

**Immune Contexture of Pancreatitis and Pancreatic Cancer:
Implications for Immunotherapy**

By

Shannon M. Liudahl

A DISSERTATION

Presented to the Cancer Biology Program
& the Oregon Health & Science University
School of Medicine

in partial fulfillment of
the requirements for the degree of

Doctor of Philosophy

August 2019



School of Medicine
Oregon Health & Science University

CERTIFICATE OF APPROVAL

This is to certify that the PhD dissertation of

Shannon M. Liudahl

has been approved

Lisa M. Coussens, PhD, Mentor/Advisor

Pepper J. Schedin, PhD, Oral Exam Committee Chair

Bernard A. Fox, PhD, Member

Rosalie C. Sears, PhD, Member

Jeffrey W. Tyner, PhD, Member

Table of Contents

List of Figures	iii
List of Tables	v
List of Abbreviations	vi
Acknowledgements.....	viii
Abstract	ix
Chapter 1: Introduction	1
The Pancreas in Health and Disease	1
<i>Pancreatic Structure and Function</i>	<i>1</i>
<i>Pancreatic Disorders.....</i>	<i>2</i>
Diabetes mellitus	2
Pancreatitis	3
Pancreatic Cancer & Neoplastic Precursors	8
Pancreatic Ductal Adenocarcinoma – An Overview	10
<i>Epidemiology, Disease Etiology, and Clinical Presentation</i>	<i>10</i>
<i>Standard Therapeutic Approaches</i>	<i>11</i>
<i>Molecular Features of PDAC.....</i>	<i>13</i>
<i>Therapeutic Targeting of Non-Immune Components of the PDAC Tumor Microenvironment</i>	<i>15</i>
Targeting Tumor Angiogenesis.....	15
Targeting Desmoplastic Stroma	16
Immunotherapy and the Immune Landscape of Pancreatic Cancer.....	18
Chapter 2: Multiplex Immunohistochemistry Reveals Phenotypic and Spatial Immune Heterogeneity in Pancreatic Ductal Adenocarcinoma	22
Introduction.....	23
Methods.....	26
Results.....	33
<i>Density of immune infiltrate is highly variable in human PDAC.....</i>	<i>33</i>
<i>Immune complexity and functional status are similar across distinct histopathological regions of PDAC resection specimens</i>	<i>41</i>
<i>Immune contexture is dynamic based on proximity to tumor.....</i>	<i>49</i>
<i>Unsupervised clustering reveals distinct immune subtypes in treatment-naïve PDAC specimens</i>	<i>53</i>
<i>Association Between Tumor Mutational Status and Immune Contexture</i>	<i>57</i>
<i>Short-term and long-term survivors exhibit different leukocyte composition</i>	<i>61</i>
<i>Neoadjuvant therapy effects on the PDAC immune microenvironment.....</i>	<i>65</i>
Discussion and Future Directions	68
Supplemental Data	72
Chapter 3: CD20 as a therapeutic target in pancreatic cancer	87
Background & Introduction	88
Materials and Methods.....	96

Results.....	103
<i>Establishing Tumor Growth Kinetics, Chemotherapy Sensitivity, and Immune Phenotypes of PDAC in C57BL/6 Mice</i>	103
<i>RTX and GA101 as monotherapy and in combination with chemotherapy</i>	108
<i>Addition of checkpoint inhibition does not improve αCD20 efficacy or alter intratumoral T cell cytotoxicity</i>	118
Discussion	125
Supplemental Data	128
Chapter 4: B lymphocytes regulate tissue response to acute pancreatic injury but are dispensable for the establishment of chronic pancreatitis.....	132
Abstract	133
Introduction.....	133
Materials and Methods.....	136
Results.....	141
<i>B cells are recruited to the pancreas following caerulein-induced acute injury and during chronic pancreatitis</i>	141
<i>Establishment and maintenance of chronic pancreatitis is B cell-independent</i>	145
<i>Acute tissue damage is reduced in the absence of B cells</i>	150
Discussion	153
Acknowledgments.....	155
Supplemental Data	156
Chapter 5: Extended Discussion.....	159
References.....	163
Appendix A: Curriculum Vitae.....	183

List of Figures

Figure 1.1 Morphological and genetic progression model of pancreatic carcinogenesis	14
Figure 2.1 Treatment-naïve PDAC tumors and adjacent tissue exhibit heterogeneous leukocyte density	40
Figure 2.2 Immune complexity in distinct histological regions of PDAC.....	48
Figure 2.3 Spatial heterogeneity of leukocytes.....	52
Figure 2.4 Unsupervised clustering of treatment-naïve PDACs based on immune complexity.....	56
Figure 2.5 Association between immune complexity and common genomic alterations in PDAC.....	60
Figure 2.6 Short-term and long-term survivors differ in leukocyte composition	64
Figure 2.7 Immune contexture of neoadjuvant-treated PDAC	67
Supplemental Figure 2.1 Myeloid biomarker panel gating strategy	72
Supplemental Figure 2.2 Lymphocyte biomarker gating strategy	73
Supplemental Figure 2.3 Functional biomarker gating strategy	74
Supplemental Figure 2.4 Leukocyte density comparisons between tissue types and sample cohorts	76
Supplemental Figure 2.5 Multiple leukocyte subpopulations are correlated with overall leukocyte density in tumor and adjacent stroma.....	77
Supplemental Figure 2.6 Intrapatient immune heterogeneity in treatment-naïve PDAC	78
Supplemental Figure 2.7 Correlations between immune subpopulation densities and overall leukocyte density in treatment-naïve tumors.....	79
Supplemental Figure 2.8 Comparisons of leukocyte population cell densities and ratios in short-term vs. long-term survivors from the treatment-naïve cohorts	81
Supplemental Figure 2.9 T cell functional profiles of short-term and long-term survivors	82
Figure 3.1 Orthotopic PDAC growth is regulated by B cells	90
Figure 3.2 α CD20-resistant B cells subvert therapeutic efficacy in orthotopic PDAC...	93
Figure 3.3 Tumor growth kinetics, chemoresponsiveness, and immune complexity of orthotopically implanted C57BL/6 PDACs	107
Figure 3.4 GA101 and RTX treatment induces significant B cell depletion in blood, spleen, and tumor.....	111
Figure 3.5 GA101 and RTX-resistant B cells in spleen are comprised of multiple B cell subpopulations	113
Figure 3.6 Combination α CD20 mAb and gemcitabine therapy does not improve antitumor response.....	117
Figure 3.7 Addition of α PD-1 mAb does not enhance therapeutic efficacy of RTX and gemcitabine	119
Figure 3.8 Addition of α PD-1 mAb does not enhance therapeutic efficacy of GA101 and gemcitabine	120
Figure 3.9 α PD-1 combination therapy is associated with increased intratumoral T cells but does not modulate myeloid frequencies.....	122
Figure 3.10 CD8 ⁺ T cell cytotoxicity and proliferation are not enhanced through combination therapy.....	124

Supplemental Figure 3.1 Genotyping of hCD20 Tg mice by flow cytometric analysis	128
Supplemental Figure 3.2 Immune complexity of end-stage orthotopic Ink4 2.2 and p53 2.1.1 FVB/n PDAC tumors	128
Supplemental Figure 3.3 Flow cytometry gating strategy used to identify myeloid and lymphoid immune lineages	129
Supplemental Figure 3.4 Flow cytometry gating strategy used to identify T cell populations	129
Figure 4.1 Treatment schematics and representative pathology of caerulein-induced acute and chronic pancreatitis	144
Figure 4.2 Tissue damage and inflammation during establishment of chronic pancreatitis is B cell-independent	147
Figure 4.3 B cell-deficiency is not associated with sustained changes in pancreatic leukocyte complexity during chronic pancreatitis	149
Figure 4.4 Acute tissue damage is reduced in the absence of B cells	152
Supplemental Figure 4.1 Pancreatic histological damage scoring criteria	156
Supplemental Figure 4.2 Cellular proliferation and apoptosis are equivalent in JH ^{+/−} and JH ^{−/−} during chronic and acute pancreatitis	157
Supplemental Figure 4.3 Resolution of tissue damage and inflammation in acute pancreatitis are FcγR- independent	158

List of Tables

Table 2.1 Baseline characteristics of 104 treatment-naïve patients with resected pancreatic adenocarcinoma	34
Table 2.2 Baseline characteristics of 13 neoadjuvant patients with resected pancreatic adenocarcinoma	35
Supplemental Table 2.1 mIHC biomarker panels.....	83
Supplemental Table 2.2 Cell lineages identified by mIHC staining	84
Supplemental Table 2.3 Correlation between leukocyte density in tumor or tumor adjacent stroma and clinical characteristics	85
Supplemental Table 2.4 List of regions of interest (ROIs) used to generate Sankey diagrams in Figure 2.3	86
Supplemental Table 2.5 Correlation between tumor cluster and clinical characteristics	86
Table 3.1 Flow cytometry antibodies used for characterization of C57BL/6 PDAC immune complexity	130
Table 3.2 Flow cytometry antibodies used for α CD20 therapeutic studies	131

List of Abbreviations

ADCC	Antibody-dependent cellular cytotoxicity
ADM	Acinar-to-ductal metaplasia
AEC	3-amino-9-ethylcarbazole
AP	Acute pancreatitis
APC	Antigen presenting cell
Breg	Regulatory B cell
BSA	Bovine serum albumin
BTK	Bruton's tyrosine kinase
CDC	Complement-dependent cytotoxicity
CIC	Circulating immune complex
CP	Chronic pancreatitis
CTLA-4	Cytotoxic T-lymphocyte-associated protein 4
DAB	3,3'-diaminobenzidine
DC	Dendritic cell
DMEM	Dulbecco's modified Eagle medium
ECM	Extracellular matrix
EDTA	Ethylenediaminetetraacetic acid
FACS	Fluorescence-activated cell sorting
FAP	Fibroblast activation protein
FBS	Fetal bovine serum
FcγR	Fc gamma receptor
FFPE	Formalin-fixed paraffin-embedded
GA101	Obinutuzumab (alternate name)
GEMM	Genetically engineered mouse model
GM-CSF	Granulocyte-macrophage colony-stimulating factor
H&E	Hematoxylin and eosin
i.p.	Intraperitoneal
i.v.	Intravenous
Ig	Immunoglobulin
IHC	Immunohistochemistry
ICAM-1	Intercellular adhesion molecule 1
ICOS	Inducible T cell co-stimulator
IFN-γ	Interferon gamma
IPMN	Intraductal papillary mucinous neoplasm
KPC mouse	<i>LSL-Kras</i> ^{G12D/+} ; <i>LSL-Trp53</i> ^{R172H/+} ; <i>Pdx-1-Cre</i> genetically engineered mouse
LAG-3	Lymphocyte-activation gene 3
mAb	Monoclonal antibody
mIHC	Multiplexed immunohistochemistry
OHSU	Oregon Health & Science University
OS	Overall survival
PanIN	Pancreatic intraepithelial neoplasia
PBMC	Peripheral blood mononuclear cell
PBS	Phosphate buffered saline

PD-1	Programmed cell death protein 1
PD-L1	Programmed death-ligand 1
PDAC	Pancreatic ductal adenocarcinoma
PDGF	Platelet-derived growth factor
PFS	Progression-free survival
PNET	Pancreatic neuroendocrine tumor
PSC	Pancreatic stellate cell
SYK	Spleen tyrosine kinase
ROI	Region of interest
ROS	Reactive oxygen species
RTX	Rituximab
TGF- β	Transforming growth factor beta
Th1	T helper 1 T cell
Th2	T helper 2 T cell
Th17	T helper 17 T cell
TIM-3	T-cell immunoglobulin and mucin-domain containing-3
TiME	Tumor immune microenvironment
TME	Tumor microenvironment
TNF- α	Tumor necrosis factor alpha
TOX	Thymocyte selection-associated HMG box protein
Treg	Regulatory T cell
VEGF	Vascular endothelial growth factor

Acknowledgements

I would like to thank my advisor, Lisa Coussens, for supporting and guiding me through the twists and turns in my projects over the years. I am without a doubt a better scientist because of you. I'm glad you took a chance on me.

Thank you to all past and present members of the Coussens lab. I could not have imagined a better group of people to call my science family over the past several years. Special thanks to Justin for making sure that the wheels never fall off. And a profound thank you to the postdoctoral fellows who have played instrumental roles in mentoring me along the way. Andy, Terry, Sushil, and Tiziana: I look up to each of you and am so grateful to have had the opportunity to work with and learn from you. Your help, encouragement, and friendship got me through all the rough parts. Thanks also to past and present members of the Schedin lab, especially Alex, Edie, and Breanna, for being excellent scientific neighbors and friends.

To the Allen-Petersens: thank you for adopting me into your family, cooking me the best dinners, and giving me pep talks when I need them most. I adore you. Kayly, Lilli, and Rick: many of my favorite grad school memories are from times we spent together. Thank you for making this fun. Courtney and Sam: a million thank-yous wouldn't be enough. You go above and beyond for me, and I am incredibly appreciative. I could not have done this without you.

Thank you to my immediate and extended family for believing wholeheartedly that I could do this and for supporting me along the way. And lastly, thank you to Matthew. Your patience and selflessness are more than I deserve. I am so lucky to have you and am so excited to start our next adventure.

Abstract

Leukocytes recruited to and persistent within chronically inflamed tissues play critical roles in fostering neoplastic progression. Immunotherapies designed to reprogram protumoral immune microenvironments have gained clinical traction in many solid tumors, but pancreatic ductal adenocarcinoma (PDAC) has thus far failed to respond to single-agent immunotherapy. Recent preclinical studies have indicated that combinatorial immunotherapy may yield improved response rates in PDAC, especially combinations intended to both reprogram immunosuppressive myeloid cells and antagonize T cell inhibitory pathways. However, the immune microenvironment of human PDAC is heterogeneous and has not been extensively characterized *in situ*. As such, functionally significant immune biomarkers are urgently needed to better stratify patients for appropriate immunotherapeutic combinations. To address this need, I used a multiplexed immunohistochemistry (mIHC) approach to comprehensively investigate and map the immune contexture – the density, composition, functional state, and spatial organization – of treatment-naïve and neoadjuvant chemotherapy-treated human PDAC surgical resections from a large, multi-institutional cohort. The resulting data affirm extensive immune heterogeneity in PDAC, both between patients and within histopathologically distinct regions of individual tumors. Our data also indicate that immune heterogeneity may be linked to molecular heterogeneity. We have revealed that high CD8⁺ T cell to CD68⁺ myeloid cell ratios are associated with improved outcomes for both treatment-naïve and neoadjuvant-treated patients. Further, we identify subgroups of tumors based upon lymphocyte and myeloid complexity that may provide a basis for stratifying patients onto rational immunotherapy combinations.

In addition to evaluation of human PDAC, my research also expands upon prior preclinical studies in the Coussens laboratory that identified B cells as mediators of PDAC progression. We previously reported a mechanism of tumor promotional crosstalk between B cells and myeloid cells resulting in tissue fibrosis, cytotoxic T cell impairment, and tumor growth. Based on these studies, I tested the hypothesis that therapeutic depletion of B cells with α CD20 monoclonal antibodies (mAbs), either as monotherapy or in combination with chemotherapy and/or α PD-1 mAb would effectively limit PDAC progression. In related studies, I tested the hypothesis that B cells regulate aspects of tissue damage and inflammation in acute and chronic pancreatitis. Using experimental murine models of pancreatitis, I report that establishment of chronic pancreatitis is B cell-independent; however, B cell deficiency is protective against acute inflammatory tissue damage. Despite pancreatitis disease pathology being driven by inflammation, immunotherapies are not currently used in disease management. These studies provide evidence that B cell-targeted therapies in recurrent acute pancreatitis could be efficacious in decreasing tissue damage and accelerating inflammatory resolution.

Finally, I discuss the broad implications and future directions of this research, with particular focus on the power of mIHC to guide patient selection for immunotherapy and to generate new hypotheses that can be taken back into preclinical models for further mechanistic investigation.

Chapter 1: Introduction

The Pancreas in Health and Disease

Pancreatic Structure and Function

The pancreas is a gland comprised of endocrine and exocrine compartments that produce hormones required for glucose homeostasis and digestive enzymes, respectively. The endocrine pancreas makes up 1-2% of total organ mass and consists of cellular clusters, known as pancreatic islets or islets of Langerhans, that are dispersed throughout the tissue and contain glucagon-producing α -cells, insulin-producing β -cells, and somatostatin-producing δ -cells [1]. Pancreatic islets are tightly interconnected to nerves and vasculature that instruct and facilitate hormone secretion in response to physiological cues [2, 3]. The exocrine pancreas constitutes the majority of the tissue area and is divided primarily between acinar cells and an extensive ductal network. Acinar cells are responsible for producing over 20 types of digestive enzymes, including amylase, lipase, and trypsin [1]. Acinar clusters form around central lumens, through which enzyme products are secreted and transported via ducts to the duodenum where they ultimately aid in digestion. Finally, pancreatic stellate cells (PSCs), a resident population of fibroblastic cells, occupy peri-acinar, peri-ductal, and peri-vascular spaces in the exocrine pancreas. In healthy tissue, PSCs are quiescent and are thought to regulate normal turnover of extracellular matrix (ECM) [4]. During injury and inflammation, PSCs are activated via inflammatory cytokines and exhibit a myofibroblast-like phenotype characterized by enhanced proliferation, cytokine and growth factor production, and ECM deposition. These attributes each contribute to tissue remodeling and wound

healing in acute inflammatory conditions but result in progressive fibrosis in the context of chronic inflammation.

Pancreatic Disorders

Both the endocrine and exocrine pancreas are susceptible to acute and chronic pathologies that significantly impact human health, including diabetes, pancreatitis, and cancer. These conditions are discussed in the following sections, with particular focus on pancreatitis and pancreatic neoplasms.

Diabetes mellitus

Nearly 10% of the United States population is estimated to have diabetes [5]. This chronic metabolic disease of the endocrine pancreas is characterized by β -cell dysfunction and is classified as either type 1 or type 2 based upon mechanism of insulin defect. Both types of diabetes are thought to arise through a complex interplay of genetic, environmental, and immune factors. Type 1 diabetes is an autoimmune disorder wherein multiple pancreatic islet-specific autoantibodies are generated against β -cells, resulting in progressive T cell-mediated β -cell destruction and consequent lack of insulin production [6]. Type 2 diabetes accounts for 90% of all diabetes cases and is characterized by impaired insulin sensitivity that causes chronic hyperinsulinemia and eventual β -cell failure and insulin insufficiency [7]. Unlike type 1 diabetes, type 2 disease does not have a clear autoimmune component but is still strongly regulated by the immune system. Obesity is a significant risk factor for type 2 diabetes, and obesity-induced inflammation in adipose tissue is thought to be a dominant mediator of metabolic dysregulation and insulin resistance [8].

Pancreatitis

Pancreatitis is an inflammatory disorder of the exocrine pancreas that can present either acutely or as a chronic fibroinflammatory disease. Acute pancreatitis (AP) is the most common cause of gastroenterological-related hospital admissions, and although mortality rates from AP have declined over the past several decades, incidence of AP is on the rise worldwide [9, 10]. Idiopathic cases of pancreatitis do occur, but there are also multiple identified etiologies of AP. Gallstone obstruction of the pancreatic duct is the most frequent cause of AP onset, and alcohol use, smoking, and obesity are lifestyle factors that also significantly increase AP risk [9]. AP ranges in severity from mild edematous disease that spontaneously resolves with supportive care, to severe necrotic disease associated with infection and/or extrapancreatic organ failure [11]. For many patients, AP is an isolated event, but a continuum has been identified in which an initial incident of AP can lead to recurrent inflammatory episodes that ultimately develop into chronic pancreatitis (CP) in a subset of cases [9, 12].

In contrast to AP, CP-associated inflammation does not fully resolve and instead leads to progressive fibrosis and tissue destruction that eventually results in exocrine and endocrine insufficiency. There are currently no therapeutic interventions to delay or reverse CP-associated tissue damage, and instead, disease management is primarily centered around pain control and pancreatic enzyme supplementation [13]. This lack of therapeutic strategies to minimize inflammation and/or slow disease progression is particularly problematic, given that CP is a strong risk factor for pancreatic cancer [14-17].

Although not all CP arises in individuals with clinically diagnosed recurrent AP, it has been postulated that subclinical, episodic acute inflammation likely precedes CP diagnosis [18]. CP shares the same lifestyle-associated risk factors as AP, with alcohol being the leading cause of CP [9]. In addition, idiopathic disease comprises approximately 25% of all CP cases, and a fraction of these are ultimately found to have an autoimmune basis [19]. Some CP cases also have hereditary underpinnings. Heritable mutations in genes encoding cationic trypsinogen (*PRSS1*) or trypsin inhibitor SPINK1 disrupt normal pancreatic protease activity, to be described below [18]. Such genomic alterations lead to early onset-pancreatitis and confer particularly high increased risk of pancreatic cancer development [9, 18].

Cellular and molecular mechanisms underlying the pathophysiology of pancreatitis are still being elucidated, but it is now well established that aberrant activation of proteases within pancreatic acini is largely responsible for initial acinar injury [20]. Proteases produced by acinar cells, such as trypsin, are synthesized in inactive pro-forms that are not activated in homeostatic states until they have reached the duodenum; however, premature protease activation within acini and pancreatic interstitium in response to etiologic stressors rapidly induces acinar injury [21]. Inflammatory factors produced by damaged acini as well as damage-associated molecular patterns (DAMPs) generated during acinar cell death rapidly recruit innate leukocytes, which then propagate further damage-promoting inflammation [22].

Human pancreatitis tissue is scarcely available for disease research, as tissue biopsies are not routine. Rodent models of acute and chronic pancreatitis have therefore been developed to enable investigation of various biological mechanisms and cellular processes of disease, including how leukocytes contribute to pathogenesis and resolution. The most widely used of these experimental models is the caerulein hyperstimulation model [23]. Caerulein is a peptide analog of cholecystokinin, a hormone produced by the duodenum that stimulates pancreatic digestive enzyme secretion. Repeated intraperitoneal administration of caerulein in rats and mice induces trypsinogen activation and inflammation, resulting in mild to moderate edematous pancreatitis [23]. Caerulein can be used to model either acute or chronic pancreatitis by modulating dosing and treatment duration accordingly. Acute pancreatitis is usually induced over the course of 1-2 days, after which the pancreas undergoes spontaneous regeneration and recovery, whereas chronic pancreatitis is induced by treating continuously for weeks or months [24-26]. Alternatively, severe necrotizing acute pancreatitis can be induced by injection of L-arginine [23]. More invasive, yet potentially more physiologically relevant, approaches of pancreatitis induction include sodium taurocholate bile acid infusion into the pancreatic duct and ductal obstruction via ligation of the pancreatic duct [23, 27]. Research incorporating these various experimental models has helped shed considerable light on immune functions in pancreatitis, particularly regarding how innate immunity regulates inflammation and tissue damage.

Neutrophil recruitment occurs very early during AP onset in response to pancreatic upregulation of neutrophil chemoattractants [28] and has profound impact on disease pathogenesis [29-31]. Neutrophils can potently stimulate trypsinogen activation and

release of reactive oxygen species (ROS) in the pancreas, thus giving rise to enhanced tissue damage and inflammation [32, 33]. Preventing neutrophil entry into the pancreas through neutrophil depletion [33, 34], blockade of integrins and selectins important for neutrophil adhesion and transendothelial migration [30, 31], or via genetic depletion of intercellular adhesion molecule 1(ICAM-1) [35] results in significant reduction in acute pancreatic injury in rodent models. There is also evidence that blocking neutrophil trafficking via inhibition of chemokine receptor CXCR2 during CP significantly reduces tissue fibrosis and acinar atrophy, although this is most likely also influenced by concurrent reduction in macrophage infiltration [28].

Conditional genetic deletion of monocytes/macrophages prior to caerulein-induced AP has also been reported to reduce pancreatitis severity [36]. Monocytes and macrophages mediate acute pancreatic damage through production of tumor necrosis factor-alpha (TNF- α), IL-1 β , IL-6, and other pro-inflammatory cytokines [37]. Interestingly, macrophages in AP have recently been found to intracellularly activate trypsinogen phagocytosed along with dying acinar cells, which then acts as a DAMP to enhance macrophage pro-inflammatory transcriptional programming and function [38].

Importantly, inflammatory macrophages have been implicated as critical instigators of acinar-to-ductal metaplasia (ADM), a process that occurs during cellular stress wherein acinar cells undergo transdifferentiation to a duct-like state that shares features with early pancreatic progenitor cells [24, 39-41]. In the case of acute damage, ADM is a reversible process, and acinar cells gradually re-differentiate as damage resolves [24]. However, under chronic inflammatory conditions, and especially in the context of acquired

oncogenic signaling, ADM persists and is speculated to be the earliest pre-neoplastic precursor of pancreatic adenocarcinoma [41, 42].

Although macrophages have well-described pro-inflammatory function in AP, evidence from mouse and human CP indicates that they are primarily transcriptionally skewed to a Th2/“M2” phenotype during chronic inflammation [43, 44]. Consistent with this, crosstalk between PSCs and macrophages via the Th2 cytokines IL-4 and IL-13 has been identified as a significant axis in the development of tissue fibrosis during CP [43]. While their transcriptional programming appears to differ between AP (Th1-like/“M1”) and CP (Th2-like/“M2”) and it is unclear precisely how or when this phenotypic shift occurs, macrophages clearly foster disease progression in both settings. This is in contrast to dendritic cells (DCs), which are reported to have opposing roles in acute versus chronic injury. Depletion of DCs during caerulein or L-arginine-induced AP pathogenesis leads to extreme exocrine necrosis and host mortality [45], whereas DCs contribute to exacerbated inflammation and tissue fibrosis in CP [46].

Though roles of innate immune cells have been extensively explored in experimental models of AP and CP, as summarized above, contributions of adaptive immunity to pancreatitis-associated tissue damage and recovery are comparatively less understood. T cells are recruited to the pancreas during experimental AP, and interferon (IFN)- γ ⁺ Th1 CD4⁺ T cells, but not CD8⁺ T cells, were reported to be positively associated with severity of tissue damage [47]. In CP, Th2 CD4⁺ T cells have been reported to form an axis with DCs that is critical for the DC-mediated fibrosis mentioned previously [46].

Apart from these studies, T cell biology in pancreatitis has not been deeply investigated. Similarly, the functional significance of B cells in pancreatitis has, until recently, been largely overlooked and is the focus of Chapter 4.

Currently, no immune-based therapeutic strategies have been successfully adopted in the clinical management of pancreatitis [48]. As experimental models of pancreatitis continue to deepen our understanding of immune and other cellular pathways involved in disease pathogenesis, tractable therapeutic targets will hopefully emerge. Therapeutic means to reverse or delay CP progression would not only improve patient quality of life but could also be cancer preventative.

Pancreatic Cancer & Neoplastic Precursors

Many types of tumors can form in the pancreas, and the subtypes range from aggressively invasive to indolent [49]. In the endocrine pancreas, pancreatic neuroendocrine tumors (PNETs) arise from pancreatic islet cells. More than half of PNET patients present with metastasis at time of diagnosis, but tumors are often slow-growing, and survival outcome is favorable compared to many other pancreatic malignancies, even with metastatic disease [50, 51]. Median overall survival for all PNET cases, including those with distant metastases, is estimated at 4.1 years [52]. The majority of pancreatic neoplasms arise in the exocrine pancreas. Of these, pancreatic ductal adenocarcinoma (PDAC) is the most common and will be the focus of the following sections this chapter, as well as Chapters 2 and 3. Rarer, morphologically distinct forms of pancreatic adenocarcinoma can also develop, such as anaplastic adenocarcinoma and adenosquamous carcinoma, which are each particularly aggressive histologic subtypes with median survival rates of 3 months

and 7 months, respectively [49]. Other rare types of exocrine tumors include acinar cell carcinoma, mucinous noncystic carcinoma, solid pseudopapillary tumors, and signet ring cell carcinoma [49]. Because incidence of these tumors is much lower than PDAC, much of the literature describing them consists of individual case studies or reports of small patient cohorts treated at a given medical center, and robust statistics on disease prognosis for some of these tumor types are unavailable.

In addition, two categories of neoplastic lesions have been identified as predominant precursors to pancreatic adenocarcinomas: intraductal papillary mucinous neoplasm (IPMN) and pancreatic intraepithelial neoplasia (PanIN) [53]. IPMNs are macroscopic cysts located in the main pancreatic duct or its major branches [54]. IPMNs are associated with invasive carcinoma in approximately one third of cases, and surgical resection is recommended if the lesion(s) are located in the main pancreatic duct or are > 3 cm as measured by radiographing imaging [54]. Approximately 10% of PDACs are estimated to arise from IPMN, but cellular and molecular features of progression from IPMN to invasive adenocarcinoma are not completely understood [55].

PanINs the most common precursor associated with PDAC. It is estimated that approximately 20% or more of all individuals over 65 years old likely have low-grade PanINs [54]. PanIN frequency and grade increase in individuals with chronic pancreatitis and PDAC compared to controls without pancreatic disease [53]. PanINs are graded from lowest to highest degree of dysplasia, and even the earliest grade PanINs are associated with genomic alterations common to PDACs [53], as will be discussed in further detail in

a later section. PanINs are frequently located in close proximity to tissue areas containing ADM, leading to the hypothesis that de-differentiated acini represent the first step in PanIN development and, by extension, that acini are a cell of origin of PDAC [53]. This concept has been supported by studies using transgenic mouse models of PanIN and PDAC development wherein acinar to ductal conversion was demonstrated to be a much more frequent origin of PanIN than normal pancreatic ductal cells [56].

Pancreatic Ductal Adenocarcinoma – An Overview

Epidemiology, Disease Etiology, and Clinical Presentation

Pancreatic ductal adenocarcinoma (PDAC) is the fourth leading cause of cancer-related mortality in the United States [57]. The median overall five-year survival rate for PDAC is only 9% [58], which is in part due to late clinical presentation and poor response to standard-of-care cytotoxic therapies. Common risk factors for PDAC include smoking, alcohol use, and obesity [59], but there are currently no biomarkers to identify individuals out of the general population who are most likely to develop PDAC. In addition to lifestyle and environmentally-associated risk factors, familial history of pancreatic cancer, certain genetic syndromes, and chronic pancreatitis are each associated with significantly elevated risk of PDAC [59].

Surgical resection remains the only potentially curative treatment for PDAC; however, only 15-20% of patients are eligible for surgery at time of diagnosis, whereas the majority of patients instead present with locally advanced disease involving major vascular and/or distant metastasis that typically precludes surgical intervention [60]. Even

when surgery is possible, disease recurrence rate for PDAC exceeds 80% [61]. Recent studies in genetically engineered mouse models (GEMMs) of PDAC have revealed that systemic dissemination of tumor cells likely occurs very early in the course of tumorigenesis [62], leading to occult metastases that become clinically detectable after removal of primary tumors and thereby limit the overall efficacy of surgery.

Because the majority of PDAC patients present with late-stage disease, there is now significant effort directed towards development of diagnostic assays to for early detection that could lead to improved patient outcomes. Germline genetic testing is now recommended for pancreatic cancer patients in order to prospectively identify first- and second-degree relatives who may benefit from screening, and surveillance trials have demonstrated the success of this approach [63, 64]. A subset of chronic pancreatitis patients that have a hereditary form of the disease may also benefit from regular cancer surveillance [65]. However, these high-risk groups with clear genetic predispositions for PDAC represent a relatively rare subset of all PDAC cases, and until biomarkers are discovered that enable specific and effective screening for the general population, improving patient outcome after PDAC diagnosis is essential.

Standard Therapeutic Approaches

For decades, standard-of-care treatment for PDAC has been single-agent or combination chemotherapy. Gemcitabine has long been a chemotherapeutic agent of choice, given its relatively low toxicity profile, ability to improve patient performance status, and modest extension of median survival time [66]. In advanced-stage disease, combining

gemcitabine with nab-paclitaxel has shown therapeutic efficacy greater than gemcitabine alone while still maintaining low toxicity, and is currently a front-line treatment option [67]. FOLFIRINOX – a combination of leucovorin, fluorouracil, irinotecan, and oxaliplatin – also confers greater median survival than gemcitabine monotherapy as front-line treatment in the metastatic setting and as adjuvant treatment for early-stage disease following tumor resection [68, 69]. However, this regimen results in considerably elevated toxicity that is not well-tolerated by all patients. Gemcitabine/capecitabine combination therapy is the current suggested alternative for patients with low performance status [70], and efficacy of gemcitabine/nab-paclitaxel compared to gemcitabine monotherapy is also being evaluated in the adjuvant setting (APACT trial, NCT01964430).

Neoadjuvant therapy is also gaining traction in PDAC, as it could improve rates of surgical margin negative (R0) resections and also provides an opportunity to convert locally advanced and borderline resectable disease into cases eligible for surgery [61, 63]. Moreover, a neoadjuvant approach ensures that patients receive some chemotherapy, as not all individuals have post-operative performance status high enough to make adjuvant treatment feasible. Either FOLFIRINOX or gemcitabine/nab-paclitaxel regimens are favored for neoadjuvant treatment, sometimes in combination with radiotherapy [71].

Importantly, even the most robust standard-of-care options fall short of delivering long-term benefit to most PDAC patients. FOLFIRINOX therapy results in a median overall survival of just 11.1 months in the metastatic setting and 54.1 months in the adjuvant

setting, whereas progression-free and metastasis-free survival intervals are considerably shorter [68, 69]. Although therapeutic outcomes have advanced considerably within the past ten years, improved combination treatments that yield more durable response rates are urgently needed.

Molecular Features of PDAC

PDACs generally harbor low relative mutational burden compared to many other solid tumors [72], but somatic alterations in four major driver genes – *KRAS*, *TP53*, *CDKN2A*, and *SMAD4* – are common and are acquired in a step-wise manner during neoplastic progression [73] (**Figure 1.1**) . Activating mutations in *KRAS* occur earliest during neoplastic progression (low grade PanIN-I) and are found in nearly all (90-100%) of PDACs [73, 74]. Inactivation of the tumor suppressor *CDKN2A* also occurs early during progression of pre-invasive neoplasia and is found in more than 80% PDACs [75]. Inactivation of *TP53* (50-70% of cases) and *SMAD4* (approximately 50% of cases) occur relatively late in neoplastic progression (high grade PanIN-3) [75]. Alterations in these four genes are independently and combinatorially associated with worse disease-free and/or overall-survival, with a higher number of these alterations associated with significantly poorer outcome [76, 77].

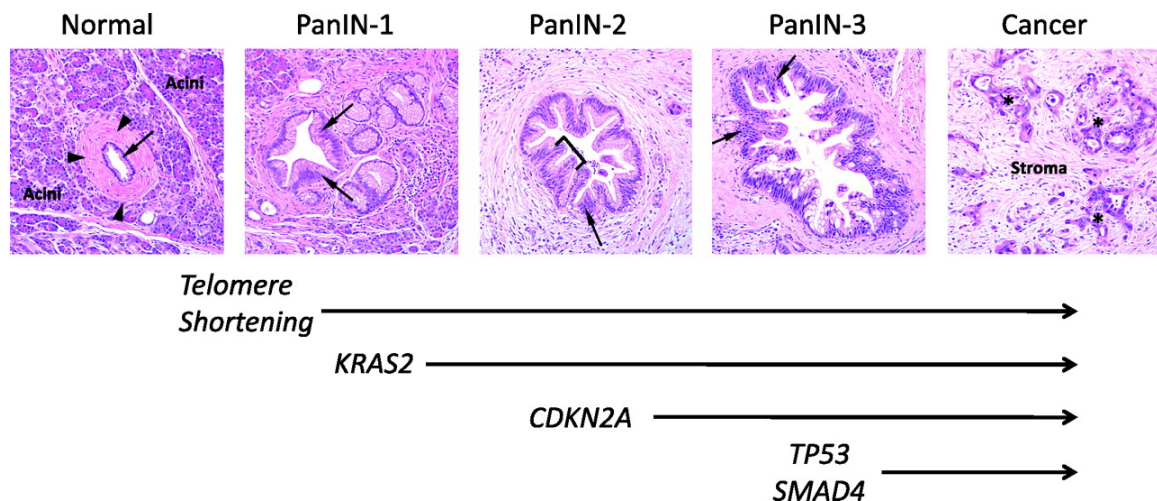


Figure 1.1 Morphological and genetic progression model of pancreatic carcinogenesis. Histological examples of a normal pancreatic duct, pancreatic intraepithelial neoplasia (PanIN) and pancreatic cancer are shown. Based on this progression model, the molecular alterations that accumulate during pancreatic carcinogenesis can be classified into early (telomere shortening and activating mutations in *KRAS2*), intermediate (inactivating mutations or epigenetic silencing of *p16/CDKN2A*) and late (inactivating mutations of *TP53* and *SMAD4*) events. Figure originally appeared in Iacobuzio-Donahue, Gut 2012 [73], and is reprinted with permission from the publisher.

One challenging aspect of moving PDAC treatment beyond cytotoxic chemotherapy is that, unlike in some other tumor types, the genomic alterations most common in this disease are not direct therapeutic targets. Several genomic and transcriptomic profiling studies of PDAC have been performed in recent years with the goal of identifying molecular subtypes that might be leveraged therapeutically to help stratify patient risk and rationally guide enrollment in clinical trials [78-83]. PDACs are reported to contain an average of 60 genomic alterations, though low prevalence of these various alterations across patient population complicates broad translation of particular targeted therapies and instead requires precision-based medicine approaches [80, 84]. Recent DNA sequencing of a cohort of 600+ PDACs revealed that roughly 25% of tumors had highly actionable mutations for which FDA-approved targeted therapies exist [82]. Notably, in a small subset of these patients who received therapy matched to their identified actionable

mutation, progression-free survival was significantly increased as compared to patients who did not received therapies tailored to their tumor mutations [82]. This underscores the clinical potential for targeted therapies in PDAC, at least in a subpopulation of patients.

Therapeutic Targeting of Non-Immune Components of the PDAC Tumor

Microenvironment

It is now widely appreciated that neoplastic cells are but one part of the equation in tumor progression and that the complex network of cancer-associated fibroblasts (CAFs), vasculature endothelial cells, lymphatic endothelial cells, and leukocytes that make up the surrounding tumor microenvironment (TME) are also essential players in tumor biology – especially with regard to how we conceive of and approach cancer therapy. Therapies directed at various constituents of the PDAC TME have been and continue to be evaluated in preclinical and clinical settings, often in combination with chemotherapy [85], although none have made significant clinical traction to this point.

Targeting Tumor Angiogenesis

Induction of tumor neoangiogenesis is a hallmark of cancer, as blood vasculature serves the critical functions of providing oxygen and nutrient supplies to growing tumors and facilitating tumor invasion [86]. Anti-angiogenic therapies targeting vascular endothelial growth factor (VEGF) and VEGF receptor (VEGFR) are approved for colorectal cancer, non-small cell lung cancer, renal cell carcinoma, pancreatic neuroendocrine tumors, and others [87], but these approaches have not demonstrated improved outcomes in PDAC in any of the clinical trials conducted to date. Phase III clinical trials evaluating

combinations of bevacizumab (a VEGF-A inhibitor) or axitinib (a VEGFR inhibitor) in combination with gemcitabine as frontline therapy for metastatic or locally advanced PDAC showed no benefit as compared to gemcitabine monotherapy [88, 89].

Additionally, the multi-target inhibitor sorafenib – which targets VEGFR, platelet-derived growth factor receptor (PDGFR) and rapidly accelerated fibrosarcoma (RAF) family kinases – did not improve progression-free or overall survival when combined with gemcitabine, despite the hope that it might have enhanced effects through impacting not only tumor angiogenesis but also signaling downstream of oncogenic KRAS [90]. In light of these clinical results, angiogenesis is not currently thought to be a particularly tractable target for further therapeutic investigation in PDAC.

Targeting Desmoplastic Stroma

A prominent feature of the PDAC TME is dense desmoplasia surrounding the neoplastic epithelium. This fibroinflammatory stroma is comprised of ECM, including collagens and hyaluronan, secreted by activated PSCs, which are the primary CAFs in the PDAC TME [91]. Dense fibrosis in PDAC increases interstitial pressure within the tumor and consequently compresses tumor vasculature and limits optimal drug perfusion [92, 93]. CAFs are also known paracrine regulators of tumor cell proliferation, angiogenesis, immune suppression, and tumor cell invasion [86]. Moreover, high levels of ECM components in human PDAC have been associated with poor survival [94]. Therefore, therapeutically targeting CAFs or other constituents of the fibrotic stroma has been of interest over the past several years. However, preclinical and clinical strategies tested thus far with the intention of reducing fibrosis have had mixed results.

Pancreas-specific deletion of αSMA^+ fibroblasts at various stages of PDAC development was reported to associate with development of more poorly differentiated tumors, increased abundance of intratumoral T regulatory cells (Tregs), and reduced survival [95]. Similarly, genomic ablation or therapeutic inhibition of Hedgehog signaling, which is active in myofibroblasts, resulted in reduced desmoplasia but also in increased tumor cell proliferation, increased tumor vascularity, and significantly reduced survival [96]. Collectively, these findings indicate that stroma can in fact restrict tumor progression rather than promote it. On the other hand, studies depleting fibroblast activation protein (FAP) $^+$ αSMA^- CAFs showed enhanced CD8 $^+$ T cell recruitment to tumors and slowed tumor growth [97]. In addition, others have reported that reprogramming CAFs via modulation of Vitamin D receptor signaling potently reduces tumor fibrosis and leads to improved chemotherapy response and extended survival [98]. These discordant effects of CAF modulation are likely due at least in part to the newly recognized phenotypic and functional heterogeneity of pancreatic CAFs that may differentially exert pro- or anti-tumoral effects [99, 100].

Much remains to be learned about CAF subtypes and CAF-targeted therapies in PDAC. As of now, one of the more successful approaches to modulate tumor stroma has been enzymatic depletion of hyaluronan. Preclinical administration of PEGylated recombinant hyaluronidase (PEGPH20) in KPC mice led to substantial stromal remodeling and decreased primary tumor growth and metastatic incidence [93]. A randomized phase II human clinical trial evaluating PEGPH20 in combination with gemcitabine/nab-paclitaxel versus gemcitabine/nab-paclitaxel alone in metastatic PDAC demonstrated modestly

improved progression-free survival (PFS), particularly in tumors with high levels of hyaluronan, but no overall survival benefit [101]. A phase III trial of PEGPH20 plus gemcitabine/nab-paclitaxel is currently ongoing in metastatic PDAs that have been pre-determined to express high levels of hyaluronan (ClinicalTrials.gov identifier: NCT02715804). If successful, this therapeutic combination will represent a milestone for implementation of a TME-directed therapy with standard of care chemotherapy in PDAC treatment.

Immunotherapy and the Immune Landscape of Pancreatic Cancer

Within the past decade, immunotherapy has revolutionized cancer treatment by improving outcomes of patients whose tumors are unresponsive or acquire resistance to standard-of-care chemo- and radiotherapies. Immune checkpoint blockade, chimeric antigen receptor (CAR) T cell therapy, vaccines against tumor neoantigens, and myeloid-targeted therapies represent several immune-oncology approaches that have demonstrated efficacy in the treatment of a variety of solid tumors [102, 103]. A major clinical goal for immunotherapy is to develop diagnostic and intervention strategies that will minimize therapeutic resistance and maximize durable therapeutic efficacy. Given the limited responsiveness to standard-of-care chemotherapies in almost all PDAC patients, considerable effort is now being put forth to identify immunotherapeutic strategies that could benefit those with this disease.

Although immunotherapy has become a cornerstone of cancer treatment in many malignancies, still only a fraction of all patients exhibit responses, and success of immunotherapeutic approaches in PDAC are still elusive [104]. PDAC is thought to be

particularly challenging due to its highly immunosuppressive TME [105]. PDACs, like most solid tumors, have co-opted tissue defense programs of the host immune system through recruitment of diverse leukocytes into the neoplastic environment that engage in tumor-promotional Th2-skewed immune functions. Through chemokine and cytokine secretion, Th2 immune programming supports tumor cell survival, angiogenesis, tissue remodeling, and fibrosis within the TME [106]. A common mechanism of tumor escape from immune surveillance is chronic activation of these Th2 responses, which is often characterized by myeloid recruitment and suppression of CD8⁺ cytotoxic T lymphocytes (CTLs).

Tumor associated macrophages (TAMs) comprise a substantial portion of the immune milieu in PDACs [107] and contribute to T cell immunosuppression via multiple direct and indirect mechanisms [103]. Tumor-infiltrating neutrophils are also associated with poor prognosis and impairment of T cell responses [108]. Preclinical studies have made promising strides in identifying therapeutic strategies to counteract immunosuppressive myeloid cells. Inhibition of the colony-stimulating factor 1 (CSF1)/colony-stimulating factor receptor (CSF1R) with a CSF1 neutralizing antibody reprogrammed TAMs toward a more inflammatory phenotype, induced infiltration of T cells into PDAC tumors, and sensitized tumors to checkpoint inhibitors [109]. In addition, blocking monocyte/macrophage and neutrophil trafficking to tumors via inhibition of myeloid chemokine receptors CCR2 and CXCR2 also revealed enhanced T cell infiltration into tumors and improved T cell effector functionality [108, 110]. Clinical trials evaluating these therapeutic strategies in human PDAC are currently underway [104].

The Coussens laboratory and others have also recently identified tumor supportive functions of B cells in preclinical murine models of PDAC [111-113]. B cells regulate immunosuppressive programming of the PDAC TME via direct secretion of immunosuppressive cytokines and through humoral immunity [111, 112]. We demonstrated that B cell-derived immunoglobulins (Igs) interact with Fc γ receptors on TAMs, resulting in macrophage polarization to a Th2-like immunosuppressive phenotype associated with increased tissue fibrosis and impaired T cell effector function [111]. Therapeutic blockade of Bruton's tyrosine kinase (BTK), a kinase downstream of the B cell receptor and Fc γ receptor, induced B cell depletion, Th1-like macrophage reprogramming, enhanced CD8⁺ T cell function, and reduced tumor growth [111]. BTK inhibitors are clinically approved for other disease indications, and results from our preclinical studies prompted clinical evaluation of the BTK inhibitor ibrutinib in PDAC, which is currently ongoing. Alternate therapeutic strategies for targeting B cells in the PDAC TME are the topic of Chapter 3.

T cell and antigen presenting cell (APC) agonists also show promise in improving antitumor immune responses in PDAC. Agonism of the CD40-CD40L signaling pathway licenses APCs, thereby promoting more effective antigen presentation to T cells, which in turn leads to T cell activation [105]. CD40 agonists used in combination with gemcitabine and nab-paclitaxel induced productive antitumor T cell responses and sensitized tumors to checkpoint inhibition in preclinical models [104, 114].

The therapies described above represent only a few of many examples of immunotherapies currently under investigation for PDAC. And while early preclinical and clinical results of these therapies are encouraging for a disease that urgently needs better treatments, more challenges are ahead with regard to identifying which subset(s) of patients are most likely to respond to particular immune-oncology agents. We recently identified mechanisms by which tumor intrinsic features give rise to extensive tumor immune heterogeneity [115]. Orthotopic implantation of isogenic tumor subclones derived from a genetically engineered mouse model of PDAC resulted in a spectrum of heterogeneous tumors that could be classified based on CD8⁺ T cell density. T cell high tumors exhibited reduced relative density of immunosuppressive myeloid cells and were sensitive to combined chemotherapy, α CD40, and checkpoint inhibition. In contrast, T cell low tumors were more heavily infiltrated by TAMs and neutrophils and were resistant to therapy [115]. Similar immune subtypes have been observed in human PDACs [116, 117] and have prognostic significance. Our recent evaluation of a small cohort of human PDAC resection specimens following treatment with a neoadjuvant tumor vaccine revealed a subgroup of patients that had densely myeloid inflamed tumors that were associated with shorter overall survival as compared to tumors with lower myeloid density [116]. Tumors with low myeloid infiltration, on the other hand, had higher densities of lymphocytes and had improved survival outcome [116]. These discoveries highlight the significance of immune heterogeneity and prompt further evaluation of immune complexity in human PDAC. A more nuanced understanding of immune heterogeneity will help stratify patients for immunotherapeutic combinations that are most likely to benefit their unique tumor landscape.

Chapter 2: Multiplex Immunohistochemistry Reveals Phenotypic and Spatial Immune Heterogeneity in Pancreatic Ductal Adenocarcinoma

Shannon M. Liudahl¹, Shamilene Sivagnanam², Courtney B. Betts¹, Vicente Morales-Oyarvide^{3,4}, Chen Yuan^{4,5}, Jonathan A. Nowak^{4,6,7}, Samuel Hwang⁸, Alison Grossblatt-Wait^{9,10}, Kenna R. Leis¹, William Larson¹, Padraic Robinson¹, Andressa Dias Costa⁸, Sara A. Varyrinen⁸, Jason Link^{10,11}, Dove Keith¹⁰, Wesley Horton^{1,2}, Meghan B. Lavoie¹, Margaret A. Tempero¹², Elizabeth M. Jaffee¹³, Brett Sheppard^{10,14}, Jeremy Goecks^{2,9}, Rosalie C. Sears^{9,10,11}, Brian M. Wolpin^{3,4,15}, and Lisa M. Coussens^{1,9,10,*}

¹Department of Cell, Developmental and Cancer Biology, Oregon Health & Science University, Portland, OR USA

²Computational Biology Program, Oregon Health & Science University, Portland, OR, USA

³Department of Medical Oncology, Dana-Farber Cancer Institute, Boston, MA, USA

⁴Harvard Medical School, Boston, MA, USA

⁵Department of Epidemiology, Harvard TH Chan School of Public Health, 677 Huntington Avenue, Boston, MA 02115, USA

⁶Department of Oncologic Pathology, Dana-Farber Cancer Institute, Boston, MA, USA

⁷Department of Pathology, Brigham and Women's Hospital and Harvard Medical School, Boston, MA, USA

⁸Department of Pathology, Oregon Health & Science University, Portland, OR, USA

⁹Knight Cancer Institute, Oregon Health & Science University, Portland, OR, USA

¹⁰Brenden-Colson Center for Pancreatic Care, Oregon Health & Science University, Portland, OR, USA

¹¹Department of Molecular and Medical Genetics, Oregon Health & Science University, Portland, OR USA

¹²Helen Diller Family Comprehensive Cancer Center and Department of Medicine, University of California, San Francisco, CA USA

¹³Departments of Oncology and Pathology, the Sidney Kimmel Comprehensive Cancer Center, the Skip Viragh Center for Pancreas Cancer Clinical Research and Patient Care at Johns Hopkins University School of Medicine, Baltimore, MD, USA

¹⁴Department of Surgery, Oregon Health & Science University, Portland, OR, USA

¹⁵Department of Medicine, Brigham and Women's Hospital, Boston, MA, USA

*Corresponding author

The contents of this chapter are the foundation for a manuscript currently in preparation, with a target submission of Fall 2019.

Introduction

Pancreatic ductal adenocarcinoma (PDAC) is the fourth leading cause of cancer-related mortality in the United States, and the current 5-year survival rate is only 9% [58]. Most patients present with late-stage metastatic disease, and even patients diagnosed at earlier stages who qualify for surgical resection have disease recurrence rates exceeding 80% [61]. Standard-of-care cytotoxic therapies only minimally extend life expectancy in this disease [68, 69], and new therapeutic combinations are urgently needed to improve PDAC outcomes.

Immunotherapies have been transformative in the treatment of many solid tumors but have yet to make an impact in PDAC [104]. With the exception of a small subset of PDAC patients with microsatellite instability (MSI) who respond to checkpoint inhibitors [118], no immunotherapeutic agents have been approved for this disease. PDAC presents particular hurdles to immunotherapy efficacy by virtue of its poor immunogenicity and highly immunosuppressive tumor immune microenvironment (TiME) [107]. A more nuanced understanding of immune contexture and heterogeneity of PDAC is needed to help stratify patients and inform rational combinations of therapies that may benefit individuals with particular tumor immune landscapes.

Much of the current characterization of PDAC heterogeneity relies upon methodologies using tissue disaggregates (e.g. DNA/RNA sequencing, flow cytometry). While these approaches, particularly molecular subtyping, have recently revealed distinct, prognostically significant classes of PDACs based upon mutational and immune

signatures [78, 79, 81], spatial context of these tumor microenvironments are largely lost in these analyses. This is particularly relevant with regard to immune evaluation, as leukocyte spatial dynamics have demonstrated prognostic significance, as evidenced by approaches such as Immunoscore used in colon cancer, which takes into account densities of cytotoxic T cells at tumor centers and at tumor margins [119].

The recent development of various multiplexed imaging approaches now enables *in situ* phenotyping and spatial characterization of multiple cell populations simultaneously [116, 120-122], and such techniques are facilitating significant advances in our understanding of immune complexity and spatial organization in PDAC. For example, several recent studies have revealed extensive T cell heterogeneity in PDAC and demonstrated that localization of CD8⁺ T cells in tumor centers but not tumor margins is prognostically significant [122-124]. However, many of these analyses focus predominantly on adaptive immune cells, and robust characterization of myeloid complexity and interpatient heterogeneity is often absent. This is particularly relevant in light of our recent report demonstrating that PDAC patients who received the neoadjuvant tumor vaccine GVAX clustered into low-myeloid inflamed and high-myeloid inflamed tumors, with high-myeloid inflamed tumors exhibiting greater T cell immunosuppression and shorter overall patient survival. [116]. Expanded studies such as these are warranted to more holistically evaluate treatment-naïve and neoadjuvant-treated tumors.

To address this need, we employed a chromogen-based multiplexed immunohistochemistry (mIHC) platform capable of deeply auditing large areas of tissue to build a comprehensive atlas of 117 clinically- and genomically-annotated human PDAC surgical resections from a multi-institutional patient population. Through mIHC profiling of lymphocyte and myeloid immune lineages in tumor, tumor adjacent stroma, immune aggregates, and adjacent normal pancreas tissue, we revealed substantial intrapatient and interpatient tumor immune heterogeneity. We identify three distinct clusters of treatment-naïve cases that have potential to serve as a baseline to inform patient stratification for immunotherapies. In addition, we demonstrate associations between immune contexture and mutational status, which has further implication for patient stratification.

Methods

Multiplexed Immunohistochemistry (mIHC) and Image Acquisition

Human PDAC surgical resection specimens were obtained with informed consent in accordance with the Declaration of Helsinki and acquired with approval from the institutional review board at Dana-Farber Cancer Institute/Brigham and Women's Cancer Center and the Oregon Pancreas Tissue Registry under Oregon Health & Science University (OHSU) IRB protocol #3609. Healthy normal pancreas was acquired through organ transplant programs at University of California San Francisco and OHSU. Tissues were fixed with 10% neutral buffered formalin, dehydrated in ethanol, and embedded with paraffin using standard protocols. Multiplexed IHC was performed on 5 μ m FFPE sections as we have previously described [116, 125, 126]. Briefly, slides were deparaffinized and stained with hematoxylin (S3301, Dako, Santa Clara, CA), followed by digital whole-slide scanning at 20X magnification on an Aperio AT2 scanner (Leica Biosystems, Wetzlar, Germany). Tissues then underwent 20 minutes heat-mediated antigen retrieval in pH 6.0 Citra solution (BioGenex, Fremont, CA), followed by endogenous peroxidase blocking in either 0.6% H₂O₂ for 20 minutes or Dako Dual Endogenous Enzyme Block (S2003, Dako, Santa Clara, CA) for 10 minutes. Protein blocking was performed for 10 minutes with 5% normal goat serum and 2.5% BSA in PBS. Primary antibody incubation was carried out for 30 to 60 minutes at room temperature or overnight at 4°C; antibodies and staining conditions are listed in **Supplemental Table 2.1**. Slides were then washed in TBST and either anti-rat, anti-mouse, or anti-rabbit Histofine Simple Stain MAX PO horseradish peroxidase (HRP)-conjugated polymer (Nichirei Biosciences, Tokyo, Japan) was applied for 30 minutes at

room temperature, followed by signal detection with AEC chromogen (Vector Laboratories, Burlingame, CA). Slides were digitally scanned following each chromogen development, followed by chromogen removal in 100% ethanol. For staining cycles with two rounds of antibody development, protein blocking was repeated after chromogen removal, and tissue sections were taken through all steps listed above from primary antibody application through chromogen development and slide scanning. At the completion of a staining cycle, chromogen was removed in 100% ethanol and the next cycle was started at the heat-mediated antigen retrieval step, in order to remove all antibodies from the previous cycle.

Tissue Annotation and Region of Interest (ROI) Selection

Whole-slide digitally scanned images for each case were reviewed by a pathologist (S.H.), and tumor-enriched tissue regions were digitally annotated. Areas of necrosis were excluded. Tumor annotations in combination with CD45 IHC staining were used to select immune-infiltrated ROIs distributed throughout the tissue. Tumor-enriched (T) ROIs within pathology annotations were evaluated for each case (117/117 cases [100%], 1-4 ROIs per case, average 21.3 mm² total area analyzed per slide), based on tissue size. The following types of intra- or extratumoral regions were also analyzed in all cases in which they were present: tumor adjacent stroma (TAS) outside of tumor annotations (94/117 cases [80%], 1-2 ROIs per case, average 8.78 mm² total area analyzed per slide); tumor adjacent normal pancreas (AN) outside of tumor annotations (41/117 cases [35%], 1-2 ROIs per case, average 3.30 mm² total area analyzed per slide), lymphocyte-dense immune aggregates (IA) within or outside of tumor annotations (68/117 [58%], 1-6 ROIs

per case, average 0.72 mm² total area analyzed per slide). For healthy normal pancreas (HN), 3 ROIs were evaluated per case (average 11.09 mm² total area analyzed per slide). Three serial formalin-fixed paraffin embedded (FFPE) tissue sections per PDAC case were used for staining of Lymphoid, Myeloid, and Functional mIHC biomarker panels. ROI number, size, and placement were maintained across serial sections from the same sample. Proximity of TAS, AN, and IA regions to nearest tumor annotation were classified as follows: Border, 75% or more of ROI area is ≤ 1 mm from tumor annotation; Spanning, 50% of ROI area is ≤ 1.0 mm of nearest annotation and 50% of area is > 1.0 mm from annotation; Distal, 75% or more of ROI area is > 1.0 mm from nearest tumor annotation. A summary of ROIs evaluated from each of these spatial categories can be found in **Supplemental Table 2.4**. To calculate cell densities of immune populations in an individual patient within particular tissue compartments (e.g. tumor), cell counts for a given cell type (e.g. CD8⁺ T cells) from each ROI were added to get total cell count, and areas of each ROI were also added. Cumulative density was then calculated with the following equation: total cell number / total area = cumulative cell density in mm².

Image Processing and Analysis

Image co-registration and processing was performed using methods adapted from our previously described image processing workflow [116, 125]. Selected ROIs from each RGB marker image were registered to the hematoxylin stained RGB image using the detectSURFfeatures algorithm in the Computer Vision Toolbox in Matlab version R2018b (The MathWorks, Inc., Natick, MA) to identify matching keypoints in the blue or red channel of the hematoxylin image with keypoints in the blue channel of the AEC

stained image. Using `estimateGeometricTransform` in the Computer Vision Toolbox, a geometric transformation was estimated using similarity that was applied to all channels of the AEC stained image. This process was used to register each marker-stained image region to the same region of the hematoxylin-stained image. This approach is a linear transformation that does not address small local, uneven deformations, however, only regions that were well-registered were included for downstream analysis.

Image processing, cell quantification, and image cytometry were performed using FIJI (FIJI Is Just ImageJ) [127], CellProfiler Version 3.5.1 [128], and FCS Express 6 Image Cytometry RUO (De Novo Software, Glendale, CA), respectively. AEC signal was extracted for quantification and visualization in FIJI using a custom macro for color deconvolution. Briefly, the FIJI plugin `Color_Deconvolution [H AEC]` was used to separate hematoxylin, followed by postprocessing steps for signal cleaning and background elimination. AEC signal was extracted in FIJI with the NIH plugin `RGB_to_CMYK`. Color deconvoluted images were rescaled and processed in Cell Profiler to quantify single cell mean intensity signal measurements for every stain. The Cell Profiler pipeline rescaled intensity of each image by dividing by the max intensity of each image, resulting in an intensity range of 0-1. The binary segmentation mask produced in FIJI was used to identify nuclei with the `IdentifyPrimaryObjects` module, and mean intensity for each object for every marker was measured using the `MeasureObjectIntensity` module. The resulting data is a csv containing the mean intensity of every cell for each marker that is subsequently used in image cytometry single cell gating. Cells were hierarchically identified and quantified by image cytometry in FCS Express. Hierarchical cell classifications and image cytometry gating strategies are

shown in **Supplemental Table 2.2** and **Supplemental Figures 2.1-2.3**. For mIHC visualization, signal-extracted images were overlaid in pseudo-color in FIJI.

Molecular Status Determination

For a subset of cases included within both cohorts, molecular status of *KRAS*, *TP53*, *CDKN2A*, and *SMAD4* was also determined by using integrated DNA sequencing and IHC approaches. Tumors from the Dana-Farber cohort underwent pyrosequencing for *KRAS* hotspot mutations, NGS sequencing using a custom massively parallel sequencing panel, and standard IHC as previously described in detail [76]. Briefly, for the Dana-Farber cohort, *KRAS* mutant versus wild-type status was determined based on sequencing results. For *TP53*, NGS data and IHC staining were used to make integrated determinations of gene status. *CDKN2A* and *SMAD4* were classified as intact (positive) or lost (negative) based on IHC [76]. For OHSU samples, DNA was extracted from FFPE tissue sections, and *KRAS*, *TP53*, and *CDKN2A* alterations were identified through DNA sequencing with either the 595 gene Tempus xT targeted cancer genome sequencing panel (Tempus, Chicago, IL) or the clinical 124 gene GeneTrails Comprehensive Solid Tumor Panel (Knight Diagnostics Laboratories, OHSU). *SMAD4* was classified as positive or negative based on IHC staining. 5 µm FFPE tissue sections were deparaffinized and subjected to 20 minutes heat-mediated antigen retrieval in pH 6.0 Citra solution (BioGenex), followed by 10 minutes endogenous peroxidase blocking in Dako Dual Endogenous Enzyme Block (Dako) and 10 minutes protein blocking with 5% normal goat serum and 2.5% BSA in PBS. Smad4 primary antibody incubation was carried out overnight at 4°C (clone B-8, #sc-7966, 1:50; Santa Cruz Biotechnology,

Dallas, TX). Slides were washed and then incubated in secondary antibody (biotinylated anti-mouse IgG, #BA-9200, 1:200; Vector Laboratories, Burlingame, CA) for 30 minutes at room temperature, followed by ABC Elite horseradish peroxidase-conjugated avidin complex (Vector Laboratories) for 30 minutes at room temperature. Signal was developed with 3,3'-diaminobenzidine (Dako) and tissues were counterstained with hematoxylin. Slides were reviewed by three pathologists (J.A.N, A.D.C., and S.A.V.) who jointly assigned Smad4 classification as previously reported [76].

Outcome Measures

Disease-free survival (DFS) was defined as time between date of surgery and date of disease recurrence. Cases with gross residual disease (R2 margin status) following surgery and cases with unknown date of disease recurrence were excluded from DFS analysis. Overall survival (OS) was defined as time between date of surgical resection and date of death from any cause or date of last clinical contact. For neoadjuvant cases, OS was defined as time from start date of neoadjuvant therapy to date of death from any cause or last clinical contact.

Statistical Analysis^S

Comparison of two groups was performed using an unpaired, two-tailed Mann-Whitney U test, and comparisons of more than two groups was performed using the Kruskal-Wallis test. Select associations were measured using the Fisher exact test for categorical variables and Wilcoxon rank-sum test for continuous variables. Correlations between

continuous variables were measured using Spearman rank correlation. For outcomes analyses (DFS and OS), Kaplan-Meier curves were generated and survival differences were measured using Mantel-Cox log-rank test. Specific statistical tests used are indicated in figure legends. * $p \leq 0.05$, ** $p \leq 0.01$, *** $p \leq 0.001$.

[§] For the final manuscript, additional statistical analyses will be incorporated that are currently in progress in collaboration with the OHSU Knight Cancer Institute Biostatistics Shared Resource.

Results

Density of immune infiltrate is highly variable in human PDAC

To profile the immune landscape of PDAC, we used an established mIHC platform [116, 125, 126] to evaluate a multi-institutional cohort of treatment-naïve (n = 104) and physician's choice neoadjuvant-treated (n = 13) surgically-resected PDACs. Clinical characteristics of patients are shown in **Table 2.1** and **Table 2.2**. Three serial FFPE sections from each patient were stained with mIHC antibody panels designed to detect and quantify lymphocyte and myeloid lineages, as well as lymphocyte functional biomarkers (**Supplemental Tables 2.1 and 2.2**). To compare leukocyte identity and density across histologically distinct areas in resected tissue, we analyzed intratumoral regions in all patient samples, and analyzed tumor adjacent stroma and tumor adjacent normal pancreas in all cases in which they were present (**Figure 2.1A**). Dense lymphoid-rich immune aggregates consistent with tertiary lymphoid structures were observed in 58% of cases and were also analyzed when present (**Figure 2.1A**).

Table 2.1 Baseline characteristics of 104 treatment-naïve patients with resected pancreatic adenocarcinoma

	Total	OHSU	DFCI	P*
Number of subjects	104	46	58	
Women, n (%)	57 (55%)	24 (52%)	33 (57%)	0.69
Age in years, median (Q1, Q3)	64.0 (56.0, 71.5)	63.5 (58.0, 71.0)	64.5 (54.0, 72.0)	0.97
Tumor location, n (%)				
Head/Uncinate	77 (74%)	36 (78%)	41 (71%)	<0.001
Body/Tail	21 (20%)	4 (9%)	17 (29%)	
Other/Unknown	6 (6%)	6 (13%)	-	
Tumor size in cm, median (Q1, Q3)**	3.0 (2.5, 4.0)	3.4 (2.5, 4.5)	3.0 (2.5, 3.5)	0.23
AJCC 8 th ed. pT stage, n (%)				
T1	11 (11%)	7 (15%)	4 (8%)	0.06
T2	62 (63%)	23 (50%)	39 (75%)	
T3	23 (24%)	15 (33%)	8 (15%)	
T4	2 (2%)	1 (2%)	1 (2%)	
Tx (cannot be assessed)	6	-	6	
AJCC 8 th ed. pN stage, n (%)				
N0	28 (27%)	12 (26%)	16 (27%)	0.64
N1	38 (36.5%)	15 (33%)	23 (40%)	
N2	38 (36.5%)	19 (41%)	19 (33%)	
Tumor differentiation, n (%)				
Well/Moderately differentiated	53 (52%)	23 (51%)	30 (54%)	0.84
Poorly differentiated/Undifferentiated	48 (48%)	22 (49%)	26 (46%)	
Unknown	3	1	2	
Resection margin status, n (%)				
R0	61 (59%)	38 (83%)	23 (40%)	<0.001
R1	40 (38%)	5 (11%)	35 (60%)	
R2	3 (3%)	3 (6%)	-	
Lymphovascular invasion, n (%)				
Negative	34 (43%)	7 (28%)	27 (50%)	0.09
Positive	45 (57%)	18 (72%)	27 (50%)	
Unknown	25	21	4	
Perineural invasion, n (%)				
Negative	12 (12%)	3 (7%)	9 (16%)	0.22
Positive	90 (88%)	42 (93%)	48 (84%)	
Unknown	2	1	1	
Adjuvant treatment, n (%)				
None	12 (11%)	5 (11%)	7 (12%)	0.50
Chemotherapy only	32 (31%)	17 (37%)	15 (26%)	
Radiation or chemoradiation only	10 (10%)	4 (9%)	6 (10%)	
Chemoradiation and chemotherapy	42 (40%)	15 (32%)	27 (47%)	
Other/Unknown	8 (8%)	5 (11%)	3 (5%)	
SMAD4, n (%)				
Lost	56 (54%)	29 (63%)	27 (47%)	0.11
Intact	48 (46%)	17 (37%)	31 (53%)	
KRAS, n (%)				
Wild-type	6 (8%)	0	6 (10%)	0.18
Mutant	74 (92%)	22 (100%)	52 (90%)	
Unknown	24	24	0	

Table continued on next page

Table 2.1 continued

	Total	OHSU	DFCI	P*
<i>TP53</i> , n (%)				0.19
Wild-type	28 (36%)	5 (23%)	23 (41%)	
Mutant	50 (64%)	17 (77%)	33 (59%)	
Unknown	26	24	2	
<i>CDKN2A</i> , n (%)				0.44
Wild-type	51 (65%)	16 (73%)	35 (62%)	
Mutant	27 (35%)	6 (27%)	21 (38%)	
Unknown	26	24	2	

Abbreviations: Q1, 25th percentile; Q3, 75th percentile; AJCC, American Joint Committee on Cancer. * *P* value for Fisher's exact test for categorical variables and Wilcoxon rank-sum test for continuous variables.

**Among 98/104 patients with available tumor size data

Table 2.2 Baseline characteristics of 13 neoadjuvant patients with resected pancreatic adenocarcinoma

	OHSU
Number of subjects	13
Women, n (%)	4 (31%)
Age in years, median (Q1, Q3)	61.0 (56.0, 69.0)
Tumor location, n (%)	
Head/Uncinate	9 (69%)
Body/Tail	2 (15%)
Other/Unknown	2 (15%)
Tumor size in cm, median (Q1, Q3)**	3.8 (2.9, 4.4)
AJCC 8 th ed. pT stage, n (%)	
T1	3 (27%)
T2	4 (36%)
T3	2 (18%)
T4	2 (18%)
Tx (cannot be assessed)	2
AJCC 8 th ed. pN stage, n (%)	
N0	7 (64%)
N1	2 (18%)
N2	2 (18%)
Nx (cannot be assessed)	2
Tumor differentiation, n (%)	
Well/Moderately differentiated	4 (31%)
Poorly differentiated/Undifferentiated	6 (46%)
Unknown	3 (23%)
Resection margin status, n (%)	
R0	9 (69%)
R1	2 (15%)
R2	2 (15%)
Lymphovascular invasion, n (%)	
Negative	5 (38%)
Positive	1 (1%)
Unknown	7 (54%)

Table continued on next page

Table 2.2 continued

	OHSU
Perineural invasion, n (%)	
Negative	0 (0%)
Positive	13 (100%)
Unknown	0
Neoadjuvant treatment, n (%)	
Chemotherapy only	7 (54%)
Radiation or chemoradiation only	1 (8%)
Chemoradiation and chemotherapy	4 (31%)
Other/Unknown	1 (8%)
Adjuvant treatment, n (%)	
None	6 (46%)
Chemotherapy only	5 (38%)
Radiation or chemoradiation only	0 (0%)
Chemoradiation and chemotherapy	0 (0%)
Other/Unknown	2 (15%)
SMAD4, n (%)	
Lost	7 (54%)
Intact	6 (46%)
KRAS, n (%)	
Wild-type	0
Mutant	9 (100%)
Unknown	4
TP53, n (%)	
Wild-type	3 (33%)
Mutant	6 (67%)
Unknown	4
CDKN2A, n (%)	
Wild-type	8 (89%)
Mutant	1 (11%)
Unknown	4

Abbreviations: Q1, 25th percentile; Q3, 75th percentile; AJCC, American Joint Committee on Cancer.

**Among 11/13 patients with available tumor size data

Intratumoral density of individual leukocyte populations, especially CD8⁺ T cells, has been associated with patient prognosis in PDAC and other malignancies [116, 122, 124, 129-131]. It is less clear, however, whether amount of total immune infiltrate in PDAC is similarly predictive of outcome as compared to evaluating infiltrating leukocyte subpopulations. To address this, we calculated cumulative cell density (cells/mm²) of all identified leukocyte subpopulations in each ROI type per patient to reflect overall leukocyte density per tissue compartment (**Figure 2.1B**). This evaluation revealed extensive heterogeneity in total leukocyte density across patients (**Figure 2.1B-C**), independent of institutional cohort (**Supplemental Figure 2.4A**). Comparison of tumor, tumor adjacent stroma, and adjacent normal pancreas from treatment-naïve cases revealed tumor adjacent stroma to have the highest leukocyte density (mean 913 cells/mm²), followed by tumor (mean 712 cells/mm²) (**Figure 2.1B**). Adjacent normal pancreas had comparatively fewer leukocytes than tumor and tumor adjacent stroma, but had notably enhanced overall density and changes in leukocyte composition as compared to cancer-free healthy pancreas resected from organ transplant donors (**Figure 2.1B, Supplemental Figure 2.4B-C**). These findings indicate that even ostensibly normal pancreas tissue adjacent to tumors is not spared from inflammation within the organ.

Intratumoral leukocyte density was strongly correlated to leukocyte density in tumor adjacent stroma in patient-matched samples (**Figure 2.1D**). However, leukocyte density in either compartment was not independently associated with overall survival or other evaluated clinical characteristics, including tumor stage and grade, perhaps indicating that

immune contexture is instead the critical stratification metric (**Figure 2.1E**, **Supplemental Figure 2.4D**, **Supplemental Table 2.3**).

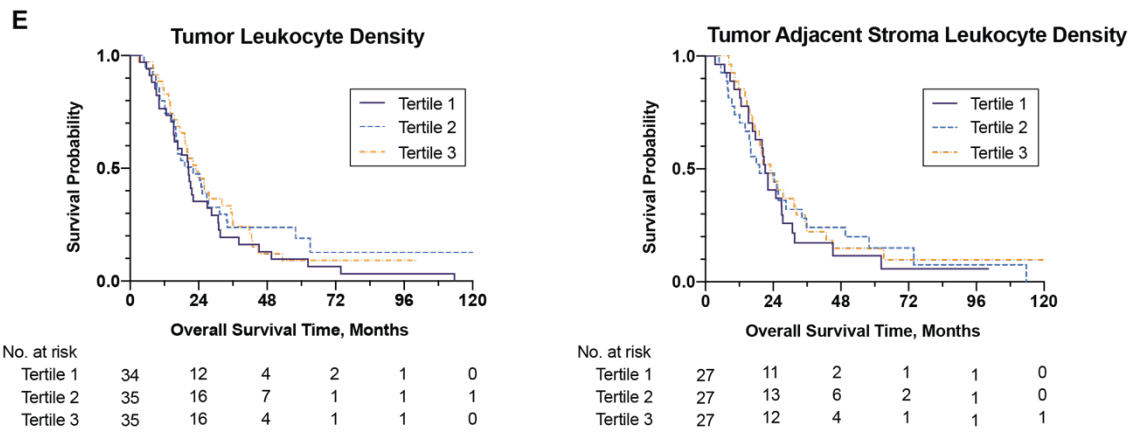
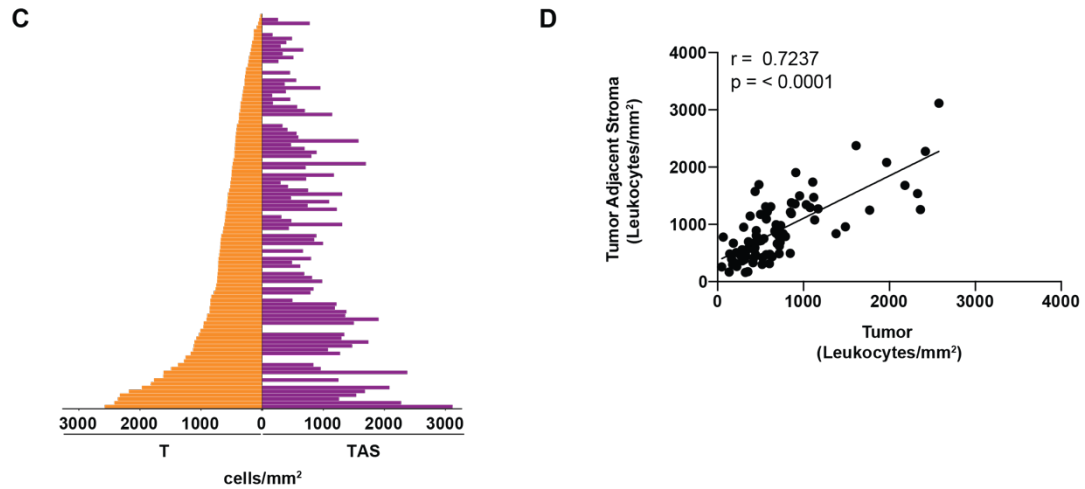
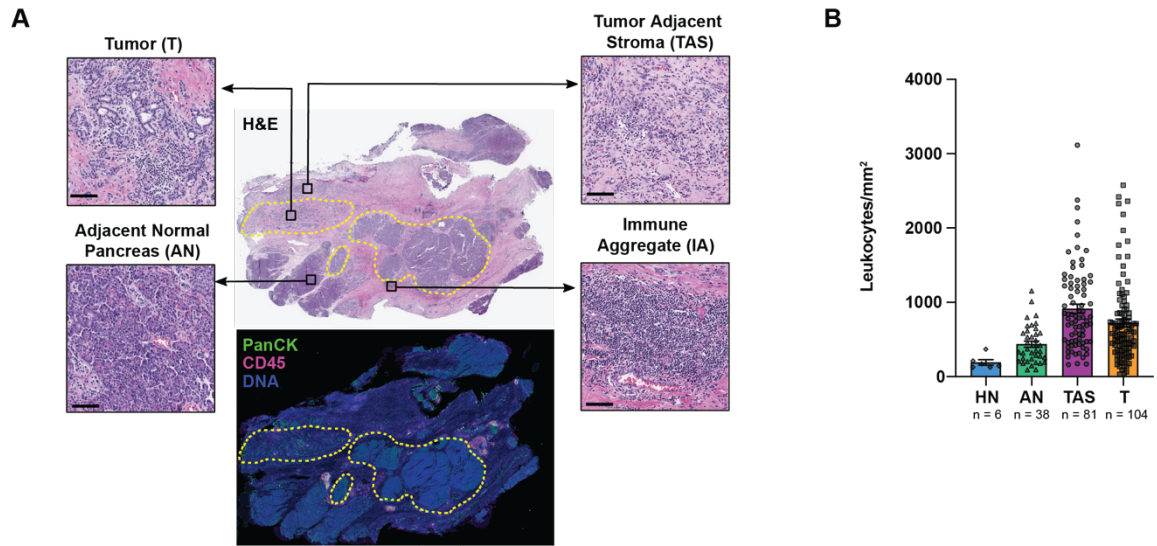


Figure 2.1 Treatment-naïve PDAC tumors and adjacent tissue exhibit heterogeneous leukocyte density. (A) Hematoxylin and eosin (H&E) stained PDAC tissue section indicating different tissue regions evaluated (top), with corresponding mIHC-stained tissue shown below in pseudocolor with CD45 (pink), pan-cytokeratin (green), and DNA (blue). Dotted yellow lines represent pathologist tumor annotations that were used to guide region selection. Scale bars equal 100 μm . (B) Total leukocyte density in healthy normal pancreas (HN, $n = 6$ patients), and from tumor adjacent normal pancreas (AN), tumor adjacent stroma (TAS), and tumor (T) from treatment-naïve PDAC cases. Data are displayed as mean \pm SEM. (C) Total leukocyte density in tumor (T, left, orange) juxtaposed to patient-matched tumor adjacent stroma (TAS, right, purple) sorted from low to high intratumoral leukocyte density (cells/ mm^2). (D) Spearman correlation of total leukocyte density in matched treatment-naïve T and TAS cases ($n = 81$ patients). (E) Kaplan-Meier analysis of treatment-naïve tumors (left) and tumor adjacent stroma (right) stratified by total leukocyte density. Tertiles were used as cutoff values for leukocyte density. Statistical significance was determined by log-rank test and $p \leq 0.05$ was considered significant.

Immune complexity and functional status are similar across distinct histopathological regions of PDAC resection specimens

To investigate parameters of leukocyte identity and heterogeneity in PDAC tissue sections in the treatment-naïve cohorts, we first determined whether there was evidence of preferential skewing toward either myeloid or lymphoid infiltrates in tumor, adjacent stroma, and/or adjacent “normal” pancreas, and revealed equivalent infiltration of both lineages within region types (**Figure 2.2A**). For deeper evaluation of immune topography (cell composition, functionality, and location), we identified 15 distinct leukocyte populations: CD8⁺ T cells, T helper cells (Th0, Th1, Th2, Th17), regulatory T cells (Tregs), CD20⁺ B cells, CD20⁻ plasmablasts and plasma cells, CD68⁺ CD163⁺ and CD68⁺ CD163⁻ cells (combined monocytes and macrophages), immature and mature dendritic cells (DCs), CD66b⁺ granulocytes (neutrophils and eosinophils), and mast cells (**Supplemental Table 2.2**).

All audited leukocyte populations were present within tumor, adjacent stroma, and adjacent normal tissue in varying proportions (**Figure 2.2B**). Densities of individual populations were similar between OHSU and DFCI treatment-naïve cohorts and was independent of tumor grade (**Supplemental Figure 2.5A-C**). Overall, proportional densities of individual populations were similar across adjacent normal pancreas, tumor adjacent stroma, and tumor, although granulocyte and monocyte/macrophage density was lowest in adjacent normal tissue, and CD8⁺ T cell and CD20⁺ cell densities were highest in adjacent stroma compared to tumor and adjacent normal (**Figure 2.2B-C**).

To understand the differentiation states of leukocyte populations in each histopathological region, we assessed CD68⁺ monocytes/macrophages for their expression of CD163, a hemoglobin scavenger receptor that is upregulated in myeloid cells with transcriptional programs consistent with Th2 inflammation and immunosuppression [132, 133]. CD163⁺ monocytes/macrophages were slightly more abundant than CD163⁻ monocytes/macrophages in all regions, consistent with potential immunosuppression (**Figure 2.2B**). Next, DC maturation status was determined based on positive or negative expression of DC-LAMP, a lysosomal glycoprotein involved in antigen processing that is almost exclusively expressed by mature DCs [134]. Immature (HLA-DP⁺ DC-LAMP⁻) DCs were significantly enriched in tumor, stroma, and adjacent normal tissue as compared to mature DC-LAMP⁺ DCs (**Figure 2.2B**). CD20⁺ B cell densities in all regions were higher than CD20⁻ immunoglobulin (Ig)-producing plasmablasts and plasma cells, indicating that the majority of B cells in and adjacent to tumor are not engaged in antibody-mediated responses. Within the T cell compartment, we delineated differentiation status of CD3⁺ CD8⁻ T cells based on positivity of canonical transcription factors (T-bet, GATA-3, RORγt, Foxp3), and found that of these T cell populations, Foxp3⁺ regulatory T cells (Tregs), Th2 helper cells, and Th0 helper cells were most abundant in tumor, adjacent stroma, and adjacent normal tissues (**Figure 2.2B**). Th0 cells are non-polarized T cells that have not differentiated into Th1, Th2, Th17, or Tregs [135]. Notably, the Th0 fraction represented here may include additional T cell subpopulations, including innate αβ T cells and γδ T cells, that could not be specifically identified with the biomarkers in our staining panels. Both innate αβ and γδ T cell subpopulations have been reported in human PDAC and were shown in preclinical

murine models of PDAC to have CD8⁺ T cell activating or suppressive function, respectively [136, 137]. These studies revealed that $\gamma\delta$ T cells comprise 40% of all CD3⁺ T cells in human PDAC [137], indicating their likely inclusion in the “Th0” population we have detected.

Collectively, our assessment of population densities and differentiation states indicates that tumor, adjacent stroma, and adjacent normal regions do not, on the basis of cell type, possess distinct immune microenvironments but instead share characteristic features of protumoral inflammation. Tumor resection specimens also enabled evaluation of lymphocytic immune aggregates, which were present in over half of treatment-naïve cases (**Figure 2.2B**). Other have previously reported lymphoid aggregates in treatment-naïve and neoadjuvant-treated PDAC resection specimens, where they were found to closely resemble lymphoid follicles in secondary lymphoid organs and were correlated with improved patient outcome [138, 139]. As anticipated, immune aggregates had the highest leukocyte density of all region types we evaluated and were primarily comprised of CD20⁺ B cells and CD3⁺ T cells. CD8⁺ T cells and Th0 helper T cells were most abundant within the T cell compartment of IAs (mean 1871 cells/mm² and 1527 cells/mm², respectively), and Th1 helper T cells, Th2 helper T cells, and regulatory T cells (Tregs) were present at lower relative densities. Mature DCs were also identified in IAs, consistent with other reports and indicative of the potential role of IAs as sites of intra- or peri-tumoral antigen presentation and T cell priming [138].

Given the heterogeneity we observed in total leukocyte density across patients in each of the tissue compartments (**Figure 2.1B-C**), we evaluated correlations between subpopulation densities and total leukocyte density to determine if any cell populations were preferentially enriched in tumors with highest overall inflammation. CD8⁺ T cells, Th0 T cells, and Tregs had the top three positive correlations with overall leukocyte density in tumor and adjacent stroma (**Supplemental Figure 2.7A**). High CD68⁺ monocyte/macrophage cell density is associated with poor survival outcomes in several solid tumor types, and low ratios of CD8⁺T cells to CD68⁺ cells are also linked to reduced survival [116, 140, 141]. Evaluation of intratumoral CD68⁺ cells revealed a moderate correlation with total leukocyte density and low correlation with CD8⁺ T cells in the treatment naïve cohorts, indicating that CD68⁺ density remains relatively consistent across hypo- and hyper-inflamed tumors and is not strongly associated with CD8⁺ T cell abundance (**Supplemental Figure 2.7B-C**).

Next, we sought to address degree of inpatient immune heterogeneity across region types. Clinical diagnostics and prospective patient stratification for cancer therapy often rely on biopsy tissue from a small area of tumor. Understanding how representative a biopsy core may be of the whole tumor immune landscape is therefore clinically relevant. A recent report demonstrated high variability in tumor-infiltrating lymphocyte density across multiple PDAC biopsies from the same patient [142]. Consistent with this finding, we observed a variable degree of inpatient immune heterogeneity in the subset of cases evaluated, with some patients exhibiting strong similarity in immune composition across ROIs from the same tissue compartment and others having high discordance between

ROIs (**Supplemental Figure 2.6**). These data affirm that a single ROI may not be reliably representative of the entire tissue compartment from which it is captured.

In addition to cellular abundance and population heterogeneity across distinct tissue regions, we next asked whether T cell functional status differed regionally, as T cell functionality is critically important for biomarker discovery and patient stratification in the context of emerging immunotherapies designed to impact T cell responses. We assessed frequency of CD3⁺ CD8⁻ T cells positive for programmed cell death protein 1 (PD-1) and inducible T cell co-stimulator (ICOS), both indicators of T cell activation, as well as the cell proliferation marker Ki67 (**Figure 2.2D**). We also assessed PD-1 and Ki67 positivity on CD3⁺ CD8⁺ T cells, as well as granzyme B (Gzmb) to interrogate cytolytic capacity (**Figure 2.2E**). Frequencies of T cells positive for these markers was similar across all tissue compartments. Notably, we observed fewer than 10% of CD3⁺ CD8⁻ cells in any of the tissue compartments that were positive for PD-1 or ICOS, and similar frequencies of PD-1 positivity were found in CD3⁺ CD8⁺ T cells (**Figure 2.2D-E**), indicating that the majority of T cells in and surrounding the tumor were potentially antigen inexperienced or had not been recently activated [143]. This was supported by equally low percentages of Ki67⁺ proliferative T cells or CD8⁺ T cells positive for granzyme B (**Figure 2.2E**). Further assessment of dual expression of PD-1 and eomesodermin (EOMES) on CD8⁺ T cells revealed that a substantial proportion of cells (28-41%) were PD-1⁻ EOMES⁺, consistent with a late effector phenotype (**Figure 2.2F**).

Finally, we interrogated CD20⁺ B cell characteristics in each tissue compartment using select differentiation and functional biomarkers and revealed that, with the exception of adjacent normal pancreas, all tissue compartments were dominated by CD27⁻ immunoglobulin (Ig)D⁻ B cells (**Figure 2.2G**). The precise function of CD27⁻ IgD⁻ B cells is unclear, as this population likely comprises a heterogeneous mix of precursor memory and other B cell subtypes; however, numerous studies have reported this B cell fraction potentially includes functionally exhausted B cells with reduced antigen presentation capacity [144, 145]. Normal adjacent pancreas contained a higher density of CD27⁻ IgD⁺ non-class switched antigen inexperienced cells than any other region, whereas B cells were pre-dominantly antigen experienced in tumor, adjacent stroma, and immune aggregates (**Figure 2.2G**).

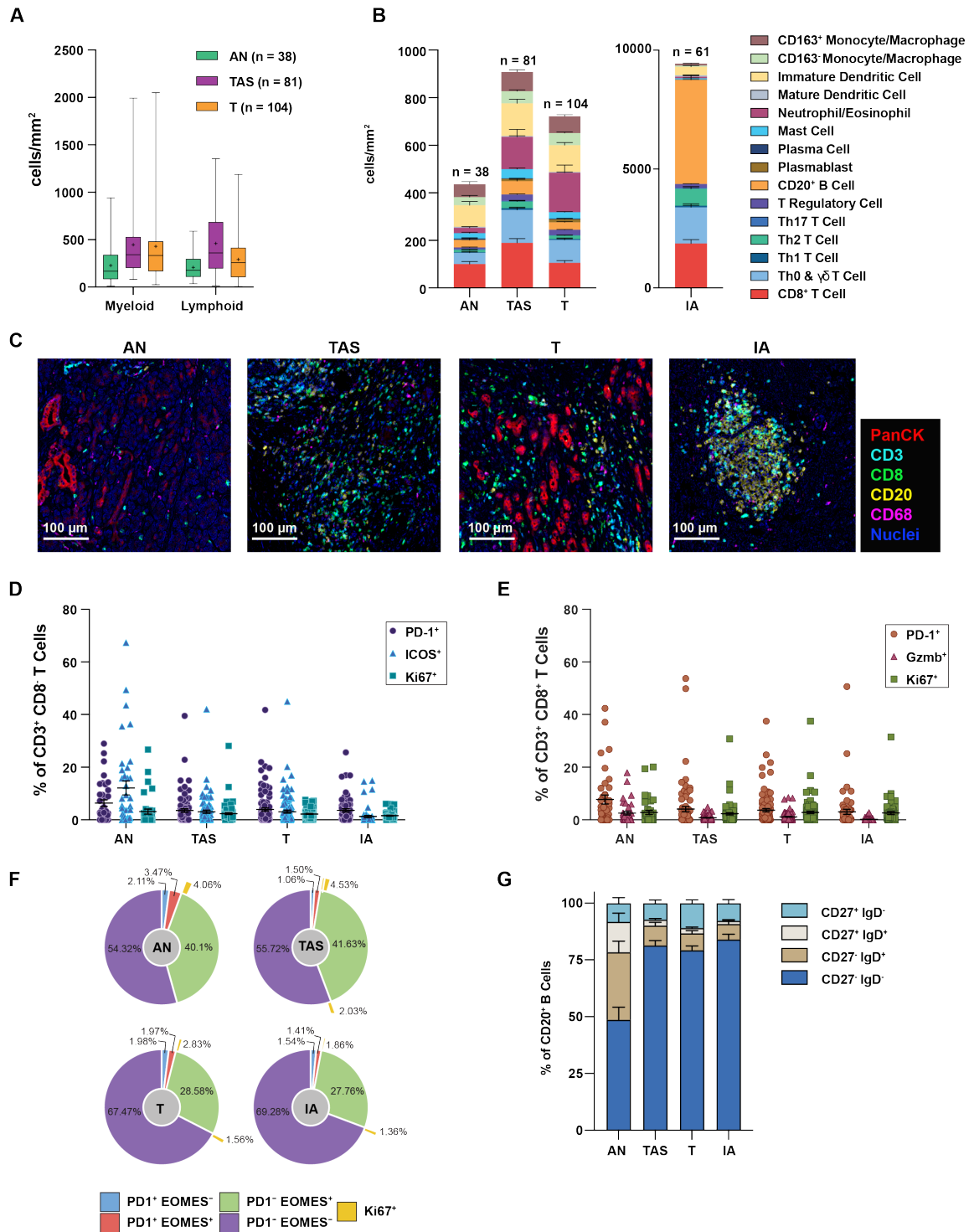


Figure 2.2 Immune complexity in distinct histological regions of PDAC (A) Myeloid and lymphoid cell densities in treatment-naïve tumor adjacent normal pancreas (AN, n = 38 patients), tumor adjacent stroma (TAS, n = 81 patients), and tumor (T, n = 104 patients). Bars, boxes, and whiskers represent median, interquartile range, and range, respectively. Means are indicated by + symbols. See Supplemental Table 2.2 for list of cell populations included in myeloid and lymphoid categories. (B) Detailed immune complexity of samples shown in (A), with the addition of immune aggregates (IA, n = 61 patients). Data are shown as mean \pm SEM. (C) Representative pseudocolored images of select immune populations from each of the tissue regions shown in (B). (D) Percentage of CD3⁺ CD8⁺ T cells positive for PD-1, ICOS, or Ki67 from samples shown in (A). (E) Percentage of CD3⁺ CD8⁺ T cells positive for PD-1, Granzyme B (Gzmb), or Ki67 from samples shown in (A). Each data point represents one patient. Data are displayed as mean \pm SEM. (F) Sunburst graphs representing percentage of CD3⁺ CD8⁺ T cells positive for PD-1, EOMES, and/or Ki67 in the indicated regions from samples evaluated in (B-D). (G) Frequency of CD27 and IgD positive cells as percentage of CD20⁺ B Cells in the indicated tissue compartments from samples shown in (A). Data are shown as mean \pm SEM.

Immune contexture is dynamic based on proximity to tumor

Spatial proximity of immune cells to invasive tumor has been demonstrated to have prognostic significance in solid malignancies [119, 121, 146]. CD8⁺ T cells have been a focus of many recent studies designed to interrogate immune topography within tumors; indeed, a recent report comparing density of CD8⁺ T cells at the tumor center versus tumor margin of surgically resected PDACs revealed differential prognostic value depending on where T cells were localized [124]. Extending this concept beyond CD8⁺ T cells alone, we hypothesized that immune milieu may differ based upon their proximity to tumor. To evaluate this, tumor adjacent stroma, adjacent normal, and immune aggregate ROIs were categorized as either “border”, “spanning border-distal”, or “distal” based upon individual ROI proximity to tumor (see Methods for detail). We generated spatial maps of tumor, border, spanning, and distal areas by averaging immune densities from all ROI types from all patients in each of these regions. Because immune aggregates have high lymphocyte abundance that would substantially skew readouts of relative cell density when simultaneously evaluating different tissue compartments, we analyzed these data both with and without immune aggregates to better appreciate their contribution to the PDAC immune landscape.

Assessment of these spatial categories without immune aggregates in treatment-naïve specimens revealed that respective densities of monocytes/macrophages, mast cells, Tregs, Th1 cells, Th2 cells, Th17 cells, plasma cells, plasmablasts, and mature DCs were relatively constant across spatial categories, including intratumoral regions (**Figure 2.3A**). Granulocytes (neutrophils and eosinophils), immature DCs, CD8⁺ T cells, and

CD20⁺ B cells exhibited greater dynamics in cell density across spatial locations (**Figure 2.3A**). Granulocytes were the densest immune population in intratumoral areas, while CD8⁺ T cells, immature DCs, and Th0/γδ T cells were the most abundant populations in all spatial areas outside of tumor. This result indicates possible exclusion of CD8⁺ T cells and immature DCs from tumor-enriched areas. Addition of immune aggregates to this analysis resulted in CD20⁺ B cell density shifting to become the highest in all spatial categories, particularly in border regions in which immune aggregates comprised over 50% of analyzed ROIs (**Figure 2.3B**).

We hypothesized that neoadjuvant therapy could potentially alter immune composition and immune spatial distribution in comparison to treatment-naïve cases, as previously described [140, 147, 148] (**Figure 2.3C-D**). We thus evaluated a small cohort of surgical resection specimens from PDAC patients that had been treated with chemotherapy and/or chemoradiation prior to surgery (**Table 2.2**). Leukocyte populations that exhibited consistent densities across spatial categories in the treatment-naïve cases had similar trends in neoadjuvant specimens (**Figure 2.2A, C**). Similar to treatment-naïve specimens, granulocytes also represented the highest density leukocyte population within neoadjuvant intratumoral regions, and we again observed enrichment of immature DCs and CD8⁺ T cells at tumor borders as compared to intratumoral areas (**Figure 2.3C**). In contrast to treatment-naïve cases, CD163⁺ monocytes/macrophages were highly enriched in all spatial categories of neoadjuvant samples, including intratumoral areas, which could indicate Th2-skewed transcriptional programming elicited in response to cytotoxic therapy, consistent with prior reports revealing increased myeloid cell recruitment

following neoadjuvant treatment [140, 148]. While Th2 responses are critical for normal wound healing and inflammatory resolution [132], chronic inflammation within the tumor microenvironment and persistence of these Th2-skewed myeloid populations also correlates with enhanced T cell suppression [103].

When immune aggregates were evaluated in neoadjuvant specimens, we again observed high densities of CD20⁺ B cells in all locations; however, granulocytes remained the highest density population in intratumoral areas, perhaps due to fewer intratumoral immune aggregates in neoadjuvant specimens as compared to treatment-naïve.

Collectively, these spatial maps reveal that overall immune contexture differs based on proximity to tumor and that immune spatial dynamics are altered in the context of neoadjuvant therapy as compared to untreated tumor resections.

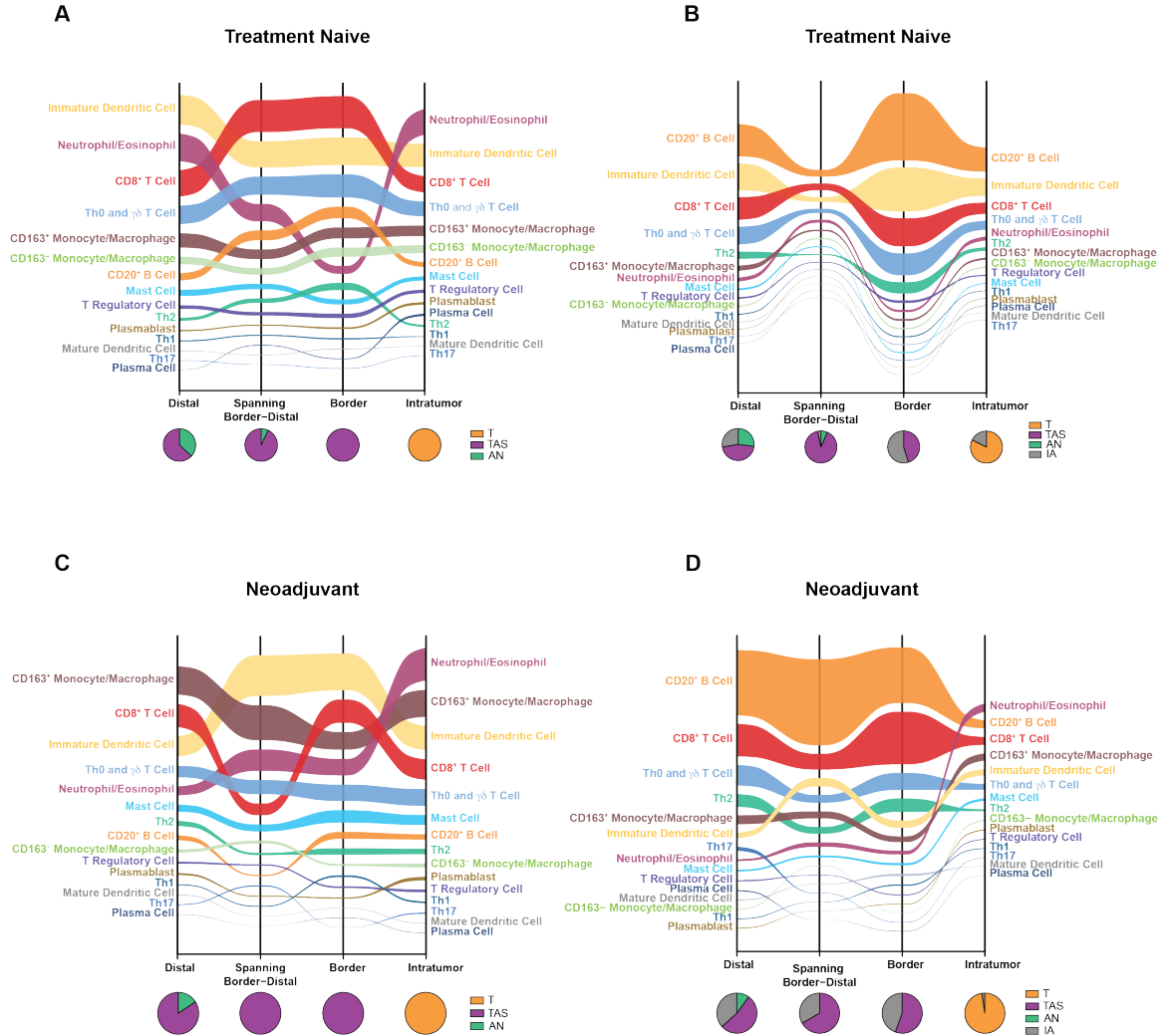


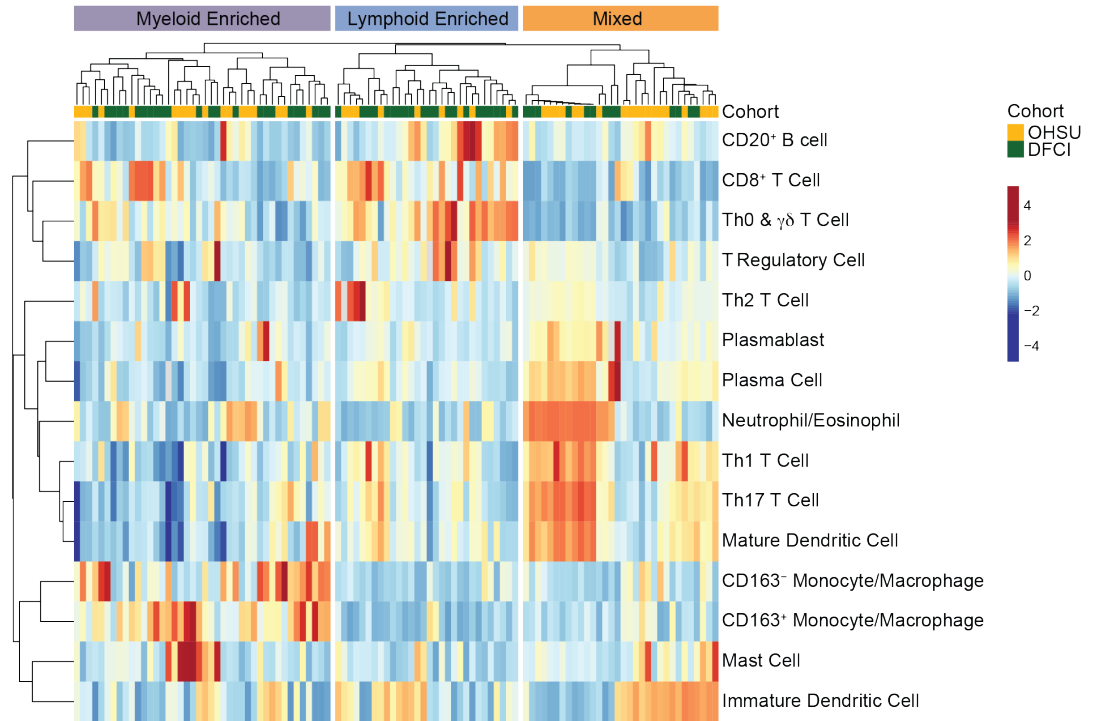
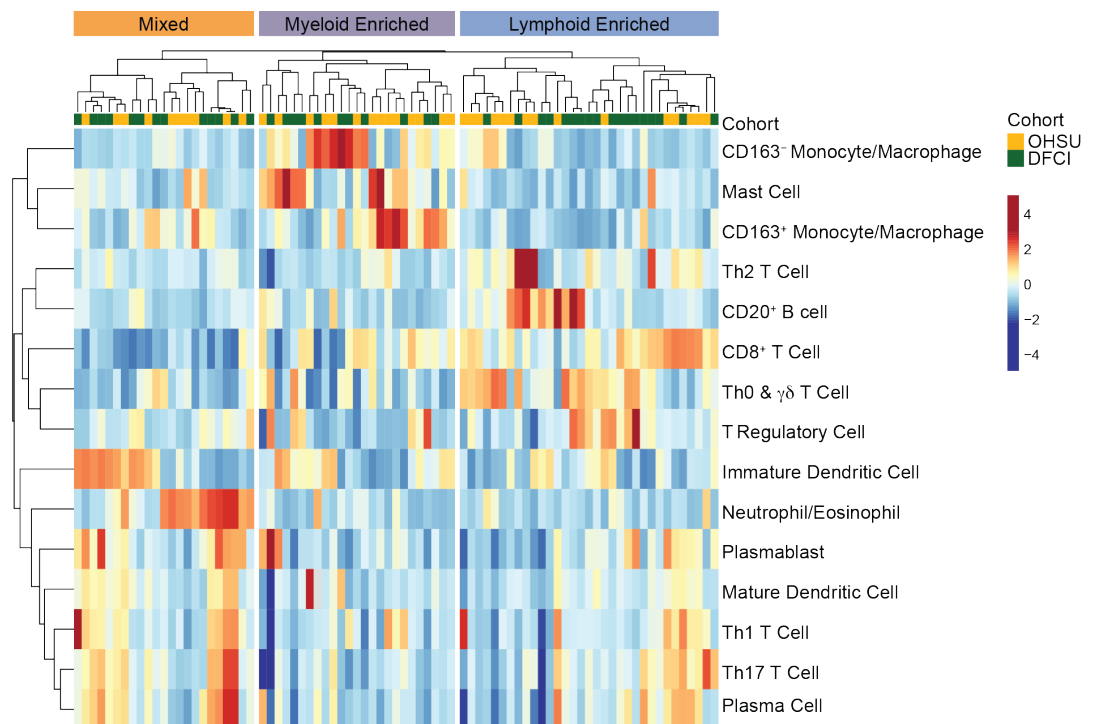
Figure 2.3 Spatial heterogeneity of leukocytes. Sankey flow diagram representing indicated leukocyte populations sorted from highest to lowest density, where line width is scaled to cell density across four spatial categories based on proximity to tumor (see Methods). Pie charts represent relative contribution of cell densities from different tissue compartments (T = tumor, TAS = tumor adjacent stroma, AN = adjacent normal pancreas, IA = immune aggregate) within each spatial category. Number of ROIs represented in diagrams is listed in Supplemental Table 2.4 (A) Data from treatment-naïve cases shown without IAs and (B) with IAs included. (C) Data from neoadjuvant cases shown without IAs and (D) with IAs.

Unsupervised clustering reveals distinct immune subtypes in treatment-naïve PDAC specimens

Previous mIHC analysis of PDACs from patients who received neoadjuvant GVAX, a granulocyte-macrophage colony-stimulating factor (GM-CSF) tumor cell vaccine, revealed that tumors clustered into two subtypes: high-myeloid inflamed and low-myeloid inflamed [116]. High myeloid inflammation was associated with significantly shorter overall survival, while low-myeloid clustered tumors had improved outcome [116]. To determine whether treatment-naïve tumors also clustered into prognostically-relevant groups that inform patient stratification, we performed unsupervised hierarchical clustering of leukocyte populations in tumor regions. Clustering revealed three broad immune phenotypes: myeloid-enriched, lymphoid-enriched, and a mixed population relatively enriched for a combination of lymphocyte and myeloid cell types (**Figure 2.4A**). Myeloid enriched tumors were relatively highest in CD163⁺ and CD163⁻ monocytes/macrophages and mast cells. Lymphoid enriched tumors were characterized by relative enrichment in CD20⁺ B cells, CD8⁺ T cells, Th0 and $\gamma\delta$ T cells, and Tregs. Mixed tumors tended to be relatively enriched for immune populations that were not enriched in the other two clusters, including neutrophils/eosinophils, mature DCs, plasma cells, and several T helper cell types. Treatment-naïve tumor adjacent stroma clustered into similar groups as compared to tumor, again demonstrating consistency in immune contexture between tumor and stroma (**Figure 2.4B**).

Since the lymphoid enriched clusters exhibited relative enrichment in T cell populations determined to be most highly correlated with overall leukocyte density (**Supplemental**

Figure 2.7A), we asked whether clusters were associated with different levels of total immune infiltrate. Although mixed clusters in both tumor and stroma had the highest overall leukocyte density, differences were not statistically significant (**Figure 2.4C**). We also evaluated whether tumor clusters differentially correlated with clinical tumor characteristics and found that there were no significant relationships between cluster and tumor stage, lymph node status, tumor differentiation, or lymphovascular invasion (**Supplemental Table 2.5**). Finally, we evaluated association of tumor and stroma clusters with overall survival and observed no significant differences in outcome based on cluster group (**Figure 2.4D**). It is possible that this lack of prognostic significance is partially attributable to immune heterogeneity within clusters, since within each cluster, differentially enriched subgroups were apparent (**Figure 2.4A-B**). These subgroups may have different survival outcomes, but sample size in this cohort was insufficiently powered for deep assessment.

A**B**

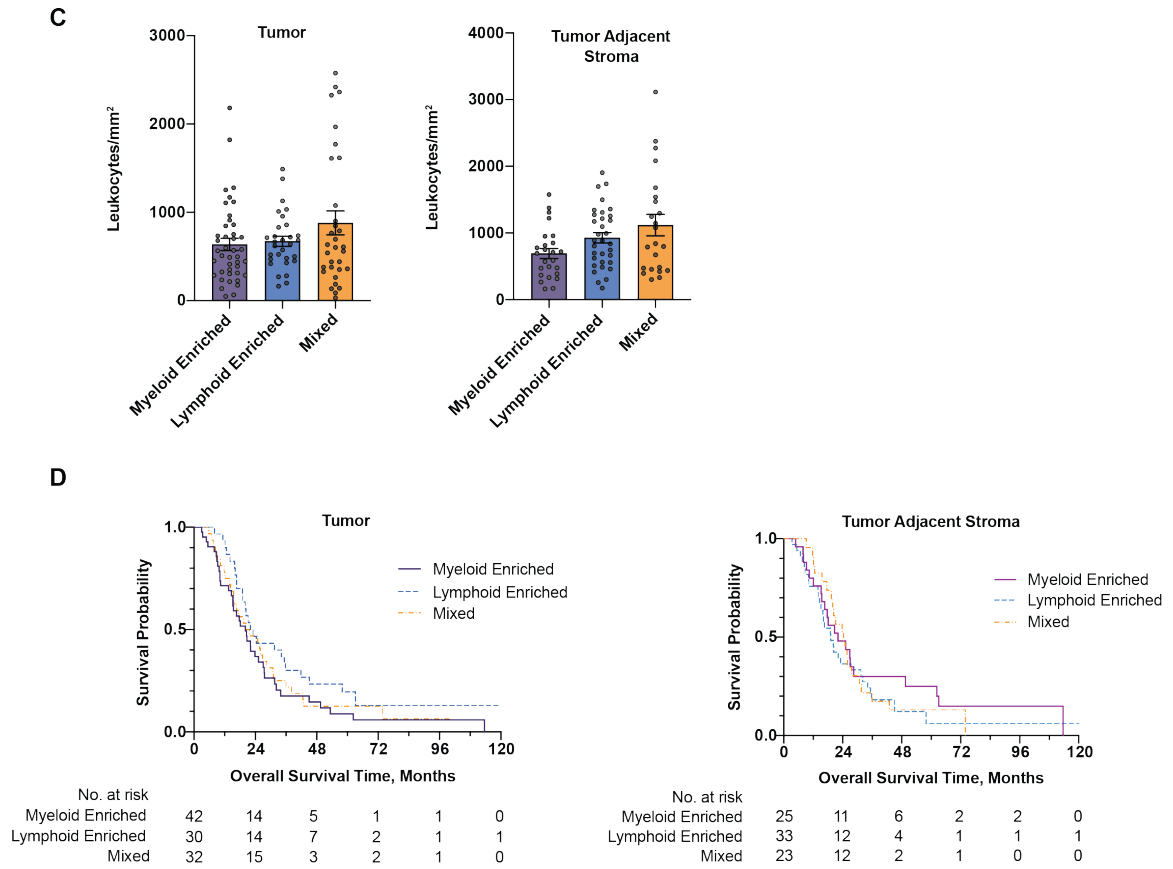


Figure 2.4 Unsupervised clustering of treatment-naïve PDACs based on immune complexity. Cell densities of 15 immune populations in **(A)** PDACs ($n = 104$ patients) and **(B)** tumor adjacent stroma ($n = 81$ patients) evaluated by unsupervised hierarchical clustering. Heatmap clusters were generated using the Pheatmap library in R software with correlation distance and average linkage. Data was patient scaled and population z-scored for visualization. Each column reflects data from one patient sample. Sample cohort is indicated in either yellow (OHSU) or green (DFCI) **(C)** Overall leukocyte density in clusters identified in **(A)** and **(B)** from tumor (left) and tumor adjacent stroma (right). Statistical significance was determined by Kruskal-Wallis test **(D)** Kaplan-Meier curves of overall survival of patients stratified by tumor cluster (left) or tumor adjacent stroma cluster (right).

Association Between Tumor Mutational Status and Immune Contexture

There is growing appreciation for the role of tumor cell intrinsic features, including genomic alterations, in shaping the tumor immune microenvironment [149]. PDACs harbor a series of common genomic alterations that are temporally associated with disease progression. Activating mutations in *KRAS* are found in nearly all PDACs and occur at the earliest stages of pre-invasive neoplasia. Alteration in the tumor suppressor *CDKN2A* also occurs in early neoplasia in > 60% of cases, whereas inactivation of *TP53* and *SMAD4* occur in late-stage progression to invasive disease in approximately 70% and 50% of cases, respectively [73]. Smad4 is a critical downstream mediator of TGF- β signaling, and its loss in PDAC has been associated with poorer disease-free and overall survival [150-154]. In addition, others have reported correlations between somatic loss of Smad4 in tumor epithelium and enhanced recruitment of immunosuppressive myeloid cells to the tumor microenvironment of other solid tumors [155]. We thus hypothesized that tumors lacking Smad4 in our cohort may show similar evidence of myeloid-mediated immunosuppression in the form of increased CD163⁺ monocyte/macrophage and/or neutrophil density that is correlated with patient survival.

Smad4 status of patients in treatment naïve cohorts were determined by IHC based on loss of Smad4 protein in neoplastic epithelium (**Figure 2.5A** and Methods). 54% of cases were classified as Smad4 negative, and univariate survival analysis revealed that Smad4 loss was significantly associated with shorter overall survival in the combined DFCI and OHSU cohort (**Figure 2.5B**). Assessment of total leukocyte density in Smad4 positive versus Smad4 negative tumors and adjacent stroma revealed that overall abundance of

immune cells was Smad4-independent (**Figure 2.5C**). We next stratified immune complexity based on Smad4 status and, in contrast to our initial hypothesis, we found that densities of all leukocyte populations were equivalent in tumor and adjacent stroma in Smad4 positive and Smad4 negative cases (**Figure 2.5D**). Since there was no evidence of Smad4 regulating immune complexity, we expanded our investigation to additional genomic alterations in a subset of treatment-naïve cases for which molecular status of *KRAS*, *CDK2NA*, and *TP53* was known. We first compared cases based solely on *KRAS* status and found that while overall leukocyte density was comparable between wild-type and mutant tumors, mutant tumors exhibited increases in intratumoral neutrophils and CD163⁺ monocytes/macrophage density, and decreases in immature DCs (**Figure 2.5E**, left panel). Incorporation of *TP53* status into this analysis revealed highly dynamic immune complexities based on mutational combinations (**Figure 2.5E**, middle panel). In particular, cases that harbor wild-type *KRAS* and mutant *TP53* exhibited ~50% reduction in overall immune infiltrate as compared to cases without alterations in either gene; however, sample size in this comparison was very low. Comparison of *KRAS* mutant tumors without or without *TP53* mutations revealed further differences in immune complexity. Total leukocyte density in *KRAS* mutant/*TP53* mutant tumors was substantially higher than observed in *KRAS* mutant/*TP53* wild-type cases, and this increased leukocyte density correlated with a striking increase in intratumoral neutrophils (**Figure 2.5E**, middle panel). These differences were still evident even with the addition of Smad4 status (**Figure 2.5E**, right panel) and indicate that while Smad4 does not appear to impact immune complexity of PDACs, alterations in *TP53* *do* correspond with altered immune infiltrate as compared to *TP53* wild-type tumors. This is consistent with recent

studies in murine models of PDAC and mammary carcinoma wherein loss of *TP53* was associated with neutrophil influx into tumors [156, 157]. Comparison of T cell functionality in *KRAS* mutant/*TP53* wild-type versus *KRAS* mutant/*TP53* wild-type is ongoing and will result in greater insight into how *TP53* alterations influence the immune microenvironment and what the functional consequences of this may be.

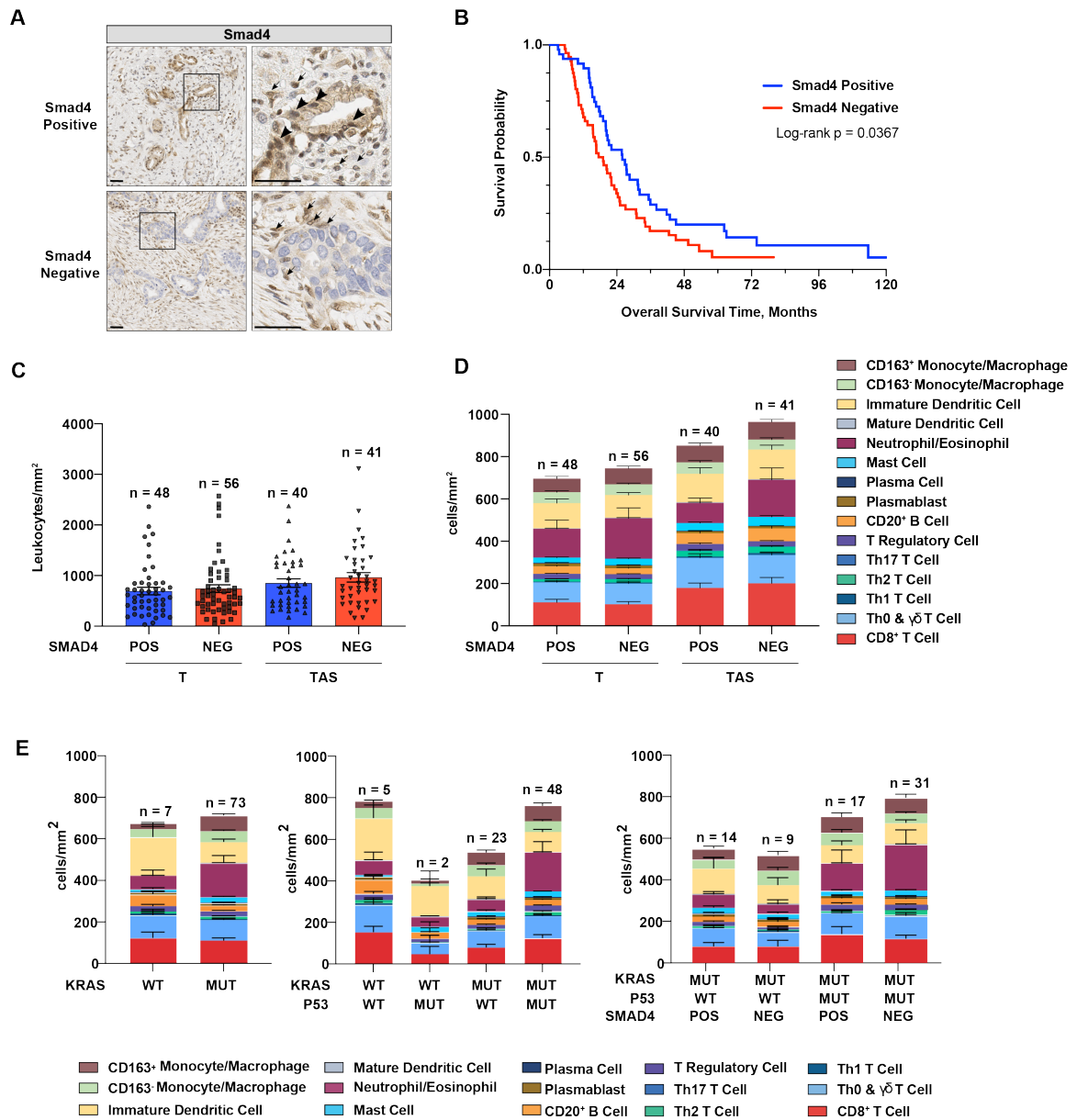


Figure 2.5 Association between immune complexity and common genomic alterations in PDAC. (A) Representative IHC of Smad4 positive (top) and Smad4 negative (bottom) PDACs. Arrowheads indicate Smad4 positive tumors cells; arrows indicate Smad4 positive stromal. Boxes on left are shown at higher magnification on right. Scale bars equal 50 μ m. **(B)** Kaplan-Meier curve of overall survival in all treatment-naïve cases ($n = 104$ patients) stratified by Smad4 status. Statistical significance was determined by log-rank test and $p \leq 0.05$ was considered significant. **(C)** Total leukocyte density in Smad4 positive and Smad4 negative tumor (T) and tumor adjacent stroma (TAS). **(D)** Immune composition of data shown in (C). **(E)** Immune complexity of tumors based on KRAS genomic status (left), by KRAS in combination with TP53 (middle), and by combinations of KRAS, TP53, and Smad4 (right). WT = wild-type, MUT = mutated, POS = positive, NEG = negative. Data are displayed as mean \pm SEM.

Short-term and long-term survivors exhibit different leukocyte composition

A recent report comparing exceptionally long-term PDAC survivors (6-year median overall survival) and short-term survivors (0.8 month median overall survival) revealed increased cytolytic CD8⁺ T cells and greater abundance of high-quality neoantigens in long-term survivors, consistent with enhanced tumor immunogenicity [131]. No individual leukocyte populations we evaluated by mIHC, including CD8⁺ T cells, were significantly associated with overall survival in treatment-naïve PDACs when assessed by univariate analysis (data not shown), but we hypothesized that stratifying patients by survival and examining only those with best and worst outcomes might more clearly reveal different immune landscapes that associate with patient prognosis. We stratified patients into short-term and long-term survivors by dividing all treatment-naïve cases into quartiles and evaluating lower quartile (short-term survivors) and upper quartile (long-term survivors) for leukocyte complexity. Long-term survivors (n = 26) had an overall median survival of 5.2 years, and short-term survivors (n = 25) had an overall median survival of 0.8 months (**Figure 2.6A**). Evaluation of leukocyte composition in short-term versus long-term survivors revealed slightly higher total leukocyte density in tumor and adjacent stroma of long-term survivors (**Figure 2.6B-C**). Further, we observed trending increases in CD8⁺ T cell and trending decreases in total CD68⁺ monocytes/macrophages in tumor and stroma of long-term survivors (**Figure 2.6C-D**). Notably, the ratio of CD8⁺ T cells to CD68⁺ monocytes/macrophages was significantly elevated in tumors of long-term survivors, with a similar trend in tumor adjacent stroma (**Figure 2.6C**). We did not observe significant increases in intratumoral mature DCs in long-term survivors, as previously reported by others [131], but immature DCs exhibited a trending increase

(**Supplemental Figure 2.8A**). Densities of other leukocyte populations were similar between short-term and long-term survivors (**Supplemental Figure 2.8A-C**).

We next evaluated whether T cell functionality in tumor and adjacent stroma differed between short-term and long-term survivors. Evaluation of CD3⁺ CD8⁺ T cells positive for either PD-1, ICOS, or Ki67 revealed comparable levels of cellular activation and proliferation in both groups (**Supplemental Figure 2.9A**). Frequencies of CD3⁺ CD8⁺ T cells single-positive for PD-1, granzyme B, and Ki67 were also equivalent between short-term and long-term survivors (**Supplemental Figure 2.9A**). Short-term and long-term survivors each had low frequency (< 3.0%) of PD-1⁺ EOMES⁺ CD8⁺ T cells, which are associated with dysfunction/exhaustion [158], but a slightly increased proportion of PD-1⁺ EOMES⁺ CD8⁺ T late effector cells were present in long-term survivors (**Supplemental 2.9B**). Together these data reveal modest but compelling differences in leukocyte complexity in treatment-naïve patients with different survival outcomes, and confirm that high ratio of CD8⁺ T cells to CD68⁺ monocytes/macrophages is associated with improved outcome, as has been reported in other solid tumors [140].

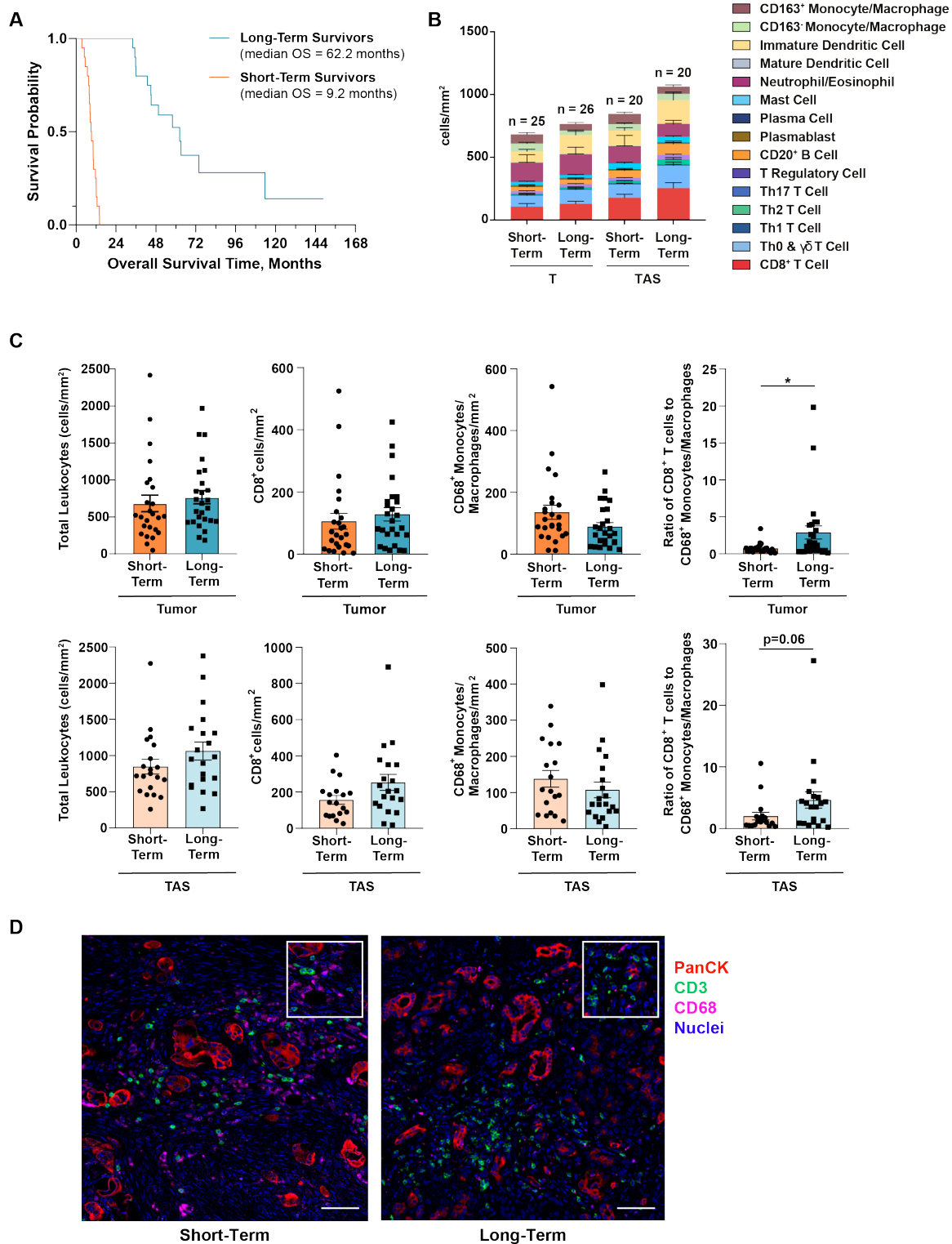


Figure 2.6 Short-term and long-term survivors differ in leukocyte composition. (A) Kaplan-Meier curve of short-term survivors (n = 25 patients) versus long-term survivors (n = 26 patients) from the treatment-naïve cohorts. Short-term survivors were defined as patients whose overall survival was within the first quartile of all treatment-naïve cases evaluated from OHSU and DFCI, and long-term survivors were defined as patients whose overall survival was within the 4th quartile. (B) Immune complexity of tumor (T) and tumor adjacent stroma (TAS) in short-term and long-term survivors. (C) Cell densities of total leukocytes, CD8⁺ T cells, CD68⁺ monocytes/macrophages, and ratio of CD8⁺ T cells to CD68⁺ monocytes/macrophages in tumor and tumor adjacent stroma). Statistical significance was determined by two-tailed, unpaired Mann-Whitney U test. * p < 0.05. Data are displayed as mean ± SEM. (D) Representative pseudocolored images of tumor from short-term (left) and long-term (right) survivors. Scale bars equals 50 µm.

Neoadjuvant therapy effects on the PDAC immune microenvironment

Only 15% of PDAC patients are eligible for surgical resection at time of diagnosis due to presence of locally advanced and/or metastatic disease [60]. Neoadjuvant chemotherapy and/or radiotherapy affords an opportunity to attempt down-staging of locally advanced or borderline resectable PDACs to resectable tumors. Recent early-phase clinical trials have demonstrated improved margin-negative (R0) resection rates and improved survival outcome following neoadjuvant therapy in borderline-resectable cases [159, 160]. It is not fully understood, however, how neoadjuvant cytotoxic therapy impacts the immune microenvironment of PDAC. Based on our earlier observations from this study indicating that neoadjuvant therapy leads to enrichment in CD163⁺ monocytes/macrophages (**Figure 2.3**), we chose to profile these samples (n = 13) more deeply with regards to leukocyte functionality and survival outcome.

Consistent with earlier data, specimens from patients that received neoadjuvant treatment revealed higher myeloid densities as compared to lymphoid densities in tumor and tumor adjacent stroma (**Figure 2.7A**). Further, total leukocyte density was slightly reduced in neoadjuvant tumors as compared to treatment-naïve tumors, and this trend was even more pronounced in tumor adjacent stroma (**Figure 2.7B**). Although size of our neoadjuvant cohort was substantially smaller than the treatment-naïve cohorts, we were interested to determine if there were trending associations with particular leukocyte populations and overall survival in the neoadjuvant cohort. Assessment of overall survival based on CD8⁺ T cell density revealed a non-significant but notable trend in improved survival of patients with high intratumoral CD8⁺ T cell density (**Figure 2.7C**). Neoadjuvant patients

with high intratumoral CD8⁺ T cell/CD68⁺ cell ratios exhibited a similar trend (**Figure 2.7C**). Interestingly, these trends were not apparent when we evaluated tumor adjacent stroma from the same patients.

Functional interrogation of CD3⁺ CD8⁻ and CD3⁺CD8⁺ T cells revealed similarities between tumor and tumor adjacent stroma (**Figure 2.7D**). We did observe an increased proportion of late effector (PD-1⁻ EOMES⁺) CD8⁺ T cells in neoadjuvant tumors (**Figure 2.7E**) as compared to treatment-naïve tumors (**Figure 2.2F**), as well as a 3-fold relative increase in Ki67⁺ PD-1⁻ EOMES⁺ cells compared to treatment naïve, perhaps indicative of a more active T cell response in neoadjuvant cases.

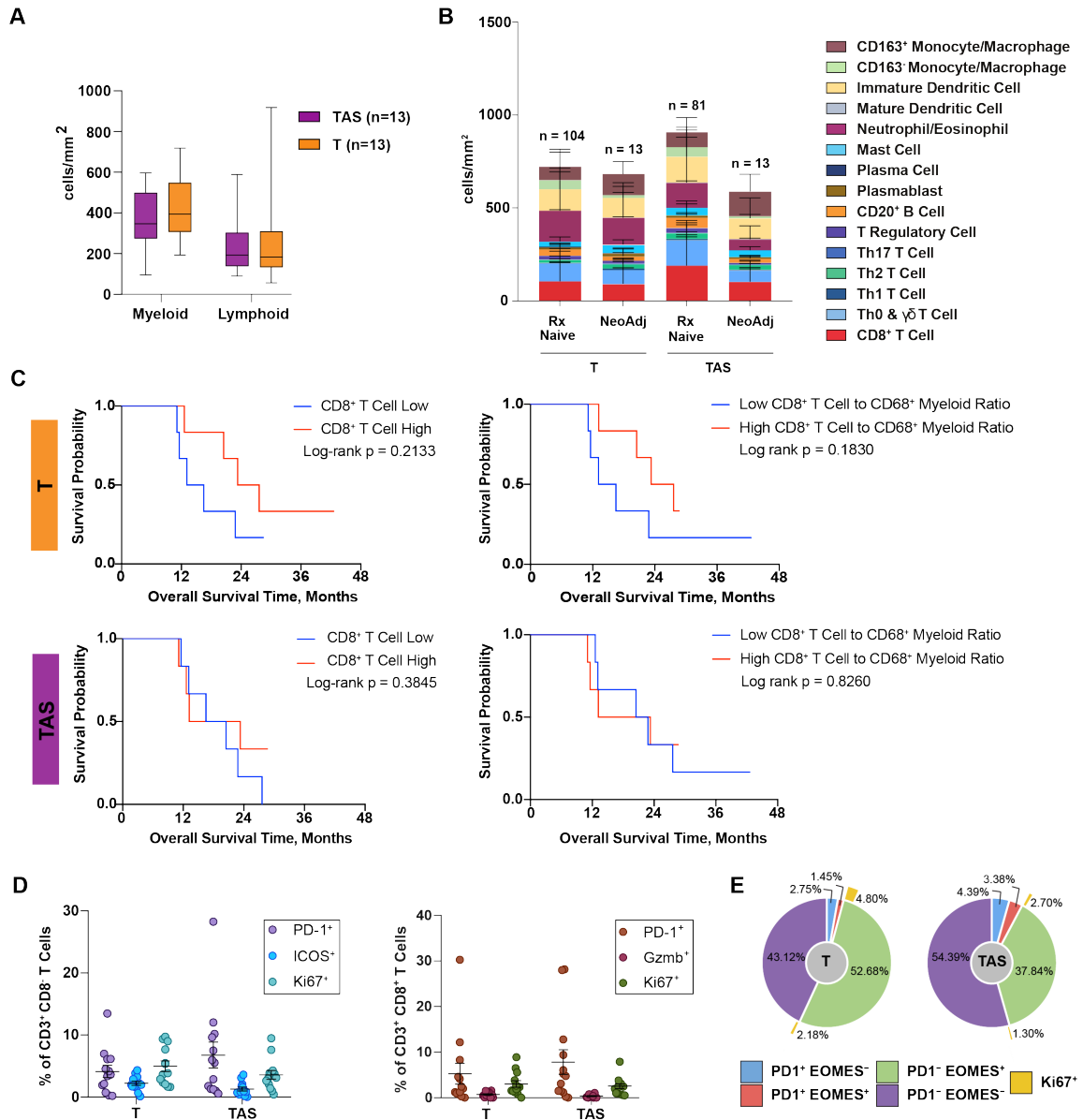


Figure 2.7 Immune contexture of neoadjuvant-treated PDAC. (A) Myeloid and lymphoid cell densities of tumor (T) and tumor adjacent stroma in 13 neoadjuvant PDAC cases from OHSU. Bars, boxes, and whiskers represent median, interquartile range, and range, respectively. (B) Immune complexity comparison between treatment-naïve (Rx Naïve, n = 104 patients) and neoadjuvant (NeoAdj, n = 13 patients) T and TAS. (C) Kaplan-Meier analyses of CD8⁺ T cell density and CD8⁺ T cell to CD68⁺ monocyte/macrophage ratio in T (top) and TAS (bottom) of neoadjuvant cases. Patients were stratified by median CD8⁺ T cell density and CD8/CD68⁺ ratio, respectively (n = 6 patients/group). (D) Frequency of CD3⁺ CD8⁺ T cells positive for PD-1, ICOS, or Ki67 (left) or frequency of CD3⁺ CD8⁺ T cells positive for PD-1, Granzyme B (Gzmb), or Ki67 (right) in the indicated tissue regions of neoadjuvant treated patients. Data are displayed as mean \pm SEM. (E) Sunburst graphs representing percentage of CD3⁺ CD8⁺ T cells positive for PD-1, EOMES, and/or Ki67 in the indicated regions in neoadjuvant patients.

Discussion and Future Directions

Emergence of multiplexed imaging methods that can be applied to FFPE tissues has opened the door to in-depth spatial characterization of human tumors and their microenvironments. Such approaches are facilitating biomarker discovery and have potential to aid in patient stratification for therapy. In this study, we utilized a chromogen-based mIHC platform to develop a pan-immune atlas of surgically resected treatment-naïve and neoadjuvant-treated PDACs. Using downstream quantitative image cytometry with hierarchical gating strategies analogous to those used in flow cytometry, we have identified and enumerated 15 individual leukocyte populations and evaluated their differentiation states and functional status. This represents the most extensive study of its kind to evaluate phenotypic and functional heterogeneity of both lymphocyte and myeloid lineages in histopathologically distinct regions of PDAC tumor resection specimens.

We demonstrate extensive immune heterogeneity at multiple levels within the PDAC TiME. Total leukocyte abundance varied considerably between patients and also between tissue regions, with tumor adjacent stroma being the most leukocyte-enriched compartment on average. Tumor adjacent stroma was also the site with the highest T cell density, as others have previously observed [123]. Notably, although T cell density was also highly heterogeneous across patients, CD8⁺ T cells, T helper cells, and Tregs collectively represented approximately one-third of all leukocytes in tumor and nearly half of all leukocytes in tumor adjacent stroma in the treatment-naïve cohorts, on average. Consistent with other reports [161], this finding indicates that PDACs are not uniformly

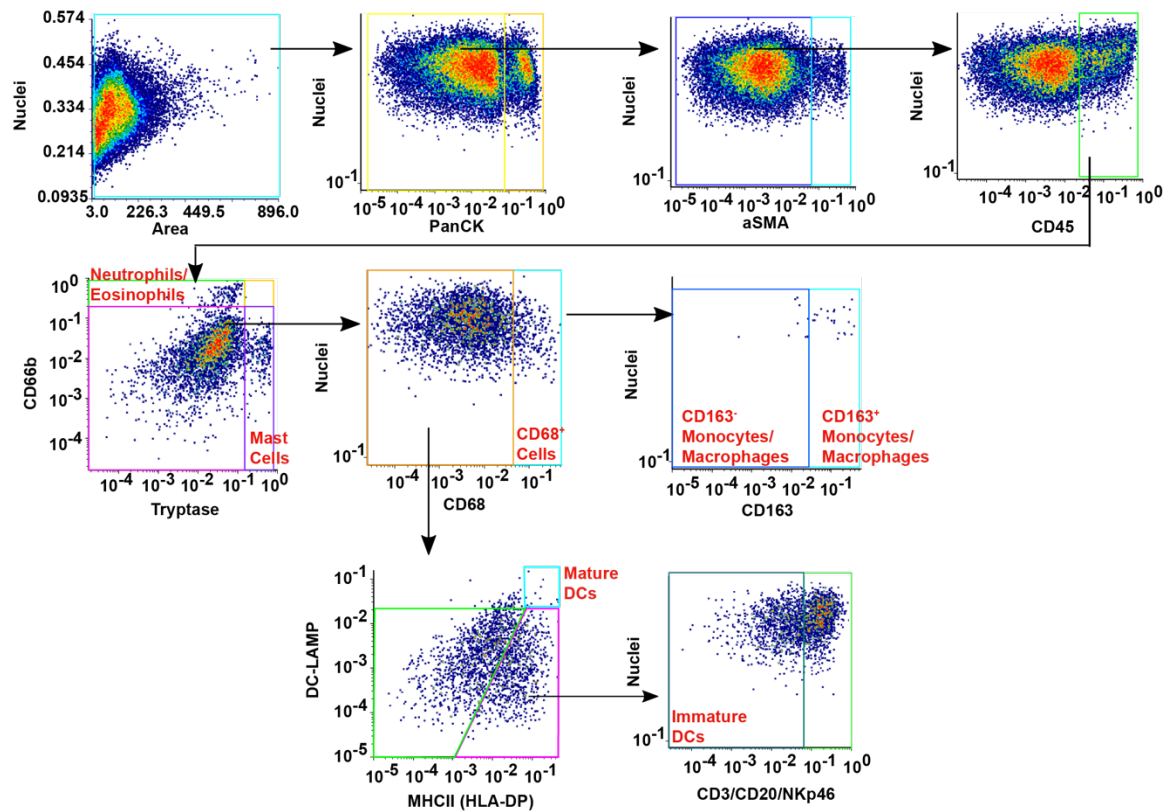
immunological deserts, but that a subset of tumors are T cell-enriched and may already be poised to respond to immunotherapies, provided they are functionally capable. This is further reflected in unsupervised clustering of treatment-naïve tumors, where we identified a lymphocyte-enriched subgroup.

Interestingly, the lymphocyte-enriched cluster was not associated with improved overall survival outcome, nor was density of CD8⁺ T cells in tumor or stroma when measured by univariate analysis. This observation is inconsistent with several other reports that indicate a strong survival advantage in PDAC patients with high levels of intratumoral CD8⁺ T cells [122, 124, 130, 154]; however, there are several potential explanations for why we did not observe this in our treatment-naïve cohorts. Firstly, ROI selection in the present study specifically compartmentalized immune aggregates from the regions in which they were found. That is, cells contained within intratumoral immune aggregate ROIs were evaluated separately from cells in tumor ROIs (**Figure 2.1A**). It is likely that integrating data from tumor and intratumoral immune aggregates will reveal stronger associations between T cells and patient outcomes, and this analysis is currently underway. It is also possible that univariate analysis is not sufficiently robust to discover prognostic associations in these cohorts and that multi-variable models would be more informative with respect to identifying prognostic immune signatures. This was the case in another recent report wherein combined assessment of CD8 and PD-L1 gene expression was prognostic, but CD8 expression alone was not [162].

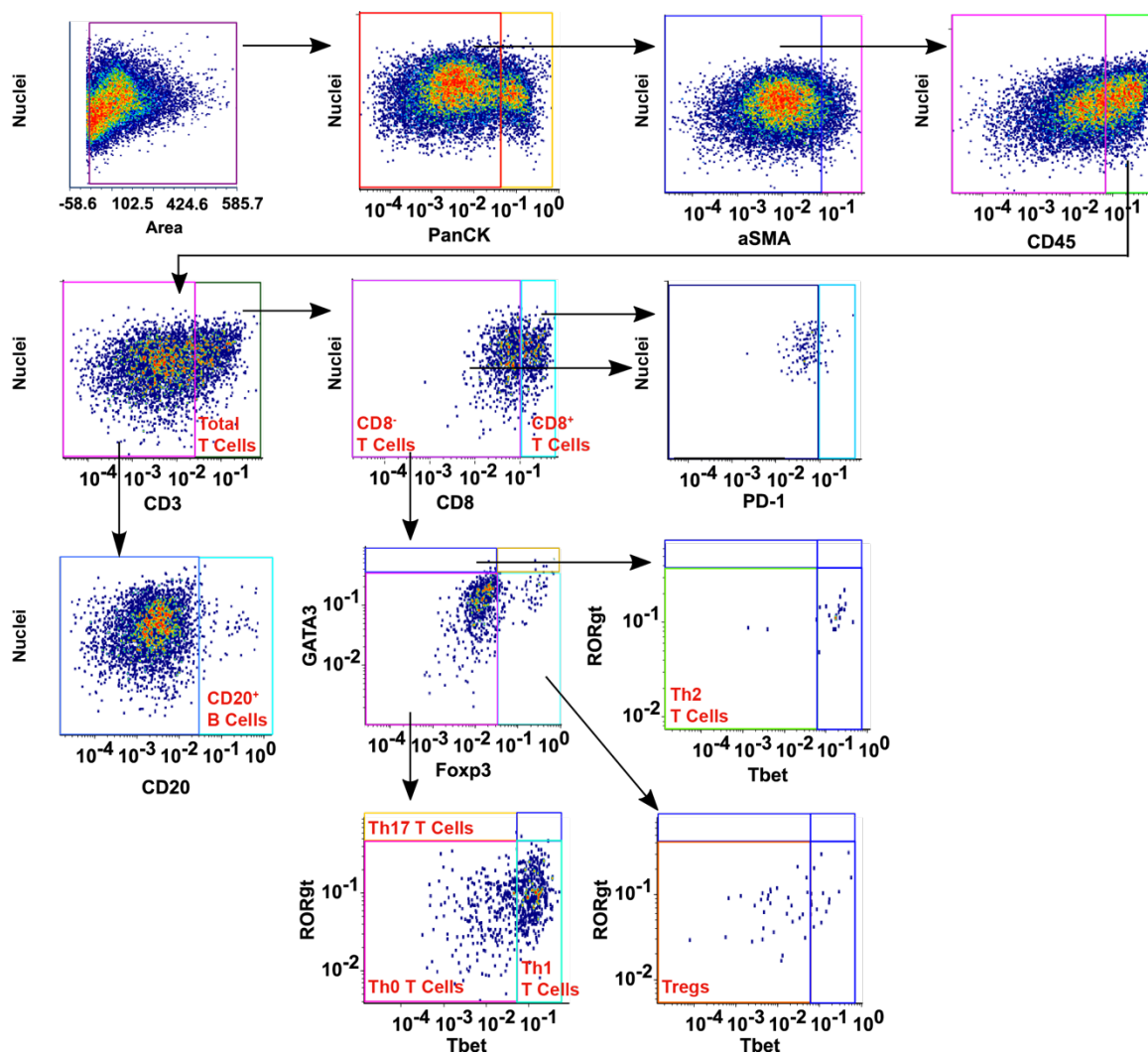
Another possibility that may underlie the lack of association between CD8⁺ T cells and survival stems from our functional interrogation that revealed less than five percent of total intratumoral CD8⁺ T cells were proliferative and even fewer were positive for granzyme B. Further, approximately 95% of all CD3⁺ T cells were negative for PD-1, thus suggesting inactivity and lack of recent antigen stimulation. PD-1 expression profiling performed by others using flow cytometry and multiplex immunofluorescence has suggested that between 30-95% of CD8⁺ T cells in treatment-naïve PDACs are PD-1⁺ [123, 161]. These reports used different PD-1 primary antibody clones in their analyses than used in the present study, which may contribute to this disparity. Nevertheless, to further explore functional identities of PD-1⁺ T cells in our study, we have designed and are validating a second T cell functional mIHC panel that includes additional biomarkers that will more clearly inform on T cell status. Among these are CD45RA and CD45RO, which will allow clearer delineation between naïve T cells and antigen-experienced T cells. Further, we are optimizing antibodies for a series of additional biomarkers that are implicated in T cell dysfunction in the context of cancer, including additional T cell co-inhibitory receptors LAG-3, CTLA-4, and TIM-3, which are each upregulated in T cells upon activation and whose cell surface expression is maintained under conditions of chronic antigen exposure [163]. We will also assess a series of emerging biomarkers of T cell exhaustion/dysfunction, including Tox, CD38, and CD39 [164-166] and Tcf1, a transcription factor expressed in memory-like T cells that have capacity to expand in tumors and generate cytotoxic antitumor effector T cells [167]. We plan to initially stain a subset of samples from our treatment naïve cohorts for these biomarkers in order to gain a more detailed perspective of T cell functionality in tumors and adjacent stroma.

T cell functionality notwithstanding, we have been able to identify three main immunotypes of PDAC based on densities of major lymphoid and myeloid lineages. While the resulting clustered groups were not independently associated with patient outcome, they still provide a highly informative view of the variable forms a PDAC immune landscape can take, and they can thus be used to predict which types of immunotherapies might be most likely to elicit antitumor responses in each group. For example, patients within the myeloid-enriched cluster with relative enrichment for CD163⁺ monocytes/macrophages might preferentially benefit from agents known to induce macrophage transcriptional reprogramming (e.g. α CSF1), whereas patients in the mixed cluster with relative enrichment in neutrophils or immature DCs might respond to therapies that attenuate neutrophil trafficking (e.g. CXCR2 blockade) and/or activate DCs (e.g. CD40 agonists), respectively. Based on our results demonstrating a potential role of *TP53* alterations in regulating tumor immune complexity, it is likely that an integrated evaluation of immune subtype and molecular status will further enhance our ability to meaningfully stratify patients. In summary, this study offers unprecedented insight into immune phenotypic and spatial heterogeneity of PDAC and offers a large baseline reference that has potential to inform prospective clinical decision-making.

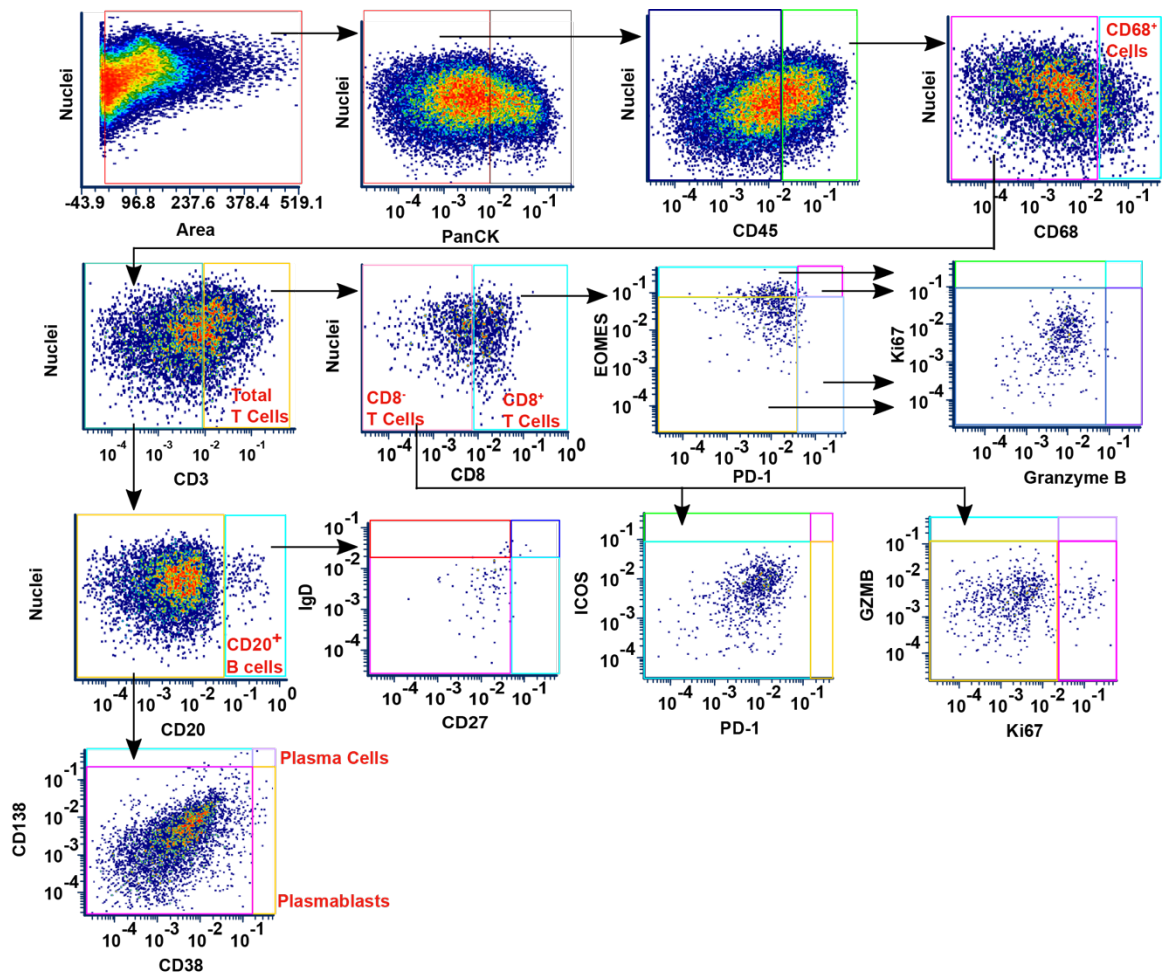
Supplemental Data



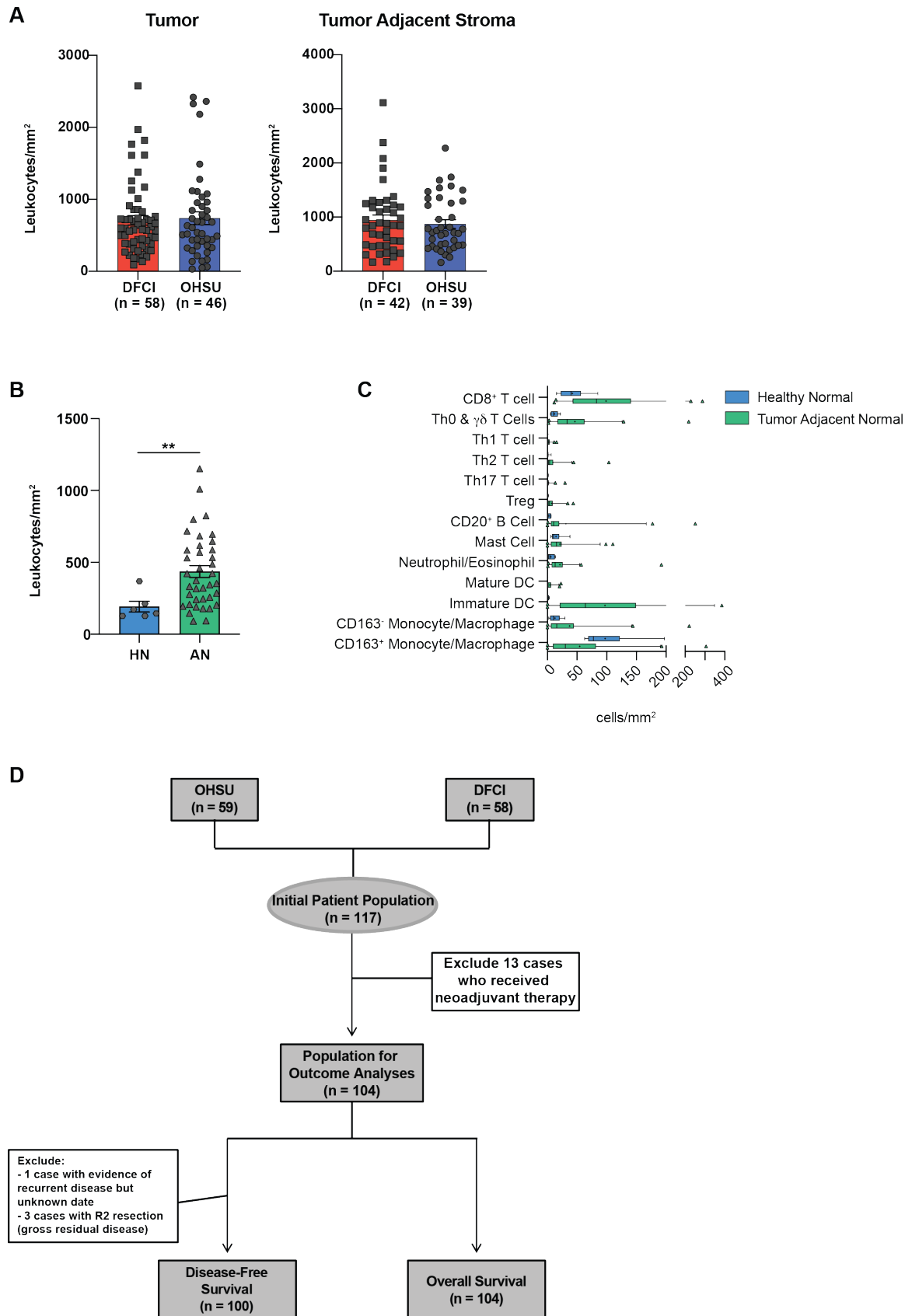
Supplemental Figure 2.1 Myeloid biomarker panel gating strategy. Image cytometry gating strategy used to evaluate myeloid cell lineages listed in Supplemental Table 2.2



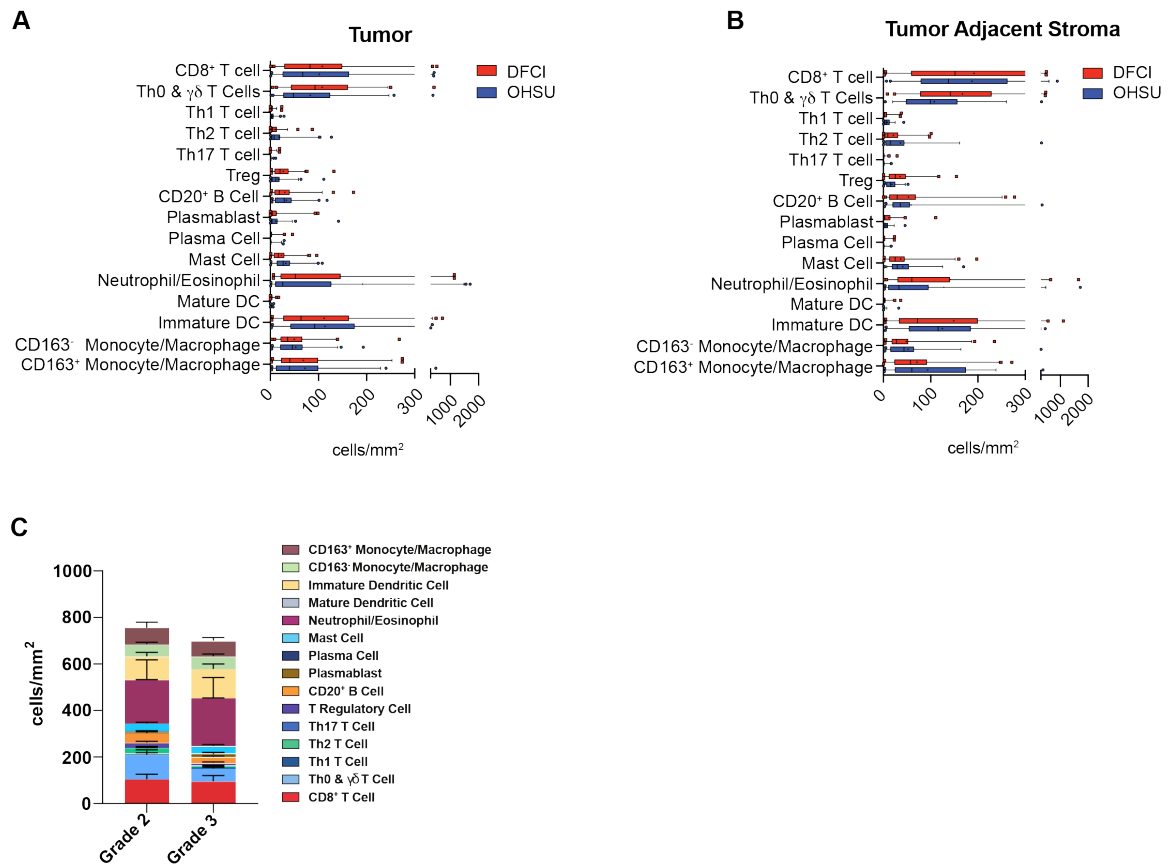
Supplemental Figure 2.2 Lymphocyte biomarker gating strategy. Image cytometry gating strategy used to evaluate lymphocyte lineages listed in Supplemental Table 2.2.



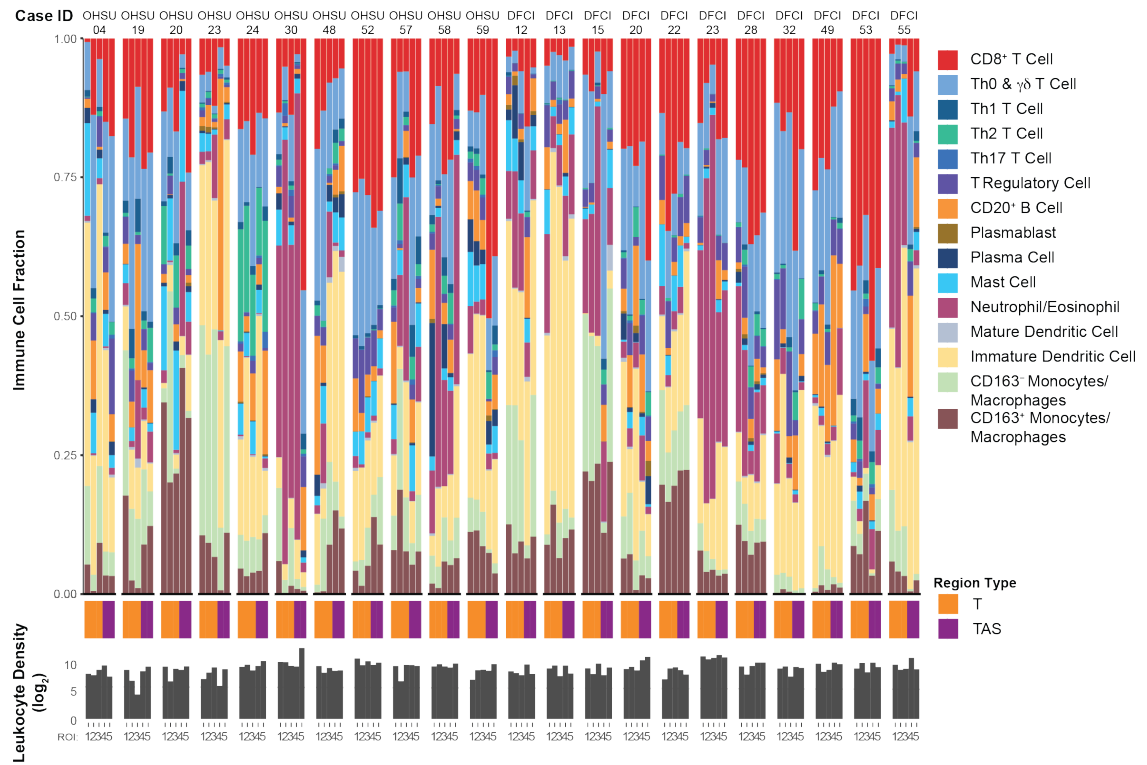
Supplemental Figure 2.3 Functional biomarker gating strategy. Image cytometry used to evaluate functional status of lymphocyte lineages listed in Supplemental Table 2.2



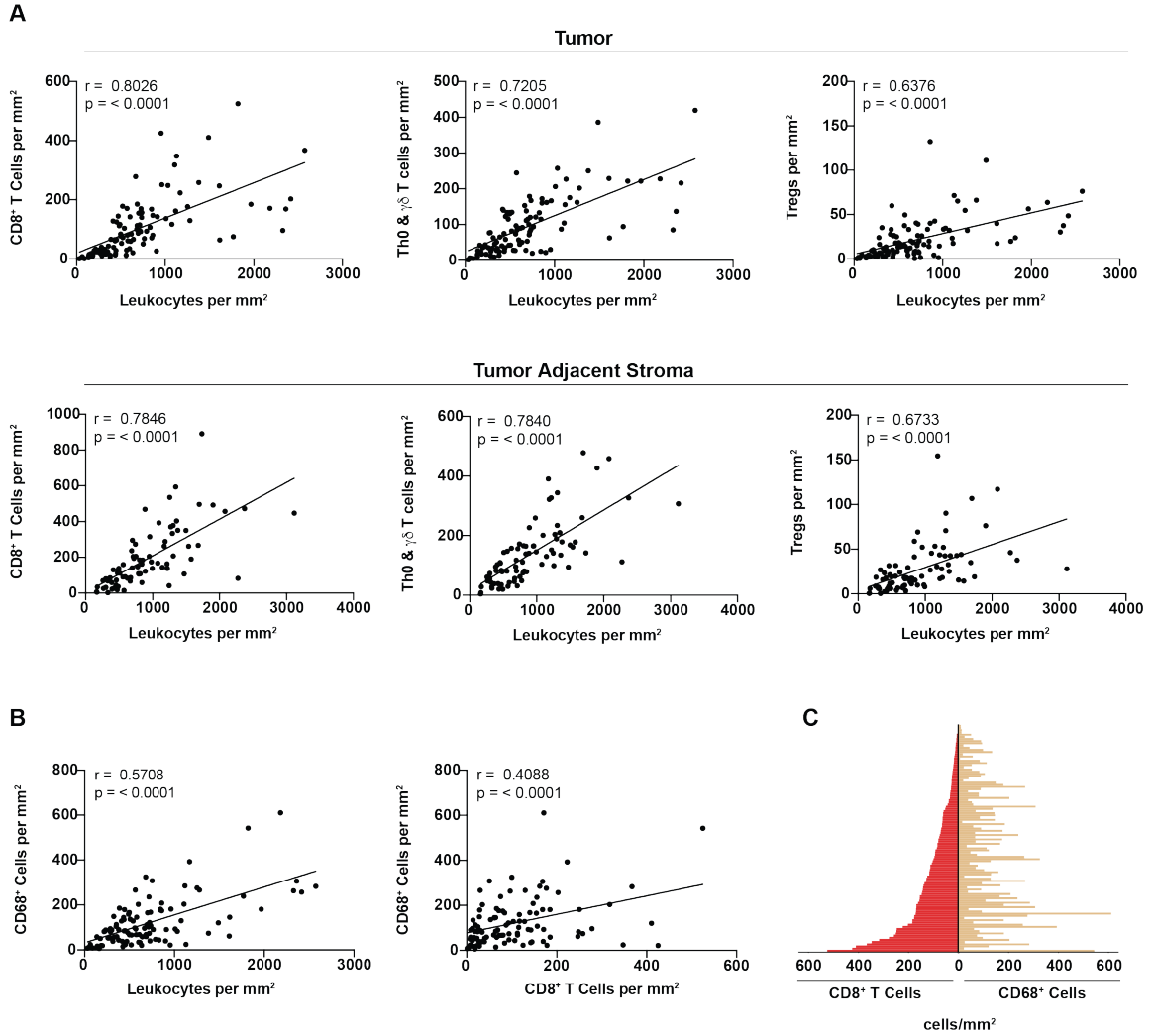
Supplemental Figure 2.4 Leukocyte density comparisons between tissue types and sample cohorts. (A) Leukocyte densities from treatment-naïve tumors and tumor adjacent stroma in Dana-Farber Cancer Institute (DFCI) and Oregon Health & Science University cohorts. **(B)** Total leukocyte density in healthy normal pancreas (HN, n = 6 patients) as compared to tumor adjacent normal pancreas (AN = 38 patients). Statistical significance was determined by two-tailed, unpaired Mann-Whitney U test. ** $p < 0.01$ **(C)** Immune composition of HN versus AN. Boxes represent interquartile range, whiskers extend to the 5th and 95th percentiles, and values outside of this range are depicted as individual points. Means are indicated by + symbols. **(D)** Flow chart of study population evaluated in survival analyses.



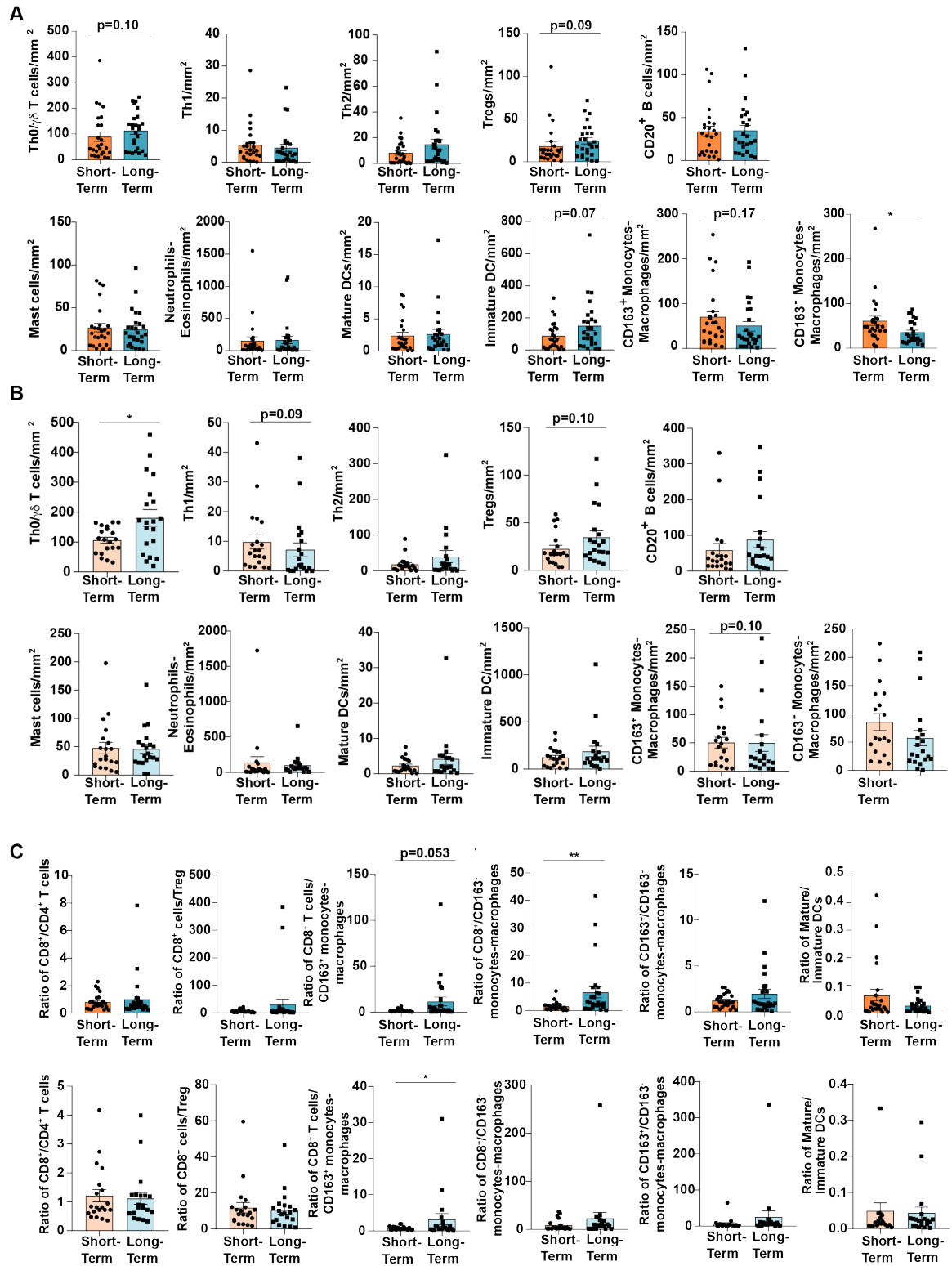
Supplemental Figure 2.5 Multiple leukocyte subpopulations are correlated with overall leukocyte density in tumor and adjacent stroma. (A) Immune composition of tumor and (B) tumor adjacent stroma of treatment-naïve cases from DFCI (n = 58 patients) and OHSU (n = 59 patients). (C) Immune composition of moderately differentiated Grade 2 tumors (n = 21 patients) and poorly differentiated Grade 3 tumors (n = 22 patients) from the OHSU treatment-naïve cohort. One Grade 1 tumor and two tumors of undetermined grade were excluded from analysis.



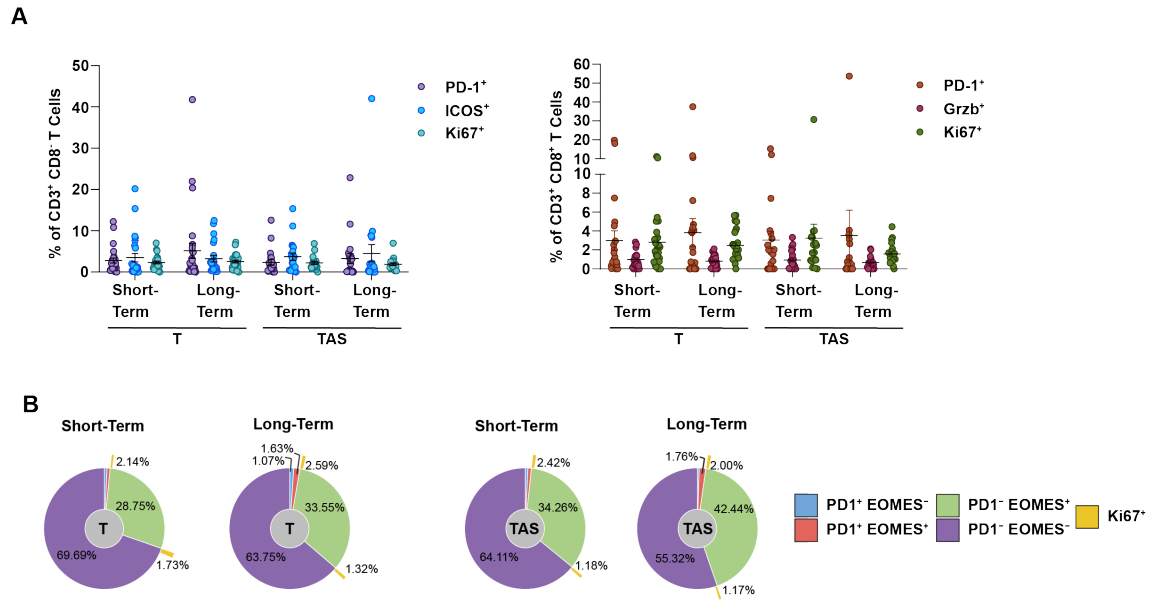
Supplemental Figure 2.6 Intrapatient immune heterogeneity in treatment-naïve PDAC. Stacked bar graphs from a representative subsample of cases from OHSU and DFCI cohorts (n = 22 patients total) illustrating relative cellular abundance of individual leukocyte populations in three tumor (T; orange) and two tumor adjacent stroma (TAS; purple) regions of interest (ROIs) from each patient. Dark gray bars (bottom) indicate total leukocyte density in log₂ scale for each ROI.



Supplemental Figure 2.7 Correlations between immune subpopulation densities and overall leukocyte density in treatment-naïve tumors. (A) Spearman correlation of total leukocyte density to CD8⁺ T cells, Th0 T cells, and Regulatory T cells (Tregs), respectively, in tumor (top) and tumor adjacent stroma (bottom). Tumor, n = 104 patients; Tumor adjacent stroma, n = 81 patients. **(B)** Spearman correlation of intratumoral leukocyte density and intratumoral CD68⁺ cells (left) and intratumoral CD68⁺ cells and CD8⁺ T cells (right). **(C)** CD8⁺ T cell density and CD68⁺ cell density in matched tumors, sorted from low to high CD8⁺ T cell density.



Supplemental Figure 2.8 Comparisons of leukocyte population cell densities and ratios in short-term vs. long-term survivors from the treatment-naïve cohorts. (A) Comparison of indicated leukocyte populations in tumor of short-term survivors (n = 25 patients) and long-term survivors (n = 26 patients). (B) Comparison of indicated leukocyte populations in tumor adjacent stroma of the short-term survivors (n = 20 patients) and long-term survivors (n = 20) for which adjacent stroma was present. (C) Ratios of leukocyte populations in tumor (top row) and tumor adjacent stroma (bottom row) from same samples as depicted in (A-B). Statistical significance was determined by two-tailed, unpaired Mann-Whitney U test. * $p \leq 0.05$, ** $p \leq 0.01$. Data are presented as mean \pm SEM.



Supplemental Figure 2.9 T cell functional profiles of short-term and long-term survivors. (A) Percentage of CD3⁺ CD8⁺ T cells positive for PD-1, ICOS, and Ki67 (left) and CD3⁺ CD8⁺ T cells positive for PD-1, Granzyme B (Gzmb), and Ki67 in tumor (T) and tumor adjacent stroma (TAS) of short-term survivors. Short-term survivors n = 25 tumors, 20 stroma; long-term survivors n = 26 tumors, 20 stroma. **(B)** Sunburst graphs depicting combinations of PD-1, EOMES, and Ki67 positivity on CD3⁺ CD8⁺ T cells from same specimens as in (A).

Supplemental Table 2.1 mIHC biomarker panels

Myeloid Panel			Cycle 1	Cycle 2	Cycle 3	Cycle 4	Cycle 5	Cycle 6
	Pre-AR	Round 1	Round 1	Round 1	Round 1	Round 1	Round 1	Round 1
Primary Antibody or Stain	Hematoxylin	CD68	DC-SIGN	DC-LAMP	CD45	CD66b	HLA-DPB1	
Clone	N/A	PG-M1	DC-28	1010E1.01	HI30	G10F5	EPR11226	
Vendor	Dako	Abcam	Santa Cruz	Novus Biologicals	ThermoFisher	BD Pharmingen	Abcam	
Catalog #	S3301	ab783	sc-65740	DDX0191P-100	1 4-0459-82	555723	ab157210	
Host Species	N/A	Mouse	Mouse	Rat	Mouse	Mouse	Rabbit	
Concentration	N/A	1:50	1:100	1:100	1:100	1:200	1:20,000	
Incubation Time	1 min	30 min @ RT	30 min @ RT	30 min @ RT	60 min @ RT	O/N @ 4°C	30 min @ RT	
		Cycle 7	Cycle 8	Cycle 9	Cycle 10	Cycle 11	Cycle 12	
		Round 1	Round 1	Round 1	Round 1	Round 1	Round 1	
Primary Antibody or Stain	CD163	PD-L1	CD3/CD20/NKp46	Tryptase	αSMA	Pan Cytokeratin		
Clone	10D6	E1L3N	SP7/SP32/195314	AA1	Polyclonal	AE1/AE3		
Vendor	ThermoFisher	CST	ThermoFisher/Abcam/R&D	Abcam	Abcam	Abcam		
Catalog #	MA5-11458	13684S	RM-9107/ab64088/MAB1850	ab2378	ab5694	ab27988		
Host Species	Rabbit	Rabbit	Rabbit/Rabbit/Mouse	Mouse	Rabbit	Mouse		
Concentration	1:100	1:100	1:150/1:1000/1:20	1:20,000	1:200	1:2000		
Incubation Time	30 min @ RT	O/N @ 4°C	30 min @ RT	30 min @ RT	30 min @ RT	30 min @ RT		

Lymphoid Panel			Cycle 1	Cycle 2	Cycle 3	Cycle 4	Cycle 5	Cycle 6	Cycle 7
	Pre-AR	Round 1	Round 1	Round 1	Round 1	Round 1	Round 1	Round 1	Round 1
Primary Antibody or Stain	Hematoxylin	PD-1	CD3	RORγt	NKp46	CD45	CD8α	T-bet	
Clone	N/A	NAT105	SP7	6F3.1	195314	HI30	C8/144B	D6N8B	
Vendor	Dako	Abcam	ThermoFisher	Millipore Sigma	R&D Systems	ThermoFisher	ThermoFisher	CST	
Catalog #	S3301	ab52587	RM-9107-S	MABF81	MAB1850	14-0459-82	MA5-13473	13232S	
Host Species	N/A	Mouse	Rabbit	Mouse	Mouse	Mouse	Mouse	Rabbit	
Concentration	N/A	1:50	1:150	1:200	1:20	1:100	1:100	1:500	
Incubation Time	1 min	30 min @ RT	30 min @ RT	30 min @ RT	30 min @ RT	60 min @ RT	30 min @ RT	O/N @ 4°C	
		Cycle 8	Cycle 9	Cycle 10	Cycle 11	Cycle 12	Cycle 13	Cycle 14	
		Round 1	Round 1	Round 1	Round 1	Round 1	Round 1	Round 1	
Primary Antibody or Stain	GATA-3	PD-L1	Foxp3	CD20	Smad4	αSMA	Pan Cytokeratin		
Clone	L50-823	E1L3N	236A/E7	SP32	B-8	Polyclonal	AE1/AE3		
Vendor	BioCare	CST	ThermoFisher	Abcam	Santa Cruz	Abcam	Abcam		
Catalog #	CM405A	13684S	14-4777-82	ab64088	sc-7966	ab5694	ab27988		
Host Species	Mouse	Rabbit	Mouse	Rabbit	Mouse	Rabbit	Mouse		
Concentration	1:50	1:100	1:40	1:1000	1:50	1:200	1:2000		
Incubation Time	O/N @ 4°C	O/N @ 4°C	30 min @ RT	60 min @ RT	O/N @ 4°C	30 min @ RT	30 min @ RT		

Functional Panel			Cycle 1	Cycle 2	Cycle 3	Cycle 4	Cycle 5	Cycle 6
	Pre-AR	Round 1	Round 1	Round 1	Round 1	Round 1	Round 1	Round 1
Primary Antibody or Stain	Hematoxylin	PD-1	CD138	CD68	CD38	CD45	IDO	
Clone	N/A	NAT105	MI15	PG-M1	38C03 (SPC32)	HI30	1F8.2	
Vendor	Dako	Abcam	ThermoFisher	Abcam	ThermoFisher	ThermoFisher	Millipore Sigma	
Catalog #	S3301	ab52587	MA5-12400	ab783	MA5-14413	14-0459-82	MAB10009	
Host Species	N/A	Mouse	Mouse	Mouse	Mouse	Mouse	Mouse	
Concentration	N/A	1:50	1:20	1:50	1:100	1:100	1:100	
Incubation Time	1 min	30 min @ RT	30 min @ RT	30 min @ RT	30 min @ RT	60 min @ RT	30 min @ RT	
		Round 2	Round 2	Round 2	Round 2	Round 2	Round 2	
Primary Antibody or Stain		PD-L1	CD4	CD3	T-bet	Granzyme B	CD278 (ICOS)	
Clone		E1L3N	SP35	SP7	D6N8B	Polyclonal	SP98	
Vendor		CST	Roche/Ventana	ThermoFisher	CST	Abcam	LifeSpan Bio	
Catalog #		3684S	790-4423	RM-9107-S	13232S	ab4059	LS-C210350	
Host Species		Rabbit	Rabbit	Rabbit	Rabbit	Rabbit	Rabbit	
Concentration		1:100	1:4	1:150	1:500	1:200	1:100	
Incubation Time		O/N @ 4°C	30 min @ RT	30 min @ RT	O/N @ 4°C	30 min @ RT	30 min @ RT	
		Cycle 7	Cycle 8	Cycle 9	Cycle 10	Cycle 11	Cycle 12	
		Round 1	Round 1	Round 1	Round 1	Round 1	Round 1	
Primary Antibody or Stain	CD8α	CD5	IgD	CD20	Pan Cytokeratin	PNAd		
Clone	C8/144B	4C7	EPR6146	SP32	AE1/AE3	MECA-79		
Vendor	ThermoFisher	ThermoFisher	Abcam	Abcam	Abcam	BD Pharmingen		
Catalog #	MA5-13473	MA5-13308	ab124795	ab64088	ab27988	553863		
Host Species	Mouse	Mouse	Rabbit	Rabbit	Mouse	Rat		
Concentration	1:100	1:40	1:200	1:1000	1:2000	1:500		
Incubation Time	30 min @ RT	O/N @ 4°C	O/N @ 4°C	60 min @ RT	30 min @ RT	O/N @ 4°C		
		Round 2	Round 2	Round 2	Round 2	Round 2	Round 2	
Primary Antibody or Stain	CD27	EOMES (Tbr2)		CD3	Ki67			
Clone	Polyclonal	Polyclonal		SP6				
Vendor	Novus Biologicals	Millipore Sigma		Millipore Sigma				
Catalog #	NBP2-38434	AB2283		275R-14				
Host Species	Rabbit	Rabbit		Rabbit				
Concentration	1:500	1:1000		1:500				
Incubation Time	30 min @ RT	30 min @ RT			30 min @ RT			

Supplemental Table 2.2 Cell lineages identified by mIHC staining

Lineage	Identification
Epithelial cells	PanCK ⁺
Myofibroblastic CAFs	PanCK ⁻ α SMA ⁺
Lymphocytes	
CD8 ⁺ T Cells	PanCK ⁻ CD45 ⁺ CD3 ⁺ CD8 ⁺
Regulatory T Cells (Tregs)	PanCK ⁻ CD45 ⁺ CD3 ⁺ CD8 ⁻ Foxp3 ⁺ GATA3 ⁻ ROR γ t ⁻ Tbet ⁻
Th0 (naïve) Helper T Cells*	PanCK ⁻ CD45 ⁺ CD3 ⁺ CD8 ⁻ Foxp3 ⁻ GATA3 ⁻ ROR γ t ⁻ Tbet ⁻
Th1 Helper T Cells	PanCK ⁻ CD45 ⁺ CD3 ⁺ CD8 ⁻ Foxp3 ⁻ GATA3 ⁻ ROR γ t ⁻ Tbet ⁻
Th2 Helper T Cells	PanCK ⁻ CD45 ⁺ CD3 ⁺ CD8 ⁻ Foxp3 ⁻ GATA3 ⁺ ROR γ t ⁻ Tbet ⁻
Th17 Helper T Cells	PanCK ⁻ CD45 ⁺ CD3 ⁺ CD8 ⁻ Foxp3 ⁻ GATA3 ⁻ ROR γ t ⁺ Tbet ⁻
B Cells	PanCK ⁻ CD45 ⁺ CD3 ⁻ CD20 ^{+/-}
Plasmablasts	PanCK ⁻ CD45 ⁺ CD3 ⁻ CD20 ⁻ CD38 ⁺ CD138 ⁻ CD27 ⁺
Plasma Cells	PanCK ⁻ CD45 ⁺ CD3 ⁻ CD20 ⁻ CD38 ⁺ CD138 ⁺ CD27 ⁺
Myeloid Cells	
Neutrophils & Eosinophils	PanCK ⁻ CD45 ⁺ CD66b ⁺
Mast Cells	PanCK ⁻ CD45 ⁺ CD66b ⁻ Tryptase ⁺
Monocytes/Macrophages	PanCK ⁻ CD45 ⁺ CD66b ⁻ Tryptase ⁻ CD68 ⁺ CD163 ^{+/-}
Immature Dendritic Cells	PanCK ⁻ CD45 ⁺ CD66b ⁻ Tryptase ⁻ CD68 ⁻ HLA-DP ⁺ DC-LAMP ⁻
Mature Dendritic Cells	PanCK ⁻ CD45 ⁺ CD66b ⁻ Tryptase ⁻ CD68 ⁻ HLA-DP ⁺ DC-LAMP ⁺

PanCK = pan cytokeratin

CAFs = cancer associated fibroblasts

*Population also includes $\gamma\delta$ T Cells and innate $\alpha\beta$ T cells

Supplemental Table 2.3 Correlation between leukocyte density in tumor or tumor adjacent stroma and clinical characteristics

Tumor	Leukocyte Density			<i>P</i> Fisher
	Tertile 1	Tertile 2	Tertile 3	
AJCC 8th ed. pT stage, n (%)				0.49
T1 (n=11)	2	5	4	
T2 (n=62)	19	23	20	
T3 (n=23)	10	6	7	
T4 (n=2)	2	0	0	
AJCC 8th ed. pN stage, n (%)				0.97
N0 (n=28)	9	10	9	
N1 (n=38)	11	13	14	
N2 (n=38)	14	12	12	
Tumor differentiation, n (%)				0.80
Well/Moderately differentiated (n=53)	17	20	16	
Poorly differentiated/Undifferentiated (n=48)	17	15	16	
Lymphovascular invasion, n (%)				0.96
Negative (n=34)	10	13	11	
Positive (n=45)	12	17	16	
Tumor Adjacent Stroma	Leukocyte Density			<i>P</i> Fisher
	Tertile 1	Tertile 2	Tertile 3	
AJCC 8th ed. pT stage, n (%)				0.22
T1 (n=9)	1	4	4	
T2 (n=49)	17	14	18	
T3 (n=17)	6	8	3	
T4 (n=2)	2	0	0	
AJCC 8th ed. pN stage, n (%)				1.00
N0 (n=23)	7	8	8	
N1 (n=31)	11	10	10	
N2 (n=27)	9	9	9	
Tumor differentiation, n (%)				0.16
Well/Moderately differentiated (n=46)	12	19	15	
Poorly differentiated/Undifferentiated (n=34)	15	8	11	
Lymphovascular invasion, n (%)				0.86
Negative (n=28)	8	11	9	
Positive (n=35)	11	11	13	

Supplemental Table 2.4 List of regions of interest (ROIs) used to generate Sankey diagrams in Figure 2.3

	Number of Intratumoral ROIs	Number of Border ROIs	Number of Spanning Border-Distal ROIs	Number of Distal ROIs	Total ROIs
Tumor (T)	312 (Rx Naïve) 40 (Neoadj)	0 (Rx Naïve) 0 (Neoadj)	0 (Rx Naïve) 0 (Neoadj)	0 (Rx Naïve) 0 (Neoadj)	312 (Rx Naïve) 40 (Neoadj)
Tumor Adjacent Stroma (TAS)	0 (Rx Naïve) 0 (Neoadj)	38 (Rx Naïve) 5 (Neoadj)	27 (Rx Naïve) 4 (Neoadj)	72 (Rx Naïve) 16 (Neoadj)	127 (Rx Naïve) 25 (Neoadj)
Adjacent Normal Pancreas (AN)	0 (Rx Naïve) 0 (Neoadj)	0 (Rx Naïve) 0 (Neoadj)	2 (Rx Naïve) 0 (Neoadj)	42 (Rx Naïve) 3 (Neoadj)	44 (Rx Naïve) 3 (Neoadj)
Immune Aggregate (IA)	67 (Rx Naïve) 1 (Neoadj)	46 (Rx Naïve) 4 (Neoadj)	1 (Rx Naïve) 2 (Neoadj)	43 (Rx Naïve) 11 (Neoadj)	157 (Rx Naïve) 18 (Neoadj)

Supplemental Table 2.5 Correlation between tumor cluster and clinical characteristics

	Tumor Cluster			P Fisher
	Myeloid Enriched	Lymphoid Enriched	Mixed	
AJCC 8th ed. pT stage, n (%)				0.60
T1 (n=11)	4	5	2	
T2 (n=62)	25	20	17	
T3 (n=23)	9	5	9	
T4 (n=2)	2	0	0	
AJCC 8th ed. pN stage, n (%)				0.82
N0 (n=28)	11	10	7	
N1 (n=38)	14	11	13	
N2 (n=38)	17	9	12	
Tumor differentiation, n (%)				0.15
Well/Moderately differentiated (n=53)	18	20	15	
Poorly differentiated/Undifferentiated (n=48)	23	10	15	
Lymphovascular invasion, n (%)				0.07
Negative (n=34)	11	14	9	
Positive (n=45)	26	10	9	

Chapter 3: CD20 as a therapeutic target in pancreatic cancer

Contributions

Shannon M. Liudahl and Lisa M. Coussens developed hypotheses, designed experiments, analyzed and interpreted data for studies described in this chapter. Andrew J. Gunderson performed initial studies involving α CD20 mAb therapy in FVB/n murine models of orthotopic PDAC. Andrew J. Gunderson and Christopher J. Chan performed initial flow cytometry immune complexity studies of FVB/n orthotopic PDAC tumors. Shannon M. Liudahl performed all other experiments, with technical assistance from Meghan B. Lavoie and Padraic S. Robinson for necropsy, tissue collection, and tissue processing.

Background & Introduction

Rituximab (RTX) is a chimeric monoclonal Ab (mAb) that specifically binds the CD20 cell surface molecule on B lymphocytes. CD20 is expressed starting at the pre-B cell stage of B cell development and is maintained in mature B cells, with the exception of immunoglobulin (Ig)-producing plasma cells, which downregulate CD20 upon differentiation [168]. RTX binding to CD20 induces antibody-dependent cellular cytotoxicity (ADCC) and complement-dependent cytotoxicity (CDC), resulting in B cell death [169]. RTX represents the first mAb to receive FDA approval for use in clinical oncology. In the decades since its first approval for non-Hodgkin's lymphoma, RTX clinical indications have expanded to additional hematologic malignancies and autoimmune diseases, including chronic lymphocytic leukemia (CLL), rheumatoid arthritis, and pemphigus vulgaris [169, 170]. The clinical success of RTX has prompted development of second generation α CD20 mAbs that have distinct modes of cellular cytotoxicity compared to RTX and also demonstrate marked clinical benefit [171]. However, clinical translation of α CD20 mAbs to solid tumors has lagged behind, despite preclinical evidence of pro-tumoral B cell functions in many solid tumor types [172].

Using a transgenic murine model of squamous cell carcinoma (SCC), the Coussens laboratory previously reported that B cell-secreted Igs form circulating immune complexes (CICs) that are deposited into premalignant skin where they bind to activating Fc γ receptors (Fc γ Rs) on myeloid cells [173, 174]. This Fc γ R engagement leads to downstream proangiogenic and tissue remodeling pathways in myeloid cells that support progressive tumor growth [174]. Notably, depletion of B cells via administration of an

anti-mouse CD20 mAb led to delayed early neoplastic progression [175]. Orthotopic SCC growth was also slowed when α CD20 mAb therapy was combined with either paclitaxel or carboplatin chemotherapy. This was partially attributable to macrophage transcriptional reprogramming that resulted in increased expression of T cell chemoattractants and increased cytotoxic CD8⁺ T cell infiltration into tumors [175].

We recently identified similar tumor supportive B cell-myeloid interactions in an orthotopic murine model of PDAC [111]. PDAC cells derived from primary pancreatic tumors from transgenic *LSL-Kras*^{G12D/+}; *Pdx-1-Cre* mice harboring null mutations in either *Trp53* (cell line p53 2.1.1) or *p16*^{Ink4a} (cell line Ink4 2.2) exhibited delayed tumor growth when orthotopically implanted into syngeneic B-cell deficient mice (JH^{-/-}) as compared to B cell proficient controls (JH^{+/-}) (**Figure 3.1**). Orthotopic PDAC growth was also significantly slowed in FcR γ ^{-/-} mice as compared to FcR γ ^{+/-} controls [111]. The observed decrease in primary tumor growth in JH^{-/-} and FcR γ ^{-/-} mice was associated with a significant decrease in tumor desmoplasia and pronounced transcriptional skewing of myeloid cells to a Th1-like program, indicating similar B cell-mediated myeloid programming in PDAC as initially observed in murine models of SCC [111].

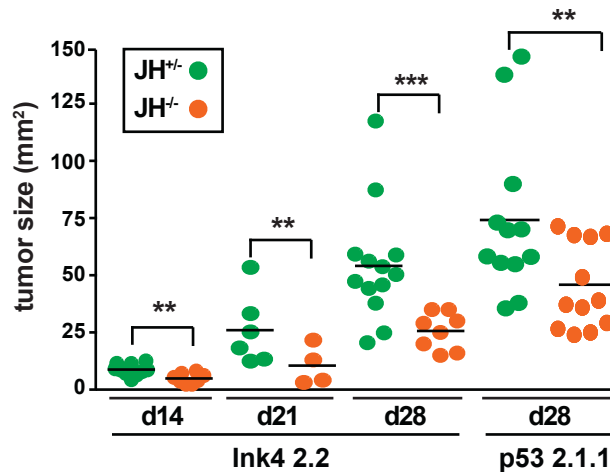


Figure 3.1 Orthotopic PDAC growth is regulated by B cells. Ink4 2.2 and p53 2.1.1–derived PDAC tumor area was quantitatively evaluated in syngeneic JH^{+/-} and JH^{-/-} in serial H&E-stained tissue sections of tumors isolated on days 14, 21, and 28 after implantation. This figure originally appeared in Gunderson et al. (2016) Bruton Tyrosine Kinase-Dependent Immune Cell Cross-Talk Drives Pancreas Cancer, Cancer Discovery, and is re-printed here with permission from the publisher.

Based on these observations in PDAC and our previous success with α CD20 mAb therapy in murine SCC, we hypothesized that α CD20 mAb treatment would be similarly efficacious in slowing PDAC growth. To test this hypothesis, syngeneic FVB/n mice were orthotopically implanted with Ink4 2.2 PDAC cells and were randomized at d14 post-tumor implant to receive either anti-mouse α CD20 mAb or a ragweed-specific isotype control mAb (α RW), plus or minus gemcitabine chemotherapy. In contrast to our observations in SCC, tumor growth was equivalent in α RW and α CD20 monotherapy groups, as well as in combination chemotherapy cohorts (**Figure 3.2A**).

Incomplete depletion of B cells during α CD20 mAb treatment has been reported in murine models [176-178]. In order to interrogate whether α CD20 mAb-resistant B cells were contributing to lack of mAb efficacy, we evaluated presence of B cells in blood, primary tumor, and spleen of α CD20 mAb-treated tumor-bearing mice at end-stage

(**Figure 3.2B-C**). Although we observed a trending decrease in B cell frequency within tumors of α CD20 mAb-treated mice as compared to controls, differences were insignificant across groups (**Figure 3.2B**). Peripheral blood mononuclear cell (PBMC) assessment revealed significant B cell depletion; however, spleen, similar to primary tumors, contained notable residual B cell populations as revealed by immunohistochemistry for the B cell biomarker B220, with particular B cell density maintained in splenic marginal zones (**Figure 3.2C**). Flow cytometric evaluation of residual intratumoral B cells in α CD20 mAb-treated mice revealed significantly elevated percentages of interleukin (IL)-10⁺ B cells (**Figure 3.2D**). IL-10 expression is a hallmark feature of immunosuppressive regulatory B cells (Bregs) and its expression on intratumoral B cells was a notable observation given the reported role of Bregs in fostering progression of PDAC and other solid tumors [112, 179, 180].

To determine whether α CD20-resistant B cells directly regulated tumor growth, we treated tumor-naïve JH^{+/-} mice with one 200 μ g dose of α CD20 mAb and isolated remaining CD19⁺ B cells from spleen 7 days later. Isolated B cells were then adoptively transferred (1.0×10^3 cells/mouse, i.v.) into syngeneic tumor-naïve JH^{-/-} recipients. Ink4 2.2 PDAC cells were orthotopically implanted into B cell recipient JH^{-/-} mice 2 days post-adoptive transfer, and tumor growth was monitored and compared to that of JH^{+/-} mice and JH^{-/-} who had not received adoptively transferred B cells. At end-stage, we observed that B cell reconstitution in JH^{-/-} mice restored tumor growth to levels of JH^{+/-} controls (**Figure 3.2E**), indicating that the residual B cell pool in α CD20 mAb-treated mice was

sufficient to foster tumor progression and likely contributed to lack of α CD20 mAb efficacy.

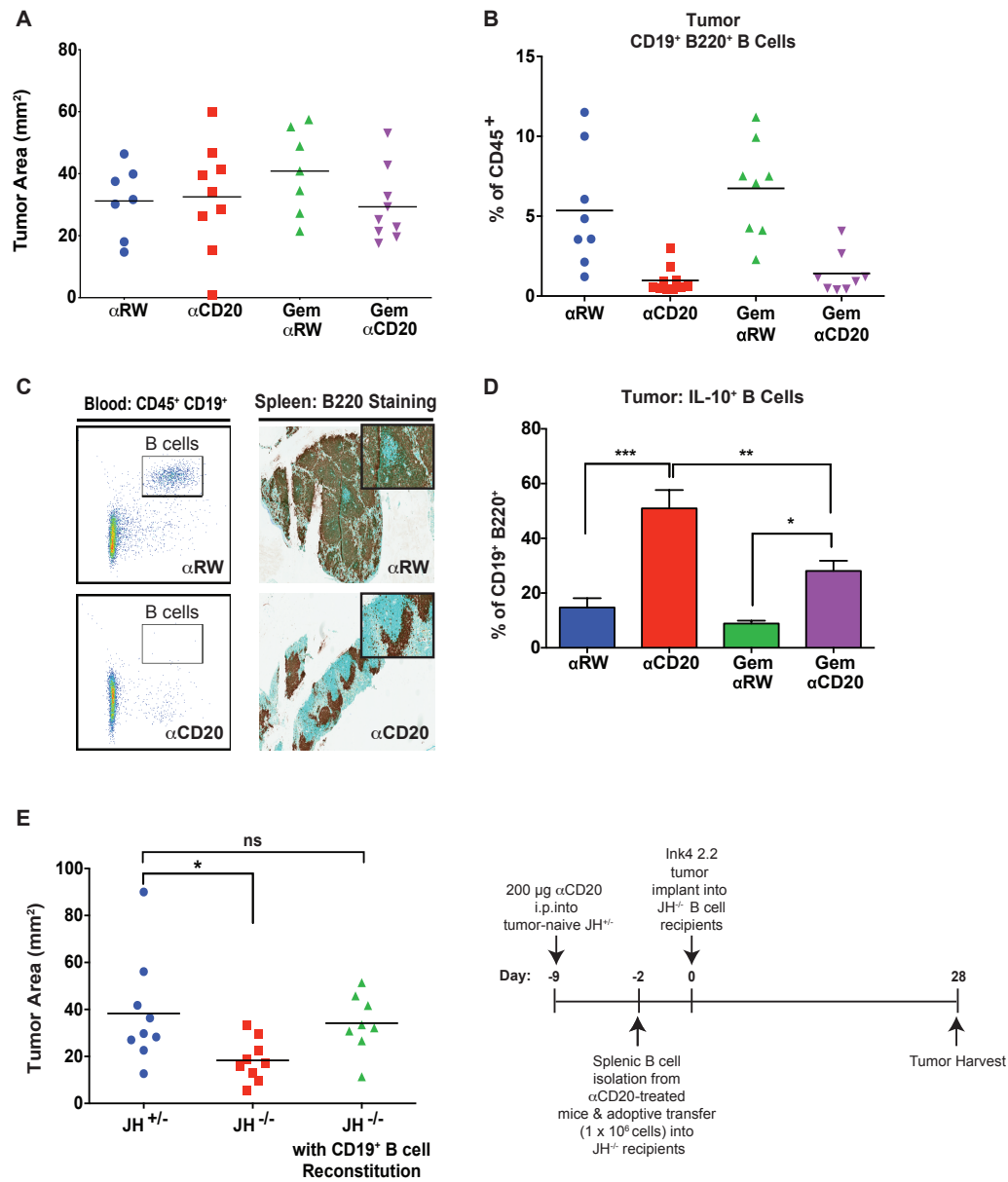


Figure 3.2 α CD20-resistant B cells subvert therapeutic efficacy in orthotopic PDAC. (A) Tumor area of end-stage Ink4 2.2 orthotopic tumors 28 days post-implantation in mice treated with α RW or α CD20 mAb +/- gemcitabine, as indicated. 200 μ g α RW or α CD20 was administered i.p. on days 14 and 21 post-tumor implant; gemcitabine was administered i.v. at 10 mg/kg body weight on days 22 and 26 post-implant. Each data point represents one mouse, $n = 7-9$ mice/group. (B) Frequency of intratumoral CD19⁺ B220⁺ B cells as a percentage of total CD45⁺ cells from mice depicted in (A). (C) Representative flow cytometry analysis of CD19⁺ B cells in peripheral blood of mice treated as indicated (left) and representative photomicrographs of B220 immunohistochemistry of spleen (right), revealing residual splenic B cells in α CD20 mAb-treated mice. (D) Percentage of intratumoral IL-10⁺ CD19⁺ B220⁺ B cells at end-stage as measured by flow cytometry. (E) Ink4 2.2 orthotopic tumor burden in JH^{+/+} B cell-proficient mice, JH^{-/-} B cell-deficient mice, and JH^{-/-} recipients of adoptively transferred residual B cells from tumor-naïve mice pre-treated with α CD20 mAb (as shown in schema on right). Significance was measured by one-way ANOVA.

Based on these results, we were motivated to explore alternative B cell depletion strategies that might impact presence of α CD20 mAb-resistant B cells and could be leveraged therapeutically. One such option was to evaluate the type II α CD20 mAb obinutuzumab (GA101), which has been reported to exhibit enhanced activity compared to type I human α CD20 mAbs, including RTX [181]. GA101 is a glycoengineered mAb specific for human CD20 that functionally differs in critical ways from type I antibodies. Whereas type I antibodies act predominantly through induction of CDC and ADCC, type II antibodies are strong inducers of direct cell death and have enhanced ADCC capability [171, 181]. Importantly, B cell depletion following GA101 administration is more rapid and complete, and GA101 therapy has been reported to result in superior tumor eradication as compared to RTX in a xenograft model of lymphoma [182-184]. We therefore hypothesized that GA101 therapy, either as monotherapy or in combination with chemotherapy and/or other immunotherapies, might result in more extensive B cell depletion and reduced tumor progression in PDAC.

Because GA101 is an anti-human mAb, administration in a murine model of PDAC required use of transgenic mice engineered to express human CD20 (hCD20 Tg^{+/+}), which have been previously established [176]. Thus, we developed a breeding colony of hCD20 Tg^{+/+} mice on the C57BL/6 strain background. In addition to evaluating GA101, hCD20 Tg^{+/+} mice also allowed us to interrogate potential efficacy of anti-human RTX, thus representing an important distinction from our prior α CD20 mAb studies in murine SCC and PDAC, which utilized a murine-specific CD20 mAb. Murine-specific mAbs are not classified as either type I or type II antibodies, and direct comparison of mAb

mechanism or extent of B cell depletion between anti-mouse and anti-human CD20 mAbs has not been reported. We hypothesized that either GA101 or RTX would exhibit enhanced anti-tumor efficacy in PDAC as compared to our previous findings and, if efficacious, would represent a more clinically relevant approach that could be rapidly translated to human PDAC, as both RTX and GA101 are FDA approved for other indications.

Materials and Methods

Cell Lines

p53 2.1.1 and Ink4 2.2 PDAC cell lines derived from transgenic mice on the FVB/n strain background have been previously described [111]. C57BL/6 murine tumor cell lines used in these experiments were derived from primary pancreatic ductal adenocarcinomas of transgenic *LSL-Kras*^{G12D/+}; *LSL-Trp53*^{R172H/+}; *Pdx-I-Cre* (KPC) mice [185]. 4662 cells were kindly provided by Dr. Robert Vonderheide (University of Pennsylvania, Philadelphia, PA). FC1199, FC1242, and FC1245 cell lines were a gift from Dr. David Tuveson (Cold Spring Harbor Laboratory, Cold Spring Harbor, NY). All murine cell lines were expanded in the Coussens laboratory and frozen at low passage number in liquid nitrogen for later use in *in vivo* studies. Human Raji (Burkitt's lymphoma) cells were generously provided by Dr. Alexey Danilov (Oregon Health & Science University, Portland, OR). Murine cells were grown in DMEM (Gibco) supplemented with 10% FBS and 1% penicillin/ streptomycin on tissue-culture treated plastic coated with 50 µg/mL rat tail Collagen I (Corning). Raji cells were grown in suspension culture in RPMI 1640 Medium with L-glutamine (Gibco), 10% FBS, and 1% penicillin/streptomycin. All cell lines tested negative for *Mycoplasma* contamination, and murine cell lines were confirmed negative (IDEXX Laboratories) for all murine pathogen species excluded from the OHSU specific pathogen-free barrier housing facility.

Mice

B cell-deficient (JH) mice contain a deletion in all J_h gene segments of the Ig heavy-chain locus that blocks formation of mature B cells. FcR γ mice lack the Fc receptor common

γ chain, resulting in deficiency of all activating Fc γ Rs. Full characterization of JH and FcR γ mice has been described elsewhere[186, 187]. Generation and characterization of transgenic mice expressing the human CD20 protein (hCD20 Tg^{+/+}) has been previously described in detail[176]. Cryopreserved sperm from hCD20 Tg mice on the C57BL/6N strain background was provided by Genentech, Inc., and the mouse line was re-derived at the OHSU Transgenic Mouse Models Core. Mice were maintained at OHSU in specific-pathogen-free facilities. hCD20 Tg genotyping was performed by flow cytometric evaluation of hCD20 expression on peripheral blood B cells (**Supplemental Figure 3.1**), and only hCD20 Tg^{+/+} mice were enrolled in experiments. All animal experiments were performed in accordance with National Institutes of Health guidelines and were approved by the Institutional Animal Care and Use Committee at OHSU.

Orthotopic Tumor Implantation and In Vivo Studies

Orthotopic implantation of murine PDAC cell lines was performed using methods we have previously described [111] with age-matched male and female mice 8-13 weeks old at time of surgery. Briefly, abdominal hair was removed with electric clippers and/or depilatory cream 1-2 days prior to surgery. At the time of surgery, mice were anesthetized with continuous isoflurane in a sterile surgical field. After confirming depth of anesthesia by toe pinch, an approximately 1.5 cm incision was made in the left abdomen, and spleen and pancreas were exteriorized. PDAC cells suspended in 50% Matrigel (Corning) and 50% serum-free DMEM (Gibco) were injected into the tail of the pancreas with a 29-gauge insulin syringe at a total volume of 30 μ L. Number of injected PDAC cells varied by cell line as follows: 4662 (1.25×10^4 cells); p53 2.1.1, Ink4 2.2,

FC1199, FC1242, and FC1245 (1.0×10^3 cells). Successful injection was confirmed by formation of a solidified Matrigel bleb in the pancreas and no apparent fluid escape. The pancreas and spleen were then returned to the peritoneal cavity, and the peritoneum was sutured and skin stapled with wound clips. Wound clips were removed 10 days after surgery. Tumors were monitored longitudinally by ultrasonography on days 10, 17, and 27 following implantation using a Vevo 2100 high-resolution imaging system (FUJIFILM VisualSonics), and tumor area (mm^2) was measured from raw ultrasound data using OsiriX DICOM Viewer software (Pixmeo). For select studies intended to establish tumor growth kinetics, tumors were instead measured by ultrasound on days 14, 21, and 27 or 28. Gemcitabine was administered i.v. at 15 mg/kg of body weight on days 18, 22, and 26 post-implantation unless otherwise indicated. mAbs were administered via i.p. injection. In FVB/n studies, 200 μg of anti-mouse αCD20 (clone 5D2, provided by Genentech) or αRW mouse IgG2a isotype was administered on days 14 and 21 post-implantation. In hCD20 studies, RTX and GA101 (provided by Roche) and mouse IgG2a (clone C1.18.4, BioXCell) were administered at 10 mg/kg or 30 mg/kg on days 10, 17, and 24 post-implantation. 250 μg of $\alpha\text{PD-1}$ (clone RMP1-14, BioXCell) or rat IgG2a (clone 2A3, BioXCell) was administered on days 18, 22, and 26 post-implantation. Animals were euthanized 28 days post-implantation, except where otherwise specified.

Flow Cytometry

Single-cell suspensions of tumor, spleen, and PBMCs used for flow cytometry were prepared as previously described [111, 188], with slight modifications. Whole blood was collected into EDTA-coated tubes via retro-orbital bleed (on-study blood collection) or

cardiac puncture (at study end-point). Plasma was extracted from whole blood after a 7-minute centrifugation at 400 x g, and red blood cells were lysed with BD Pharm Lyse (BD Biosciences), leaving PBMCs. Tumor and spleen were collected following cardiac perfusion with 10 mL PBS supplemented with 10 U/mL heparin (Sigma-Aldrich) to clear peripheral blood. To prepare single-cell suspensions, tumor was manually minced then enzymatically digested at 37°C for 30 minutes with constant stirring in DMEM containing 1.0 mg/mL soybean trypsin inhibitor (VWR), 1.0 mg/mL collagenase IV (Gibco), and 50 U/mL DNase I (Roche). Cells were passed through a 100 µm mesh filter and washed with FACS buffer (PBS with 0.5% BSA and 2.0 mM EDTA), followed by 5 minutes centrifugation at 400 x g. Spleen was mashed and passed through a 40 µm filter, followed by red blood cell lysis with BD Pharm Lyse, and 5 minutes centrifugation at 400 x g. To prevent non-specific antibody binding, Fc blocking was performed by re-suspending and incubating cells for 30 minutes on wet ice with rat anti-mouse CD16/CD32 mAb (2.4G2, 1:200, BD Bioscience) in PBS also containing Live/Dead Fixable Aqua stain (1:500, Invitrogen) to distinguish viable from dead cells. Cells were centrifuged at 400 x g for 5 minutes, then incubated for 30 minutes at 4°C in 100 µL FACS buffer containing fluorescently-conjugated antibodies against cell surface antigens, as listed in **Table 3.1** and **Table 3.2**. Cells were then washed in 100 µL FACS buffer and centrifuged as before. For intracellular staining, the Foxp3 Transcription Factor Staining Kit (Invitrogen) was used according to manufacturer instructions. Cells not requiring intracellular staining were fixed in BD Cytofix Buffer (BD Biosciences) for 15 minutes, followed by a final wash in FACS buffer. All cells were stored in 200 µL FACS buffer at 4°C until running on a BD Fortessa with FACSDiva software (BD Biosciences). Data

were analyzed with FlowJo software (FlowJo LLC). Flow cytometry gating strategies are depicted in **Figure 3.5** and **Supplemental Figures 3.3 and 3.4**.

For B cell reconstitution experiments, splenocytes were harvested and stained as described above, followed by fluorescence activated cell sorting (FACS) for isolation of CD19⁺ B cells. Cells were sorted using a BD Influx sorter with FACSDiva software.

In Vitro α CD20 Binding Assay

To verify binding affinities of RTX and GA101, Raji cells (1×10^5 cells per well of a 96-well plate) were incubated with either RTX or GA101 (0.01-10 μ g/mL) diluted in FACS buffer for 30 minutes at 4°C. Cells were spun down for 5 minutes at 400 x g and incubated in Live/Dead Fixable Aqua stain (1:1000, Invitrogen) in PBS for 30 minutes at 4°C. After washing in FACS buffer and spinning down, cells were incubated for an additional 30 minutes at 4°C in PE-conjugated goat F(ab')₂ anti-mouse IgG secondary antibody (1:50, STAR105, Bio-Rad), washed, and fixed for 15 minutes in BD Cytofix (BD Biosciences). All conditions were tested in triplicate. Data was acquired on an LSR-II flow cytometer (BD Biosciences), and mean fluorescence intensity of PE in viable cells was calculated using FlowJo software (FlowJo LLC).

Histology and Immunohistochemistry

Tissues from cardiac-perfused mice were fixed in 10% neutral-buffered formalin for 16 hours, processed through a series of graded alcohols and xylenes, and embedded in paraffin wax using standard procedures. Hematoxylin and eosin (H&E) staining was performed on 5 μ m thick formalin-fixed paraffin-embedded (FFPE) sections on a Jung

Autostainer XL (Leica Biosystems). For immunohistochemical detection of B cells, 5 μ m FFPE sections were baked at 60°C for 30 minutes, deparaffinized, and subjected to heat-mediated antigen retrieval in 95°C Citra pH 6.0 solution (BioGenex) for 15 minutes in a vegetable steamer (Oster 5712). Slides were cooled for 15 minutes at room temperature, and endogenous peroxidases were blocked by submersion in 0.6% hydrogen peroxide in methanol for 20 minutes at room temperature, followed by washes in TBST. Protein blocking was conducted for 30 minutes at room temperature in PBS containing 5% normal goat serum and 2.5% BSA, followed by application and incubation of rat anti-mouse CD45R/B220 primary antibody (RA3-6B2, #550286, 1:500; BD Pharmingen) for 1 hour at room temperature in a humidified chamber. Tissue sections were then washed in TBST, incubated in biotinylated anti-rat secondary antibody (#BA-4001, 1:200; Vector Laboratories) for 30 minutes, washed, and incubated in horseradish peroxidase-conjugated avidin complex (ABC Elite, Vector Laboratories) for 30 minutes. 3,3'-diaminobenzidine (DAB) chromogen was applied to tissues for 90 seconds for signal detection, and sections were counterstained in 0.01% methyl green for 2 minutes, followed by dehydration and coverslipping with Permount mounting medium (Fisher Scientific). Slides were scanned at 20X magnification on an Aperio AT2 digital slide scanner (Leica Biosystems).

Statistical Analysis

All statistical analyses were performed using Prism versions 6 and 8 for Mac (GraphPad Software). Unpaired t-tests were used to compare 2 groups, and one-way ANOVA with Tukey's multiple comparisons test was used to evaluate differences between more than 2

groups. Specific tests used are identified in figure legends. p values < 0.05 were considered statistically significant, with * $p < 0.05$, ** $p < 0.01$, *** $p < 0.001$, **** $p < 0.0001$.

Results

Establishing Tumor Growth Kinetics, Chemotherapy Sensitivity, and Immune

Phenotypes of PDAC in C57BL/6 Mice

Our previous research identifying pro-tumoral functions of B cells in pancreatic cancer relied upon PDAC cell lines derived from transgenic KPC mice maintained on the FVB/n strain background, and therefore used syngeneic FVB/n mice as orthotopic tumor recipients[111]. Since hCD20 transgenic mice used for the present studies were developed on the C57BL/6 strain background, we acquired four primary murine PDAC cell lines (4662, FC199, FC1242, FC1245) derived from C57BL/6 KPC mice previously characterized by other investigators using *in vivo* and *ex vivo* analyses [189, 190]. To assess tumor kinetics and histopathology of each of these cell lines, tumor cells were orthotopically implanted into the pancreas of syngeneic C57BL/6 mice at inoculum densities recommended by the laboratories of cell origin, and tumor growth was longitudinally measured by ultrasound imaging starting between days 10-14 post-implantation (**Figure 3.3A**). Of the cell lines evaluated, FC1245 displayed the most aggressive primary tumor growth kinetics, which led to marked decline in overall animal health and necessitated a humane study end point at day 23. Upon necropsy, a majority (14 of 16) FC1245 tumor-bearing mice exhibited macroscopic tumor outgrowth throughout the peritoneal cavity (data not shown). All other cell lines displayed growth kinetics within similar ranges to what we have previously observed in analogous studies using FVB/n mice. Histopathologic review of H&E-stained tumor sections from study end points revealed FC1199 tumors to be moderately differentiated, FC1245 tumors to be moderately to poorly differentiated, and FC1242 and 4662 to be poorly differentiated

(**Figure 3.3B**). Tumors from each cell line contained prominent ischemic central necrosis and/or geographic necrosis, and all tumors exhibited high mitotic index (≥ 10 mitotic cells / 10 high powered fields), based on review by a pathologist (Terry Morgan, MD; Oregon Health & Science University).

Innate and acquired resistance to standard-of-care chemotherapies is common in human PDAC [191, 192] . To evaluate chemo-responsiveness of these different murine tumors *in vivo*, we administered gemcitabine (15 mg/kg of body weight) on days 18, 22, and 26 post-implantation, as we have previously described in PDAC studies on the FVB/n strain background [111]. Among the four tumor lines assessed, 4662 tumor-bearing mice were the only group that demonstrated significant chemotherapy-mediated slowing in tumor growth at experimental end point (**Figure 3.3C**). FC1245 tumor-bearing mice required euthanasia one day following the second gemcitabine dose, thereby prohibiting a complete assessment of response to therapy; however, there was no significant difference in tumor area (**Figure 3.3C**), volume, or weight (data not shown) at end stage between the control and gemcitabine groups. To query whether the observed gemcitabine resistance in the other cell lines was dose-dependent, we treated an additional cohort of FC1199 tumor-bearing mice with high-dose gemcitabine (60 mg/kg of body weight), which resulted in no significant effect on primary tumor growth kinetics (**Figure 3.3C**).

In addition to characterizing tumor kinetics and chemo-responsiveness, we assessed tumor immune complexity in untreated and gemcitabine-treated end stage tumors by flow cytometry (**Figure 3.3D**). In other studies, we reported that isogenic tumor subclones derived from KPC mice possess tumor cell-intrinsic properties giving rise to a high

degree of intratumoral immune heterogeneity, which in turn significantly impacts response to chemo- and immunotherapy [115]. Importantly, these prior studies revealed that tumors from KPC-derived tumor subclones can be subdivided into T cell high and T cell low groups, where increased T cell abundance is predictive of therapeutic response. Of the four cell lines evaluated herein, immune profiles of primary orthotopic tumors generated from each cell line were not significantly different with or without chemotherapy (**Figure 3.3D**). All tumors exhibited myeloid-dominant immune complexities, with MHCII⁻ CD11b⁺ Ly6G⁺ Ly6C^{int} neutrophils and MHCII⁻ CD11b⁺ Ly6G⁻ Ly6C⁻ immature myeloid cells collectively comprising approximately 40% or more of the total CD45⁺ compartment (**Figure 3.3D**). FC1199 tumors displayed highest overall neutrophil abundance of the four tumors evaluated (60.5% of CD45⁺ cells), and 4662 and FC1242 tumors had highest MHCII⁺ CD11b⁺ F4/80⁺ CD11c^{+/-} macrophage infiltration (10.1% and 12.9% of CD45⁺ cells, respectively). T and B lymphocytes were comparatively sparse in all tumor types (2.9-12.0% lymphocytes of total CD45⁺ cells). 4662 tumors had highest average CD8⁺ T cell abundance; however, even in these tumors, CD8⁺ T cells represented < 2% of total immune cells, falling into the range of T cell low KPC subclones previously characterized.

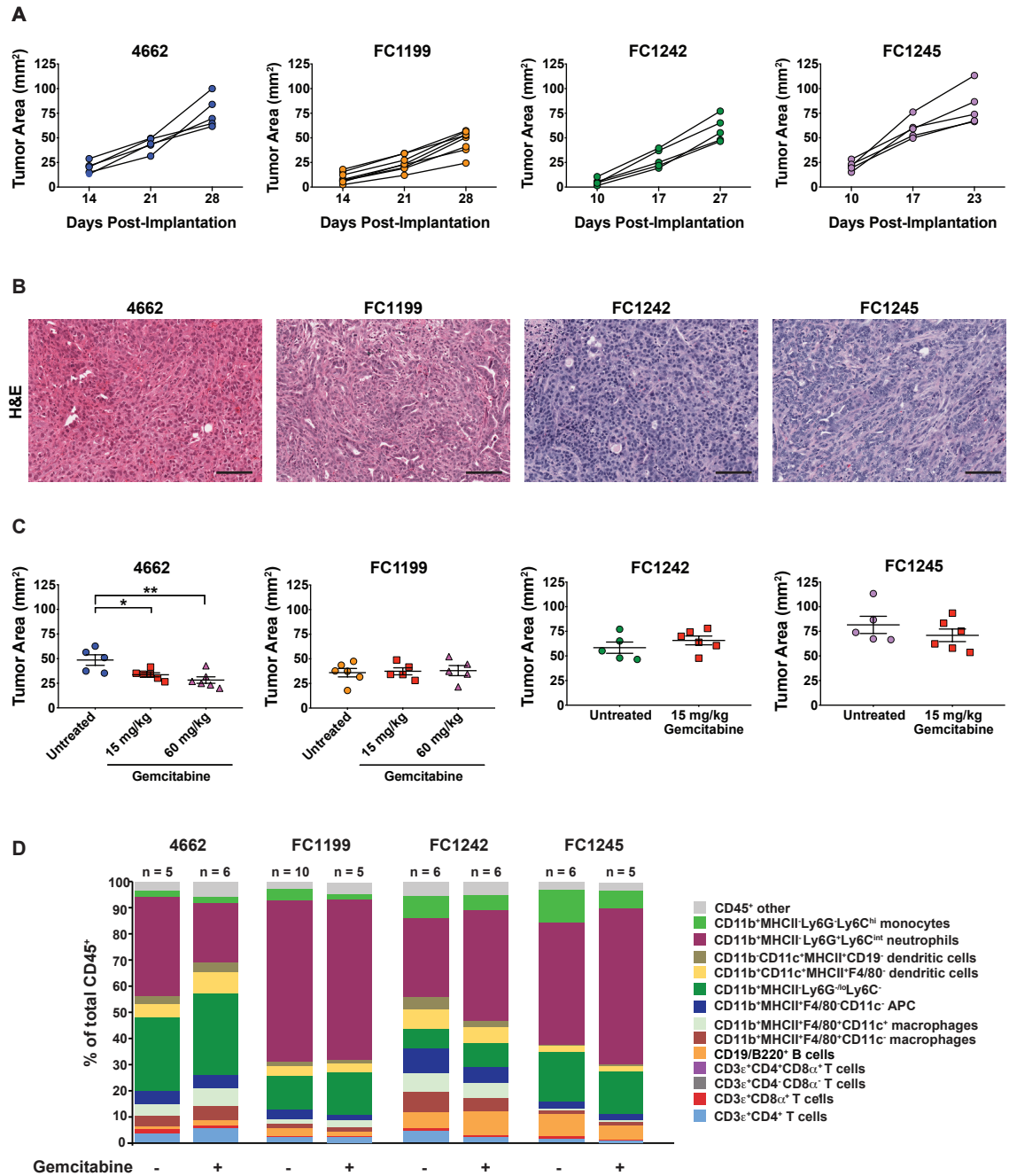


Figure 3.3 Tumor growth kinetics, chemoresponsiveness, and immune complexity of orthotopically implanted C57BL/6 PDACs. (A) Tumor areas of PDAC tumors derived from indicated primary PDAC cell lines, measured longitudinally by ultrasound. (B) Representative histopathology of end-stage untreated tumors by H&E staining. Scale bars equal 100 μm . (C) End-stage tumor area of untreated mice compared to mice receiving 15 mg/kg or 60 mg/kg gemcitabine, as indicated. 4662, FC1199, and FC1242 tumor-bearing animals received gemcitabine i.v. on days 18, 22, and 26 post-tumor implant, and FC1245 tumor-bearing animals received gemcitabine on days 18 and 22. Each data point represents one mouse. Statistical significance was determined by unpaired t-test for comparison of two groups, or by one-way ANOVA for comparison of three groups. (D) Leukocyte composition of untreated and gemcitabine-treated end-stage tumors as measured by flow cytometry and identified using the lineage markers indicated (right). Data in each bar segment represents mean subpopulation frequency as a percent of viable CD45⁺ leukocytes.

RTX and GA101 as monotherapy and in combination with chemotherapy

Given the overall similarities in tumor kinetics, chemo-responsiveness, and immune profile of 4662 tumors to our established FVB/n PDAC models (**Figure 3.1** and **Supplemental Figure 3.2**), we selected this cell line for continued use in α CD20 therapeutic studies. Prior to initiating α CD20 mAb treatment in hCD20 Tg^{+/+} mice, we first confirmed that tumor growth was equivalent in hCD20 Tg^{+/+} and wild-type animals (**Figure 3.4A**). We also validated respective binding affinities of RTX and GA101 prior to *in vivo* administration (**Figure 3.4B**). Consistent with previous reports, level of GA101 binding to human Raji cells at saturating antibody concentrations was approximately half that of RTX, which is a characteristic feature of type II antibodies [181, 183].

We next sought to determine optimal *in vivo* doses of RTX and GA101 to achieve maximal B cell depletion in the periphery and in tissues, including orthotopic pancreatic tumors. Beginning at day 10 post-tumor implant and every 7 days thereafter until end point, GA101, RTX, or isotype control was administered i.p. at either 10 mg/kg or 30 mg/kg (**Figure 3.4C**). We did not observe slowed tumor growth or tumor regression in GA101 or RTX-treated mice as compared to isotype-treated tumor-bearing controls (**Figure 3.4C**), and therefore evaluated end-stage tumor, spleen, and blood to assess frequency of mAb-resistant B cells that could be mediating progressive tumor growth. Flow cytometry evaluation of CD19⁺ B cells revealed significant B cell reduction in all tissues from GA101 and RTX treatment groups at both doses tested (**Figure 3.4D**), indicating superior overall depletion with both human α CD20 mAbs as compared to the

murine α CD20 mAb used in prior studies (**Figure 3.2B**). Immunohistochemical staining of tumor and spleen tissue sections for the B cell identification marker B220 corroborated these flow cytometry data (**Figure 3.4E-F**), although B220⁺ cells were still clearly detectable in spleen, particularly in RTX-treated mice (**Figure 3.4E**).

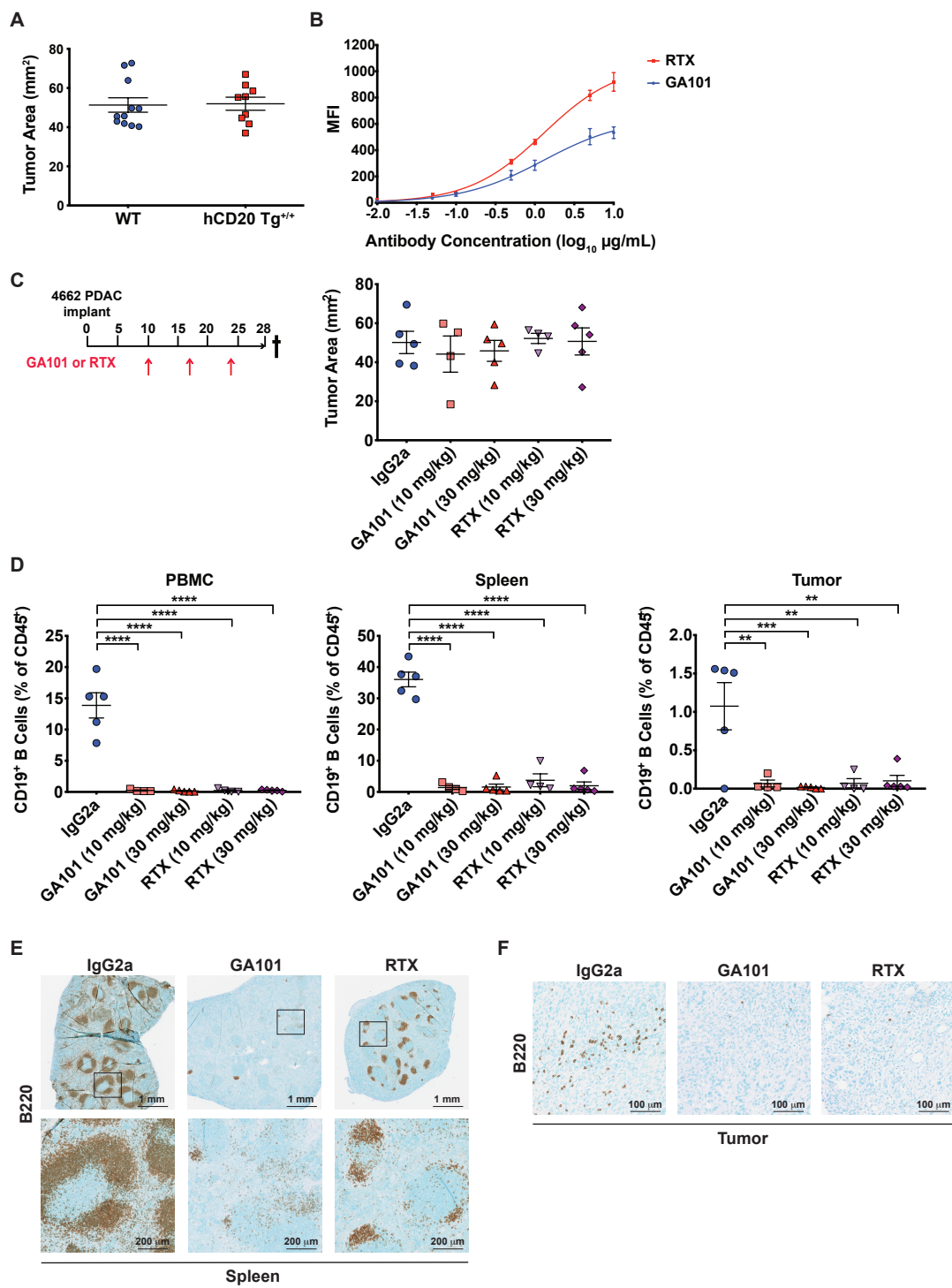


Figure 3.4 GA101 and RTX treatment induces significant B cell depletion in blood, spleen, and tumors. (A) End-stage tumor area of orthotopic 4662 PDAC tumors implanted into either wild-type C57BL/6 or hCD20 Tg^{+/+} mice. (B) In vitro antibody binding-assay comparing GA101 and RTX binding to cultured Raji cells at mAb concentrations indicated. Raji cells were incubated in either GA101 or RTX for 30 minutes followed by staining with PE-conjugated secondary IgG. Mean fluorescence intensity (MFI) of PE signal was determined by flow cytometry. Conditions were tested in triplicate and data shown represent average MFI. (C) End-stage tumor area of 4662 orthotopic PDAC tumors from mice treated as indicated in the treatment schematic (left) with GA101 or RTX at 10 mg/kg or 30 mg/kg on days 10, 17, and 24 post-tumor implant. (D) Flow cytometric evaluation of CD19⁺ B cell frequency in peripheral blood (left), spleen (middle), and tumor (right) of mice in the indicated treatment groups at day 28 end point. Statistical significance was determined by one-way ANOVA. (E) Representative images of B220 staining of spleen isolated from orthotopic tumor-bearing mice at end stage, following treatment with 10 mg/kg doses of either IgG2a, GA101, or RTX. Squares in top images indicate regions shown at higher magnification below. (F) Representative images of B220 staining of end-stage tumors from mice treated as in (E).

Phenotyping of splenic B cells revealed that the majority of remaining B cells in GA101 and RTX groups were CD19⁺ CD93⁺ transitional cells, CD19⁺ CD21^{lo} CD23⁻ IgD⁺ follicular cells, and CD19⁺ CD21⁻ CD23⁻ IgD⁻ memory cells, whereas CD19⁺ CD5⁺ CD1d⁺ Bregs were relatively infrequent (< 3% of total CD19⁺ B cells) (**Figure 3.5**).

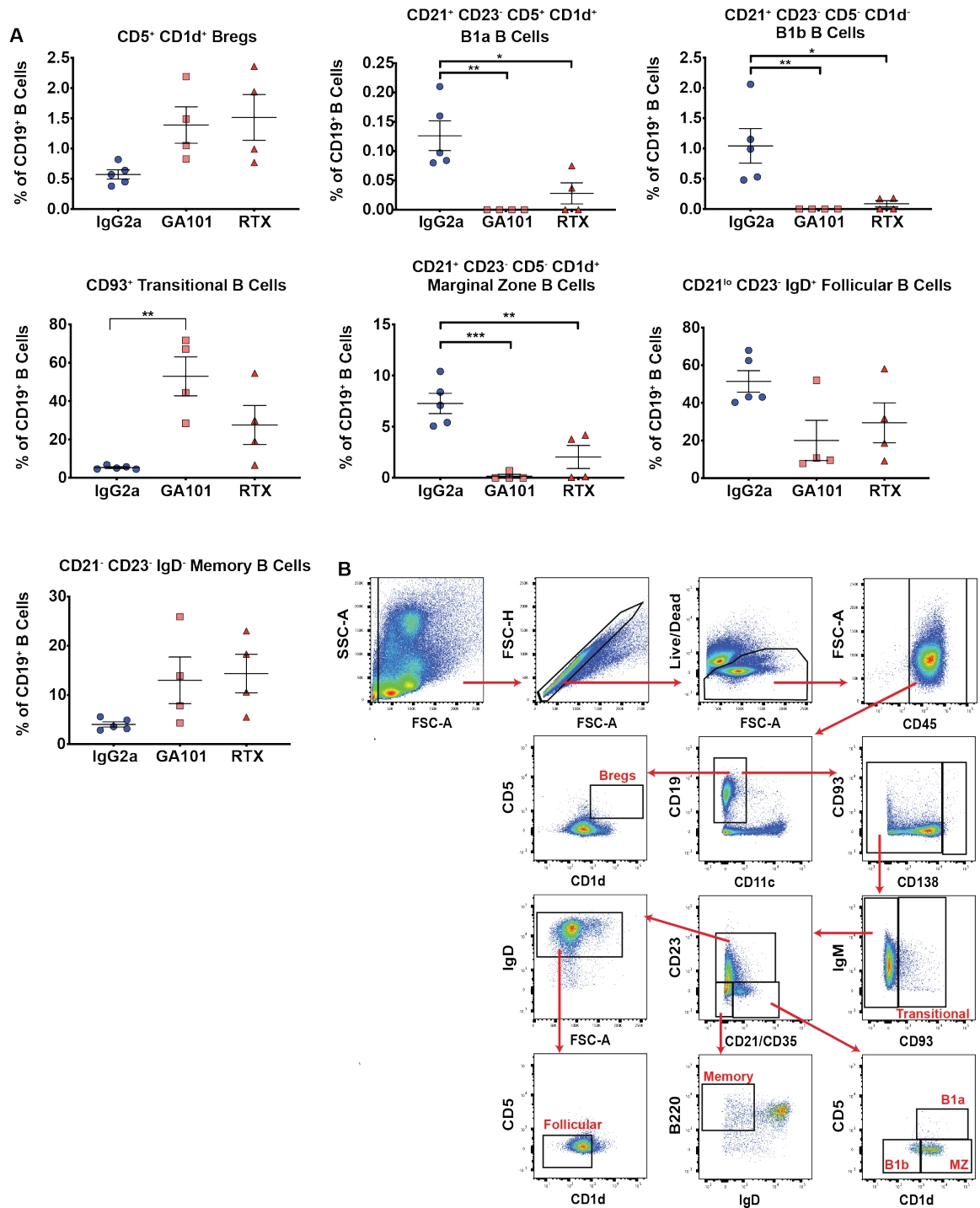


Figure 3.5 GA101 and RTX-resistant B cells in spleen are comprised of multiple B cell subpopulations. (A) Flow cytometry quantification of the indicated splenic B cell populations from tumor-bearing mice following a full course of α CD20 mAb therapy. Data are displayed as percentage of total CD19⁺ B cells. Each data point represents one mouse, $n = 4$ -5/group. Significance was assessed by one-way ANOVA. (B) Flow cytometry gating strategy used to identify B cell subpopulations evaluated in (A).

Although various subpopulations of B cells are capable of secreting IL-10 and other immunosuppressive cytokines in a context-dependent manner [193], low frequency of total intratumoral B cells and of a CD5⁺ CD1d⁺ Breg population in GA101 and RTX-treated spleens led us to hypothesize that mAb-resistant B cells may not be primary mediators of progressive tumor growth in this context. In SCC, we reported that α CD20 *monotherapy* delays tumor growth in mice receiving treatment prior to tumor inoculation but not in mice receiving α CD20 after SCCs are well established [175]. However, combination treatment with α CD20 and chemotherapy significantly enhanced anti-tumor response in established SCCs compared to α CD20 monotherapy [175]. Based on these results, we reasoned that combining α CD20 mAb therapy with cytotoxic chemotherapy could similarly enhance therapeutic efficacy in the context of established PDAC.

To test this hypothesis, we initiated GA101 or RTX treatment and confirmed peripheral B cell depletion prior to beginning the gemcitabine chemotherapy cycle (**Figure 3.6A-B**). Combination GA101/gemcitabine treatment delayed end-stage tumor growth significantly as compared to GA101 monotherapy, but neither GA101 nor RTX in combination with gemcitabine enhanced response compared to gemcitabine alone (**Figure 3.6C**). To determine whether CD8⁺ T cell exclusion from tumors or limited T cell cytotoxic function might underlie apparent lack of synergy between α CD20 and gemcitabine, we quantified intratumoral CD8⁺ T cells in tumor single cell suspensions by flow cytometry (**Figure 3.6D**) and observed no significant difference in their abundance across treatment groups. The majority of intratumoral CD8⁺ T cells in all treatment arms were positive for the immune checkpoint molecule programmed cell death ligand-1 (PD-

1) (**Figure 3.6E**). PD-1 is expressed following T cell activation, but sustained expression of PD-1 can also be indicative of T cell exhaustion [194]. Only a limited percentage (< 12%) of PD-1⁺ CD8⁺ T cells co-expressed Granzyme B or CD107a (**Figure 3.6F-G**), reflecting that a minority of these T cells were engaging in cytotoxic function within the tumor microenvironment.

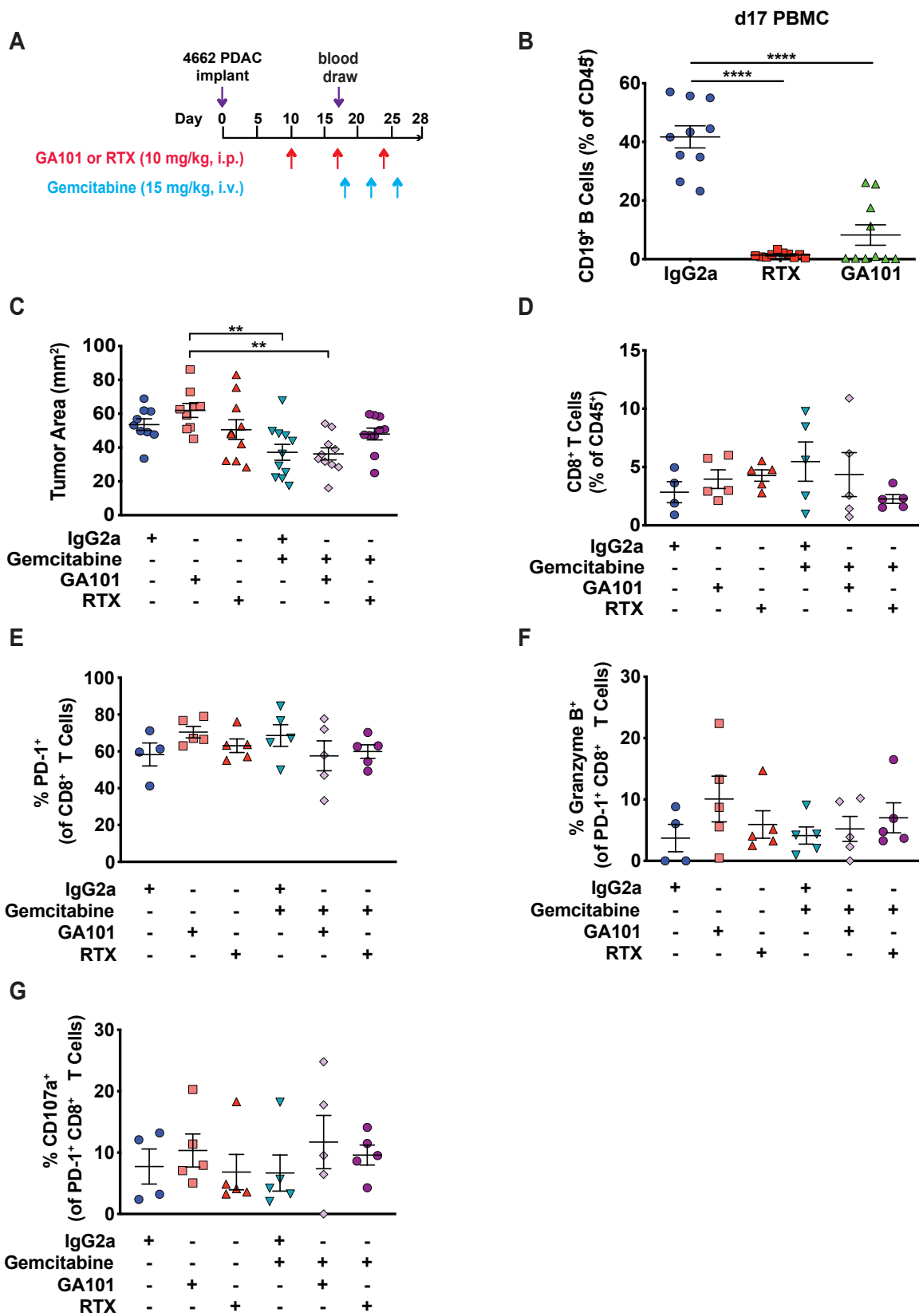


Figure 3.6 Combination α CD20 mAb and gemcitabine therapy does not improve antitumor response. (A) Schema for therapeutic administration of GA101 or RTX (10 mg/kg i.p., beginning on day 10) and gemcitabine (15 mg/kg i.v., beginning on day 18). (B) Frequency of circulating CD19⁺ B cells one week following first dose of GA101 or RTX as assessed by flow cytometry. (C) End-stage tumor areas from indicated treatment groups as measured by ultrasonography. Data from 2 independent experiments are shown. n = 4-5/group per experiment (D) Percentage of intratumoral CD3⁺ CD8⁺ T cells at day 28 end point as determined by flow cytometry. (E) Percentage of intratumoral PD-1⁺ cells of CD8⁺ T cells at end-stage by flow cytometry analysis. (F-G) Frequency of Granzyme B⁺ and CD107a⁺ cells out of intratumoral PD-1⁺ CD8⁺ T cells. Statistical significance was determined by one-way ANOVA.

Addition of checkpoint inhibition does not improve α CD20 efficacy or alter intratumoral T cell cytotoxicity

Given that a large proportion of intratumoral CD8⁺ T cells were PD-1⁺ in all treatment groups, we hypothesized that addition of an antagonist α PD-1 mAb to the α CD20/gemcitabine treatment regimen might enhance anti-tumor T cell functionality and lead to reduced tumor burden. Contrary to this prediction, combination of RTX with α PD-1 (with or without gemcitabine) revealed no therapeutic efficacy as compared to isotype controls (**Figure 3.7A-C**). Similarly, combinations of GA101, α PD-1, and gemcitabine failed to significantly impact tumor burden (**Figure 3.8A-C**).

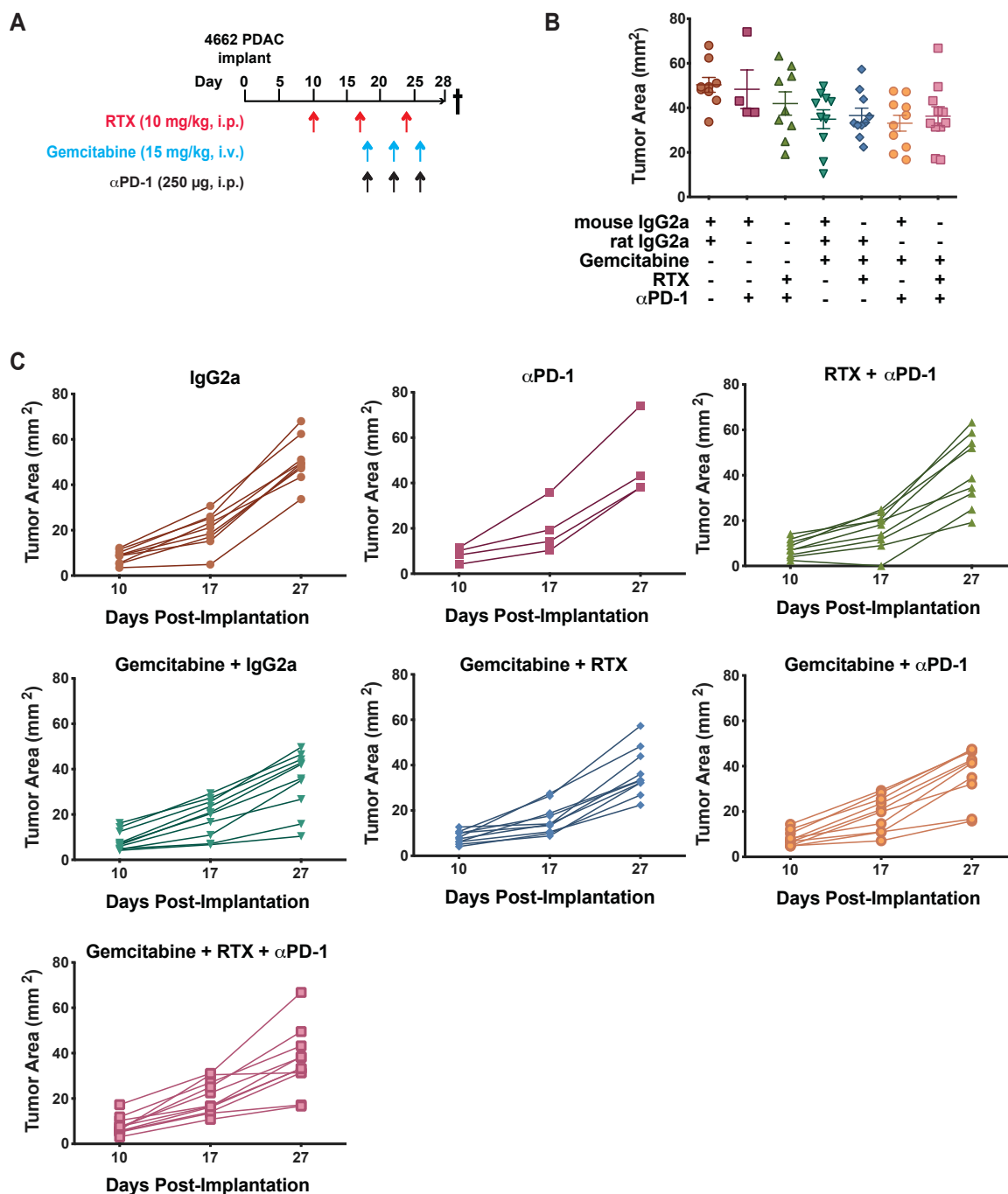


Figure 3.7 Addition of αPD-1 mAb does not enhance therapeutic efficacy of RTX and gemcitabine. (A) Schema depicting combinatorial treatment with RTX (10 mg/kg i.v., beginning at day 10), and concurrent administration of gemcitabine (15 mg/kg i.v.) and αPD-1 (250 μg i.p.) on days 18, 22, and 26. **(B)** End-stage tumor area as measured by ultrasonography for the indicated treatment groups. Data shown are from 2 independent experiments. n = 4-5/treatment group per experiment. Statistical significance was assessed by one-way ANOVA. **(C)** Longitudinal tumor growth as measured by ultrasonography on days 10, 17, and 27 post-implant in the treatment groups indicated.

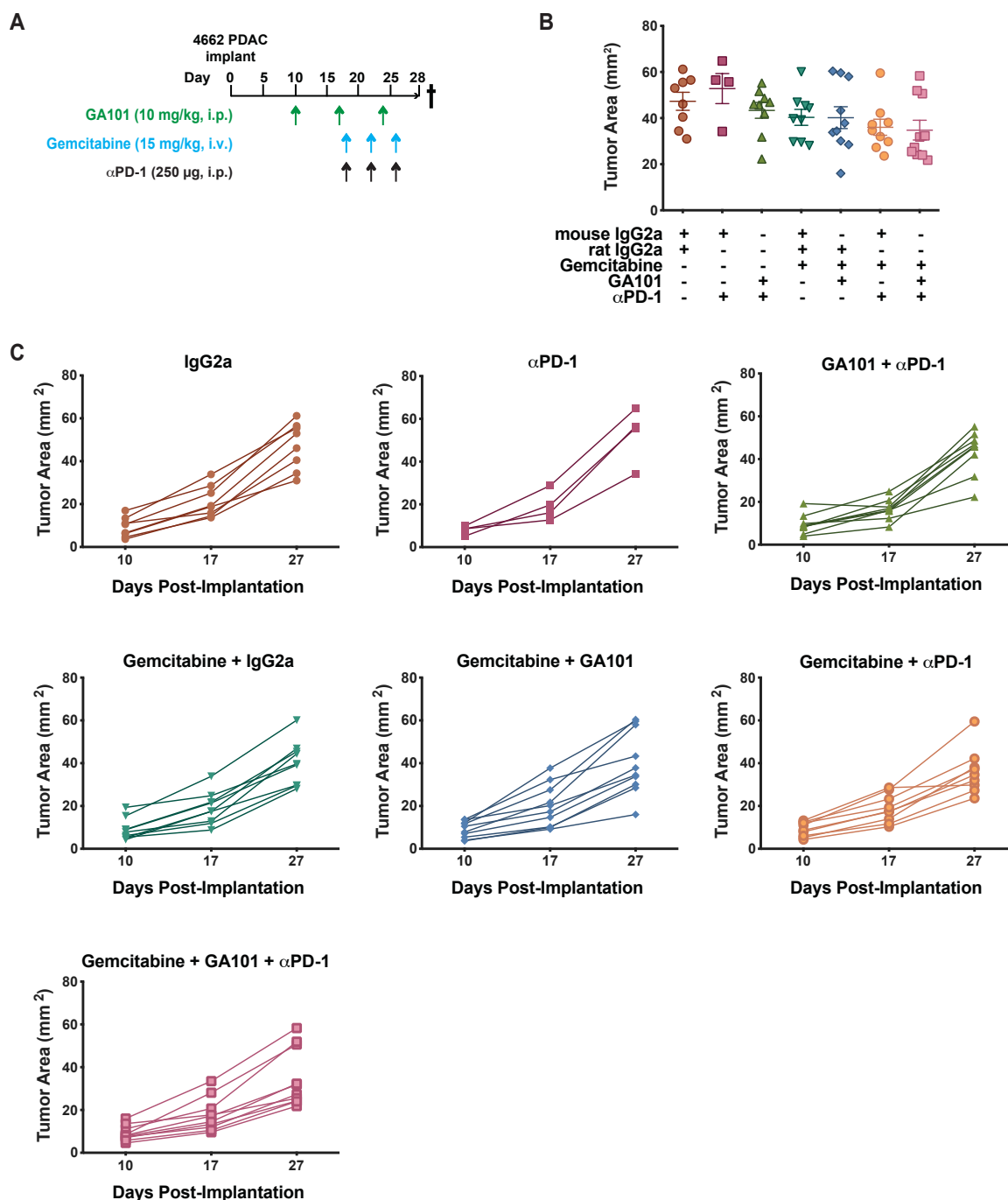


Figure 3.8 Addition of αPD-1 mAb does not enhance therapeutic efficacy of GA101 and gemcitabine. (A) Schema depicting combinatorial treatment with GA101 (10 mg/kg i.v., beginning at day 10), and concurrent administration of gemcitabine (15 mg/kg i.v.) and αPD-1 (250 μg i.p.) on days 18, 22, and 26. (B) End-stage tumor area as measured by ultrasonography for the indicated treatment groups. Data shown are from 2 independent experiments. $n = 3-5$ /treatment group per experiment. Statistical significance was assessed by one-way ANOVA. (C) Longitudinal tumor growth as measured by ultrasonography on days 10, 17, and 27 post-implant in the treatment groups indicated.

To determine whether the tumor immune microenvironment was impacted by triple combination therapy, we profiled immune populations by flow cytometry in end-stage tumors. B cells were significantly depleted in tumors of mice receiving either RTX or GA101, but frequency of total CD45⁺ immune cells was unchanged in any group as compared to isotype control (**Figure 3.9A**). Intratumoral MHCII⁺ CD11b⁺ Ly6C^{int} Ly6G⁻ monocytes were significantly reduced in most groups receiving gemcitabine as compared to isotype controls, which is in line with other reports indicating decreased monocyte frequency in tissues following gemcitabine treatment [195-197]; however, dendritic cell, macrophage, and neutrophil frequencies were equivalent in all treatment groups (**Figure 3.9A**). We also evaluated T cells and observed significant increases in total CD3⁺ T cells in the gemcitabine/ α PD-1 dual therapy group and the GA101/gemcitabine/ α PD-1 triple therapy arm, and trending increases in all other α PD-1 combination arms as compared to isotype only controls (**Figure 3.9B**). This was consistent with trending increases in CD8⁺ T cells in α PD-1 arms and significant or trending increases in CD4⁺ T cells in the same treatment groups, which were unattributable to increases in CD4⁺ Foxp3⁺ T regulatory cells. Collectively, these data reveal that α PD-1 therapy enhances T cell recruitment to and/or retention within orthotopic PDAC tumors.

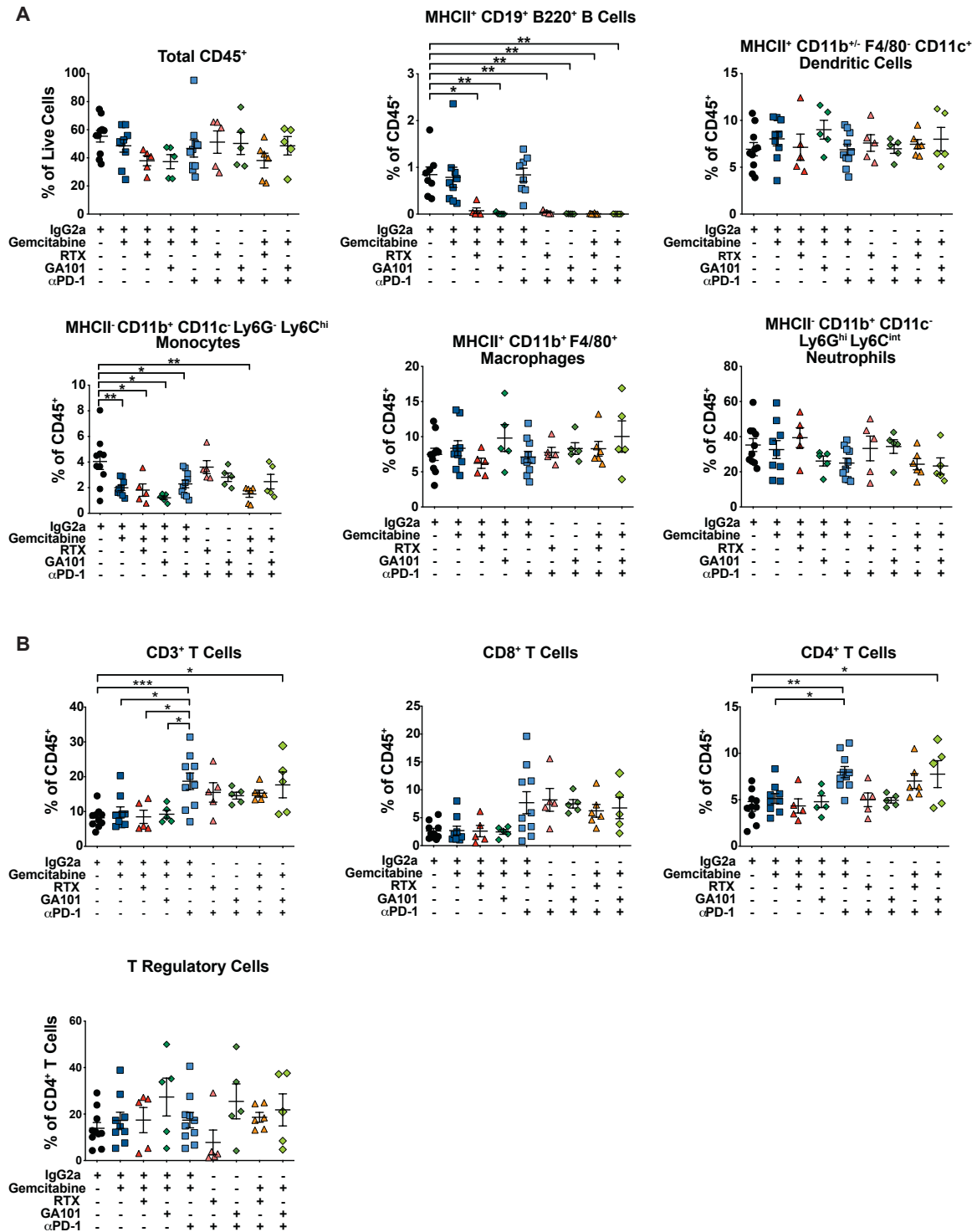


Figure 3.9 α PD-1 combination therapy is associated with increased intratumoral T cells but does not modulate myeloid frequencies. Flow cytometric analysis of total intratumoral CD45⁺ immune cells, B cells, myeloid lineages (A) and T cell populations (B) at day 28 end-stage from a subset of mice shown in Figure 3.7 and Figure 3.8. Significance was determined by one-way ANOVA.

Despite increases in T cell abundance with α PD-1 therapy, we predicted that T cell antitumor functionality was not significantly improved in any of the treatment arms, given unchanged tumor burden (**Figure 3.7, Figure 3.8**). Assessment of CD62L and CD44 cell surface expression on CD8⁺ T cells revealed that the majority of CD8⁺ T cells in all groups were CD44⁺ CD62L⁻, indicative of an effector memory subtype (**Figure 3.10A**). We then evaluated PD-1 and eomesodermin (EOMES) on CD44⁺ CD62L⁻ CD8⁺ T cells and found that the largest subgroups across all treatment arms were PD-1⁻ EOMES⁺ and PD-1⁺ EOMES⁺, characteristic of late effector/memory cells and exhausted cells, respectively (**Figure 3.10B**). Surprisingly, PD-1⁺ EOMES⁺ frequency was significantly decreased in all groups receiving α PD-1 mAb except for the RTX/gemcitabine/ α PD-1 group, and was concomitant with increases in the PD-1⁻ EOMES⁺ cell fraction. While these results indicated skewing from a potentially dysfunctional/exhausted state to an effector phenotype in CD8⁺ T cells of mice receiving α PD-1 combinations, CD8⁺ T cells did not exhibit increased expression of Granzyme B, CD107a, or Ki-67 (**Figure 3.10C-D**), indicating no enhancement in cytotoxicity or proliferation, and providing an explanation for the progressive tumor growth observed in all treatment groups.

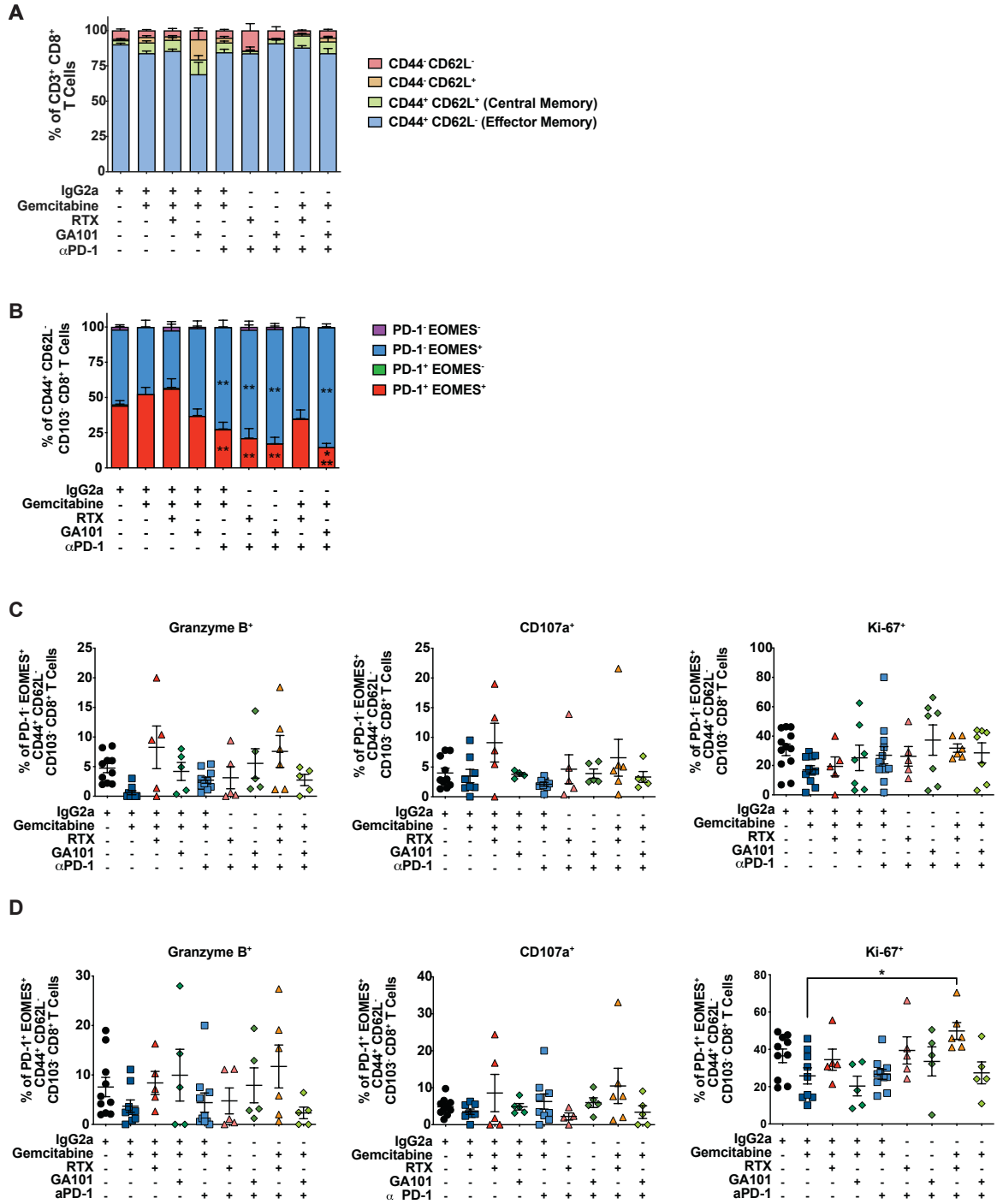


Figure 3.10 CD8⁺ T cell cytotoxicity and proliferation are not enhanced through combination therapy. (A) Flow cytometric assessment of CD44 and CD62L expression on CD103⁺ CD8⁺ T cells in end-stage PDACs from mice shown in Figure 3.9. (B) PD-1 and EOMES expression on CD44⁺ CD62L⁻ CD103⁺ CD8⁺ T cells in end-stage PDAC from mice in treatment groups shown. (C-D) Frequency of Granzyme B, CD107a, and Ki-67 positive cells in PD-1⁻ EOMES⁺ and PD-1⁺ EOMES⁺ subpopulations from (B). Statistical significance was determined by one-way ANOVA.

Discussion

Immunotherapies have transformed treatment of numerous malignancies, but effectively harnessing the potential of immunotherapy in PDAC remains a clinical hurdle. Several types of immunotherapies evaluated thus far in human PDAC have failed to yield significant clinical improvements, with the exception of α PD-L1 treatment in a small subset of patients with micro-satellite instability (MSI) high tumors that are predicted to have high levels of neoantigens to which T cells may respond [104]. Moving forward, it will be critical to identify rational combinations of immunotherapies and standard-of-care chemo- and radiotherapies that can target multiple facets of the immunosuppressive PDAC TME.

We and others recently identified B cells as important regulators of PDAC progression in preclinical murine models [111-113]. B cell-targeted therapies, such as α CD20 mAbs, are already a mainstay in the treatment of B cell malignancies and autoimmune diseases, and we hypothesized that α CD20 mAbs may also be effectively translated to PDAC. Herein, we provide evidence that neither murine α CD20 mAb treatment, nor treatment with human α CD20 mAbs RTX or GA101 as monotherapy or in combination with gemcitabine confer significant reduction in PDAC growth in murine models. Furthermore, human α CD20 mAb therapy did not sensitize PDACs to α PD-1 or augment CD8⁺ T cell cytotoxicity.

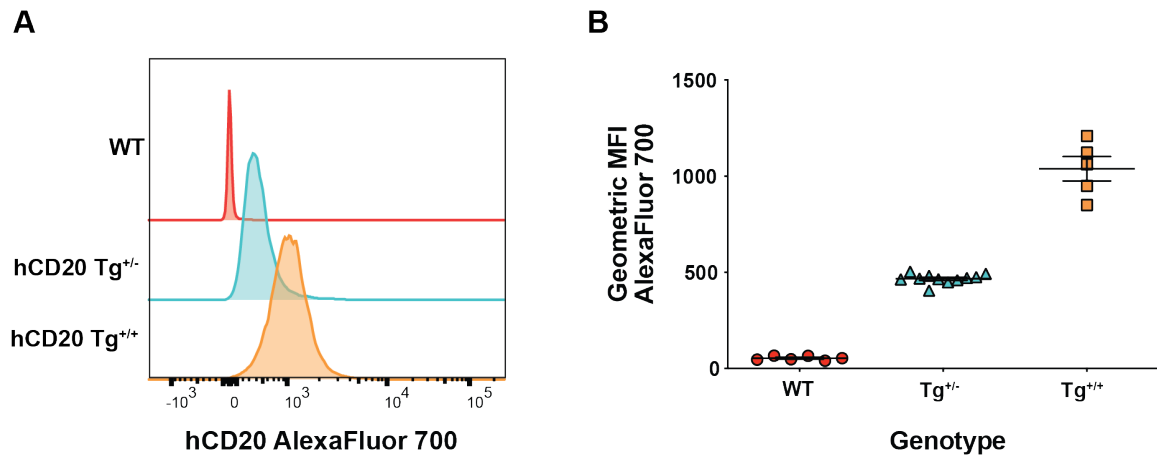
Lack of observed efficacy in the evaluated α CD20 mAb combinations likely has multiple underlying causes. We found that B cells resistant to murine α CD20 mAb therapy in FVB/n mice can rescue PDAC growth when adoptively transferred into syngeneic JH^{-/-} mice, underscoring incomplete B cell depletion as a significant aspect of murine α CD20 mAb failure. Although GA101 and RTX treatment in hCD20 Tg^{+/+} mice resulted in robust B cell depletion in the periphery and in tissues at both mAb doses tested, we still detected low levels of mAb-resistant B cell populations following these treatments, particularly in spleen. It is unclear precisely if and how these GA101 and RTX-resistant splenic B cells may contribute to tumor progression, but it is possible that they could be sources of immunosuppressive soluble factors (e.g. IL-10, IL-35) and/or Igs that may reinforce protumoral myeloid functions in the tumor through pathways we have previously identified [111, 175]. Indeed, others have reported detectable levels of IL-10 and IL-35 from splenic B cells of tumor-bearing KPC mice [198]. Examining the transcriptional profiles of the various residual splenic B cell populations could help determine whether these cells are likely to be blunting therapeutic efficacy. In addition, it has been reported that peritoneal B cells are also strongly resistant to murine α CD20 mAb therapy [177], and Ig-producing plasma cells do not express CD20 and are thereby spared from α CD20 mAb-induced depletion. These B cell populations were not evaluated in the present studies, but future interrogation of their frequency and functionality following α CD20 mAb treatment could be informative.

Our prior research in SCC and PDAC revealed significant interplay between humoral immunity and macrophage transcriptional programming, which ultimately regulates T

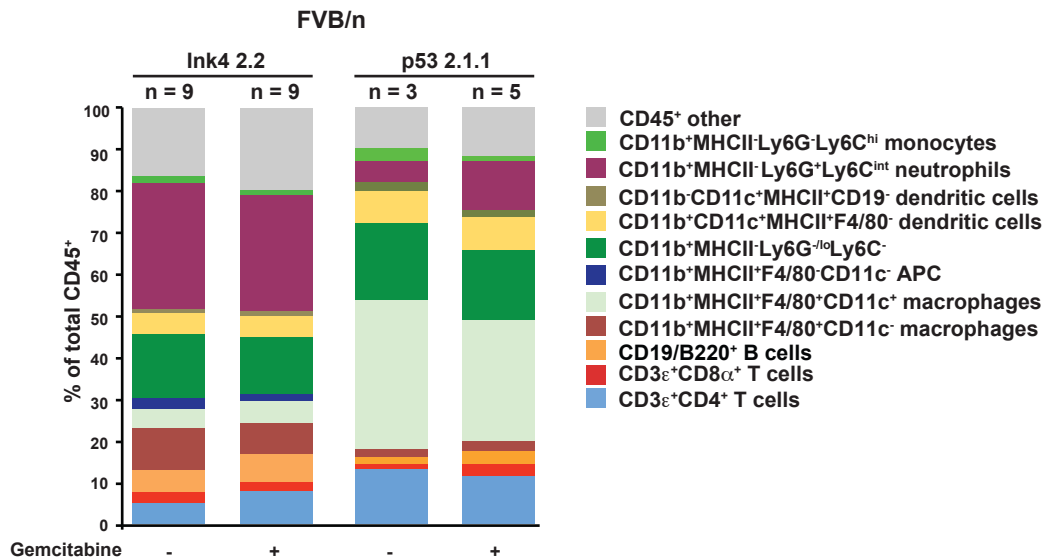
cell recruitment and function [111, 175]. It is also possible that mAb treatment is not sufficiently mediating Th1-skewing of intratumoral myeloid cells and is thus why we did not observe improved T cell functionality. Intratumoral macrophage frequencies were equivalent in all treatment groups, but transcriptional profiles were not evaluated.

Collectively, these results do not support clinical translation of α CD20 mAb in PDAC, although mechanism(s) of resistance to treatment remain to be fully elucidated. However, other approaches of targeting B cells in PDAC have clinical potential. Bruton's Tyrosine Kinase (BTK) inhibitors, including ibrutinib and acalabrutinib, block BTK pathway activation downstream of the B cell receptor, resulting in arrested B cell maturation and B cell death [199]. Importantly, BTK activation also occurs downstream of Fc γ R in myeloid cells, and when we treated late-stage PDAC-bearing mice with ibrutinib plus gemcitabine, we observed Th1-skewing of macrophages and dendritic cells, increased presence of intratumoral effector and memory CD8⁺ T cells, and significant tumor suppression [111]. These results highlight the potential importance of simultaneously impacting B cell and myeloid function in PDAC, whereas targeting B cells alone through mAb depletion is insufficient. Moreover, because we observed increased cytotoxic effector T cells in ibrutinib-treated mice, it is possible that BTK inhibitors may synergize with α PD-1 and/or co-stimulatory mAbs to further bolster antitumor T cell functionality.

Supplemental Data



Supplemental Figure 3.1 Genotyping of hCD20 Tg mice by flow cytometric analysis. (A) Representative histograms of hCD20 expression on CD45⁺ CD19⁺ B220⁺ peripheral B cells from hCD20 Tg^{+/-} and hCD20 Tg^{+/+} mice as compared to wild-type (WT) C57BL/6 control. (B) Geometric mean fluorescence staining intensity of hCD20 (conjugated to AlexaFluor 700 fluorophore) on B cells by flow cytometry. Genotype of hCD20 mice was determined by MFI distribution compared to known WT controls.



Supplemental Figure 3.2 Immune complexity of end-stage orthotopic Ink4 2.2 and p53 2.1.1 FVB/n PDAC tumors, as evaluated by flow cytometry in chemo-naïve and gemcitabine-treated mice.

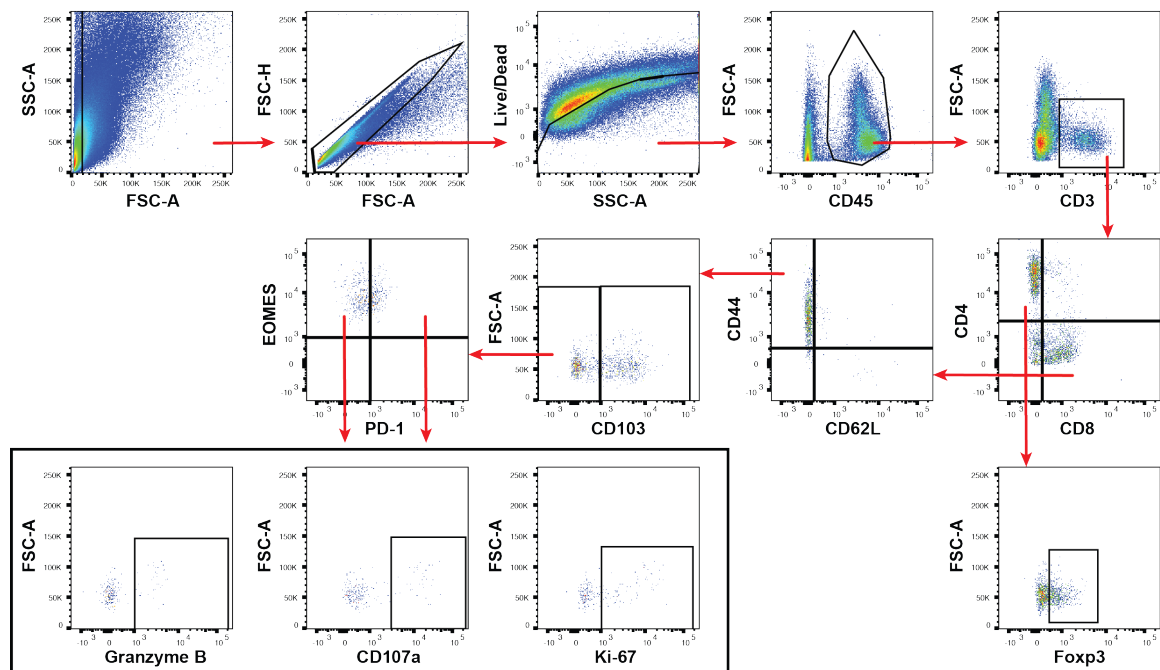
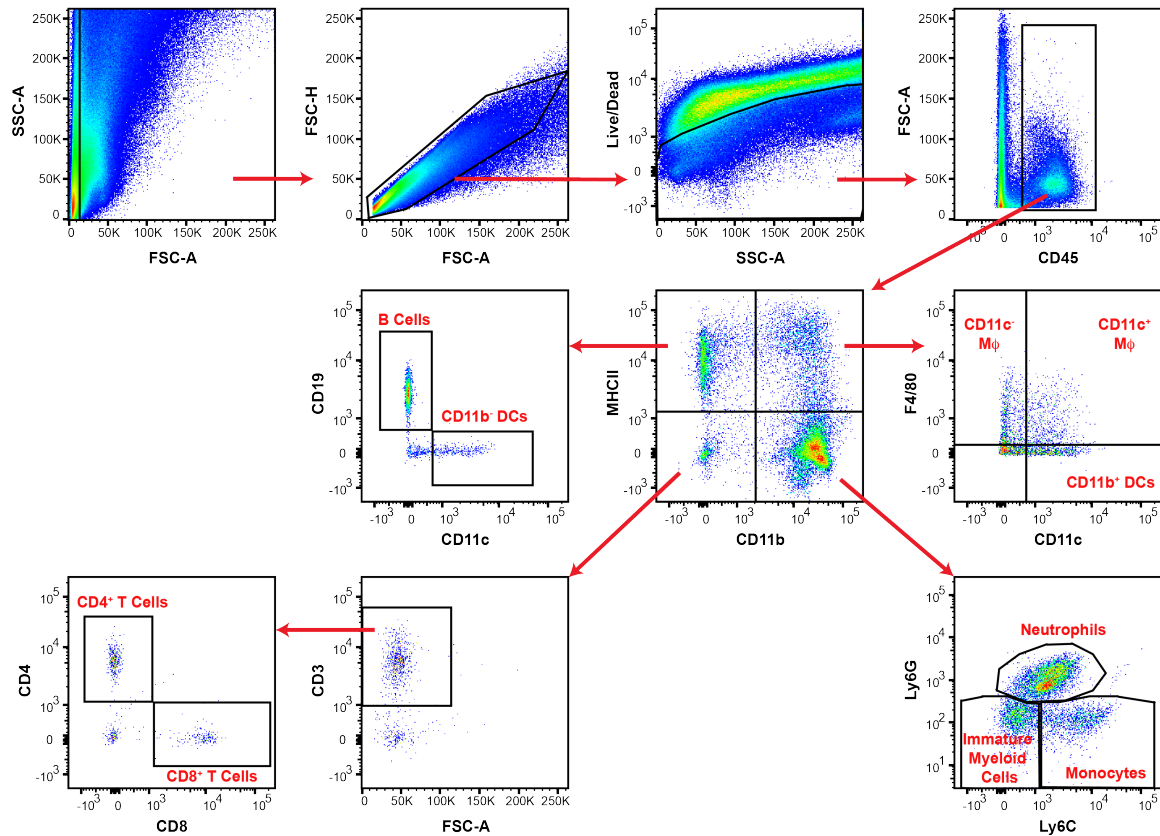


Table 3.1 Flow cytometry antibodies used for characterization of C57BL/6 PDAC immune complexity

Combined Myeloid & Lymphoid Panel				
Antibody	Clone	Concentration	Source	Catalog #
CD11b FITC	M1/70	1:200	BioLegend	101206
CD11c APC-eFluor780	N418	1:400	eBioscience	47-0114-82
CD16/32 Unconjugated	2.4G2	1:200	BD Pharmingen	553142
CD19 Brilliant Violet 650	6D5	1:400	BioLegend	115541
CD3 ϵ Brilliant Violet 786	17A2	1:200	BD Horizon	564010
CD4 Brilliant Violet 605	RM4-5	1:400	BD Horizon	563151
CD45 PE-Cy7	30-F11	1:4000	BD Pharmingen	561868
CD8 α Brilliant Violet 711	53-6.7	1:200	BD Horizon	563046
F4/80 APC	BM8	1:400	BioLegend	123116
Foxp3 PE	FJK-16s	1:200	eBioscience	12-5773-82
Live Dead Aqua		1:1000	Invitrogen	L34957
Ly6C PerCP	HK1.4	1:400	BioLegend	128028
Ly6G Alexa Fluor 700	1A8	1:400	BioLegend	127622
MHCII eFluor450	M5/114.15.2	1:1000	eBioscience	48-5321-82

Table 3.2 Flow cytometry antibodies used for α CD20 therapeutic studies

1. T Cell Phenotyping Panel				
Antibody	Clone	Concentration	Source	Catalog #
CD103 Brilliant Violet 605	2E7	1:100	BioLegend	121433
CD107a PE-Dazzle	1D4B	1:200	BioLegend	121624
CD16/32 Unconjugated	2.4G2	1:200	BD Pharmingen	553142
CD279 (PD-1) PE-Cy7	J43	1:400	eBioscience	25-9985-82
CD3 ϵ Brilliant Violet 786	17A2	1:200	BD Horizon	564010
CD4 PE	GK1.5	1:400	BioLegend	100408
CD44 Brilliant Violet 650	IM7	1:400	BioLegend	103049
CD45 APC-eFluor780	30-F11	1:1000	eBioscience	47-0451-82
CD62L Alexa Fluor 700	MEL-14	1:100	eBioscience	56-0621-82
CD8 α Brilliant Violet 711	53-6.7	1:200	BD Horizon	563046
EOMES PerCP-eFluor710	Dan11mag	1:100	eBioscience	46-4875-82
Foxp3 APC	FJK-16s	1:200	eBioscience	17-5773-82
Granzyme B eFluor450	NGZB	1:50	eBioscience	48-8898-82
Ki67 FITC	B56	1:10	BD Pharmingen	556026
Live Dead Aqua		1:1000	Invitrogen	L34957
2. Myeloid Panel				
Antibody	Clone	Concentration	Source	Catalog #
B220 Brilliant Violet 786	RA3-6B2	1:200	BD Horizon	563894
CD103 PE-CF594	M290	1:400	BD Horizon	565849
CD11b Brilliant Violet 711	M1/70	1:400	BD Horizon	563168
CD11c Brilliant Violet 605	N418	1:400	BioLegend	11734
CD16/32 Unconjugated	2.4G2	1:200	BD Pharmingen	553142
CD19 PerCP-Cy5.5	6D5	1:200	BioLegend	115534
CD274 (PD-L1) PE-Cy7	10F.9G2	1:200	BioLegend	124314
CD279 (PD-1) PE	J43	1:200	eBioscience	12-9985-82
CD45 FITC	30-F11	1:500	BD Pharmingen	553080
CD80 Brilliant Violet 650	16-10A1	1:200	BD Horizon	563687
CD86 Alexa Fluor 700	GL-1	1:200	BD Pharmingen	560581
F4/80 APC	BM8	1:200	BioLegend	123116
Live Dead Aqua		1:1000	Invitrogen	L34957
Ly6C PerCP	HK1.4	1:400	BioLegend	128028
Ly6G APC-Cy7	1A8	1:400	BioLegend	127624
MHCII eFluor450	M5/114.15.2	1:1000	eBioscience	48-5321-82
3. B Cell Phenotyping Panel				
Antibody	Clone	Concentration	Source	Catalog #
B220 Brilliant Violet 786	RA3-6B2	1:400	BD Horizon	563894
CD11c Brilliant Violet 605	N418	1:400	BioLegend	117334
CD138 PE	281-2	1:200	BD Pharmingen	553714
CD16/32 Unconjugated	2.4G2	1:200	BD Pharmingen	553142
CD19 Brilliant Violet 650	6D5	1:400	BioLegend	115541
CD1d Brilliant Violet 421	1B1	1:400	BD Horizon	562712
CD21/35 FITC	eBio4E3	1:400	eBioscience	11-0212-82
CD23 PE-Cy7	B3B4	1:400	eBioscience	25-0232-82
CD45 APC-eFluor780	30-F11	1:1000	eBioscience	47-0451-82
CD5 PerCP	53-7.3	1:400	BioLegend	100616
CD93 PE-eFluor594	AA4.1	1:200	BD Horizon	563805
huCD20 Alexa Fluor 700	2H7	1:400	BioLegend	302322
IgD Brilliant Violet 711	11-26c.2a	1:400	BioLegend	405731
IgM APC	II/41	1:400	eBioscience	17-5790-82
Live Dead Aqua		1:1000	Invitrogen	L34957

Chapter 4: B lymphocytes regulate tissue response to acute pancreatic injury but are dispensable for the establishment of chronic pancreatitis

Shannon M. Liudahl¹, Ruben Sanchez Flores Jr.², Meghan B. Lavoie¹, Kenna R. Leis¹,
Konjit Betre¹, and Lisa M. Coussens^{1,2,3,*}

¹Department of Cell, Developmental and Cancer Biology; Oregon Health and Science University; Portland, OR USA

²Knight Cancer Institute; Oregon Health and Science University; Portland, OR USA

³Brenden-Colson Center for Pancreatic Care; Oregon Health and Science University, Portland, OR, USA

*Corresponding Author:

Lisa M. Coussens, Ph.D.

Hildegard Lamfrom Chair in Basic Science

Professor and Chair, Department of Cell, Developmental, and Cancer Biology

Associate Director for Basic Research, Knight Cancer Institute

Oregon Health & Science University

2720 S.W. Moody Avenue

Mail Code KR-CDCB

Portland, OR 97201

Voice: 503-494-7811

Email: coussenl@ohsu.edu

This chapter is comprised of a manuscript in preparation for *The American Journal of Pathology*, to be submitted Fall 2019.

Abstract

Pancreatitis is an inflammatory disease of the exocrine pancreas that is associated with considerable morbidity and elevated risk of pancreatic cancer. Recurrent acute pancreatitis can lead to chronic fibroinflammatory pancreatitis, which is characterized by irreversible tissue damage and organ dysfunction. B cells have been reported to regulate neoplastic progression in the pancreas, but functional significance of B cells in pancreatitis remains unclear. Here, we report that B cells are recruited to the pancreas during experimental chronic and acute pancreatitis and have different roles in these two inflammatory contexts. We demonstrate that exocrine damage, leukocyte recruitment, and tissue fibrosis during early establishment of chronic pancreatitis are B cell-independent. In contrast, B-cell deficient mice exhibited accelerated pancreatic recovery following acute injury, implicating B cells as significant mediators of inflammation and tissue damage during acute pancreatitis. These data indicate potential for B cell-targeted therapies to mitigate tissue injury in patients suffering from recurrent acute pancreatitis.

Introduction

B cells are central mediators of humoral immunity and are important contributors to pathogen clearance and host defense through their roles in immunoglobulin (Ig) production, cytokine secretion, and antigen presentation. However, B cells are also appreciated to promote pathogenesis of several autoimmune diseases and some solid tumors [172, 200, 201]. We and others recently reported tumor promotional roles for B cells and downstream B cell-regulated signaling pathways in pancreatic ductal adenocarcinoma (PDAC) [111-113, 202]. These studies revealed multiple B cell subtypes

capable of supporting neoplastic progression via B cell secretion of pro-survival and immunosuppressive cytokines, as well as through induction of Th2-skewed myeloid transcriptional programs following binding of Ig-containing immune complexes to transmembrane Fc γ receptors (Fc γ Rs) on myeloid cells [17, 111]. Immune complex activation of Fc γ Rs leads to activation of spleen tyrosine kinase- (Syk) and Bruton's tyrosine kinase (BTK)-dependent signaling cascades implicated in proangiogenic, profibrotic, and T cell suppressive activities [174, 175]. Genetic deletion of B cells in murine models of PDAC slowed neoplastic progression and primary tumor growth [111, 112]. Moreover, therapeutic B cell depletion with α CD20 monoclonal antibody (mAb) slowed progression of pre-invasive neoplasia, and treatment of tumor-bearing mice with a small-molecule BTK inhibitor in combination with gemcitabine chemotherapy limited tissue fibrosis and relieved T cell suppression, resulting in slowed primary tumor growth and improved survival [201, 202]. Given these findings, we hypothesized that B cells might also be functionally significant mediators of acute and/or chronic pancreatitis onset or recovery from acute inflammatory tissue injury.

Pancreatitis is a leading cause of gastroenterological hospitalization in the United States [9]. Acute pancreatitis ranges from mild, self-limiting disease to severe necrotic disease associated with systemic organ failure [203]. Inflammation associated with acute onset pancreatitis typically resolves and the pancreas returns to a homeostatic state over a period of weeks. Chronic pancreatitis, however, is characterized by progressive tissue fibrosis, sustained inflammatory infiltration, acinar cell atrophy, and pancreatic enzyme insufficiency [13]. Current treatment strategies for chronic pancreatitis aim to improve

patient quality of life but are neither curative nor fully preventative with regards to ongoing tissue damage. Notably, sustained inflammation and tissue damage in patients with chronic pancreatitis enhance the relative risk of pancreatic cancer in this patient population [15, 17].

Pathogenesis of pancreatitis is rooted in recruitment of innate leukocytes and inflammation-associated tissue injury [37]. In acute pancreatitis, neutrophils are potent mediators of intra-acinar protease activation and are sources of reactive oxygen species that contribute to cellular damage [28, 30, 32, 33]. Macrophages also contribute to acute tissue injury through production of inflammatory cytokines and proteinases that promote acinar de-differentiation to a duct-like phenotype (acinar-to-ductal metaplasia; ADM), and they are significant regulators of fibrosis in chronic pancreatitis [40, 43].

Comparatively little has been reported on potential roles of the adaptive immune system during acute pancreatitis initiation or resolution, or during progressive chronic disease. A recent study demonstrated that B cell depletion enhanced tissue recovery in established chronic pancreatitis [204], but it remains unclear whether B cells also regulate the onset of chronic pancreatitis. Similarly, the role of B cells in acute pancreatitis initiation and recovery is unknown. To address these gaps, we investigated the functional significance of B cells in these temporal phases pancreatic damage and report herein that B cells are not significant regulators of chronic pancreatitis establishment in experimental mouse models, but do play a significant role in the resolution phase of acute pancreatitis.

Materials and Methods

Animal Studies

All animal experiments were performed in compliance with National Institutes of Health guidelines and were approved by the Oregon Health & Science University Institutional Animal Care and Use Committee. Generation and characterization of B cell-deficient (JH^{-/-}) and FcR γ -deficient ($\gamma^{-/-}$) mice has been previously described [174, 186, 187]. JH^{+/-} and FcR γ ^{+/-} were backcrossed a minimum of five generations into FVB/NJ (Stock No. 001800, The Jackson Laboratory, Bar Harbor, ME) and were housed in specific-pathogen-free facilities. 7 to 11 week old female JH and FcR γ mice were used for caerulein-induced pancreatitis. Acute pancreatitis was induced by seven hourly intraperitoneal (i.p.) injections of caerulein (50 μ g/kg body weight; Sigma-Aldrich, St. Louis, MO) for two consecutive days, and pancreata were harvested for analysis three and seven days following the final caerulein injection. Chronic pancreatitis was induced as previously described [26, 28], with minor modification: caerulein was administered i.p. at 0.23 mg/kg body weight once per day for 5 consecutive days, followed by two rest days, for up to four weeks. Pancreata were harvested one day following the final caerulein injection at indicated time points. All experiments were repeated at least twice with $n \geq 3$ per experimental group.

Histology & Pancreatic Damage Scoring

Pancreata were collected from PBS cardiac-perfused mice, and tissue was immediately transferred to 10% neutral-buffered formalin for overnight fixation. Following fixation, tissues were processed and paraffin embedding using standard protocols. Deparaffinized

5 μ m tissue sections were hematoxylin and eosin (H&E) stained using a Jung Autostainer XL (Leica Biosystems, Wetzlar, Germany). Masson's Trichrome staining was performed using the American MasterTech Masson Trichrome Stain Kit (#KTMTR, American MasterTech, Lodi, CA) according to manufacturer recommendations. Tissue damage scoring of caerulein pancreatitis tissues was performed on H&E slides by two independent reviewers blinded to mouse genotype and treatment group. Four randomly selected regions were evaluated per mouse using a scoring system adapted from Folias et al. [205]. Lobular integrity and acinar damage (de-differentiation and necrosis) were each scored from 0-3 for each region, and individual scores from these categories from every region were added to obtain a combined histology score (minimum combined score = 0, maximum combined score = 24). Scoring criteria are detailed in Supplemental Figure 4.1.

Immunohistochemistry

To identify proliferating cells by immunohistochemistry (IHC), mice received an i.p. injection of bromodeoxyuridine (BrdU; Roche, Basel, Switzerland) dissolved in PBS (50 mg/kg of mouse body weight) 90 minutes prior to sacrifice. For IHC staining, deparaffinized tissue sections were subjected to 20 minutes endogenous peroxidase blocking in 0.6% hydrogen peroxide in methanol and 15 minute heat-mediated antigen retrieval in 95°C Citra pH 6.0 solution (BioGenex Laboratories, Fremont, CA). Slides were cooled for 15 minutes, washed 3 x 2 minutes in PBS or TBST, and incubated in protein blocking buffer (5% normal goat serum (Gibco, Waltham, MA)/2.5% BSA (Fisher Scientific, Waltham, MA)/PBS (Gibco)) for 30 minutes. Tissues were incubated

in primary antibody diluted in 0.5X blocking buffer for 1.0 hour at room temperature, washed, and incubated in species-appropriate biontynlated secondary antibody for 30 minutes at room temperature. The following primary antibodies were used: rat anti-mouse BrdU (BU1/75 (ICR1), #MCA2060, 1:2000; Bio-Rad, Hercules, CA), rat anti-mouse CD45R/B220 (RA3-6B2, #550286, 1:500; BD Biosciences, San Jose, CA), rat anti-mouse CD45 (30-F11, #550539, 1:500; BD Biosciences), rabbit anti-mouse cleaved caspase-3 (polyclonal, #9661, 1:200; Cell Signaling Technology, Danvers, MA), rabbit anti-mouse Sox9 (polyclonal, #AB5535, 1:20,000; MilliporeSigma, Burlington, MA). Secondary antibodies used were: biotinylated anti-rabbit IgG (#BA-1000, 1:500; Vector Laboratories, Burlingame, CA) and biotinylated anti-rat IgG (#BA-9401, 1:500, Vector Laboratories). After secondary antibody staining and washing, slides were incubated for 30 minutes in ABC Elite horseradish peroxidase-conjugated avidin complex (Vector Laboratories), washed, and signal was developed with 3,3'-diaminobenzidine (Dako, Santa Clara, CA). Slides were counterstained with 0.01% methyl green, dehydrated, coverslipped with Permount medium (Fisher Scientific), and digitally scanned at 20X magnification on an Aperio Scanscope AT or AT2 slide scanner (Leica Biosystems). Quantification of immunohistochemical staining from caerulein pancreatitis experiments was performed on 18 total 300 x 300 μ m fields per slide using the Color Deconvolution v9 macro in Aperio ImageScope software (Leica Biosystems).

Flow Cytometry

Mice were cardiac perfused with PBS/heparin to clear circulating leukocytes prior to tissue collection. Pancreas single-cell suspensions were prepared as we have previously

reported [111]. Briefly, pancreata were finely minced with scissors, and tissue pieces were enzymatically digested for 15 minutes at 37°C with constant stirring in serum-free DMEM (Gibco) containing 1.0 mg/mL soybean trypsin inhibitor (Gibco), 1.0 mg/mL collagenase IV (Gibco), and 50 U/mL DNase I (Roche). Following digestion, cells were passed through a 100 µm mesh filter and washed with FACS buffer (PBS with 0.5% BSA and 2.0 mM EDTA), followed by a 5-minute centrifugation at 400 x g. To distinguish viable from dead cells, cells were incubated with Live/Dead Fixable Aqua stain (1:1000, Invitrogen) for 30 minutes on ice. Cells were centrifuged as before, then incubated for 30 minutes on ice with the following fluorescently-conjugated antibodies: CD3 (Brilliant Violet 785, clone 17A2, 1:100, BioLegend, San Diego, CA), CD4 (Brilliant Violet 605, clone RM4-5, 1:200, BioLegend), CD8α (PerCP-Cy5.5, clone 53-6.7, 1:200, BioLegend), CD11b (FITC, clone M1/70, 1:200, BioLegend), CD11c (APC-eFluor780, clone N418, 1:200, eBioscience, Waltham, MA), CD16/32 (PE, clone 93, 1:400, eBioscience), CD19 (Brilliant Violet 650, clone 6D5, 1:400, BioLegend), CD45 (PE-Cy7, clone 30-F11, 1:4000, eBioscience), CD64 (Brilliant Violet 711, clone X54-5/7.1, 1:400, BioLegend), F4/80 (APC, clone BM8, 1:400, BioLegend), Ly6C (PerCP, clone HK1.4, 1:400, BioLegend), Ly6G (Alexa Fluor 700, clone 1A8, 1:400, BioLegend), MHC Class II (eFluor450, clone M5/114.15.2, 1:1000, eBioscience). After staining, cells were fixed in BD Cytofix Buffer (BD Biosciences) for 15 minutes followed by a final wash in FACS buffer. Cells were stored in FACS buffer at 4°C until running on a BD Fortessa cytometer with FACSDiva software (BD Biosciences). Data were analyzed with FlowJo v10 software (FlowJo LLC, Ashland, OR).

Statistical Analysis

Statistical analyses were performed using GraphPad Prism 8 (GraphPad Software, San Diego, CA). Two-way ANOVA with Sidak multiple comparisons test was used for evaluation of two or more groups across multiple time points. The D'Agostino-Pearson test was used to evaluate normal distribution of samples in all experiments. When samples were not normally distributed, data were transformed using probit function prior to two-way ANOVA. Untransformed data are displayed for all figures, and data are presented with means \pm SEM. p values of < 0.05 were considered statistically significant, with * $p < 0.05$, ** $p < 0.01$, *** $p < 0.001$, and **** $p < 0.0001$.

Results

B cells are recruited to the pancreas following caerulein-induced acute injury and during chronic pancreatitis

To evaluate different phases of acute and chronic pancreatic inflammation, we employed established murine models of caerulein-induced pancreatitis [23]. Caerulein is a cholecystokinin analog that, when administered at supraphysiological levels, induces intrapancreatic protease activity, pancreatic edema, immune infiltration, and acinar de-differentiation and cell death [206]. When administered acutely, caerulein treatment results in an initial phase of inflammatory tissue damage that is followed by resolution and tissue regeneration within the course of several days [24, 39, 207]. Repeated caerulein treatment over multiple weeks promotes chronic inflammation and extensive tissue remodeling, including mild to moderate fibrosis, that reflect features also observed in human chronic pancreatitis [43].

Using these models, we first examined pancreas histopathology at multiple time points following acute caerulein administration and during establishment of chronic pancreatitis (**Figure 4.1A**). H&E-stained pancreata harvested three days after acute caerulein treatment exhibited expected morphologic indicators of damage, including acinar cell enlargement, increased interlobular and intralobular space, and acinar de-differentiation, which were moderately resolved by day 7 (**Figure 4.1A**). In addition to these observed exocrine changes, immunohistochemical staining for leukocyte common antigen (i.e. CD45) confirmed an increase in pancreatic leukocyte infiltration following caerulein treatment (**Figure 4.1A**). Notably, staining for the B cell marker B220 revealed that while

few B cells were typically present in homeostatic pancreas, acute insult resulted in B cell trafficking to inflamed pancreatic tissue (**Figure 4.1A**). Similar histopathologic features of tissue damage were observed in pancreata treated chronically with caerulein for two to four weeks (**Figure 4.1B**). As in acute pancreatitis, we observed B cell infiltration during chronic caerulein treatment (**Figure 4.1B**), supporting our hypothesis that B cells might be have significant function at one or more temporal stages of pancreatitis.

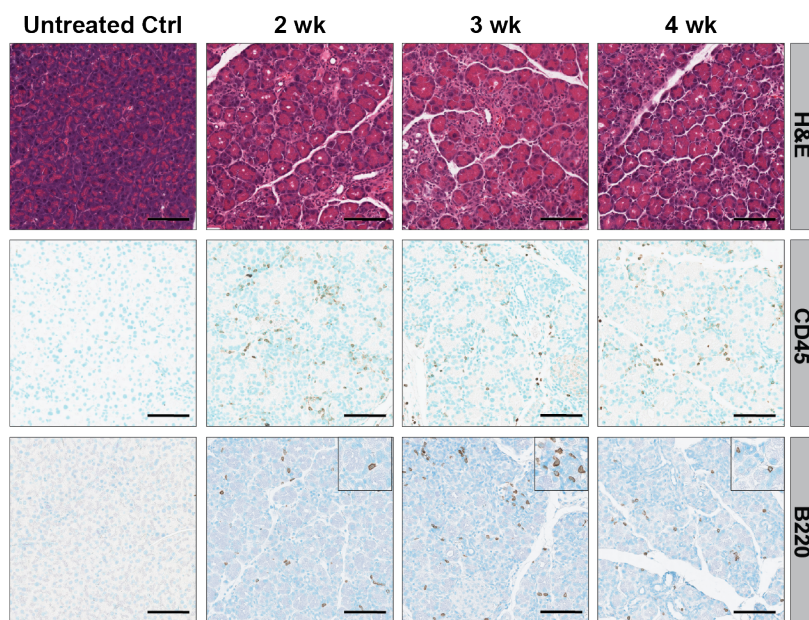
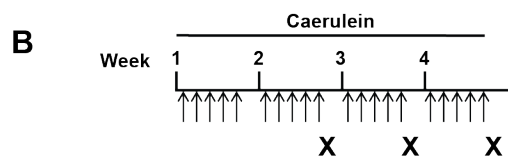
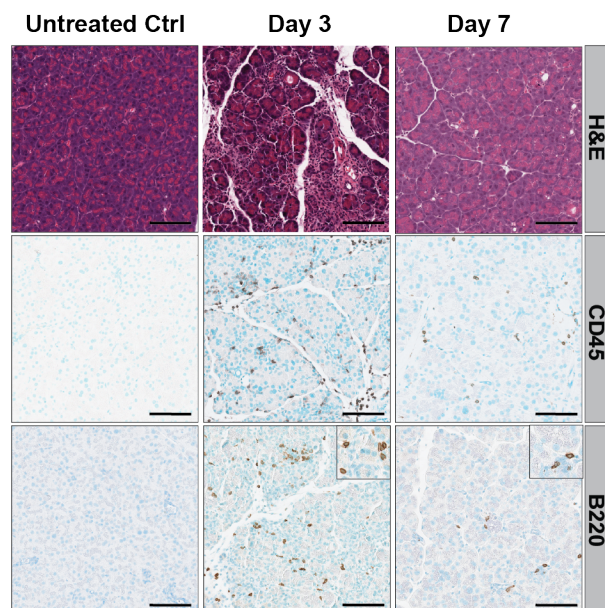
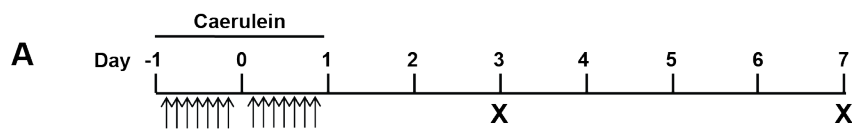


Figure 4.1 Treatment schematics and representative pathology of caerulein-induced acute and chronic pancreatitis. (A) Schema for acute caerulein pancreatitis in which mice were administered seven hourly i.p. injections of caerulein (50 µg/kg) for two consecutive days (denoted by arrows). Pancreas was harvested on Day 3 and Day 7 following final caerulein administration (indicated by X's). Representative images of pancreas stained with hematoxylin & eosin (H&E), CD45, and B220 from wild-type untreated baseline control or wild-type mice treated with caerulein. Pancreata of treated mice were harvested at indicated time points. (B) Schema for chronic caerulein pancreatitis in which mice were administered one 0.23 mg/kg dose of caerulein five days per week, followed by two rest days. Pancreata were harvested after the second, third, and fourth weeks of treatment (indicated by X's). Representative staining of pancreas with H&E and immunostaining for CD45 and B220 are shown from an untreated control and from wild-type caerulein-treated mice at indicated time points.

Establishment and maintenance of chronic pancreatitis is B cell-independent

We first sought to determine whether B cells regulated establishment of tissue damage during chronic pancreatitis. Caerulein was administered as previously indicated (**Figure 4.1B**) to mice lacking mature B cells ($JH^{-/-}$ mice) and to heterozygous $JH^{+/-}$ controls, and pancreata were examined at weekly intervals beginning at two weeks of treatment. We developed a histologic scoring system to evaluate pancreatic lobular integrity and acinar cell damage following caerulein treatment (see Methods and Supplemental Figure 4.1). Based on this scoring, tissue damage was confirmed to be elevated in both genotypes at all evaluated on-treatment time points as compared to respective pre-treatment baseline controls (**Figure 4.2A**); however, severity of damage was equivalent between genotypes (**Figure 4.2A**). Consistent with this, assessment of $CD45^{+}$ cells revealed that leukocyte abundance in $JH^{+/-}$ and $JH^{-/-}$ was comparable across time points (**Figure 4.2B**). To evaluate damage-induced acinar-to-ductal metaplasia (ADM), we evaluated expression of Sox9, an early pancreatic progenitor cell marker that is re-expressed in acini undergoing ADM [39, 56]. Using Sox9 positivity as an additional readout of tissue damage and remodeling, we observed > 5-fold increases in $Sox9^{+}$ cells that were maintained throughout the treatment course in both $JH^{+/-}$ and $JH^{-/-}$ mice (**Figure 4.2C**). Mild tissue fibrosis was also evident during caerulein treatment and was similar in both genotypes (**Figure 4.2D**).

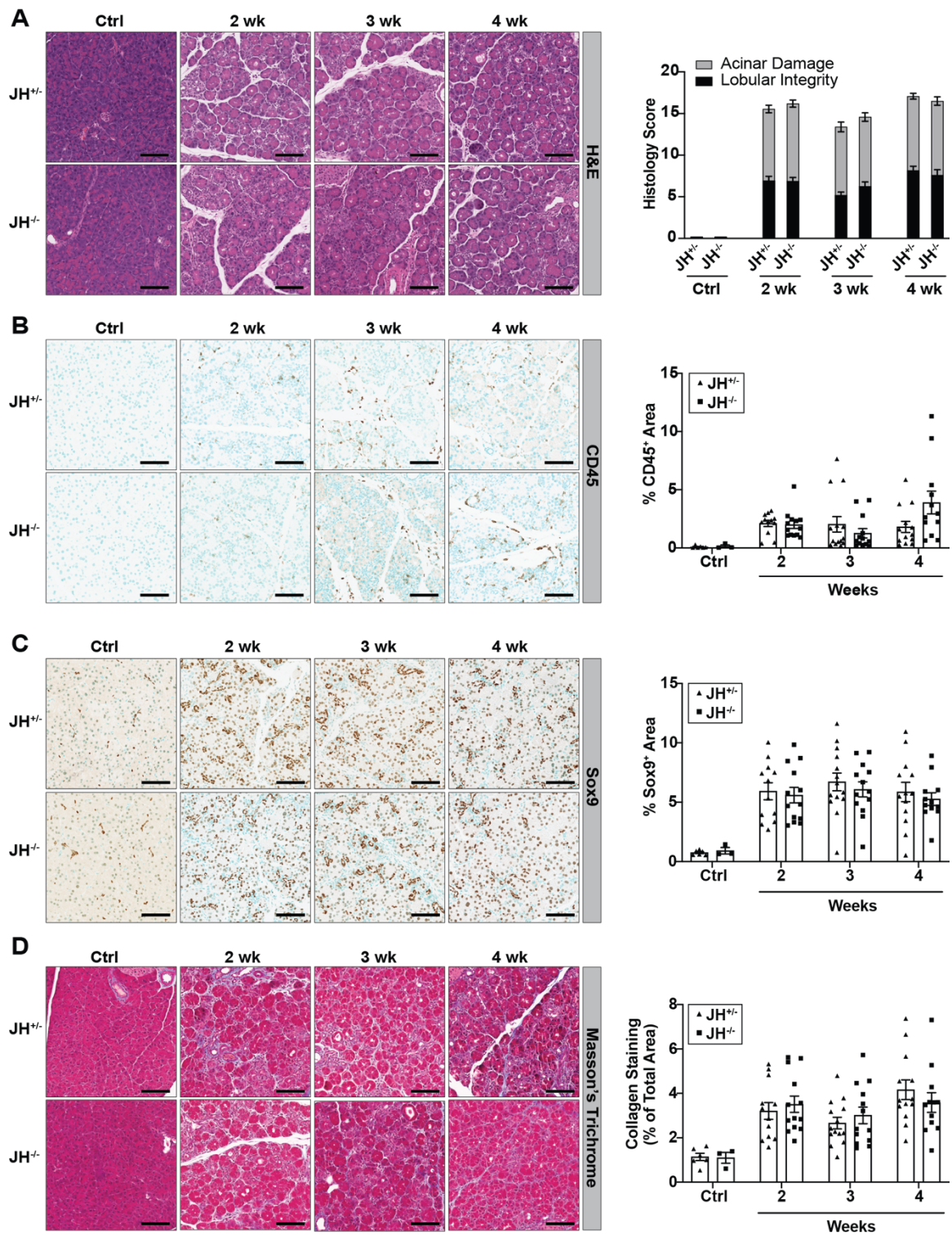


Figure 4.2 Tissue damage and inflammation during establishment of chronic pancreatitis is B cell-independent. (A) Representative hematoxylin and eosin (H&E) staining of JH^{+/+} and JH^{-/-} pancreas from untreated baseline controls (Ctrl) and from mice after 2 weeks, 3 weeks, and 4 weeks caerulein treatment, as described in Figure 1. Corresponding tissue damage scoring is shown on the right based on scoring criteria detailed in Methods and Supplemental Figure 1. Representative images and quantification of (B) CD45 staining, (C) Sox9 staining, and (D) Masson's trichrome staining. Staining quantification is presented as % positively stained area of total evaluated tissue area. Scale bars equal 100 μ m. Data from two independent experiments are shown and each data point represents one mouse; n = 3-14 mice/group. Statistical significance was determined by two-way ANOVA.

Although overall abundance of CD45⁺ cells in JH^{+/-} and JH^{-/-} mice was similar during chronic pancreatitis, we also audited frequencies of individual leukocyte populations to investigate whether immune complexity was altered in the context of B cell deficiency. Dendritic cells (DCs), monocytes, and macrophages exhibited transient increases in JH^{-/-} mice as compared to JH^{+/-} controls at two weeks, three weeks, and four weeks, respectively (**Figure 4.3**). DCs and macrophages have been identified as positive regulators of tissue fibrosis during chronic pancreatitis [37, 44, 46], but the observed similarities in collagen deposition between JH^{+/-} and JH^{-/-} mice (**Figure 4.2D**) indicated that profibrotic functions of these innate leukocyte populations were not mediated by B cells. Together, these data reveal that establishment of chronic pancreatitis is B cell-independent, at least in the model investigated.

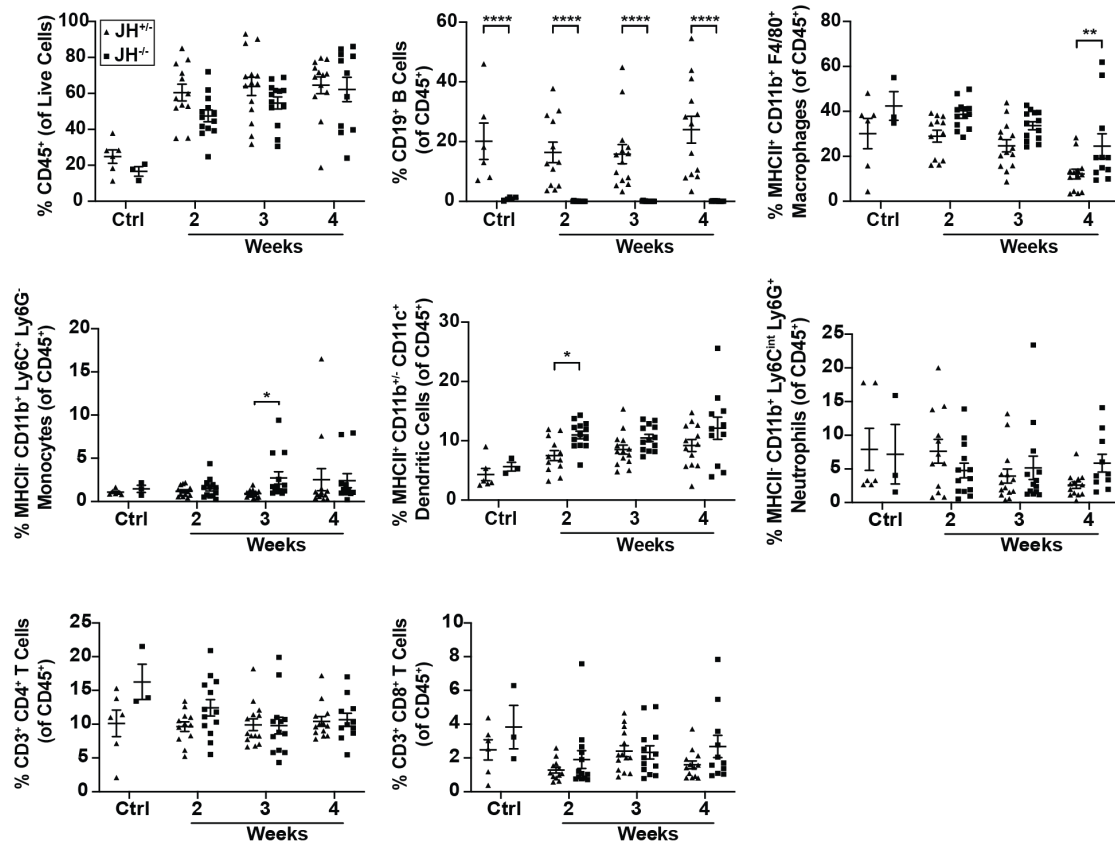


Figure 4.3 B cell-deficiency is not associated with sustained changes in pancreatic leukocyte complexity during chronic pancreatitis. Flow cytometric evaluation of indicated leukocyte populations in pancreata of $JH^{+/-}$ (triangles) and $JH^{-/-}$ mice (squares) treated with caerulein for the indicated durations. Data from two independent experiments are shown and each data point represents one mouse; $n = 3-14$ mice/group. Statistical significance was determined by two-way ANOVA.

Acute tissue damage is reduced in the absence of B cells

To determine the functional significance of B cells during acute pancreatitis, we administered caerulein for two consecutive days to $JH^{-/-}$ and $JH^{+/-}$ mice. Scoring of H&E-stained pancreas sections from day 3 following caerulein cessation revealed significantly reduced pancreatic damage in B cell-deficient mice as compared to B cell-proficient controls, which was attributable to both reduced tissue edema (i.e. improved lobular integrity) and limited acinar de-differentiation and necrosis in $JH^{-/-}$ mice (**Figure 4.4A**). Leukocyte infiltration was also significantly decreased in the absence of B cells at day 3 (**Figure 4.4B**), as were number of cells positive for Sox9 (**Figure 4.4C**). At day 7, trending decreases in histology score, immune infiltrate, and Sox9-positive cells were evident in $JH^{-/-}$ mice, although these differences were not statistically significant and both genotypes exhibited progressive damage resolution compared to day 3. Histological quantification of cellular proliferation and apoptosis by BrdU and cleaved caspase-3 staining, respectively, revealed that these parameters were equivalent across genotypes at all time points examined (**Figure 4.4D-E**, **Supplemental Figure 4.2C-D**).

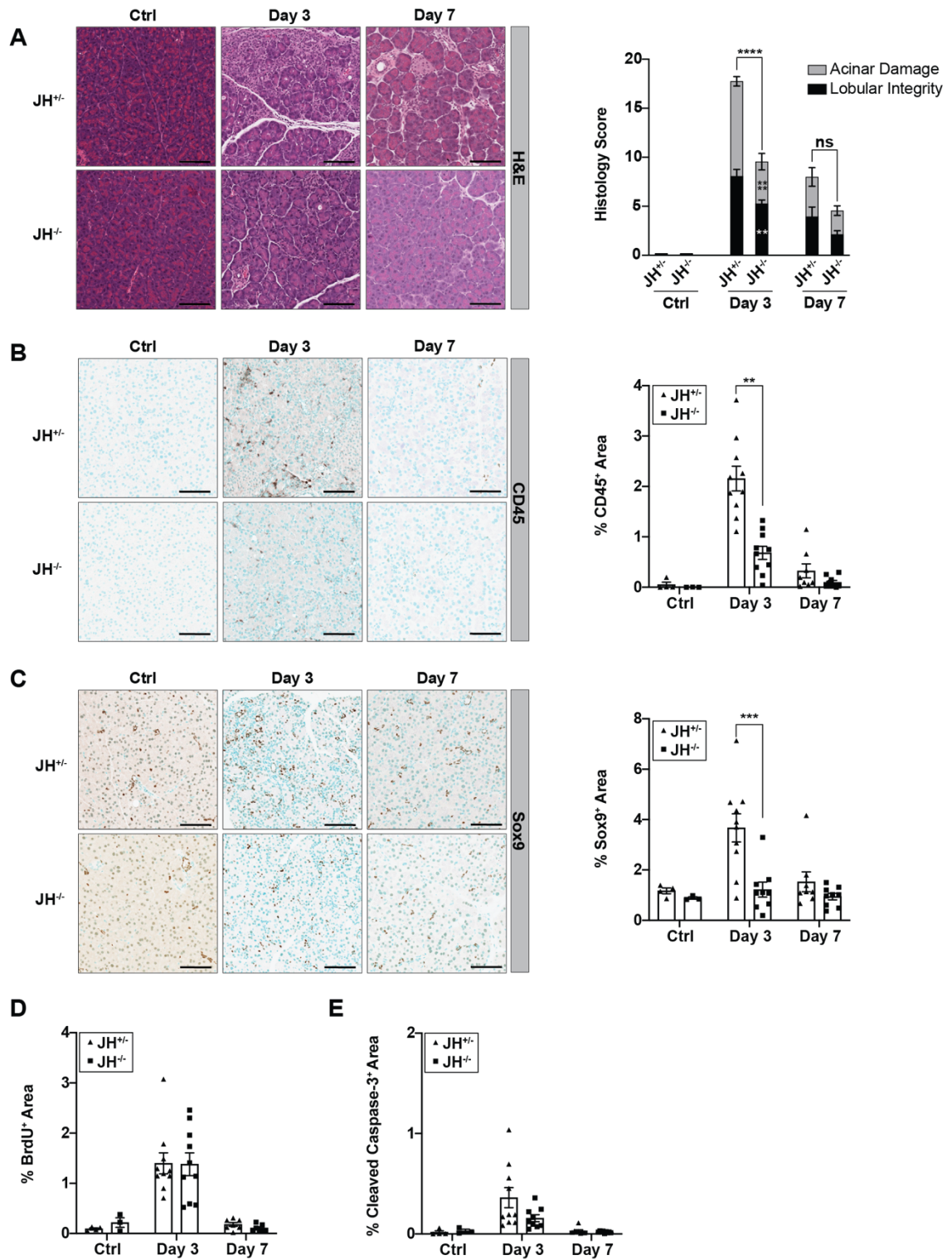


Figure 4.4 Acute tissue damage is reduced in the absence of B cells. **A)** Representative hematoxylin and eosin (H&E) staining of JH^{+/-} and JH^{-/-} pancreas from untreated baseline controls (Ctrl) and from mice on day 3 and day 7 following caerulein treatment, as described in Figure 1. Corresponding tissue damage scoring is shown on the right based on scoring criteria detailed in Methods and Supplemental Figure 1. Representative images and quantification of **(B)** CD45 staining and **(C)** Sox9 staining from pancreata harvested at the indicated time points. **(D-E)** Immunohistochemistry quantification of BrdU and cleaved caspase-3 staining. Staining quantification is presented as % positively stained area of total evaluated tissue area. Scale bars equal 100 μ m. Data from two independent experiments are shown and each data point represents one mouse; n = 3-10 mice/group. Statistical significance was determined by two-way ANOVA.

Since we have previously reported that B cells foster cutaneous squamous cell carcinoma and PDAC progression via Ig binding to Fc γ Rs on myeloid cells, that in turn regulates downstream pro-tumoral myeloid transcriptional programming and functionality [111, 174, 175], we sought to determine whether acute pancreatic damage was also mediated by analogous Ig-Fc γ R interactions. Thus, we evaluated parameters of acute pancreatitis in FcR $\gamma^{+/+}$ and FcR $\gamma^{-/-}$ mice. Histologic evaluation revealed that pancreatic damage, CD45⁺ leukocyte abundance, and number of Sox9⁺ cells did not differ significantly between FcR $\gamma^{+/+}$ and FcR $\gamma^{-/-}$ (**Supplemental Figure 4.3A-C**), thereby indicating that alternate mechanisms underlie B cell-mediated acute tissue damage in response to caerulein. Collectively, these findings implicate B cells as regulators of acute pancreatitis and indicate that B cell deficiency confers protection against acute pancreatic injury and metaplasia in early phases of the damage response through as-yet unidentified function(s).

Discussion

In the present study, we provide evidence that B cells play a significant role in regulating resolution of acute pancreatitis but are dispensable during establishment of chronic disease. We demonstrate herein using a murine model of caerulein-induced chronic pancreatitis that extent of exocrine damage, cell death, and tissue fibrosis are comparable in B cell-proficient and –deficient mice, thus affirming that B cells are neither protective nor damage promotional throughout a month-long establishment of chronic inflammation. Lee and colleagues recently reported that therapeutic depletion of B cells with α CD20 mAb after three weeks of chronic caerulein treatment accelerated tissue

regeneration [204]. However, as the authors indicated, tissue repair following caerulein withdrawal is unique to experimental chronic pancreatitis models and does not recapitulate the irreversible tissue damage found in human disease. Therefore, it was also important to understand whether B cells are functional mediators of chronic pancreatitis establishment or maintenance, as this would have more direct implications for potential therapeutic intervention and tissue damage prevention in humans. Given the results of the present study, efficacy of B cell-directed therapies in chronic pancreatitis would not be anticipated.

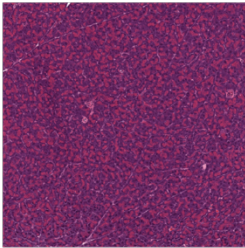
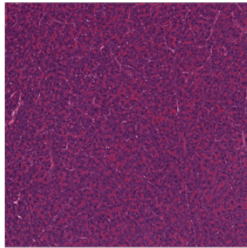
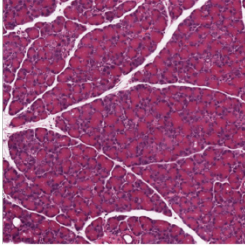
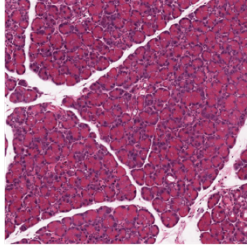
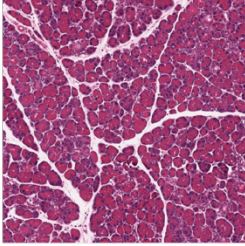
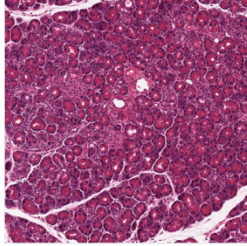
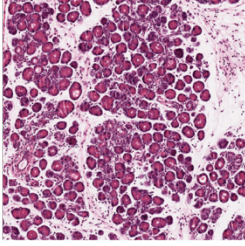
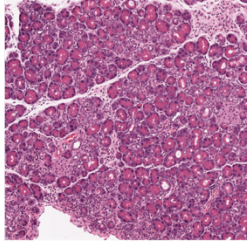
In contrast to results in chronic pancreatitis, we did reveal decreased tissue damage following acute caerulein treatment in mice lacking B cells. Together with the previous findings of Lee et al., these results indicate that B cells contribute to impaired tissue recovery in the pancreas following inflammatory insult. This is also consistent with experimental models of acute injury in heart, liver, and kidney that demonstrated B cell-mediated impairment of normal tissue repair and function following damage [208-210]. Future investigations are warranted to delineate specific mechanism(s) underlying B cell-mediated regulation of acute pancreatic recovery, as revealing these mechanisms could lead to improved therapeutic options for patients suffering from recurrent acute pancreatitis and its associated tissue damage.

Acknowledgments

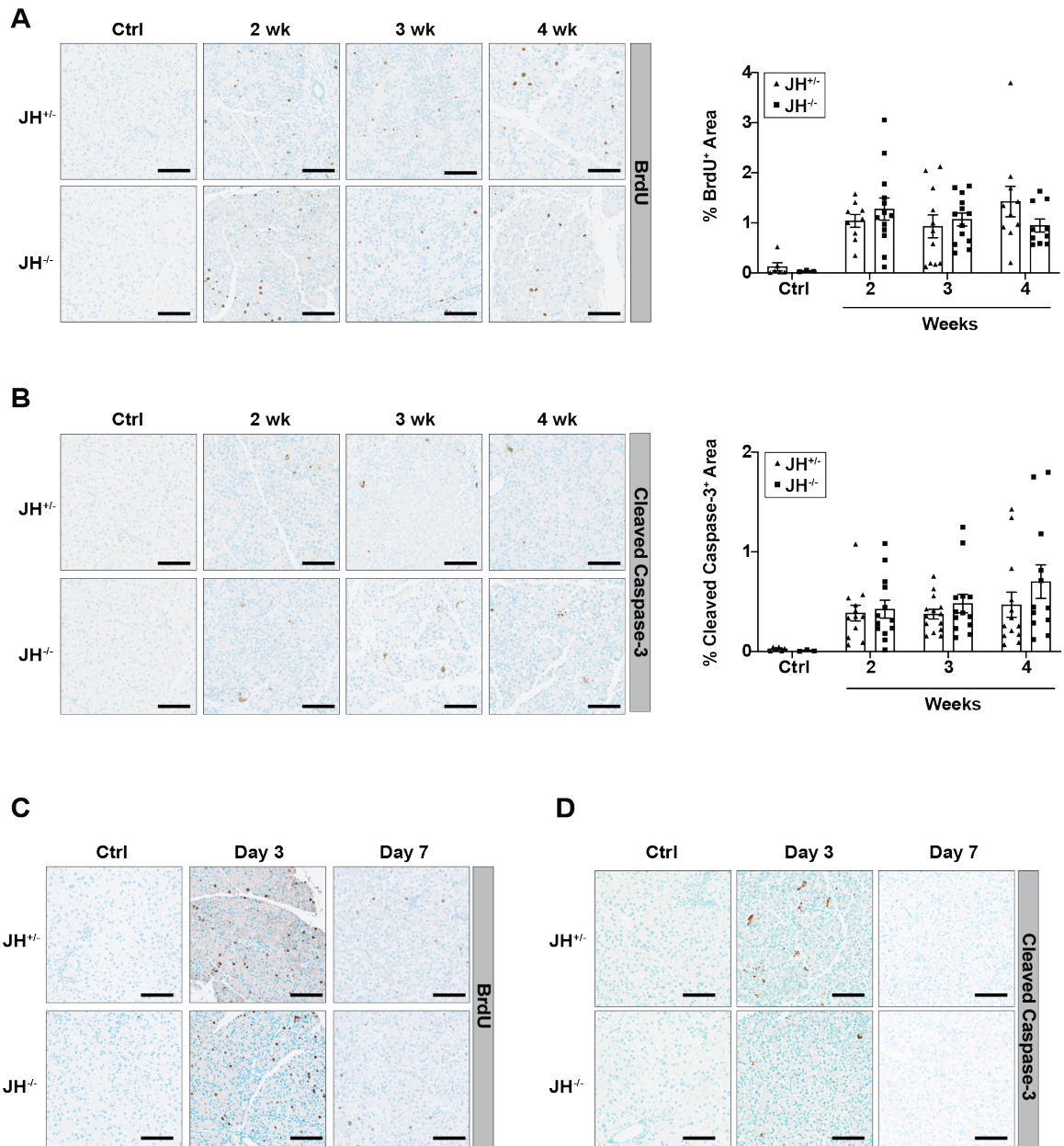
The authors thank the Oregon Health and Science University Histopathology and Flow Cytometry Shared Resources and the Brenden-Colson Center for Pancreatic Care. We are grateful to past and present members of the Coussens laboratory for insightful discussion, to Jo Hill for technical assistance, and to Justin Tibbitts for regulatory oversight and animal husbandry.

S.M.L. designed and performed experiments, analyzed and interpreted data, and wrote the manuscript; R.S.F., M.B.L., K.R.L., and K.B. acquired and analyzed histologic data; L.M.C. supervised the project, designed experiments, interpreted data, wrote and edited the manuscript and provided funding for the study.

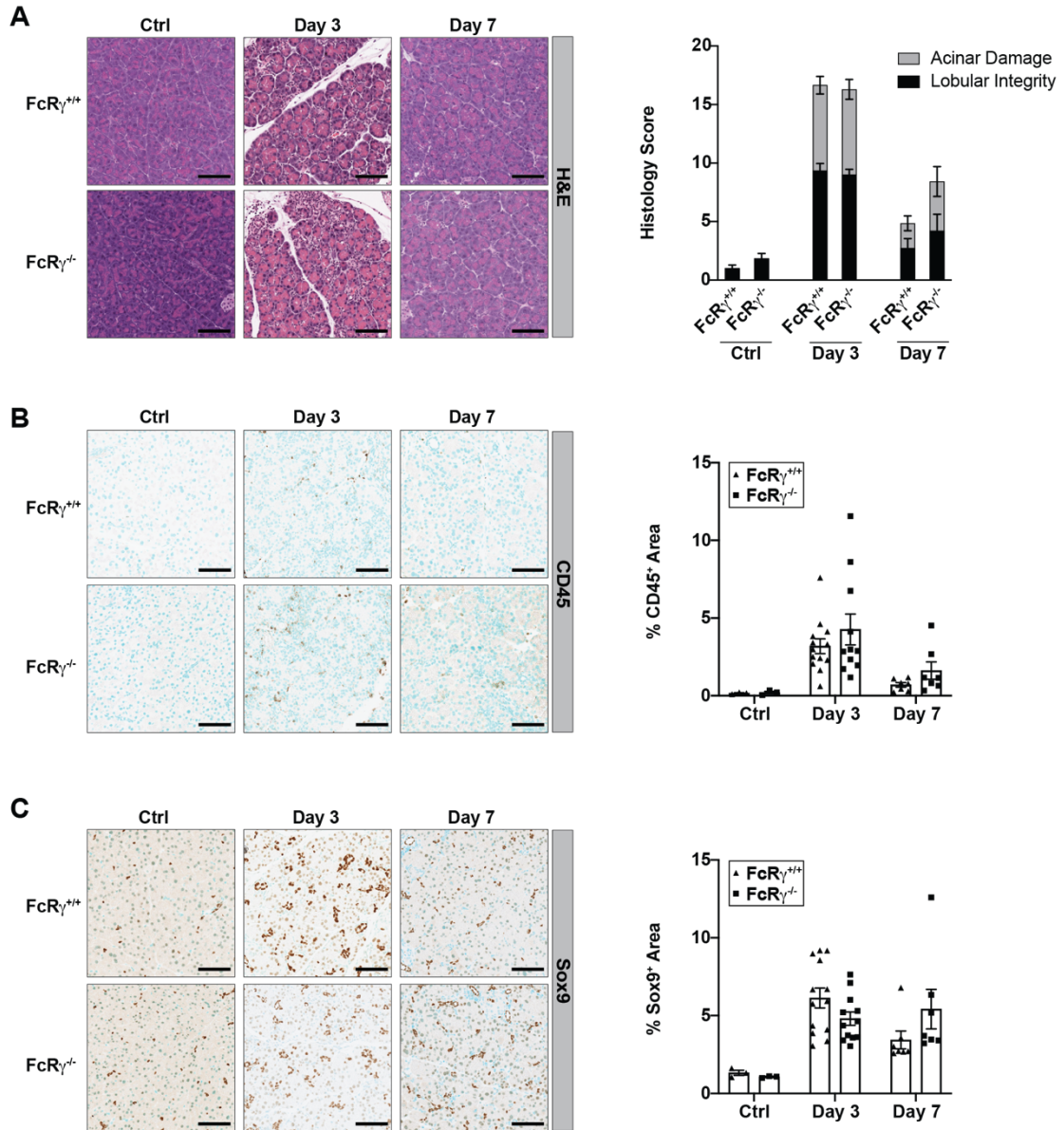
Supplemental Data

Lobular Integrity	Acinar Damage
 <p>0 No abnormality</p>	 <p>0 No abnormality</p>
 <p>1 Mild interlobular space and/or intralobular space</p>	 <p>1 < 10% acinar de-differentiation or death but with abnormal acinar size</p>
 <p>2 Moderate interlobular space and intralobular space</p>	 <p>2 10-30% acinar de-differentiation or death</p>
 <p>3 Severe interlobular space and intralobular space</p>	 <p>3 > 30% acinar de-differentiation or death</p>

Supplemental Figure 4.1 Pancreatic histological damage scoring criteria. Hematoxylin and eosin (H&E) stained pancreata of caerulein-treated mice were evaluated for two parameters: lobular integrity and acinar damage. Lobular integrity measures change in inter- and intra-lobular spaces and is reflective of pancreatic edema. The acinar damage score encompasses both acinar de-differentiation/metaplasia and necrosis. Scoring for each parameter increased with damage severity on a scale from 0 to 3. Scores from each parameter were added from 4 fields of view per mouse and resulted in a cumulative histology score. Representative images of each scoring category are shown.



Supplemental Figure 4.2 Cellular proliferation and apoptosis are equivalent in JH^{+/-} and JH^{-/-} during chronic and acute pancreatitis. (A) Representative images of BrdU staining in JH^{+/-} and JH^{-/-} at the chronic pancreatitis time points indicated (left) and corresponding IHC quantification (right). Data shown are from two independent experiments. n = 3-14/group. (B) Representative cleaved caspase-3 staining from the same chronic pancreatitis experiments included in (A). (C-D) Representative BrdU (left) and cleaved caspase-3 staining corresponding to acute pancreatitis experiments shown in Figure 3.3. All scale bars equal 100 μ m.



Supplemental Figure 4.3 Resolution of tissue damage and inflammation in acute pancreatitis are FcγR-independent. $FcR\gamma^{+/+}$ and $FcR\gamma^{-/-}$ mice were treated acutely with caerulein (seven hourly 50 $\mu\text{g}/\text{kg}$ i.p. doses of caerulein on two consecutive days) and pancreas was harvested on day 3 and day 7 following final caerulein injection. **(A)** Representative H&E-stained pancreata from untreated controls (Ctrl) and pancreata from caerulein-treated mice at the indicated time points (left) with corresponding histology damage score (right). **(B-C)** Representative staining and quantification of CD45 and Sox9 from pancreas evaluated at the indicated time points. Scale bars equal 100 μm . Data shown are from two independent experiments. $n = 3-13/\text{group}$.

Chapter 5: Extended Discussion

The research projects described herein share the common goal of identifying immune biomarkers and immunotherapeutic targets that could be leveraged to improve patient care and/or outcome. In our extensive mIHC-based evaluation of human PDAC (Chapter 2), we identified immune subtypes of treatment-naïve and neoadjuvant-treated tumors that can now serve as a baseline reference for patient stratification and response to immunotherapies. This is a critical advancement in the PDAC field, as no other studies to date have provided equally comprehensive lymphoid and myeloid complexity data and spatial analysis at near single-cell resolution. Such immune subtyping of human PDACs should be considered a critical aspect of patient management for guiding future (pre)clinical validation of immunotherapy combinations.

In support of our data revealing multiple immune subtypes of human PDAC, we recently reported that murine PDAC isogenic subclones isolated from GEMM PDAC models cluster into myeloid-enriched and lymphoid-enriched subgroups similar to subtypes we observed in human tumors [115]. Immune characterization of additional murine cell lines (Chapter 3) further exemplified the existence of immune heterogeneity in preclinical rodent models of PDAC. Moving forward, this heterogeneity could be strategically leveraged to study mechanisms of immunotherapy response and resistance in tumors with known immune complexities. Murine PDAC cell lines from the libraries developed in our past and present studies can be rationally selected based upon immune features and utilized to investigate novel therapeutic combinations and drug sequencing strategies in tractable *in vivo* orthotopic tumor implantation models. Therapeutic responses can also be

evaluated and directly compared across murine tumors with distinct immune profiles, and resulting information can then be translated back to human disease.

Our mIHC study answered several outstanding questions regarding how the PDAC immune landscape is associated with patient outcome and has prompted multiple new questions to be addressed in future studies, including:

- Does PDAC immune contexture change as disease progresses from early stage to advanced metastatic disease?
- How extensive is inpatient immune heterogeneity, and what are implications of inpatient heterogeneity for research and clinical management of disease?
- How is immune contexture associated with other stromal and tumor-intrinsic features?

All human specimens evaluated in the mIHC studies described herein were derived from patients presenting with primary non-metastatic PDAC, and thus represent only ~15% of total PDACs. Future studies should therefore strive to determine whether immune signatures found in non-metastatic primary tumors are similar to late-stage primary tumors that have already metastasized. In addition, understanding if and how immune contexture of primary tumors differs from metastatic lesions is also an important component of successfully predicting patient response to therapy and stratifying outcomes. The Coussens laboratory is beginning to address this through mIHC of late-stage primary and metastatic PDAC lesions from patients enrolled in immunotherapy

clinical trials. Preliminary results from a small number of pre-treatment patient samples indicate that advanced stage primary tumors cluster together and are distinct from non-metastatic PDACs, and that PDAC liver metastases cluster separately from late-stage primary tumors. These observations support the concept that immune contexture evolves with disease progression and that early and advanced stage tumors should not necessarily be expected to respond equivalently to the same types of immunotherapeutic combinations. Immune profiling of additional advanced primary tumors and metastases is a clear next step in order to build an atlas of late disease stages comparable to the one we have created here for non-metastatic PDAC. Atlas resources such as these will be invaluable for developing or selecting therapeutic regimens with potential to target cells or protumoral pathways shared between primary and metastatic sites. Additionally, characterization of immune contexture in late stage metastatic disease could lead to identification of new therapeutic biomarkers specific for disease stage.

In addition to the immune heterogeneity existing between disease stages and between individual patients within a single disease stage, our data also revealed presence of *intrapatient* immune heterogeneity. Intrapatient heterogeneity is particularly important to consider when analyzing and interpreting data from IHC studies relying on small quantities of tissue, such as biopsies or tissue microarray (TMA) cores. For advanced PDAC cases in which surgical resection is infeasible, or in the context of clinical trials that include longitudinal on-treatment tissue sampling, biomarker detection is limited to blood and biopsy specimens. High intratumoral immune heterogeneity could limit ability to reliably evaluate immune contexture or treatment responsiveness if only a single

biopsy is used. Ongoing multivariate statistical evaluation of inpatient heterogeneity in our mIHC dataset will help predict minimum number of biopsy passes required to optimally represent tumor immune contexture. This information could set an important precedent for tissue-based research in PDAC and other solid tumors.

Collectively, mIHC has tremendous potential for biomarker discovery in cancer. While our current mIHC analysis is focused almost exclusively on immune parameters, the high adaptability of this methodology readily permits future analyses evaluating immune contexture in tandem with contexture of other significant aspects of the PDAC TME (e.g. vasculature, fibroblasts). Integration of mIHC-derived stromal signatures and PDAC molecular subtyping could also move the field an important step further by enabling assessment of how tumor intrinsic factors shape the TME, or vice versa. These integrated approaches will lead to even greater patient stratification that will give rise to improved therapeutic responses and prolonged survival in patients suffering from this difficult disease.

References

1. Paniccia, A., Schulick, RD, *Pancreatic physiology and functional assessment*, in *Blumgart's Surgery of the Liver, Biliary Tract, and Pancreas*, W. Jarnagin, Editor. 2017, Elsevier.
2. Ballian, N. and F.C. Brunicardi, Islet vasculature as a regulator of endocrine pancreas function. *World J Surg*, 2007. 31(4): p. 705-14.
3. Thorens, B., Neural regulation of pancreatic islet cell mass and function. *Diabetes Obes Metab*, 2014. 16 Suppl 1: p. 87-95.
4. Apte, M.V., R.C. Pirola, and J.S. Wilson, Pancreatic stellate cells: a starring role in normal and diseased pancreas. *Front Physiol*, 2012. 3: p. 344.
5. *National diabetes statistics report, 2017*. 2017, Centers for Disease Control and Prevention.
6. DiMeglio, L.A., C. Evans-Molina, and R.A. Oram, Type 1 diabetes. *Lancet*, 2018. 391(10138): p. 2449-2462.
7. Chatterjee, S., K. Khunti, and M.J. Davies, Type 2 diabetes. *Lancet*, 2017. 389(10085): p. 2239-2251.
8. Wellen, K.E. and G.S. Hotamisligil, Inflammation, stress, and diabetes. *J Clin Invest*, 2005. 115(5): p. 1111-9.
9. Yadav, D. and A.B. Lowenfels, The epidemiology of pancreatitis and pancreatic cancer. *Gastroenterology*, 2013. 144(6): p. 1252-61.
10. Krishna, S.G., A.K. Kamboj, P.A. Hart, A. Hinton, and D.L. Conwell, The Changing Epidemiology of Acute Pancreatitis Hospitalizations: A Decade of Trends and the Impact of Chronic Pancreatitis. *Pancreas*, 2017. 46(4): p. 482-488.
11. Wu, B.U. and P.A. Banks, Clinical management of patients with acute pancreatitis. *Gastroenterology*, 2013. 144(6): p. 1272-81.
12. Nojgaard, C., U. Becker, P. Matzen, J.R. Andersen, C. Holst, and F. Bendtsen, Progression from acute to chronic pancreatitis: prognostic factors, mortality, and natural course. *Pancreas*, 2011. 40(8): p. 1195-200.
13. Forsmark, C.E., Management of chronic pancreatitis. *Gastroenterology*, 2013. 144(6): p. 1282-91 e3.
14. Lowenfels, A.B., P. Maisonneuve, G. Cavallini, R.W. Ammann, P.G. Lankisch, J.R. Andersen, E.P. Dimagno, A. Andren-Sandberg, and L. Domellof, Pancreatitis and the risk of pancreatic cancer. International Pancreatitis Study Group. *N Engl J Med*, 1993. 328(20): p. 1433-7.
15. Raimondi, S., A.B. Lowenfels, A.M. Morselli-Labate, P. Maisonneuve, and R. Pezzilli, Pancreatic cancer in chronic pancreatitis; aetiology, incidence, and early detection. *Best Pract Res Clin Gastroenterol*, 2010. 24(3): p. 349-58.
16. Bang, U.C., T. Benfield, L. Hyldstrup, F. Bendtsen, and J.E. Beck Jensen, Mortality, cancer, and comorbidities associated with chronic pancreatitis: a Danish nationwide matched-cohort study. *Gastroenterology*, 2014. 146(4): p. 989-94.
17. Kirkegaard, J., F.V. Mortensen, and D. Cronin-Fenton, Chronic Pancreatitis and Pancreatic Cancer Risk: A Systematic Review and Meta-analysis. *Am J Gastroenterol*, 2017. 112(9): p. 1366-1372.

18. Whitcomb, D.C., Genetic risk factors for pancreatic disorders. *Gastroenterology*, 2013. 144(6): p. 1292-302.
19. Keller, J. and P. Layer, Idiopathic chronic pancreatitis. *Best Pract Res Clin Gastroenterol*, 2008. 22(1): p. 105-13.
20. Mayerle, J., M. Sendler, E. Hegyi, G. Beyer, M.M. Lerch, and M. Sahin-Toth, Genetics, Cell Biology, and Pathophysiology of Pancreatitis. *Gastroenterology*, 2019. 156(7): p. 1951-1968 e1.
21. Saluja, A., V. Dudeja, R. Dawra, and R.P. Sah, Early Intra-Acinar Events in Pathogenesis of Pancreatitis. *Gastroenterology*, 2019. 156(7): p. 1979-1993.
22. Hoque, R., A.F. Malik, F. Gorelick, and W.Z. Mehal, Sterile inflammatory response in acute pancreatitis. *Pancreas*, 2012. 41(3): p. 353-7.
23. Lerch, M.M. and F.S. Gorelick, Models of acute and chronic pancreatitis. *Gastroenterology*, 2013. 144(6): p. 1180-93.
24. Jensen, J.N., E. Cameron, M.V. Garay, T.W. Starkey, R. Gianani, and J. Jensen, Recapitulation of elements of embryonic development in adult mouse pancreatic regeneration. *Gastroenterology*, 2005. 128(3): p. 728-41.
25. Fukuda, A., S.C. Wang, J.P.t. Morris, A.E. Folias, A. Liou, G.E. Kim, S. Akira, K.M. Boucher, M.A. Firpo, S.J. Mulvihill, and M. Hebrok, Stat3 and MMP7 contribute to pancreatic ductal adenocarcinoma initiation and progression. *Cancer Cell*, 2011. 19(4): p. 441-55.
26. Guerra, C., A.J. Schuhmacher, M. Canamero, P.J. Grippo, L. Verdaguer, L. Perez-Gallego, P. Dubus, E.P. Sandgren, and M. Barbacid, Chronic pancreatitis is essential for induction of pancreatic ductal adenocarcinoma by K-Ras oncogenes in adult mice. *Cancer Cell*, 2007. 11(3): p. 291-302.
27. Sendler, M., G. Beyer, U.M. Mahajan, V. Kauschke, S. Maertin, C. Schurmann, G. Homuth, U. Volker, H. Volzke, W. Halangk, T. Wartmann, F.U. Weiss, P. Hegyi, M.M. Lerch, and J. Mayerle, Complement Component 5 Mediates Development of Fibrosis, via Activation of Stellate Cells, in 2 Mouse Models of Chronic Pancreatitis. *Gastroenterology*, 2015. 149(3): p. 765-76 e10.
28. Steele, C.W., S.A. Karim, M. Foth, L. Rishi, J.D. Leach, R.J. Porter, C. Nixon, T.R. Jeffry Evans, C.R. Carter, R.J. Nibbs, O.J. Sansom, and J.P. Morton, CXCR2 inhibition suppresses acute and chronic pancreatic inflammation. *J Pathol*, 2015. 237(1): p. 85-97.
29. Zaninovic, V., A.S. Gukovskaya, I. Gukovsky, M. Mouria, and S.J. Pandol, Cerulein upregulates ICAM-1 in pancreatic acinar cells, which mediates neutrophil adhesion to these cells. *Am J Physiol Gastrointest Liver Physiol*, 2000. 279(4): p. G666-76.
30. Awla, D., A. Abdulla, S. Zhang, J. Roller, M.D. Menger, S. Regner, and H. Thorlacius, Lymphocyte function antigen-1 regulates neutrophil recruitment and tissue damage in acute pancreatitis. *Br J Pharmacol*, 2011. 163(2): p. 413-23.
31. Hartman, H., A. Abdulla, D. Awla, B. Lindkvist, B. Jeppsson, H. Thorlacius, and S. Regner, P-selectin mediates neutrophil rolling and recruitment in acute pancreatitis. *Br J Surg*, 2012. 99(2): p. 246-55.
32. Awla, D., A. Abdulla, I. Syk, B. Jeppsson, S. Regner, and H. Thorlacius, Neutrophil-derived matrix metalloproteinase-9 is a potent activator of trypsinogen in acinar cells in acute pancreatitis. *J Leukoc Biol*, 2012. 91(5): p. 711-9.

33. Gukovskaya, A.S., E. Vaquero, V. Zaninovic, F.S. Gorelick, A.J. Lusa, M.L. Brennan, S. Holland, and S.J. Pandol, Neutrophils and NADPH oxidase mediate intrapancreatic trypsin activation in murine experimental acute pancreatitis. *Gastroenterology*, 2002. 122(4): p. 974-84.
34. Sandoval, D., A. Gukovskaya, P. Reavey, S. Gukovsky, A. Sisk, P. Braquet, S.J. Pandol, and S. Poucell-Hatton, The role of neutrophils and platelet-activating factor in mediating experimental pancreatitis. *Gastroenterology*, 1996. 111(4): p. 1081-91.
35. Frossard, J.L., A. Saluja, L. Bhagat, H.S. Lee, M. Bhatia, B. Hofbauer, and M.L. Steer, The role of intercellular adhesion molecule 1 and neutrophils in acute pancreatitis and pancreatitis-associated lung injury. *Gastroenterology*, 1999. 116(3): p. 694-701.
36. Perides, G., E.R. Weiss, E.S. Michael, J.M. Laukkanen, J.S. Duffield, and M.L. Steer, TNF-alpha-dependent regulation of acute pancreatitis severity by Ly-6C(hi) monocytes in mice. *J Biol Chem*, 2011. 286(15): p. 13327-35.
37. Habtezion, A., Inflammation in acute and chronic pancreatitis. *Curr Opin Gastroenterol*, 2015. 31(5): p. 395-9.
38. Sendler, M., F.U. Weiss, J. Golchert, G. Homuth, C. van den Brandt, U.M. Mahajan, L.I. Partecke, P. Doring, I. Gukovsky, A.S. Gukovskaya, P.R. Wagh, M.M. Lerch, and J. Mayerle, Cathepsin B-Mediated Activation of Trypsinogen in Endocytosing Macrophages Increases Severity of Pancreatitis in Mice. *Gastroenterology*, 2018. 154(3): p. 704-718 e10.
39. Morris, J.P.t., D.A. Cano, S. Sekine, S.C. Wang, and M. Hebrok, Beta-catenin blocks Kras-dependent reprogramming of acini into pancreatic cancer precursor lesions in mice. *J Clin Invest*, 2010. 120(2): p. 508-20.
40. Liou, G.Y., H. Doppler, B. Necela, M. Krishna, H.C. Crawford, M. Raimondo, and P. Storz, Macrophage-secreted cytokines drive pancreatic acinar-to-ductal metaplasia through NF-kappaB and MMPs. *J Cell Biol*, 2013. 202(3): p. 563-77.
41. Liou, G.Y. and P. Storz, Inflammatory macrophages in pancreatic acinar cell metaplasia and initiation of pancreatic cancer. *Oncoscience*, 2015. 2(3): p. 247-51.
42. Storz, P., Acinar cell plasticity and development of pancreatic ductal adenocarcinoma. *Nat Rev Gastroenterol Hepatol*, 2017. 14(5): p. 296-304.
43. Xue, J., V. Sharma, M.H. Hsieh, A. Chawla, R. Murali, S.J. Pandol, and A. Habtezion, Alternatively activated macrophages promote pancreatic fibrosis in chronic pancreatitis. *Nat Commun*, 2015. 6: p. 7158.
44. Liou, G.Y., L. Bastea, A. Fleming, H. Doppler, B.H. Edenfield, D.W. Dawson, L. Zhang, N. Bardeesy, and P. Storz, The Presence of Interleukin-13 at Pancreatic ADM/PanIN Lesions Alters Macrophage Populations and Mediates Pancreatic Tumorigenesis. *Cell Rep*, 2017. 19(7): p. 1322-1333.
45. Bedrosian, A.S., A.H. Nguyen, M. Hackman, M.K. Connolly, A. Malhotra, J. Ibrahim, N.E. Cieza-Rubio, J.R. Henning, R. Barilla, A. Rehman, H.L. Pachter, M.V. Medina-Zea, S.M. Cohen, A.B. Frey, D. Acehan, and G. Miller, Dendritic cells promote pancreatic viability in mice with acute pancreatitis. *Gastroenterology*, 2011. 141(5): p. 1915-26 e1-14.

46. Ochi, A., A.H. Nguyen, A.S. Bedrosian, H.M. Mushlin, S. Zarbakhsh, R. Barilla, C.P. Zambirinis, N.C. Fallon, A. Rehman, Y. Pylayeva-Gupta, S. Badar, C.H. Hajdu, A.B. Frey, D. Bar-Sagi, and G. Miller, MyD88 inhibition amplifies dendritic cell capacity to promote pancreatic carcinogenesis via Th2 cells. *J Exp Med*, 2012. 209(9): p. 1671-87.
47. Demols, A., O. Le Moine, F. Desalle, E. Quertinmont, J.L. Van Laethem, and J. Deviere, CD4(+) T cells play an important role in acute experimental pancreatitis in mice. *Gastroenterology*, 2000. 118(3): p. 582-90.
48. Xue, J., V. Sharma, and A. Habtezion, Immune cells and immune-based therapy in pancreatitis. *Immunol Res*, 2014. 58(2-3): p. 378-86.
49. Stauffer, J.A. and H.J. Asbun, Rare Tumors and Lesions of the Pancreas. *Surg Clin North Am*, 2018. 98(1): p. 169-188.
50. Scott, A.T. and J.R. Howe, Evaluation and Management of Neuroendocrine Tumors of the Pancreas. *Surg Clin North Am*, 2019. 99(4): p. 793-814.
51. Akirov, A., V. Larouche, S. Alshehri, S.L. Asa, and S. Ezzat, Treatment Options for Pancreatic Neuroendocrine Tumors. *Cancers (Basel)*, 2019. 11(6).
52. Brooks, J.C., R.M. Shavelle, and K.N. Vavra-Musser, Life expectancy in pancreatic neuroendocrine cancer. *Clin Res Hepatol Gastroenterol*, 2019. 43(1): p. 88-97.
53. Hruban, R.H., A. Maitra, and M. Goggins, Update on pancreatic intraepithelial neoplasia. *Int J Clin Exp Pathol*, 2008. 1(4): p. 306-16.
54. Matthaei, H., R.D. Schulick, R.H. Hruban, and A. Maitra, Cystic precursors to invasive pancreatic cancer. *Nat Rev Gastroenterol Hepatol*, 2011. 8(3): p. 141-50.
55. Patra, K.C., N. Bardeesy, and Y. Mizukami, Diversity of Precursor Lesions For Pancreatic Cancer: The Genetics and Biology of Intraductal Papillary Mucinous Neoplasm. *Clin Transl Gastroenterol*, 2017. 8(4): p. e86.
56. Kopp, J.L., G. von Figura, E. Mayes, F.F. Liu, C.L. Dubois, J.P.t. Morris, F.C. Pan, H. Akiyama, C.V. Wright, K. Jensen, M. Hebrok, and M. Sander, Identification of Sox9-dependent acinar-to-ductal reprogramming as the principal mechanism for initiation of pancreatic ductal adenocarcinoma. *Cancer Cell*, 2012. 22(6): p. 737-50.
57. Tempero, M.A., M.P. Malafa, E.G. Chiorean, B. Czito, C. Scaife, A.K. Narang, C. Fountzilas, B.M. Wolpin, M. Al-Hawary, H. Asbun, S.W. Behrman, A.B. Benson, E. Binder, D.B. Cardin, C. Cha, V. Chung, M. Dillhoff, E. Dotan, C.R. Ferrone, G. Fisher, J. Hardacre, W.G. Hawkins, A.H. Ko, N. LoConte, A.M. Lowy, C. Moravek, E.K. Nakakura, E.M. O'Reilly, J. Obando, S. Reddy, S. Thayer, R.A. Wolff, J.L. Burns, and G. Zuccarino-Catania, Pancreatic Adenocarcinoma, Version 1.2019. *J Natl Compr Canc Netw*, 2019. 17(3): p. 202-210.
58. Howlader N, N.A., Krapcho M, Miller D, Brest A, Yu M, Ruhl J, Tatalovich Z, Mariotto A, Lewis DR, Chen HS, Feuer EJ, Cronin KA (eds), *SEER Cancer Statistics Review, 1975-2016*. 2019, National Cancer Institute: Bethesda, MD.
59. Midha, S., S. Chawla, and P.K. Garg, Modifiable and non-modifiable risk factors for pancreatic cancer: A review. *Cancer Lett*, 2016. 381(1): p. 269-77.
60. White, R.R. and A.M. Lowy, Clinical Management: Resectable Disease. *Cancer J*, 2017. 23(6): p. 343-349.

61. Garrido-Laguna, I. and M. Hidalgo, Pancreatic cancer: from state-of-the-art treatments to promising novel therapies. *Nat Rev Clin Oncol*, 2015. 12(6): p. 319-34.
62. Rhim, A.D., E.T. Mirek, N.M. Aiello, A. Maitra, J.M. Bailey, F. McAllister, M. Reichert, G.L. Beatty, A.K. Rustgi, R.H. Vonderheide, S.D. Leach, and B.Z. Stanger, EMT and dissemination precede pancreatic tumor formation. *Cell*, 2012. 148(1-2): p. 349-61.
63. Tempero, M.A., NCCN Guidelines Updates: Pancreatic Cancer. *J Natl Compr Canc Netw*, 2019. 17(5.5): p. 603-605.
64. Vasen, H., I. Ibrahim, C.G. Ponce, E.P. Slater, E. Matthai, A. Carrato, J. Earl, K. Robbers, A.M. van Mil, T. Potjer, B.A. Bonsing, W.H. de Vos Tot Nederveen Cappel, W. Bergman, M. Wasser, H. Morreau, G. Kloppel, C. Schicker, M. Steinkamp, J. Figiel, I. Esposito, E. Mocci, E. Vazquez-Sequeiros, A. Sanjuanbenito, M. Munoz-Beltran, J. Montans, P. Langer, V. Fendrich, and D.K. Bartsch, Benefit of Surveillance for Pancreatic Cancer in High-Risk Individuals: Outcome of Long-Term Prospective Follow-Up Studies From Three European Expert Centers. *J Clin Oncol*, 2016. 34(17): p. 2010-9.
65. Lo, W., M.C. Morris, S.A. Ahmad, and S.H. Patel, Screening patients at high risk for pancreatic cancer-Is it time for a paradigm shift? *J Surg Oncol*, 2019.
66. Burris, H.A., 3rd, M.J. Moore, J. Andersen, M.R. Green, M.L. Rothenberg, M.R. Modiano, M.C. Cripps, R.K. Portenoy, A.M. Storniolo, P. Tarassoff, R. Nelson, F.A. Dorr, C.D. Stephens, and D.D. Von Hoff, Improvements in survival and clinical benefit with gemcitabine as first-line therapy for patients with advanced pancreas cancer: a randomized trial. *J Clin Oncol*, 1997. 15(6): p. 2403-13.
67. Von Hoff, D.D., T. Ervin, F.P. Arena, E.G. Chiorean, J. Infante, M. Moore, T. Seay, S.A. Tjulandin, W.W. Ma, M.N. Saleh, M. Harris, M. Reni, S. Dowden, D. Laheru, N. Bahary, R.K. Ramanathan, J. Tabernero, M. Hidalgo, D. Goldstein, E. Van Cutsem, X. Wei, J. Iglesias, and M.F. Renschler, Increased survival in pancreatic cancer with nab-paclitaxel plus gemcitabine. *N Engl J Med*, 2013. 369(18): p. 1691-703.
68. Conroy, T., P. Hammel, M. Hebbar, M. Ben Abdelghani, A.C. Wei, J.L. Raoul, L. Chone, E. Francois, P. Artru, J.J. Biagi, T. Lecomte, E. Assenat, R. Faroux, M. Ychou, J. Volet, A. Sauvanet, G. Breysacher, F. Di Fiore, C. Cripps, P. Kavan, P. Texereau, K. Bouhier-Leporrier, F. Khemissa-Akouz, J.L. Legoux, B. Juzyna, S. Gourgou, C.J. O'Callaghan, C. Jouffroy-Zeller, P. Rat, D. Malka, F. Castan, J.B. Bachet, G. Canadian Cancer Trials, and G.I.P.G. the Unicancer, FOLFIRINOX or Gemcitabine as Adjuvant Therapy for Pancreatic Cancer. *N Engl J Med*, 2018. 379(25): p. 2395-2406.
69. Conroy, T., F. Desseigne, M. Ychou, O. Bouche, R. Guimbaud, Y. Becouarn, A. Adenis, J.L. Raoul, S. Gourgou-Bourgade, C. de la Fouchardiere, J. Bennisouna, J.B. Bachet, F. Khemissa-Akouz, D. Pere-Verge, C. Delbaldo, E. Assenat, B. Chauffert, P. Michel, C. Montoto-Grillot, M. Ducreux, U. Groupe Tumeurs Digestives of, and P. Intergroup, FOLFIRINOX versus gemcitabine for metastatic pancreatic cancer. *N Engl J Med*, 2011. 364(19): p. 1817-25.
70. Neoptolemos, J.P., D.H. Palmer, P. Ghaneh, E.E. Psarelli, J.W. Valle, C.M. Halloran, O. Faluyi, D.A. O'Reilly, D. Cunningham, J. Wadsley, S. Darby, T.

- Meyer, R. Gillmore, A. Anthoney, P. Lind, B. Glimelius, S. Falk, J.R. Izbicki, G.W. Middleton, S. Cummins, P.J. Ross, H. Wasan, A. McDonald, T. Crosby, Y.T. Ma, K. Patel, D. Sherriff, R. Soomal, D. Borg, S. Sothi, P. Hammel, T. Hackert, R. Jackson, M.W. Buchler, and C. European Study Group for Pancreatic, Comparison of adjuvant gemcitabine and capecitabine with gemcitabine monotherapy in patients with resected pancreatic cancer (ESPAC-4): a multicentre, open-label, randomised, phase 3 trial. *Lancet*, 2017. 389(10073): p. 1011-1024.
71. Raufi, A.G., G.A. Manji, J.A. Chabot, and S.E. Bates, Neoadjuvant Treatment for Pancreatic Cancer. *Semin Oncol*, 2019. 46(1): p. 19-27.
 72. Yarchoan, M., L.A. Albacker, A.C. Hopkins, M. Montesion, K. Murugesan, T.T. Vithayathil, N. Zaidi, N.S. Azad, D.A. Laheru, G.M. Frampton, and E.M. Jaffee, PD-L1 expression and tumor mutational burden are independent biomarkers in most cancers. *JCI Insight*, 2019. 4(6).
 73. Iacobuzio-Donahue, C.A., Genetic evolution of pancreatic cancer: lessons learnt from the pancreatic cancer genome sequencing project. *Gut*, 2012. 61(7): p. 1085-94.
 74. Ying, H., P. Dey, W. Yao, A.C. Kimmelman, G.F. Draetta, A. Maitra, and R.A. DePinho, Genetics and biology of pancreatic ductal adenocarcinoma. *Genes Dev*, 2016. 30(4): p. 355-85.
 75. Hidalgo, M., Pancreatic cancer. *N Engl J Med*, 2010. 362(17): p. 1605-17.
 76. Qian, Z.R., D.A. Robinson, J.A. Nowak, V. Morales-Oyarvide, R.F. Dunne, M.M. Kozak, M.W. Welch, L.K. Brais, A. Da Silva, T. Li, W. Li, A. Masuda, J. Yang, Y. Shi, M. Gu, Y. Masugi, J. Bui, C.L. Zellers, C. Yuan, A. Babic, N. Khalaf, A. Aguirre, K. Ng, R.A. Miksad, A.J. Bullock, D.T. Chang, J.F. Tseng, T.E. Clancy, D.C. Linehan, J.J. Findeis-Hosey, L.A. Doyle, A.R. Thorner, M. Ducar, B. Wollison, A. Laing, W.C. Hahn, M. Meyerson, C.S. Fuchs, S. Ogino, J.L. Hornick, A.F. Hezel, A.C. Koong, and B.M. Wolpin, Association of Alterations in Main Driver Genes With Outcomes of Patients With Resected Pancreatic Ductal Adenocarcinoma. *JAMA Oncol*, 2018. 4(3): p. e173420.
 77. Yachida, S., C.M. White, Y. Naito, Y. Zhong, J.A. Brosnan, A.M. Macgregor-Das, R.A. Morgan, T. Saunders, D.A. Laheru, J.M. Herman, R.H. Hruban, A.P. Klein, S. Jones, V. Velculescu, C.L. Wolfgang, and C.A. Iacobuzio-Donahue, Clinical significance of the genetic landscape of pancreatic cancer and implications for identification of potential long-term survivors. *Clin Cancer Res*, 2012. 18(22): p. 6339-47.
 78. Collisson, E.A., A. Sadanandam, P. Olson, W.J. Gibb, M. Truitt, S. Gu, J. Cooc, J. Weinkle, G.E. Kim, L. Jakkula, H.S. Feiler, A.H. Ko, A.B. Olshen, K.L. Danenberg, M.A. Tempero, P.T. Spellman, D. Hanahan, and J.W. Gray, Subtypes of pancreatic ductal adenocarcinoma and their differing responses to therapy. *Nat Med*, 2011. 17(4): p. 500-3.
 79. Moffitt, R.A., R. Marayati, E.L. Flate, K.E. Volmar, S.G. Loeza, K.A. Hoadley, N.U. Rashid, L.A. Williams, S.C. Eaton, A.H. Chung, J.K. Smyla, J.M. Anderson, H.J. Kim, D.J. Bentrem, M.S. Talamonti, C.A. Iacobuzio-Donahue, M.A. Hollingsworth, and J.J. Yeh, Virtual microdissection identifies distinct tumor- and

- stroma-specific subtypes of pancreatic ductal adenocarcinoma. *Nat Genet*, 2015. 47(10): p. 1168-78.
80. Waddell, N., M. Pajic, A.M. Patch, D.K. Chang, K.S. Kassahn, P. Bailey, A.L. Johns, D. Miller, K. Nones, K. Quek, M.C. Quinn, A.J. Robertson, M.Z. Fadlullah, T.J. Bruxner, A.N. Christ, I. Harliwong, S. Idrisoglu, S. Manning, C. Nourse, E. Nourbakhsh, S. Wani, P.J. Wilson, E. Markham, N. Cloonan, M.J. Anderson, J.L. Fink, O. Holmes, S.H. Kazakoff, C. Leonard, F. Newell, B. Poudel, S. Song, D. Taylor, N. Waddell, S. Wood, Q. Xu, J. Wu, M. Pinese, M.J. Cowley, H.C. Lee, M.D. Jones, A.M. Nagrial, J. Humphris, L.A. Chantrill, V. Chin, A.M. Steinmann, A. Mawson, E.S. Humphrey, E.K. Colvin, A. Chou, C.J. Scarlett, A.V. Pinho, M. Giry-Laterriere, I. Rومان, J.S. Samra, J.G. Kench, J.A. Pettitt, N.D. Merrett, C. Toon, K. Epari, N.Q. Nguyen, A. Barbour, N. Zeps, N.B. Jamieson, J.S. Graham, S.P. Niclou, R. Bjerkvig, R. Grutzmann, D. Aust, R.H. Hruban, A. Maitra, C.A. Iacobuzio-Donahue, C.L. Wolfgang, R.A. Morgan, R.T. Lawlor, V. Corbo, C. Bassi, M. Falconi, G. Zamboni, G. Tortora, M.A. Tempero, I. Australian Pancreatic Cancer Genome, A.J. Gill, J.R. Eshleman, C. Pilarsky, A. Scarpa, E.A. Musgrove, J.V. Pearson, A.V. Biankin, and S.M. Grimmond, Whole genomes redefine the mutational landscape of pancreatic cancer. *Nature*, 2015. 518(7540): p. 495-501.
 81. Bailey, P., D.K. Chang, K. Nones, A.L. Johns, A.M. Patch, M.C. Gingras, D.K. Miller, A.N. Christ, T.J. Bruxner, M.C. Quinn, C. Nourse, L.C. Murtaugh, I. Harliwong, S. Idrisoglu, S. Manning, E. Nourbakhsh, S. Wani, L. Fink, O. Holmes, V. Chin, M.J. Anderson, S. Kazakoff, C. Leonard, F. Newell, N. Waddell, S. Wood, Q. Xu, P.J. Wilson, N. Cloonan, K.S. Kassahn, D. Taylor, K. Quek, A. Robertson, L. Pantano, L. Mincarelli, L.N. Sanchez, L. Evers, J. Wu, M. Pinese, M.J. Cowley, M.D. Jones, E.K. Colvin, A.M. Nagrial, E.S. Humphrey, L.A. Chantrill, A. Mawson, J. Humphris, A. Chou, M. Pajic, C.J. Scarlett, A.V. Pinho, M. Giry-Laterriere, I. Rومان, J.S. Samra, J.G. Kench, J.A. Lovell, N.D. Merrett, C.W. Toon, K. Epari, N.Q. Nguyen, A. Barbour, N. Zeps, K. Moran-Jones, N.B. Jamieson, J.S. Graham, F. Duthie, K. Oien, J. Hair, R. Grutzmann, A. Maitra, C.A. Iacobuzio-Donahue, C.L. Wolfgang, R.A. Morgan, R.T. Lawlor, V. Corbo, C. Bassi, B. Rusev, P. Capelli, R. Salvia, G. Tortora, D. Mukhopadhyay, G.M. Petersen, I. Australian Pancreatic Cancer Genome, D.M. Munzy, W.E. Fisher, S.A. Karim, J.R. Eshleman, R.H. Hruban, C. Pilarsky, J.P. Morton, O.J. Sansom, A. Scarpa, E.A. Musgrove, U.M. Bailey, O. Hofmann, R.L. Sutherland, D.A. Wheeler, A.J. Gill, R.A. Gibbs, J.V. Pearson, N. Waddell, A.V. Biankin and S.M. Grimmond, Genomic analyses identify molecular subtypes of pancreatic cancer. *Nature*, 2016. 531(7592): p. 47-52.
 82. Pishvaian, M.J., R.J. Bender, D. Halverson, L. Rahib, A.E. Hendifar, S. Mikhail, V. Chung, V.J. Picozzi, D. Sohal, E.M. Blais, K. Mason, E.E. Lyons, L.M. Matrisian, J.R. Brody, S. Madhavan, and E.F. Petricoin, 3rd, Molecular Profiling of Patients with Pancreatic Cancer: Initial Results from the Know Your Tumor Initiative. *Clin Cancer Res*, 2018. 24(20): p. 5018-5027.
 83. Puleo, F., R. Nicolle, Y. Blum, J. Cros, L. Marisa, P. Demetter, E. Quertinmont, M. Svrcek, N. Elarouci, J. Iovanna, D. Franchimont, L. Verset, M.G. Galdon, J. Deviere, A. de Reynies, P. Laurent-Puig, J.L. Van Laethem, J.B. Bachet, and R.

- Marechal, Stratification of Pancreatic Ductal Adenocarcinomas Based on Tumor and Microenvironment Features. *Gastroenterology*, 2018. 155(6): p. 1999-2013 e3.
84. Jones, S., X. Zhang, D.W. Parsons, J.C. Lin, R.J. Leary, P. Angenendt, P. Mankoo, H. Carter, H. Kamiyama, A. Jimeno, S.M. Hong, B. Fu, M.T. Lin, E.S. Calhoun, M. Kamiyama, K. Walter, T. Nikolskaya, Y. Nikolsky, J. Hartigan, D.R. Smith, M. Hidalgo, S.D. Leach, A.P. Klein, E.M. Jaffee, M. Goggins, A. Maitra, C. Iacobuzio-Donahue, J.R. Eshleman, S.E. Kern, R.H. Hruban, R. Karchin, N. Papadopoulos, G. Parmigiani, B. Vogelstein, V.E. Velculescu, and K.W. Kinzler, Core signaling pathways in human pancreatic cancers revealed by global genomic analyses. *Science*, 2008. 321(5897): p. 1801-6.
 85. Feig, C., A. Gopinathan, A. Neesse, D.S. Chan, N. Cook, and D.A. Tuveson, The pancreas cancer microenvironment. *Clin Cancer Res*, 2012. 18(16): p. 4266-76.
 86. Hanahan, D. and R.A. Weinberg, Hallmarks of cancer: the next generation. *Cell*, 2011. 144(5): p. 646-74.
 87. Jayson, G.C., R. Kerbel, L.M. Ellis, and A.L. Harris, Antiangiogenic therapy in oncology: current status and future directions. *Lancet*, 2016. 388(10043): p. 518-29.
 88. Kindler, H.L., D. Niedzwiecki, D. Hollis, S. Sutherland, D. Schrag, H. Hurwitz, F. Innocenti, M.F. Mulcahy, E. O'Reilly, T.F. Wozniak, J. Picus, P. Bhargava, R.J. Mayer, R.L. Schilsky, and R.M. Goldberg, Gemcitabine plus bevacizumab compared with gemcitabine plus placebo in patients with advanced pancreatic cancer: phase III trial of the Cancer and Leukemia Group B (CALGB 80303). *J Clin Oncol*, 2010. 28(22): p. 3617-22.
 89. Kindler, H.L., T. Ioka, D.J. Richel, J. Bennouna, R. Letourneau, T. Okusaka, A. Funakoshi, J. Furuse, Y.S. Park, S. Ohkawa, G.M. Springett, H.S. Wasan, P.C. Trask, P. Bycott, A.D. Ricart, S. Kim, and E. Van Cutsem, Axitinib plus gemcitabine versus placebo plus gemcitabine in patients with advanced pancreatic adenocarcinoma: a double-blind randomised phase 3 study. *Lancet Oncol*, 2011. 12(3): p. 256-62.
 90. Goncalves, A., M. Gilibert, E. Francois, L. Dahan, H. Perrier, R. Lamy, D. Re, R. Largillier, M. Gasmi, X. Tchiknavorian, B. Esterni, D. Genre, L. Moureau-Zabotto, M. Giovannini, J.F. Seitz, J.R. Delpero, O. Turrini, P. Viens, and J.L. Raoul, BAYPAN study: a double-blind phase III randomized trial comparing gemcitabine plus sorafenib and gemcitabine plus placebo in patients with advanced pancreatic cancer. *Ann Oncol*, 2012. 23(11): p. 2799-805.
 91. Kalluri, R., The biology and function of fibroblasts in cancer. *Nat Rev Cancer*, 2016. 16(9): p. 582-98.
 92. Olive, K.P., M.A. Jacobetz, C.J. Davidson, A. Gopinathan, D. McIntyre, D. Honess, B. Madhu, M.A. Goldgraben, M.E. Caldwell, D. Allard, K.K. Frese, G. Denicola, C. Feig, C. Combs, S.P. Winter, H. Ireland-Zecchini, S. Reichelt, W.J. Howat, A. Chang, M. Dhara, L. Wang, F. Ruckert, R. Grutzmann, C. Pilarsky, K. Izeradjene, S.R. Hingorani, P. Huang, S.E. Davies, W. Plunkett, M. Egorin, R.H. Hruban, N. Whitebread, K. McGovern, J. Adams, C. Iacobuzio-Donahue, J. Griffiths, and D.A. Tuveson, Inhibition of Hedgehog signaling enhances delivery

- of chemotherapy in a mouse model of pancreatic cancer. *Science*, 2009. 324(5933): p. 1457-61.
93. Provenzano, P.P., C. Cuevas, A.E. Chang, V.K. Goel, D.D. Von Hoff, and S.R. Hingorani, Enzymatic targeting of the stroma ablates physical barriers to treatment of pancreatic ductal adenocarcinoma. *Cancer Cell*, 2012. 21(3): p. 418-29.
 94. Whatcott, C.J., C.H. Diep, P. Jiang, A. Watanabe, J. LoBello, C. Sima, G. Hostetter, H.M. Shepard, D.D. Von Hoff, and H. Han, Desmoplasia in Primary Tumors and Metastatic Lesions of Pancreatic Cancer. *Clin Cancer Res*, 2015. 21(15): p. 3561-8.
 95. Ozdemir, B.C., T. Pentcheva-Hoang, J.L. Carstens, X. Zheng, C.C. Wu, T.R. Simpson, H. Laklai, H. Sugimoto, C. Kahlert, S.V. Novitskiy, A. De Jesus-Acosta, P. Sharma, P. Heidari, U. Mahmood, L. Chin, H.L. Moses, V.M. Weaver, A. Maitra, J.P. Allison, V.S. LeBleu, and R. Kalluri, Depletion of carcinoma-associated fibroblasts and fibrosis induces immunosuppression and accelerates pancreas cancer with reduced survival. *Cancer Cell*, 2014. 25(6): p. 719-34.
 96. Rhim, A.D., P.E. Oberstein, D.H. Thomas, E.T. Mirek, C.F. Palermo, S.A. Sastra, E.N. Dekleva, T. Saunders, C.P. Becerra, I.W. Tattersall, C.B. Westphalen, J. Kitajewski, M.G. Fernandez-Barrena, M.E. Fernandez-Zapico, C. Iacobuzio-Donahue, K.P. Olive, and B.Z. Stanger, Stromal elements act to restrain, rather than support, pancreatic ductal adenocarcinoma. *Cancer Cell*, 2014. 25(6): p. 735-47.
 97. Feig, C., J.O. Jones, M. Kraman, R.J. Wells, A. Deonarine, D.S. Chan, C.M. Connell, E.W. Roberts, Q. Zhao, O.L. Caballero, S.A. Teichmann, T. Janowitz, D.I. Jodrell, D.A. Tuveson, and D.T. Fearon, Targeting CXCL12 from FAP-expressing carcinoma-associated fibroblasts synergizes with anti-PD-L1 immunotherapy in pancreatic cancer. *Proc Natl Acad Sci U S A*, 2013. 110(50): p. 20212-7.
 98. Sherman, M.H., R.T. Yu, D.D. Engle, N. Ding, A.R. Atkins, H. Tiriach, E.A. Collisson, F. Connor, T. Van Dyke, S. Kozlov, P. Martin, T.W. Tseng, D.W. Dawson, T.R. Donahue, A. Masamune, T. Shimosegawa, M.V. Apte, J.S. Wilson, B. Ng, S.L. Lau, J.E. Gunton, G.M. Wahl, T. Hunter, J.A. Drebin, P.J. O'Dwyer, C. Liddle, D.A. Tuveson, M. Downes, and R.M. Evans, Vitamin D receptor-mediated stromal reprogramming suppresses pancreatitis and enhances pancreatic cancer therapy. *Cell*, 2014. 159(1): p. 80-93.
 99. Biffi, G., T.E. Oni, B. Spielman, Y. Hao, E. Elyada, Y. Park, J. Preall, and D.A. Tuveson, IL1-Induced JAK/STAT Signaling Is Antagonized by TGFbeta to Shape CAF Heterogeneity in Pancreatic Ductal Adenocarcinoma. *Cancer Discov*, 2019. 9(2): p. 282-301.
 100. Elyada, E., M. Bolisetty, P. Laise, W.F. Flynn, E.T. Courtois, R.A. Burkhart, J.A. Teinor, P. Belleau, G. Biffi, M.S. Lucito, S. Sivajothi, T.D. Armstrong, D.D. Engle, K.H. Yu, Y. Hao, C.L. Wolfgang, Y. Park, J. Preall, E.M. Jaffee, A. Califano, P. Robson, and D.A. Tuveson, Cross-Species Single-Cell Analysis of Pancreatic Ductal Adenocarcinoma Reveals Antigen-Presenting Cancer-Associated Fibroblasts. *Cancer Discov*, 2019.

101. Hingorani, S.R., L. Zheng, A.J. Bullock, T.E. Seery, W.P. Harris, D.S. Sigal, F. Braiteh, P.S. Ritch, M.M. Zalupski, N. Bahary, P.E. Oberstein, A. Wang-Gillam, W. Wu, D. Chondros, P. Jiang, S. Khelifa, J. Pu, C. Aldrich, and A.E. Hendifar, HALO 202: Randomized Phase II Study of PEGPH20 Plus Nab-Paclitaxel/Gemcitabine Versus Nab-Paclitaxel/Gemcitabine in Patients With Untreated, Metastatic Pancreatic Ductal Adenocarcinoma. *J Clin Oncol*, 2018. 36(4): p. 359-366.
102. Chen, D.S. and I. Mellman, Oncology meets immunology: the cancer-immunity cycle. *Immunity*, 2013. 39(1): p. 1-10.
103. DeNardo, D.G. and B. Ruffell, Macrophages as regulators of tumour immunity and immunotherapy. *Nat Rev Immunol*, 2019. 19(6): p. 369-382.
104. Morrison, A.H., K.T. Byrne, and R.H. Vonderheide, Immunotherapy and Prevention of Pancreatic Cancer. *Trends Cancer*, 2018. 4(6): p. 418-428.
105. Vonderheide, R.H., The Immune Revolution: A Case for Priming, Not Checkpoint. *Cancer Cell*, 2018. 33(4): p. 563-569.
106. Hanahan, D. and L.M. Coussens, Accessories to the crime: functions of cells recruited to the tumor microenvironment. *Cancer Cell*, 2012. 21(3): p. 309-22.
107. Karamitopoulou, E., Tumour microenvironment of pancreatic cancer: immune landscape is dictated by molecular and histopathological features. *Br J Cancer*, 2019. 121(1): p. 5-14.
108. Steele, C.W., S.A. Karim, J.D.G. Leach, P. Bailey, R. Upstill-Goddard, L. Rishi, M. Foth, S. Bryson, K. McDaid, Z. Wilson, C. Eberlein, J.B. Candido, M. Clarke, C. Nixon, J. Connelly, N. Jamieson, C.R. Carter, F. Balkwill, D.K. Chang, T.R.J. Evans, D. Strathdee, A.V. Biankin, R.J.B. Nibbs, S.T. Barry, O.J. Sansom, and J.P. Morton, CXCR2 Inhibition Profoundly Suppresses Metastases and Augments Immunotherapy in Pancreatic Ductal Adenocarcinoma. *Cancer Cell*, 2016. 29(6): p. 832-845.
109. Zhu, Y., B.L. Knolhoff, M.A. Meyer, T.M. Nywening, B.L. West, J. Luo, A. Wang-Gillam, S.P. Goedegebuure, D.C. Linehan, and D.G. DeNardo, CSF1/CSF1R blockade reprograms tumor-infiltrating macrophages and improves response to T-cell checkpoint immunotherapy in pancreatic cancer models. *Cancer Res*, 2014. 74(18): p. 5057-69.
110. Nywening, T.M., B.A. Belt, D.R. Cullinan, R.Z. Panni, B.J. Han, D.E. Sanford, R.C. Jacobs, J. Ye, A.A. Patel, W.E. Gillanders, R.C. Fields, D.G. DeNardo, W.G. Hawkins, P. Goedegebuure, and D.C. Linehan, Targeting both tumour-associated CXCR2(+) neutrophils and CCR2(+) macrophages disrupts myeloid recruitment and improves chemotherapeutic responses in pancreatic ductal adenocarcinoma. *Gut*, 2018. 67(6): p. 1112-1123.
111. Gunderson, A.J., M.M. Kaneda, T. Tsujikawa, A.V. Nguyen, N.I. Affara, B. Ruffell, S. Gorjestani, S.M. Liudahl, M. Truitt, P. Olson, G. Kim, D. Hanahan, M.A. Tempero, B. Sheppard, B. Irving, B.Y. Chang, J.A. Varner, and L.M. Coussens, Bruton Tyrosine Kinase-Dependent Immune Cell Cross-talk Drives Pancreas Cancer. *Cancer Discov*, 2016. 6(3): p. 270-85.
112. Pylayeva-Gupta, Y., S. Das, J.S. Handler, C.H. Hajdu, M. Coffre, S.B. Koralov, and D. Bar-Sagi, IL35-Producing B Cells Promote the Development of Pancreatic Neoplasia. *Cancer Discov*, 2016. 6(3): p. 247-55.

113. Lee, K.E., M. Spata, L.J. Bayne, E.L. Buza, A.C. Durham, D. Allman, R.H. Vonderheide, and M.C. Simon, Hif1a Deletion Reveals Pro-Neoplastic Function of B Cells in Pancreatic Neoplasia. *Cancer Discov*, 2016. 6(3): p. 256-69.
114. Byrne, K.T. and R.H. Vonderheide, CD40 stimulation obviates innate sensors and drives T cell immunity in cancer. *Cell Reports*, 2016. 15(12): p. 2719-2732.
115. Li, J., K.T. Byrne, F. Yan, T. Yamazoe, Z. Chen, T. Baslan, L.P. Richman, J.H. Lin, Y.H. Sun, A.J. Rech, D. Balli, C.A. Hay, Y. Sela, A.J. Merrell, S.M. Liudahl, N. Gordon, R.J. Norgard, S. Yuan, S. Yu, T. Chao, S. Ye, T.S.K. Eisinger-Mathason, R.B. Faryabi, J.W. Tobias, S.W. Lowe, L.M. Coussens, E.J. Wherry, R.H. Vonderheide, and B.Z. Stanger, Tumor Cell-Intrinsic Factors Underlie Heterogeneity of Immune Cell Infiltration and Response to Immunotherapy. *Immunity*, 2018. 49(1): p. 178-193 e7.
116. Tsujikawa, T., S. Kumar, R.N. Borkar, V. Azimi, G. Thibault, Y.H. Chang, A. Balter, R. Kawashima, G. Choe, D. Sauer, E. El Rassi, D.R. Clayburgh, M.F. Kulesz-Martin, E.R. Lutz, L. Zheng, E.M. Jaffee, P. Leyshock, A.A. Margolin, M. Mori, J.W. Gray, P.W. Flint, and L.M. Coussens, Quantitative Multiplex Immunohistochemistry Reveals Myeloid-Inflamed Tumor-Immune Complexity Associated with Poor Prognosis. *Cell Rep*, 2017. 19(1): p. 203-217.
117. Wartenberg, M., S. Cibi, I. Zlobec, E. Vassela, S. Eppenberger-Castori, L. Terracciano, M.D. Eichmann, M. Worni, B. Gloor, A. Perren, and E. Karamitopoulou, Integrated Genomic and Immunophenotypic Classification of Pancreatic Cancer Reveals Three Distinct Subtypes with Prognostic/Predictive Significance. *Clinical Cancer Research*, 2018. 24(18): p. 4444-4454.
118. Le, D.T., J.N. Durham, K.N. Smith, H. Wang, B.R. Bartlett, L.K. Aulakh, S. Lu, H. Kemberling, C. Wilt, B.S. Luber, F. Wong, N.S. Azad, A.A. Rucki, D. Laheru, R. Donehower, A. Zaheer, G.A. Fisher, T.S. Crocenzi, J.J. Lee, T.F. Greten, A.G. Duffy, K.K. Ciombor, A.D. Eyring, B.H. Lam, A. Joe, S.P. Kang, M. Holdhoff, L. Danilova, L. Cope, C. Meyer, S. Zhou, R.M. Goldberg, D.K. Armstrong, K.M. Bever, A.N. Fader, J. Taube, F. Housseau, D. Spetzler, N. Xiao, D.M. Pardoll, N. Papadopoulos, K.W. Kinzler, J.R. Eshleman, B. Vogelstein, R.A. Anders, and L.A. Diaz, Jr., Mismatch repair deficiency predicts response of solid tumors to PD-1 blockade. *Science*, 2017. 357(6349): p. 409-413.
119. Pages, F., B. Mlecnik, F. Marliot, G. Bindea, F.S. Ou, C. Bifulco, A. Lugli, I. Zlobec, T.T. Rau, M.D. Berger, I.D. Nagtegaal, E. Vink-Borger, A. Hartmann, C. Geppert, J. Kolwelter, S. Merkel, R. Grutzmann, M. Van den Eynde, A. Jouret-Mourin, A. Kartheuser, D. Leonard, C. Remue, J.Y. Wang, P. Bavi, M.H.A. Roehrl, P.S. Ohashi, L.T. Nguyen, S. Han, H.L. MacGregor, S. Hafezi-Bakhtiari, B.G. Wouters, G.V. Masucci, E.K. Andersson, E. Zavadova, M. Vocka, J. Spacek, L. Petruzella, B. Konopasek, P. Dundr, H. Skalova, K. Nemejcova, G. Botti, F. Tatangelo, P. Delrio, G. Ciliberto, M. Maio, L. Laghi, F. Grizzi, T. Fredriksen, B. Buttard, M. Angelova, A. Vasaturo, P. Maby, S.E. Church, H.K. Angell, L. Lafontaine, D. Bruni, C. El Sissy, N. Haicheur, A. Kirilovsky, A. Berger, C. Lagorce, J.P. Meyers, C. Paustian, Z. Feng, C. Ballesteros-Merino, J. Dijkstra, C. van de Water, S. van Lent-van Vliet, N. Knijn, A.M. Musina, D.V. Scripcariu, B. Popivanova, M. Xu, T. Fujita, S. Hazama, N. Suzuki, H. Nagano, K. Okuno, T. Torigoe, N. Sato, T. Furuhashi, I. Takemasa, K. Itoh, P.S. Patel, H.H.

- Vora, B. Shah, J.B. Patel, K.N. Rajvik, S.J. Pandya, S.N. Shukla, Y. Wang, G. Zhang, Y. Kawakami, F.M. Marincola, P.A. Ascierto, D.J. Sargent, B.A. Fox, and J. Galon, International validation of the consensus Immunoscore for the classification of colon cancer: a prognostic and accuracy study. *Lancet*, 2018. 391(10135): p. 2128-2139.
120. Lin, J.R., B. Izar, S. Wang, C. Yapp, S. Mei, P.M. Shah, S. Santagata, and P.K. Sorger, Highly multiplexed immunofluorescence imaging of human tissues and tumors using t-CyCIF and conventional optical microscopes. *Elife*, 2018. 7.
 121. Keren, L., M. Bosse, D. Marquez, R. Angoshtari, S. Jain, S. Varma, S.R. Yang, A. Kurian, D. Van Valen, R. West, S.C. Bendall, and M. Angelo, A Structured Tumor-Immune Microenvironment in Triple Negative Breast Cancer Revealed by Multiplexed Ion Beam Imaging. *Cell*, 2018. 174(6): p. 1373-1387 e19.
 122. Carstens, J.L., P. Correa de Sampaio, D. Yang, S. Barua, H. Wang, A. Rao, J.P. Allison, V.S. LeBleu, and R. Kalluri, Spatial computation of intratumoral T cells correlates with survival of patients with pancreatic cancer. *Nat Commun*, 2017. 8: p. 15095.
 123. Stromnes, I.M., A. Hulbert, R.H. Pierce, P.D. Greenberg, and S.R. Hingorani, T-cell Localization, Activation, and Clonal Expansion in Human Pancreatic Ductal Adenocarcinoma. *Cancer Immunol Res*, 2017. 5(11): p. 978-991.
 124. Masugi, Y., T. Abe, A. Ueno, Y. Fujii-Nishimura, H. Ojima, Y. Endo, Y. Fujita, M. Kitago, M. Shinoda, Y. Kitagawa, and M. Sakamoto, Characterization of spatial distribution of tumor-infiltrating CD8(+) T cells refines their prognostic utility for pancreatic cancer survival. *Mod Pathol*, 2019.
 125. Banik, G., C.B. Betts, S.M. Liudahl, S. Sivagnanam, R. Kawashima, T. Cotechini, W. Larson, J. Goecks, S.I. Pai, D.R. Clayburgh, T. Tsujikawa, and L.M. Coussens, High-dimensional multiplexed immunohistochemical characterization of immune contexture in human cancers. *Methods in Enzymology*, 2019.
 126. Means, C., D.R. Clayburgh, L. Maloney, D. Sauer, M.H. Taylor, M.L. Shindo, L.M. Coussens, and T. Tsujikawa, Tumor immune microenvironment characteristics of papillary thyroid carcinoma are associated with histopathological aggressiveness and BRAF mutation status. *Head Neck*, 2019.
 127. Schindelin, J., I. Arganda-Carreras, E. Frise, V. Kaynig, M. Longair, T. Pietzsch, S. Preibisch, C. Rueden, S. Saalfeld, B. Schmid, J.Y. Tinevez, D.J. White, V. Hartenstein, K. Eliceiri, P. Tomancak, and A. Cardona, Fiji: an open-source platform for biological-image analysis. *Nat Methods*, 2012. 9(7): p. 676-82.
 128. Carpenter, A.E., T.R. Jones, M.R. Lamprecht, C. Clarke, I.H. Kang, O. Friman, D.A. Guertin, J.H. Chang, R.A. Lindquist, J. Moffat, P. Golland, and D.M. Sabatini, CellProfiler: image analysis software for identifying and quantifying cell phenotypes. *Genome Biol*, 2006. 7(10): p. R100.
 129. Fridman, W.H., F. Pages, C. Sautes-Fridman, and J. Galon, The immune contexture in human tumours: impact on clinical outcome. *Nat Rev Cancer*, 2012. 12(4): p. 298-306.
 130. Ino, Y., R. Yamazaki-Itoh, K. Shimada, M. Iwasaki, T. Kosuge, Y. Kanai, and N. Hiraoka, Immune cell infiltration as an indicator of the immune microenvironment of pancreatic cancer. *Br J Cancer*, 2013. 108(4): p. 914-23.

131. Balachandran, V.P., M. Luksza, J.N. Zhao, V. Makarov, J.A. Moral, R. Remark, B. Herbst, G. Askan, U. Bhanot, Y. Senbabaoglu, D.K. Wells, C.I.O. Cary, O. Grbovic-Huezo, M. Attiyeh, B. Medina, J. Zhang, J. Loo, J. Saglimbeni, M. Abu-Akeel, R. Zappasodi, N. Riaz, M. Smoragiewicz, Z.L. Kelley, O. Basturk, I. Australian Pancreatic Cancer Genome, R. Garvan Institute of Medical, H. Prince of Wales, H. Royal North Shore, G. University of, H. St Vincent's, Q.B.M.R. Institute, C.f.C.R. University of Melbourne, I.f.M.B. University of Queensland, H. Bankstown, H. Liverpool, C.O.B.L. Royal Prince Alfred Hospital, H. Westmead, H. Fremantle, H. St John of God, H. Royal Adelaide, C. Flinders Medical, P. Envoi, H. Princess Alexandria, H. Austin, I. Johns Hopkins Medical, A.R.-N.C.f.A.R.o. Cancer, M. Gonen, A.J. Levine, P.J. Allen, D.T. Fearon, M. Merad, S. Gnjjatic, C.A. Iacobuzio-Donahue, J.D. Wolchok, R.P. DeMatteo, T.A. Chan, B.D. Greenbaum, T. Merghoub, and S.D. Leach, Identification of unique neoantigen qualities in long-term survivors of pancreatic cancer. *Nature*, 2017. 551(7681): p. 512-516.
132. Mantovani, A., S.K. Biswas, M.R. Galdiero, A. Sica, and M. Locati, Macrophage plasticity and polarization in tissue repair and remodelling. *J Pathol*, 2013. 229(2): p. 176-85.
133. Ruffell, B. and L.M. Coussens, Macrophages and therapeutic resistance in cancer. *Cancer Cell*, 2015. 27(4): p. 462-72.
134. de Saint-Vis, B., J. Vincent, S. Vandenabeele, B. Vanbervliet, J.J. Pin, S. Ait-Yahia, S. Patel, M.G. Mattei, J. Banchereau, S. Zurawski, J. Davoust, C. Caux, and S. Lebecque, A novel lysosome-associated membrane glycoprotein, DC-LAMP, induced upon DC maturation, is transiently expressed in MHC class II compartment. *Immunity*, 1998. 9(3): p. 325-36.
135. Miner, K.T. and M. Croft, Generation, persistence, and modulation of Th0 effector cells: role of autocrine IL-4 and IFN-gamma. *J Immunol*, 1998. 160(11): p. 5280-7.
136. Hundeyin, M., E. Kurz, A. Mishra, J.A. Kochen Rossi, S.M. Liudahl, K.R. Leis, H. Mehrotra, M. Kim, L.E. Torres, A. Ogunsakin, J. Link, R.C. Sears, S. Sivagnanam, J. Goecks, K.S. Islam, I. Dolgalev, S. Savadkar, W. Wang, B. Aykut, J. Leinwand, B. Diskin, S. Adam, M. Israr, M. Gelas, J. Lish, K. Chin, M.S. Farooq, B. Wadowski, J. Wu, S. Shah, D.O. Adeegbe, S. Pushalkar, V. Vasudevaraja, D. Saxena, K.K. Wong, L.M. Coussens, and G. Miller, Innate alphabeta T cells Mediate Antitumor Immunity by Orchestrating Immunogenic Macrophage Programming. *Cancer Discov*, 2019.
137. Daley, D., C.P. Zambirinis, L. Seifert, N. Akkad, N. Mohan, G. Werba, R. Barilla, A. Torres-Hernandez, M. Hundeyin, V.R.K. Mani, A. Avanzi, D. Tipples, R. Narayanan, J.E. Jang, E. Newman, V.G. Pillarisetty, M.L. Dustin, D. Bar-Sagi, C. Hajdu, and G. Miller, gammadelta T Cells Support Pancreatic Oncogenesis by Restraining alphabeta T Cell Activation. *Cell*, 2016. 166(6): p. 1485-1499 e15.
138. Lutz, E.R., A.A. Wu, E. Bigelow, R. Sharma, G. Mo, K. Soares, S. Solt, A. Dorman, A. Wamwea, A. Yager, D. Laheru, C.L. Wolfgang, J. Wang, R.H. Hruban, R.A. Anders, E.M. Jaffee, and L. Zheng, Immunotherapy converts nonimmunogenic pancreatic tumors into immunogenic foci of immune regulation. *Cancer Immunol Res*, 2014. 2(7): p. 616-31.

139. Hiraoka, N., Y. Ino, R. Yamazaki-Itoh, Y. Kanai, T. Kosuge, and K. Shimada, Intratumoral tertiary lymphoid organ is a favourable prognosticator in patients with pancreatic cancer. *Br J Cancer*, 2015. 112(11): p. 1782-90.
140. DeNardo, D.G., D.J. Brennan, E. Rexhepaj, B. Ruffell, S.L. Shiao, S.F. Madden, W.M. Gallagher, N. Wadhvani, S.D. Keil, S.A. Junaid, H.S. Rugo, E.S. Hwang, K. Jirstrom, B.L. West, and L.M. Coussens, Leukocyte complexity predicts breast cancer survival and functionally regulates response to chemotherapy. *Cancer Discov*, 2011. 1(1): p. 54-67.
141. Diana, A., L.M. Wang, Z. D'Costa, A. Azad, M.A. Silva, Z. Soonawalla, P. Allen, S. Liu, W.G. McKenna, R.J. Muschel, and E. Fokas, Prognostic role and correlation of CA9, CD31, CD68 and CD20 with the desmoplastic stroma in pancreatic ductal adenocarcinoma. *Oncotarget*, 2016. 7(45): p. 72819-72832.
142. Ino, Y., S. Oguro, R. Yamazaki-Itoh, S. Hori, K. Shimada, and N. Hiraoka, Reliable evaluation of tumor-infiltrating lymphocytes in pancreatic cancer tissue biopsies. *Oncotarget*, 2019. 10(10): p. 1149-1159.
143. Bally, A.P., J.W. Austin, and J.M. Boss, Genetic and Epigenetic Regulation of PD-1 Expression. *J Immunol*, 2016. 196(6): p. 2431-7.
144. Centuori, S.M., C.J. Gomes, S.S. Kim, C.W. Putnam, B.T. Larsen, L.L. Garland, D.W. Mount, and J.D. Martinez, Double-negative (CD27(-)IgD(-)) B cells are expanded in NSCLC and inversely correlate with affinity-matured B cell populations. *J Transl Med*, 2018. 16(1): p. 30.
145. Wu, Y.C., D. Kipling, and D.K. Dunn-Walters, The relationship between CD27 negative and positive B cell populations in human peripheral blood. *Front Immunol*, 2011. 2: p. 81.
146. Kather, J.N., M. Suarez-Carmona, P. Charoentong, C.A. Weis, D. Hirsch, P. Bankhead, M. Horning, D. Ferber, I. Kel, E. Herpel, S. Schott, I. Zornig, J. Utikal, A. Marx, T. Gaiser, H. Brenner, J. Chang-Claude, M. Hoffmeister, D. Jager, and N. Halama, Topography of cancer-associated immune cells in human solid tumors. *Elife*, 2018. 7.
147. Ruffell, B., A. Au, H.S. Rugo, L.J. Esserman, E.S. Hwang, and L.M. Coussens, Leukocyte composition of human breast cancer. *Proc Natl Acad Sci U S A*, 2012. 109(8): p. 2796-801.
148. Parra, E.R., P. Villalobos, C. Behrens, M. Jiang, A. Pataer, S.G. Swisher, W.N. William, Jr., J. Zhang, J. Lee, T. Cascone, J.V. Heymach, M.A. Forget, C. Haymaker, C. Bernatchez, N. Kalhor, A. Weissferdt, C. Moran, J. Zhang, A. Vaporciyan, D.L. Gibbons, B. Sepesi, and Wistuba, II, Effect of neoadjuvant chemotherapy on the immune microenvironment in non-small cell lung carcinomas as determined by multiplex immunofluorescence and image analysis approaches. *J Immunother Cancer*, 2018. 6(1): p. 48.
149. Wellenstein, M.D. and K.E. de Visser, Cancer-Cell-Intrinsic Mechanisms Shaping the Tumor Immune Landscape. *Immunity*, 2018. 48(3): p. 399-416.
150. Blackford, A., O.K. Serrano, C.L. Wolfgang, G. Parmigiani, S. Jones, X. Zhang, D.W. Parsons, J.C. Lin, R.J. Leary, J.R. Eshleman, M. Goggins, E.M. Jaffee, C.A. Iacobuzio-Donahue, A. Maitra, J.L. Cameron, K. Olino, R. Schulick, J. Winter, J.M. Herman, D. Laheru, A.P. Klein, B. Vogelstein, K.W. Kinzler, V.E.

- Velculescu, and R.H. Hruban, SMAD4 gene mutations are associated with poor prognosis in pancreatic cancer. *Clin Cancer Res*, 2009. 15(14): p. 4674-9.
151. Iacobuzio-Donahue, C.A., B. Fu, S. Yachida, M. Luo, H. Abe, C.M. Henderson, F. Vilardell, Z. Wang, J.W. Keller, P. Banerjee, J.M. Herman, J.L. Cameron, C.J. Yeo, M.K. Halushka, J.R. Eshleman, M. Raben, A.P. Klein, R.H. Hruban, M. Hidalgo, and D. Laheru, DPC4 gene status of the primary carcinoma correlates with patterns of failure in patients with pancreatic cancer. *J Clin Oncol*, 2009. 27(11): p. 1806-13.
 152. Oshima, M., K. Okano, S. Muraki, R. Haba, T. Maeba, Y. Suzuki, and S. Yachida, Immunohistochemically detected expression of 3 major genes (CDKN2A/p16, TP53, and SMAD4/DPC4) strongly predicts survival in patients with resectable pancreatic cancer. *Ann Surg*, 2013. 258(2): p. 336-46.
 153. Tascilar, M., H.G. Skinner, C. Rosty, T. Sohn, R.E. Wilentz, G.J. Offerhaus, V. Adsay, R.A. Abrams, J.L. Cameron, S.E. Kern, C.J. Yeo, R.H. Hruban, and M. Goggins, The SMAD4 protein and prognosis of pancreatic ductal adenocarcinoma. *Clin Cancer Res*, 2001. 7(12): p. 4115-21.
 154. Wang, W.Q., L. Liu, H.X. Xu, C.T. Wu, J.F. Xiang, J. Xu, C. Liu, J. Long, Q.X. Ni, and X.J. Yu, Infiltrating immune cells and gene mutations in pancreatic ductal adenocarcinoma. *Br J Surg*, 2016. 103(9): p. 1189-99.
 155. Yamamoto, T., K. Kawada, Y. Itatani, S. Inamoto, R. Okamura, M. Iwamoto, E. Miyamoto, T.F. Chen-Yoshikawa, H. Hirai, S. Hasegawa, H. Date, M.M. Taketo, and Y. Sakai, Loss of SMAD4 Promotes Lung Metastasis of Colorectal Cancer by Accumulation of CCR1+ Tumor-Associated Neutrophils through CCL15-CCR1 Axis. *Clin Cancer Res*, 2017. 23(3): p. 833-844.
 156. Wormann, S.M., L. Song, J. Ai, K.N. Diakopoulos, M.U. Kurkowski, K. Gorgulu, D. Ruess, A. Campbell, C. Doglioni, D. Jodrell, A. Neesse, I.E. Demir, A.P. Karpathaki, M. Barenboim, T. Hagemann, S. Rose-John, O. Sansom, R.M. Schmid, M.P. Protti, M. Lesina, and H. Algul, Loss of P53 Function Activates JAK2-STAT3 Signaling to Promote Pancreatic Tumor Growth, Stroma Modification, and Gemcitabine Resistance in Mice and Is Associated With Patient Survival. *Gastroenterology*, 2016. 151(1): p. 180-193 e12.
 157. Wellenstein, M.D., S.B. Coffelt, D.E.M. Duits, M.H. van Miltenburg, M. Slagter, I. de Rink, L. Henneman, S.M. Kas, S. Prekovic, C.S. Hau, K. Vrijland, A.P. Drenth, R. de Korte-Grimmerink, E. Schut, I. van der Heijden, W. Zwart, L.F.A. Wessels, T.N. Schumacher, J. Jonkers, and K.E. de Visser, Loss of p53 triggers WNT-dependent systemic inflammation to drive breast cancer metastasis. *Nature*, 2019.
 158. Wherry, E.J. and M. Kurachi, Molecular and cellular insights into T cell exhaustion. *Nat Rev Immunol*, 2015. 15(8): p. 486-99.
 159. Murphy, J.E., J.Y. Wo, D.P. Ryan, W. Jiang, B.Y. Yeap, L.C. Drapek, L.S. Blaszkowsky, E.L. Kwak, J.N. Allen, J.W. Clark, J.E. Faris, A.X. Zhu, L. Goyal, K.D. Lillemoe, T.F. DeLaney, C. Fernandez-Del Castillo, C.R. Ferrone, and T.S. Hong, Total Neoadjuvant Therapy With FOLFIRINOX Followed by Individualized Chemoradiotherapy for Borderline Resectable Pancreatic Adenocarcinoma: A Phase 2 Clinical Trial. *JAMA Oncol*, 2018. 4(7): p. 963-969.

160. Murphy, J.E., J.Y. Wo, D.P. Ryan, J.W. Clark, W. Jiang, B.Y. Yeap, L.C. Drapek, L. Ly, C.V. Baglini, L.S. Blaszkowsky, C.R. Ferrone, A.R. Parikh, C.D. Weekes, R.D. Nipp, E.L. Kwak, J.N. Allen, R.B. Corcoran, D.T. Ting, J.E. Faris, A.X. Zhu, L. Goyal, D.L. Berger, M. Qadan, K.D. Lillemoe, N. Talele, R.K. Jain, T.F. DeLaney, D.G. Duda, Y. Boucher, C. Fernandez-Del Castillo, and T.S. Hong, Total Neoadjuvant Therapy With FOLFIRINOX in Combination With Losartan Followed by Chemoradiotherapy for Locally Advanced Pancreatic Cancer: A Phase 2 Clinical Trial. *JAMA Oncol*, 2019.
161. Shibuya, K.C., V.K. Goel, W. Xiong, J.G. Sham, S.M. Pollack, A.M. Leahy, S.H. Whiting, M.M. Yeh, C. Yee, S.R. Riddell, and V.G. Pillarisetty, Pancreatic ductal adenocarcinoma contains an effector and regulatory immune cell infiltrate that is altered by multimodal neoadjuvant treatment. *PLoS One*, 2014. 9(5): p. e96565.
162. Danilova, L., W.J. Ho, Q. Zhu, T. Vithayathil, A. De Jesus-Acosta, N.S. Azad, D.A. Laheru, E.J. Fertig, R. Anders, E.M. Jaffee, and M. Yarchoan, Programmed Cell Death Ligand-1 (PD-L1) and CD8 Expression Profiling Identify an Immunologic Subtype of Pancreatic Ductal Adenocarcinomas with Favorable Survival. *Cancer Immunol Res*, 2019. 7(6): p. 886-895.
163. Anderson, A.C., N. Joller, and V.K. Kuchroo, Lag-3, Tim-3, and TIGIT: Co-inhibitory Receptors with Specialized Functions in Immune Regulation. *Immunity*, 2016. 44(5): p. 989-1004.
164. Scott, A.C., F. Dundar, P. Zumbo, S.S. Chandran, C.A. Klebanoff, M. Shakiba, P. Trivedi, L. Menocal, H. Appleby, S. Camara, D. Zamarin, T. Walther, A. Snyder, M.R. Femia, E.A. Comen, H.Y. Wen, M.D. Hellmann, N. Anandasabapathy, Y. Liu, N.K. Altorki, P. Lauer, O. Levy, M.S. Glickman, J. Kaye, D. Betel, M. Philip, and A. Schietinger, TOX is a critical regulator of tumour-specific T cell differentiation. *Nature*, 2019. 571(7764): p. 270-274.
165. Alfei, F., K. Kanev, M. Hofmann, M. Wu, H.E. Ghoneim, P. Roelli, D.T. Utzschneider, M. von Hoesslin, J.G. Cullen, Y. Fan, V. Eisenberg, D. Wohlleber, K. Steiger, D. Merkler, M. Delorenzi, P.A. Knolle, C.J. Cohen, R. Thimme, B. Youngblood, and D. Zehn, TOX reinforces the phenotype and longevity of exhausted T cells in chronic viral infection. *Nature*, 2019. 571(7764): p. 265-269.
166. Khan, O., J.R. Giles, S. McDonald, S. Manne, S.F. Ngiew, K.P. Patel, M.T. Werner, A.C. Huang, K.A. Alexander, J.E. Wu, J. Attanasio, P. Yan, S.M. George, B. Bengsch, R.P. Staupe, G. Donahue, W. Xu, R.K. Amaravadi, X. Xu, G.C. Karakousis, T.C. Mitchell, L.M. Schuchter, J. Kaye, S.L. Berger, and E.J. Wherry, TOX transcriptionally and epigenetically programs CD8(+) T cell exhaustion. *Nature*, 2019. 571(7764): p. 211-218.
167. Siddiqui, I., K. Schaeuble, V. Chennupati, S.A. Fuertes Marraco, S. Calderon-Copete, D. Pais Ferreira, S.J. Carmona, L. Scarpellino, D. Gfeller, S. Pradervand, S.A. Luther, D.E. Speiser, and W. Held, Intratumoral Tcf1(+)PD-1(+)CD8(+) T Cells with Stem-like Properties Promote Tumor Control in Response to Vaccination and Checkpoint Blockade Immunotherapy. *Immunity*, 2019. 50(1): p. 195-211 e10.
168. Tedder, T.F. and P. Engel, CD20: a regulator of cell-cycle progression of B lymphocytes. *Immunol Today*, 1994. 15(9): p. 450-4.

169. Salles, G., M. Barrett, R. Foa, J. Maurer, S. O'Brien, N. Valente, M. Wenger, and D.G. Maloney, Rituximab in B-Cell Hematologic Malignancies: A Review of 20 Years of Clinical Experience. *Adv Ther*, 2017. 34(10): p. 2232-2273.
170. Musette, P. and J.D. Bouaziz, B Cell Modulation Strategies in Autoimmune Diseases: New Concepts. *Front Immunol*, 2018. 9: p. 622.
171. Beers, S.A., C.H. Chan, R.R. French, M.S. Cragg, and M.J. Glennie, CD20 as a target for therapeutic type I and II monoclonal antibodies. *Semin Hematol*, 2010. 47(2): p. 107-14.
172. Yuen, G.J., E. Demissie, and S. Pillai, B lymphocytes and cancer: a love-hate relationship. *Trends Cancer*, 2016. 2(12): p. 747-757.
173. de Visser, K.E., L.V. Korets, and L.M. Coussens, De novo carcinogenesis promoted by chronic inflammation is B lymphocyte dependent. *Cancer Cell*, 2005. 7(5): p. 411-23.
174. Andreu, P., M. Johansson, N.I. Affara, F. Pucci, T. Tan, S. Junankar, L. Korets, J. Lam, D. Tawfik, D.G. DeNardo, L. Naldini, K.E. de Visser, M. De Palma, and L.M. Coussens, FcRgamma activation regulates inflammation-associated squamous carcinogenesis. *Cancer Cell*, 2010. 17(2): p. 121-34.
175. Affara, N.I., B. Ruffell, T.R. Medler, A.J. Gunderson, M. Johansson, S. Bornstein, E. Bergsland, M. Steinhoff, Y. Li, Q. Gong, Y. Ma, J.F. Wiesen, M.H. Wong, M. Kulesz-Martin, B. Irving, and L.M. Coussens, B cells regulate macrophage phenotype and response to chemotherapy in squamous carcinomas. *Cancer Cell*, 2014. 25(6): p. 809-821.
176. Gong, Q., Q. Ou, S. Ye, W.P. Lee, J. Cornelius, L. Diehl, W.Y. Lin, Z. Hu, Y. Lu, Y. Chen, Y. Wu, Y.G. Meng, P. Gribling, Z. Lin, K. Nguyen, T. Tran, Y. Zhang, H. Rosen, F. Martin, and A.C. Chan, Importance of cellular microenvironment and circulatory dynamics in B cell immunotherapy. *J Immunol*, 2005. 174(2): p. 817-26.
177. Hamaguchi, Y., J. Uchida, D.W. Cain, G.M. Venturi, J.C. Poe, K.M. Haas, and T.F. Tedder, The peritoneal cavity provides a protective niche for B1 and conventional B lymphocytes during anti-CD20 immunotherapy in mice. *J Immunol*, 2005. 174(7): p. 4389-99.
178. Laws, L.H., C.E. Parker, G. Cherala, Y. Koguchi, A. Waisman, M.K. Slifka, M.H. Oberbarnscheidt, J.S. Obhrai, M.Y. Yeung, and L.V. Riella, Inflammation Causes Resistance to Anti-CD20-Mediated B Cell Depletion. *Am J Transplant*, 2016. 16(11): p. 3139-3149.
179. Das, S. and D. Bar-Sagi, BTK signaling drives CD1d(hi)CD5(+) regulatory B-cell differentiation to promote pancreatic carcinogenesis. *Oncogene*, 2019. 38(17): p. 3316-3324.
180. Schwartz, M., Y. Zhang, and J.D. Rosenblatt, B cell regulation of the anti-tumor response and role in carcinogenesis. *J Immunother Cancer*, 2016. 4: p. 40.
181. Mossner, E., P. Brunker, S. Moser, U. Puntener, C. Schmidt, S. Herter, R. Grau, C. Gerdes, A. Nopora, E. van Puijenbroek, C. Ferrara, P. Sondermann, C. Jager, P. Strein, G. Fertig, T. Friess, C. Schull, S. Bauer, J. Dal Porto, C. Del Nagro, K. Dabbagh, M.J. Dyer, S. Poppema, C. Klein, and P. Umana, Increasing the efficacy of CD20 antibody therapy through the engineering of a new type II anti-

- CD20 antibody with enhanced direct and immune effector cell-mediated B-cell cytotoxicity. *Blood*, 2010. 115(22): p. 4393-402.
182. Bologna, L., E. Gotti, M. Manganini, A. Rambaldi, T. Intermesoli, M. Introna, and J. Golay, Mechanism of action of type II, glycoengineered, anti-CD20 monoclonal antibody GA101 in B-chronic lymphocytic leukemia whole blood assays in comparison with rituximab and alemtuzumab. *J Immunol*, 2011. 186(6): p. 3762-9.
 183. Herter, S., F. Herting, O. Mundigl, I. Waldhauer, T. Weinzierl, T. Fauti, G. Muth, D. Ziegler-Landesberger, E. Van Puijenbroek, S. Lang, M.N. Duong, L. Reslan, C.A. Gerdes, T. Friess, U. Baer, H. Burtscher, M. Weidner, C. Dumontet, P. Umana, G. Niederfellner, M. Bacac, and C. Klein, Preclinical activity of the type II CD20 antibody GA101 (obinutuzumab) compared with rituximab and ofatumumab in vitro and in xenograft models. *Mol Cancer Ther*, 2013. 12(10): p. 2031-42.
 184. Herting, F., T. Friess, S. Bader, G. Muth, G. Holzlwimmer, N. Rieder, P. Umana, and C. Klein, Enhanced anti-tumor activity of the glycoengineered type II CD20 antibody obinutuzumab (GA101) in combination with chemotherapy in xenograft models of human lymphoma. *Leuk Lymphoma*, 2014. 55(9): p. 2151-5160.
 185. Hingorani, S.R., L. Wang, A.S. Multani, C. Combs, T.B. Deramautd, R.H. Hruban, A.K. Rustgi, S. Chang, and D.A. Tuveson, Trp53R172H and KrasG12D cooperate to promote chromosomal instability and widely metastatic pancreatic ductal adenocarcinoma in mice. *Cancer Cell*, 2005. 7(5): p. 469-83.
 186. Chen, J., M. Trounstein, F.W. Alt, F. Young, C. Kurahara, J.F. Loring, and D. Huszar, Immunoglobulin gene rearrangement in B cell deficient mice generated by targeted deletion of the JH locus. *Int Immunol*, 1993. 5(6): p. 647-56.
 187. Takai, T., M. Li, D. Sylvestre, R. Clynes, and J.V. Ravetch, FcR gamma chain deletion results in pleiotrophic effector cell defects. *Cell*, 1994. 76(3): p. 519-29.
 188. Medler, T.R., D. Murugan, W. Horton, S. Kumar, T. Cotechini, A.M. Forsyth, P. Leyshock, J.J. Leitenberger, M. Kulesz-Martin, A.A. Margolin, Z. Werb, and L.M. Coussens, Complement C5a Fosters Squamous Carcinogenesis and Limits T Cell Response to Chemotherapy. *Cancer Cell*, 2018. 34(4): p. 561-578 e6.
 189. Evans, R.A., M.S. Diamond, A.J. Rech, T. Chao, M.W. Richardson, J.H. Lin, D.L. Bajor, K.T. Byrne, B.Z. Stanger, J.L. Riley, N. Markosyan, R. Winograd, and R.H. Vonderheide, Lack of immunoediting in murine pancreatic cancer reversed with neoantigen. *JCI Insight*, 2016. 1(14).
 190. Engle, D.D., H. Tiriach, K.D. Rivera, A. Pommier, S. Whalen, T.E. Oni, B. Alagesan, E.J. Lee, M.A. Yao, M.S. Lucito, B. Spielman, B. Da Silva, C. Schoepfer, K. Wright, B. Creighton, L. Afinowicz, K.H. Yu, R. Grutzmann, D. Aust, P.A. Gimotty, K.S. Pollard, R.H. Hruban, M.G. Goggins, C. Pilarsky, Y. Park, D.J. Pappin, M.A. Hollingsworth, and D.A. Tuveson, The glycan CA19-9 promotes pancreatitis and pancreatic cancer in mice. *Science*, 2019. 364(6446): p. 1156-1162.
 191. Amrutkar, M. and I.P. Gladhaug, Pancreatic Cancer Chemoresistance to Gemcitabine. *Cancers (Basel)*, 2017. 9(11).
 192. Seth, S., C.Y. Li, I.L. Ho, D. Corti, S. Loponte, L. Sapio, E. Del Poggetto, E.Y. Yen, F.S. Robinson, M. Peoples, T. Karpinet, A.K. Deem, T. Kumar, X. Song, S.

- Jiang, Y. Kang, J. Fleming, M. Kim, J. Zhang, A. Maitra, T.P. Heffernan, V. Giuliani, G. Genovese, A. Futreal, G.F. Draetta, A. Carugo, and A. Viale, Pre-existing Functional Heterogeneity of Tumorigenic Compartment as the Origin of Chemoresistance in Pancreatic Tumors. *Cell Rep*, 2019. 26(6): p. 1518-1532 e9.
193. Rosser, E.C. and C. Mauri, Regulatory B cells: origin, phenotype, and function. *Immunity*, 2015. 42(4): p. 607-12.
 194. Bengsch, B., T. Ohtani, O. Khan, M. Setty, S. Manne, S. O'Brien, P.F. Gherardini, R.S. Herati, A.C. Huang, K.M. Chang, E.W. Newell, N. Bovenschen, D. Pe'er, S.M. Albelda, and E.J. Wherry, Epigenomic-Guided Mass Cytometry Profiling Reveals Disease-Specific Features of Exhausted CD8 T Cells. *Immunity*, 2018. 48(5): p. 1029-1045 e5.
 195. Suzuki, E., V. Kapoor, A.S. Jassar, L.R. Kaiser, and S.M. Albelda, Gemcitabine selectively eliminates splenic Gr-1+/CD11b+ myeloid suppressor cells in tumor-bearing animals and enhances antitumor immune activity. *Clin Cancer Res*, 2005. 11(18): p. 6713-21.
 196. Ding, Z.C., X. Lu, M. Yu, H. Lemos, L. Huang, P. Chandler, K. Liu, M. Walters, A. Krasinski, M. Mack, B.R. Blazar, A.L. Mellor, D.H. Munn, and G. Zhou, Immunosuppressive myeloid cells induced by chemotherapy attenuate antitumor CD4+ T-cell responses through the PD-1-PD-L1 axis. *Cancer Res*, 2014. 74(13): p. 3441-53.
 197. Zhu, J., H. Chen, X. Huang, S. Jiang, and Y. Yang, Ly6C(hi) monocytes regulate T cell responses in viral hepatitis. *JCI Insight*, 2016. 1(17): p. e89880.
 198. Spear, S., J.B. Candido, J.R. McDermott, C. Ghirelli, E. Maniati, S.A. Beers, F.R. Balkwill, H.M. Kocher, and M. Capasso, Discrepancies in the Tumor Microenvironment of Spontaneous and Orthotopic Murine Models of Pancreatic Cancer Uncover a New Immunostimulatory Phenotype for B Cells. *Front Immunol*, 2019. 10: p. 542.
 199. Hendriks, R.W., S. Yuvaraj, and L.P. Kil, Targeting Bruton's tyrosine kinase in B cell malignancies. *Nat Rev Cancer*, 2014. 14(4): p. 219-32.
 200. Rawlings, D.J., G. Metzler, M. Wray-Dutra, and S.W. Jackson, Altered B cell signalling in autoimmunity. *Nat Rev Immunol*, 2017. 17(7): p. 421-436.
 201. Gunderson, A.J. and L.M. Coussens, B cells and their mediators as targets for therapy in solid tumors. *Exp Cell Res*, 2013. 319(11): p. 1644-9.
 202. Masso-Valles, D., T. Jauset, E. Serrano, N.M. Sodik, K. Pedersen, N.I. Affara, J.R. Whitfield, M.E. Beaulieu, G.I. Evan, L. Elias, J. Arribas, and L. Soucek, Ibrutinib exerts potent antifibrotic and antitumor activities in mouse models of pancreatic adenocarcinoma. *Cancer Res*, 2015. 75(8): p. 1675-81.
 203. Habtezion, A., A.S. Gukovskaya, and S.J. Pandol, Acute Pancreatitis: A Multifaceted Set of Organelle and Cellular Interactions. *Gastroenterology*, 2019. 156(7): p. 1941-1950.
 204. Lee, K.E., M. Spata, R. Maduka, R.H. Vonderheide, and M.C. Simon, Hif1alpha Deletion Limits Tissue Regeneration via Aberrant B Cell Accumulation in Experimental Pancreatitis. *Cell Rep*, 2018. 23(12): p. 3457-3464.
 205. Folias, A.E., C. Penaranda, A.L. Su, J.A. Bluestone, and M. Hebrok, Aberrant innate immune activation following tissue injury impairs pancreatic regeneration. *PLoS One*, 2014. 9(7): p. e102125.

- 206. Kim, H., Cerulein pancreatitis: oxidative stress, inflammation, and apoptosis. *Gut Liver*, 2008. 2(2): p. 74-80.
- 207. Siveke, J.T., C. Lubeseder-Martellato, M. Lee, P.K. Mazur, H. Nakhai, F. Radtke, and R.M. Schmid, Notch signaling is required for exocrine regeneration after acute pancreatitis. *Gastroenterology*, 2008. 134(2): p. 544-55.
- 208. Zouggari, Y., H. Ait-Oufella, P. Bonnin, T. Simon, A.P. Sage, C. Guerin, J. Vilar, G. Caligiuri, D. Tsiantoulas, L. Laurans, E. Dumeau, S. Kotti, P. Bruneval, I.F. Charo, C.J. Binder, N. Danchin, A. Tedgui, T.F. Tedder, J.S. Silvestre, and Z. Mallat, B lymphocytes trigger monocyte mobilization and impair heart function after acute myocardial infarction. *Nat Med*, 2013. 19(10): p. 1273-80.
- 209. Novobrantseva, T.I., G.R. Majeau, A. Amatucci, S. Kogan, I. Brenner, S. Casola, M.J. Shlomchik, V. Kotliansky, P.S. Hochman, and A. Ibraghimov, Attenuated liver fibrosis in the absence of B cells. *J Clin Invest*, 2005. 115(11): p. 3072-82.
- 210. Jang, H.R., M.T. Gandolfo, G.J. Ko, S.R. Satpute, L. Racusen, and H. Rabb, B cells limit repair after ischemic acute kidney injury. *J Am Soc Nephrol*, 2010. 21(4): p. 654-65.

Appendix A: Curriculum Vitae

Shannon M. Liudahl

Cancer Biology Graduate Program, School of Medicine
Oregon Health & Science University
2720 SW Moody Avenue, Portland, OR 97201
Lab: (503) 494-9859 | Cell: (541) 225-7999
liudahl@ohsu.edu

Education

August 2019 (anticipated)	Ph.D. Cancer Biology Program Department of Cell, Developmental & Cancer Biology Oregon Health & Science University, Portland, OR
2017	Graduate Certificate in Human Investigations Human Investigations Program, Oregon Clinical & Translational Research Institute, Oregon Health & Science University, Portland, OR
2012	B.S. Micro/Molecular Biology , Portland State University, Portland, OR University Honors Program <i>Magna cum laude</i> with Biology Departmental Honors

Research Experience

2012-present	Doctoral Research Cancer Biology Graduate Program, Oregon Health & Science University Ph.D. Supervisor: Lisa M. Coussens, Ph.D. <u>Research</u> : My research has focused, in part, on identifying the role of B lymphocytes in regulating neoplastic progression in models of chronic pancreatitis and pancreatic ductal adenocarcinoma, and has included preclinical trials evaluating B cell depletion in combination with chemotherapy and α PD-1. I also contributed to the development of a multiplex immunohistochemistry platform I am implementing to deeply profile the immune microenvironment of human pancreatic tumors to determine associations between immune landscape, tumor mutational status, and survival outcomes.
2011-2012	Undergraduate Research Assistant Department of Biology, Portland State University Honors Thesis Advisor: Jeffrey D. Singer, Ph.D. Undergraduate Honors Thesis: <i>Analysis of Enzyme/Substrate Interactions During Cell Cycle Progression Using Fluorescence Resonance Energy Transfer</i>
2011	Summer Student <i>Section of Cancer Genomics, National Cancer Institute, National Institutes of Health</i> Principal Investigator: Thomas Ried, M.D.

Additional Scientific Training

2015	Workshop on Modeling Human Cancer in Mice <i>The Jackson Laboratory, Bar Harbor, ME</i>
------	---

Honors & Awards

Competitive Funding:

2017	Knight Cancer Institute Graduate Stipend Award
2014-2015	Ruth L. Kirschstein NIH T32 - OHSU Program in Molecular & Cellular Biosciences
2014	N.L. Tartar Trust Fellowship (Oregon Health & Science University)

Other:

2018	Keystone Symposia Travel Scholarship
2017, 2018	OHSU All-Hill Student Council <i>Leadership in Student Service</i> award nominee
2015	Gordon Research Conference Travel Award for Invited Short Talk
2011	Throckmorton Scholarship (Portland State Univ. Honors Program)
2010-2011	Portland State University Dean's List
2009-2010	Portland State University President's List
2008-2012	Oregon Laurels Undergraduate Merit Scholarship
2008-2012	Eugene Airport Rotary Foundation Scholarship

Publications

i. Peer-Reviewed Research Articles

Liudahl SM, Sivagnanam S, Betts CB, Morales-Oyarvide V, Yuan C, Nowak JA, Hwang S, Grossblatt-Wait A, Leis KR, Larson W, Robinson P, Dias Costa A, Varyrynen SA, Link J, Keith D, Horton W, Tempero, MA, Jaffee EM, Sheppard B, Goecks J, Sears RC, Wolpin BA, Coussens LM. Multiplex immunohistochemistry reveals phenotypic and spatial immune heterogeneity in pancreatic ductal adenocarcinoma. *Manuscript in preparation*.

Liudahl SM, Sanchez Flores Jr, R, Lavoie MB, Leis KR, Betre K, Coussens LM. B lymphocytes regulate tissue response to acute pancreatic injury but are dispensable for the establishment of chronic pancreatitis. *Manuscript in preparation*.

Link J, **Liudahl SM**, Betts CB, Sivagnanam S, Leis KR, McDonnell M, Pelz C, Johnson B, Hamman K, Keith D, Sampson J, Morgan TK, Lopez CD, Coussens LM, Sears RC. Tumor immunity associated with long-term survival of a patient with chemotherapy-resistant metastatic pancreatic adenocarcinoma and familial predisposition to the disease. *Manuscript in preparation*.

Michaelis KA, Norgard MA, Zhu X, Levasseur PR, Sivagnanam S, **Liudahl SM**, Burfeind KG, Olson B, Pelz KR, Angeles Ramos D, Olive KP, Coussens LM, Morgan TK, Marks DL. (2019) The TLR7/8 agonist R848 remodels tumor and host immune responses to promote survival in pancreatic cancer. *Manuscript accepted at Nature Communications*.

Banik G, Betts CB, **Liudahl SM**, Sivagnanam S, Kawashima R, Cotechini T, Larson W, Clayburgh DR, Tsujikawa T, Coussens LM. High-dimensional multiplexed immunohistochemical characterization of immune contexture in human cancers. (2019) *Methods in Enzymology*, In press, DOI: 10.1016/bs.mie.2019.05.039

Hundeyin M, Kurz E, Mishra A, Kochen Rossi JA, **Liudahl SM**, Leis KR, Mehrotra H, Kim M, Torres LE, Ogunsankin A, Link J, Sears RC, Sivagnanam S, Goecks J, Sadeq Islam KM, Dolgalev I, Savadkar S, Wang W, Aykut B, Leinwand J, Diskin B, Adam S, Israr M, Gelas M, Lish J, Chin K, Saad Farooq M, Wadowski B, Wu J, Shah S, Adeegbe D, Pushalkar S, Vasudevaraja V, Saxena D, Wong K, Coussens LM, Miller G. (2019) Innate $\alpha\beta$ T cells mediate antitumor immunity by orchestrating immunogenic macrophage programming. *Cancer Discov.* 9:1288-1305. PMCID: PMC6726581

Li J, Byrne KT, Yan F, Yamazoe T, Chen Z, Baslan T, Richman LP, Lin J, Sun YH, Rech AJ, Balli D, Hay CA, Sela Y, Merrell AJ, **Liudahl SM**, Gordon N, Norgard RJ, Yuan S, Yu S, Chao T, Ye S, Eisinger- Mathason TSK, Faryabi RB, Tobias JW, Lowe S, Coussens LM, Wherry EJ, Vonderheide RH, Stanger BZ. (2018) Tumor cell-intrinsic factors underlie immune heterogeneity and therapeutic response. *Immunity* 49:173-193. PMCID: PMC6707727

Gunderson AJ, Kaneda MM, Tsujikawa T, Nguyen AV, Affara NI, Ruffell B, Gorjestani S, **Liudahl SM**, Truitt M, Olson P, Kim G, Hanahan D, Tempero MA, Sheppard B, Irving B, Chang BY, Varner JA, Coussens LM. (2016) Bruton tyrosine kinase-dependent immune crosstalk drives pancreas cancer. *Cancer Discov.* 6:270-285. PMCID: PMC4783268

ii. Book Chapters, Commentaries & Reviews

Liudahl SM and Coussens LM. (2018) To help or to harm: dynamic roles of CD4⁺ T helper cells in solid tumor microenvironments. Book chapter in: Immunology Vol. 1 - Immunotoxicology, Immunopathology, and Immunotherapy (M.A. Hayat, Ed.), Elsevier/Academic Press, *Chapter 8*, 97-116.

Liudahl SM and Coussens LM. (2018) B cells as biomarkers: predicting immune checkpoint therapy adverse events. *J Clin Invest.* 128:577-579. PMID: 293094

Presentations

National & International

Oral Presentation: “Multiplex Immunohistochemistry to Evaluate Immune Heterogeneity in Pancreatic Cancer: Implications for Effective Immune Therapy” Next Generation Dx Summit, Washington D.C., August 2019

Poster: “Correlations between Smad4 status and leukocyte complexity in human pancreatic cancer” Keystone Symposia – Cancer Immunotherapy: Combinations; Montreal, Quebec, Canada, March 2018.

Poster: “Regulation of pancreatic cancer progression via therapeutic inhibition of Bruton’s tyrosine kinase and related Tec-family kinases”. Cancer Biology Training Consortium (CABTRAC) Annual Meeting; Stevenson, WA, October 2017.

Oral Presentation: “Immune Regulation of Pancreatic Cancer”. 7th Annual Tumor Microenvironment Network (TMEN) Junior Investigators Meeting; National Institutes of Health, Bethesda, MD, May 2016.

Oral Presentation: “B Cells Regulate Tissue Damage During Pancreatitis”. Gordon Research Conference on Pancreatic Diseases; Mount Holyoke College, South Hadley, MA, July 2015.

Poster: “Leukocyte involvement in the initiation and maintenance of pancreatitis”. Keystone Symposia – Immune Evolution in Cancer; Whistler, British Columbia, Canada, March 2014.

Local/Institutional

Oral Presentation: “Leukocyte Complexity, Mutational Status, and Survival Outcomes in Human Pancreatic Cancer”. OHSU Cancer Biology Program Student Seminar Series, Portland, OR, November 2018.

Oral Presentation: “Leukocyte Complexity, Mutational Status, and Survival Outcomes in Human Pancreatic Cancer”. PNW Tumor Microenvironment Symposium, Portland, OR, October 2018.

Oral Presentation: “Leukocyte Complexity, Mutational Status, and Survival Outcomes in Human Pancreatic Cancer”. OHSU Cancer Biology Program Student Seminar Series, Portland, OR, June 2018.

Oral Presentation: “Blockade of BTK Promotes Anti-Tumor Immunity in Pancreatic Cancer – Implications for Early-Stage Disease”. OHSU Cancer Biology Program Student Seminar Series, Portland, OR, November 2016.

Oral Presentation: “Blockade of Kinases BTK and ITK Promotes Anti-Tumor Immunity in Pancreatic Cancer”. OHSU Cell, Developmental & Cancer Biology Graduate Student Retreat, Portland, OR, September 2016.

Poster: “B Cells Regulate Tissue Damage During Pancreatitis”. Oregon Biosciences Association Annual Meeting, Portland, OR, September 2015

Poster: “B Cells Regulate Tissue Damage During Pancreatitis”. Cell, Developmental & Cancer Biology – OHSU Center for Spatial Systems Biomedicine Joint Retreat, Stevenson, WA, August 2015.

Oral Presentation: “Identifying the Role of B Cells in Pancreatitis.” OHSU Cancer Biology Program Student Seminar Series, Portland, OR, June 2015.

Poster: “B Cells Regulate the Initiation and Maintenance of Pancreatitis”. OHSU Program in Molecular and Cellular Biosciences Annual Retreat, Welches, OR, September 2014.

Poster: “B Cells Regulate the Initiation and Maintenance of Pancreatitis”. PancWest Symposium, Portland, OR, September 2014.

Poster: “Leukocyte involvement in the initiation and maintenance of pancreatitis”. Oregon Health & Science University Research Week, May 2014.

Poster: “Leukocyte involvement in the initiation and maintenance of pancreatitis”. OHSU Knight Cancer Institute Retreat, October 2013.

Leadership & Service

Leadership & Outreach

2018	Conference Assistant, Keystone Symposia - Cancer Immunotherapy: Combinations <u>Roles:</u> Prepare conference Program Report and Meeting Summary for the Keystone Symposia co-chaired by Drs. Chris Boshoff, Leiping Chen, and Lisa Coussens that took place in March 2018 in Montreal, QC.
2015-2017	OHSU Graduate Student Organization Vice President (2016-2017), Treasurer (2015-2016) <u>Roles:</u> Co-direct monthly student meetings, lead GSO Travel Award steering committee, attend monthly Graduate Faculty Council and OHSU Student Council meetings, serve on GSO student award selection committees, student advocacy, event development and planning, budget preparation, website development and maintenance
2015-2016	OHSU Cell, Developmental & Cancer Biology Student Retreat Planning Committee Member <u>Roles:</u> Plan and coordinate scientific and career development activities, keynote speaker selection and invitation, abstract selection
2015	<i>On Track OHSU!</i> Volunteer <u>Roles:</u> Participate in scientific outreach activities and provide academic and career guidance to underrepresented high school students in the Portland metro area
2014	OHSU Program in Molecular & Cellular Biosciences Retreat Planning Committee Member <u>Roles:</u> Develop student breakout sessions, keynote speaker selection

Mentoring & Teaching Experience

Mentoring

- 2018 Ruben Sanchez Flores Jr., High School Student
OHSU Ted R. Lilley CURE Internship Program, June-August 2018
- *Received Best Poster award at OHSU intern poster session*
- Padraic Robinson, Research Assistant – Coussens Lab, OHSU
- Kenna Leis, Research Assistant – Coussens Lab, OHSU
- 2017 Hannah Zhao, Undergraduate Student (University of Southern California)
OHSU CDCB Summer Internship Program, June-August 2017
- Rowan Talbot-Guerette, Undergraduate Student (University of Rhode Island)
OHSU CDCB Summer Internship Program, June-August 2017

Teaching

- 2018 Lecturer, *"How to Read a Journal Article"* – OHSU Cell, Developmental & Cancer
Biology Summer Internship Program
- 2015 Teaching Assistant for CANB 613/CELL 613 Tissue Biology, OHSU

Memberships to Professional Societies

- 2018-present American Association for Cancer Research